Proline-Quaterthiophene Hybrids: Synthesis and Self-Assembly

Dissertation

zur Erlangung des akademischen Grades

Dr. rer. nat.

der Fakultät für Naturwissenschaften

der Universität Ulm

vorgelegt von

Angela Digennaro

aus Milano

2016

Amtierender Dekan: Prof. Dr. Peter Dürre

1. Gutachter: Prof. Dr. Peter Bäuerle

2. Gutachter: Prof. Dr. Tanja Weil

Tag der Promotionsprüfung: 06. Juli 2016

Fakultät für Naturwissenschaften, Universität Ulm 2016

"Those who say it cannot be done

should not interrupt those who are doing it”

Anonymus

I would like to express my sincere gratitude to my mentor, Prof. Dr. Peter Bäuerle, for the interesting and challenging topic, the great working conditions, and the possibility he gave me to take part to national and international conferences.

Thanks to my cooperation partners: Prof. Dr. Helma Wennemers, Dr. Francelin Bouillère, Dr. Urszula Lewandowska, Dr. Gururaj Joshi, Prof. Dr. Müllen, Dr. Long Chen, and Dr. Wojciech Zajaczkowsk. I would like to acknowledge the Volkswagen Foundation for the financial support. Thanks to the group of Prof. Dr. Mika Linden for the performance of DLS measurements, and to the group of Prof. Dr. Paul Walther for the help they gave me during the TEM measurements.

Many thanks to Dr. Elena Mena-Osteritz for the precious support she gave me for the understanding of many aspects of my PhD project, for her guidance in the use of AFM, and, more important, for the sensitivity she has shown during difficult periods. Thanks to Dr. Sylvia Schmid for helping me and stand by me during these years of research. Thanks to Dr. Günther Götz, whom I will always remember for his patience in helping me with most of the laboratory instrumentations, and his true love for my native country, Italia. Thanks to Dr. Gisela Schultz for her essential help in the fabrication of solar cells and the result interpretation. Many thanks go to Dr. Markus Wunderlin for all the mass spectra, for his help concerning all the possible and imaginable computer problems and other aspects. My thanks go also to Mrs. Maria Heuschmid and Mrs. Ingrid Bopp for their patient assistance in all the bureaucratic problems, which are quite a lot and not so easy to understand for foreign people. Thousand thanks to all OC II colleagues: you were the best I could wish to work with. A particular thanks go to my best friends Eduard (so-called Edoardo) Brier, Dr. (!) Martina Gatys, Dr. Mirjam Löbert, and all the colleagues passed through “Lab 4104”: you made my days.

Incommensurable thanks go to all my friends, Italian and not, from Ulm, from Italy, or other countries. In particular, thank you Ilaria Cappadona, Novella Guidi, Giuseppe Oliveri, and Marco Balducci for our lunch time together (and offered coffee); Francesca Mannella, Ivonne Brock and many others: you were always able to turn my bad days in positive ones and to support and bear me all these years. *Dulcis in fundo*, I would like to thank with all my love my boyfriend, Bernd, who supports and tolerates me most of the time -Italian girls can be pretty annoying sometimes- in all situations with all his love, and my family, who supported and helped me when I decided to come to Deutschland, and they still do, with all their unconditional love.

Table of Contents

Abbreviation

A	adenosine, acceptor
AFM	atomic force microscopy
Ala	alanine
Arg	arginine
Asp	aspartic acid
a_0	headgroup area
BChl	bacteriochlorophyll
BHJSC	bulk heterojunction solar cell
Boc	*tert*-butoxycarbonyl
CAC	critical aggregation concentration
CB	chlorobenzene
CD	circular dichroism
CI	chemical ionization
CuAAC	Cu(I)-catalyzed azide-alkyne 1,3-dipolar Huisgen cycloaddition
CV	cyclic voltammetry
D	donor
d	day
d	doublet
dd	doublet of doublets
DAN	dialcoxynaphtalene
DBTTC	dibenzotetrathienocoronene

DCE	1,2-dichloroethane
DCM	dichloromethane
DCTB	(2-[(2*E*)-3-(4-*tert*-butylphenyl)-2-methylprop-2-enyliden]malononitrile)
DCV	2,2´-dicyanovinyl
DFT	density functional theory
DHN	dihydroxynaphtalene
DLS	dynamic light scattering
DMF	*N,N*-dimethylformamide
DNA	deoxyribonucleic acid
$E_{g,CV}$	electrochemical gap
$E_{g,opt}$	optical gap
EDG	electron donating group
EDTA	ethylenediaminetetraacetic acid
e.g.	*lat.: "exempli gratia"; engl.: "for example"*
EI	electron ionization
Em	emission
eq.	equivalent
EWG	elecron withdrawing group
Fc/Fc^+	ferrocene/ferrocenium couple
FF	fill factor
FMO	frontier molecular orbital
FT-IR	fourier transform infrared spectroscopy
GIDX	grazing incidence X-ray diffraction

GISAX	grazing incidence small Angle X-ray
GIWAX	grazing incidence wide angle X-ray
Gly	glycine
Glu	glutamic acid
Gln	glutamine
h	hour
HBC	hexa-*peri*-hexabenzocoronene
His	histidine
HOMO	highest occupied molecular orbital
HOPG	highly oriented pyrolytic graphite
HPLC	high performance liquid chromatography
HRMS	high resolution mass spectrometry
HTL	hole transporting layer
ICT	intramolecular charge transfer
Ile	isoleucine
ITO	indium-doped tin oxide
J	coupling constant
J_{SC}	short-circuit current density
l_0	hydrophobic length
LDA	lithium diisopropilamide
Leu	leucine
LUMO	lowest unoccupied molecular orbital
Lys	lysine

M	molar
m	multiplet
MALDI	matrix assisted laser desorption ionization
MeOH	methanol
M. p.	melting point
MS	mass spectrometry
NBS	*N*-bromosuccinimide
n-BuLi	*n*-butyl lithium
NDI	naphthalenetetracarboxylic diimide
NMR	nuclear magnetic resonance
OFET	organic field effect transistor
OLED	organic light emitting diode
OPV	oligo(*p*-phenylenevinylene), organic photovoltaic
OSC	organic solar cell
OT	oligothiophene
Ox	oxidation
P	packing parameter
P3HT	poly(3-hexylthiophene)
Pas	peptide amphiphiles
$PC_{61}BM$	[6,6]-phenyl-C_{61}-butyric acid methyl ester
$PC_{71}BM$	[6,6]-phenyl-C_{71}-butyric acid methyl ester
PCE	power conversion efficiency
PDI	perylene diimide

PEDOT	poly(3,4-ethylenedioxythiophene)
PEO	poly(ethylene oxide)
Phe	phenylalanine
PP	polyproline
Ppm	parts per million
Pro	proline
PSD	position-sensitive detector
PSS	polystyrenesulfonic acid
PT	polythiophene
PTCI	perylene tetracarboxydiimide
rt	room temperature
Red	reduction
s	singlet
SA	self-assembly
SCCNT	stacked-cup carbon nanotube
SMOSC	small molecule organic solar cell
S_N2	nucleophilic substitution
STM	scanning tunneling microscopy
SWNT	single-walled carbon nanotube
t	triplet
T	temperature
TBAF	tetra-*n*-butylammonium fluoride
TBAHFP	tetra-*n*-butylammonium hexafluorophosphate

TEM	transmission electron microscopy
THF	tetrahydrofurane
TLC	thin layer chromatography
TMS	trimethylsilyl
TOF	time of flight
UV/Vis	ultraviolet/visible
V	voltage
v	hydrophobic volume
Val	valine
V_{oc}	open-circuit voltage
XRD	X-Ray diffraction
δ	chemical shift
ε	molar extinction coefficient
λ	wavelength
μ	dipole moment
4T	quaterthiophene

Chapter 1

Aim of the Thesis

Since the discovery of highly conducting polyacetylene by Shirakawa, MacDiarmid, and Heeger in 1977,[1] π-conjugated systems have attracted great attention as materials for the development and production of a new generation of electronics. Big efforts are currently made to improve the properties of such devices. In fact, because of the low cost, the large area coverage, and the processability and structural flexibility of the organic semiconductors, organic electronics are largely preferred over inorganic electronics.[2]

In particular, in recent years, polymers and oligomers based on thiophene (***Chart 1.1***) have gained immense interest in this field and find versatile application in organic light emitting diodes (OLEDs)[3], organic field effect transistors (OFETs)[4], or organic solar cells (OSCs).[5]

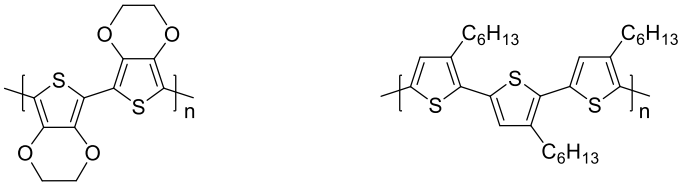

1.1 **1.2**

Chart 1.1. *Structures of poly(3,4-ethylenedioxythiophene) (PEDOT)* ***1.1*** *and poly(3-hexyl-thiophene) (P3HT)* ***1.2****.*

Because the performance of the electronic devices directly depends on the self-organization of the active material in the bulk, chiral polythiophenes (PTs) and oligothiophenes (OTs) were reported as promising scaffolds for the construction of functional nanoarchitectures.[6–8] A more recent approach combines various π-conjugated segments with biological motifs such as peptides[9–13] or carbohydrates,[14,15] most of them in a symmetric A–B–A structure. These are capable of interacting via a broad variety of non-covalent forces such as π–π, van-der-Waals, dipole-dipole, and hydrogen bond interactions. The resulting nanostructures were reported to follow the secondary structural motifs of the incorporated biosegments, *e.g.*, α-helices or β-sheets (***Figure 1.1***).

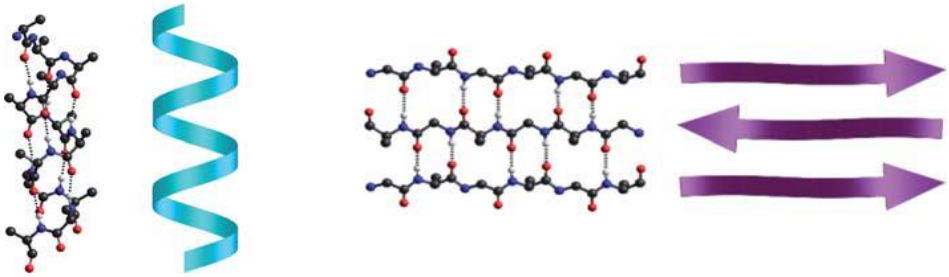

Figure 1.1. *Examples of peptide secondary structure motifs: left: α-helical backbone (here: poly-alanine); right: antiparallel β-sheet (here: a glycinealanine sequence).*[16] Reproduced from *J. Mater. Chem*. **2010**, *20,* 3563-3578 with permission of The Royal Society of Chemistry.

With this in mind, the aim of my thesis was to create and control a new generation of ordered mesoscopic materials which could be applied in macroscopic organic electronic devices (***Figure 1.2***).

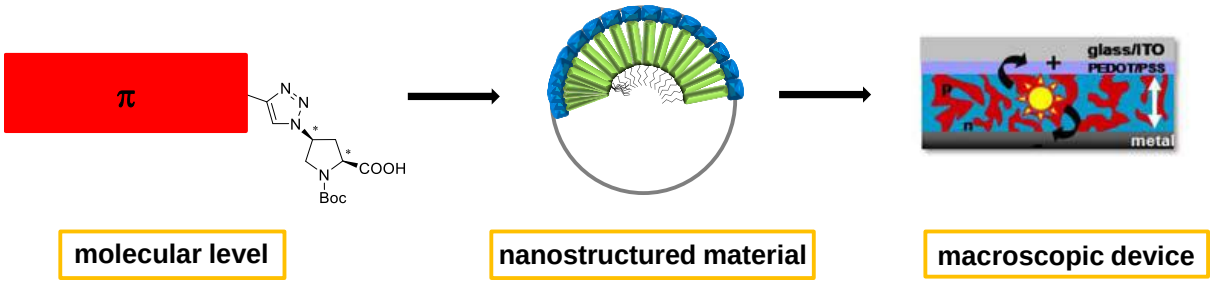

Figure 1.2*. Hierarchical development of integrated molecular components in functional macroscopic devices on increasing length scale: From molecular level (synthesis) to nanostructured mesoscopic materials (self-assembly) to macroscopic organic electronic devices (electronic properties).*

In order to avoid the often used synthesis and isolation of larger peptides, in 2010, our group presented one of the first example of non-symmetrical A-B system by introducing a single amino acid, such as a functionalized monoproline, into a conjugated hybrid: a quaterthiophene decorated by lateral dodecyl chains in β-position was combined via click chemistry with a *N*-Boc-protected monoproline (***Chart 1.2***).[17]

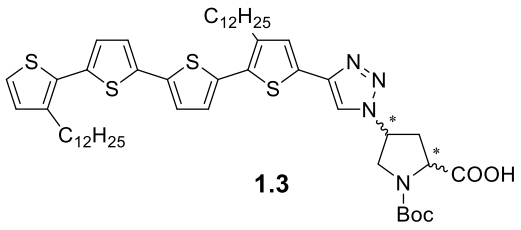

Chart 1.2. *Structure of quaterthiophene-proline hybrid* ***1.3****.*

Because such system showed the ability to self-assemble in organized suprastructures, I decided to focus my research on the improvement of this molecule by making diverse structural changes. These should lead to higher order nanostructured materials. To do so, my first step was to replace the long lateral dodecyl chains with hexyl rests (***Chart 1.3***). This structural change should allow the π-conjugated backbones to get closer to each other in the self-assembled aggregates.

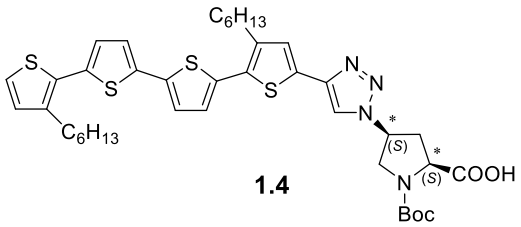

1.4

Chart 1.3. *Structure of quaterthiophene-proline hybrid* ***1.4****.*

To further increase the amphiphilic character of such a quaterthiophene-proline hybrid, an ulterior step was to remove the hindering lateral hexyl chains and to introduce diverse alkyl moieties at the 5'''-position of the 4T (***Chart 1.4***). This change should also prevent the oxidation of the semiconductor at this position.

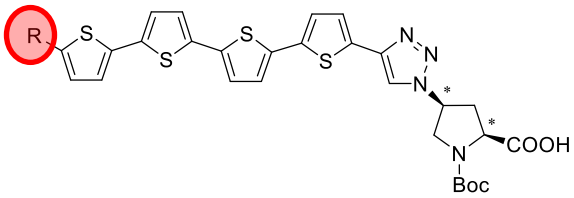

1.5 R = $-C_3H_7$, $-C_6H_{13}$, $-C_6H_{13}(C_2H_5)$

Chart 1.4. *Structure of quaterthiophene-proline hybrid* ***1.5****.*

Another relevant issue in this development process was the solubility of the target molecules. For this reason, it was necessary to replace the free carboxylic acid with an ester function; in this way the formation of H-bonds is prevented, hence they cannot affect the self-assembly anymore, and the molecular solubility increases (***Chart 1.5***).

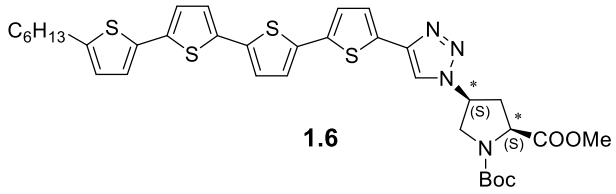

1.6

Chart 1.5. *Structure of quaterthiophene-methyl ester proline hybrid* ***1.6****.*

Because one challenge of my PhD research was the application of the synthesized hybrids in macroscopic organic electronic devices, in particular OSCs, an additional structural development was necessary: the introduction of an acceptor in the biohybrid structure such as a dicyanovinyl group (***Chart 1.6***).

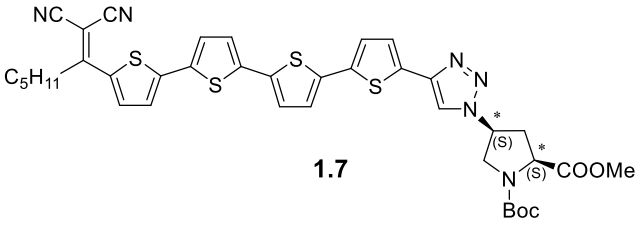

1.7

Chart 1.6. *Structure of DCV-quaterthiophene-proline hybrid* ***1.7****.*

The investigations carried out on the conjugates **1.4**-**1.7** with respect to their self-assembling properties will clearly show the formation of aggregates, in which the chromophores are organized in a chiral fashion. Circularly shaped suprastructures will be observed in the solid state. Additionally, first tests of such aggregates in OSC devices will be reported.

References

[1] C. K. Chiang, C. R. Fincher, Y. W. Park, A. J. Heeger, H. Shirakawa, E. J. Louis, S. C. Gau, A. G. MacDiarmid, *Phys. Rev. Lett.* **1977**, *39*, 1098–1101.

[2] H. Klauk in *Organic Electronics II*, (Ed. H. Klauk), Wiley-VCH Verlag & Co. KGaA, Weinheim, **2012**.

[3] *"Handbook of Oligo- and Polythiophenes"*: P. Bäuerle in *Electronic Materials: The Oligomeric Approach* (Ed.: D. Fichou), Wiley-VCH, Weinheim **1999**, 89–181.

[4] A. Mishra, C.-Q. Ma, P. Bäuerle, *Chem. Rev.* **2009**, *109*, 1141–1278.

[5] A. L. Groenendaal, F. Jonas, D. Freitag, H. Pielartzik, J. R. Reynolds, *Adv. Mater.* **2000**, *12*, 481–494.

[6] a) B. F. M. Kilbinger, A. P. H. J. Schenning, F. Goldoni, W. J. Feast, E. W. Meijer, *J. Am. Chem. Soc.* **2000**, *122*, 1820–1821; b) O. Henze, W. J. Feast, F. Gardebien, P. Jonkheijm, R. Lazzaroni, P. Leclere, E. W. Meijer, A. P. H. J. Schenning, *J. Am. Chem. Soc.* **2006**, *128*, 5923–5929.

[7] K. P. R. Nilsson, A. Herland, P. Hammarstrom, O. Inganäs, *Biochemistry* **2005**, *44*, 3718–3724.

[8] M. Melucci, G. Barbarella, M. Gazzano, M. Cavallini, F. Biscarini, A. Bongini, F. Piccinelli, M. Monari, M. Bandini, A. Umani-Ronchi, P. Biscarini, *Chem. Eur. J.* **2006**, *12*, 7304–7312.

[9] a) H. A. Klok, A. Rösler, G. Götz, E. Mena-Osteritz, P. Bäuerle, *Org. Biomol. Chem.* **2004**, *2*, 3541–3544; b) E.-K. Schillinger, E. Mena-Osteritz, J. Hentschel, H. G. Börner, P. Bäuerle, *Adv. Mater.* **2009**, *21*, 1562–1567; c) A. K. Shaytan, E.-K. Schillinger, P. G. Khalatur, E. Mena-Osteritz, J. Hentschel, H. G. Börner, P. Bäuerle, A. R. Khokhlov, *ACS Nano* **2011**, *5*, 6894–6909.

[10] S. R. Diegelmann, J. M. Gorham, J. D. Tovar, *J. Am. Chem. Soc.* **2008**, *130*, 13840–13841.

[11] a) D. A. Stone, L. Hsu, S. I. Stupp, *Soft Matter* **2009**, *5*, 1990–1993; b) J. A. Lehrman, H. Cui, W.-W. Tsai, T. J. Moyer, S. I. Stupp, *Chem. Commun.* **2012**, *48*, 9711–9713.

[12] R. J. Kumar, J. M. MacDonald, T. B. Singh, L. J. Waddington, A. B. Holmes, *J. Am. Chem. Soc.* **2011**, *133*, 8564–8573.

[13] L. Tian, R. Szilluweit, R. Marty, L. Bertschi, M. Zerson, E.-C. Spitzner, R. Magerle, H. Frauenrath, *Chem. Sci.* **2012**, *3*, 1512–1521.

[14] I.-B. Kim, J. N. Wilson, U. H. F. Bunz, *Chem. Commun.* **2005**, 1273–1275.

[15] S. Schmid, A.Mishra, P. Bäuerle, *Chem. Commun.* **2011**, *47*, 1324–1326.

[16] A. Jatsch, E.-K. Schillinger, S. Schmid, P. Bäuerle, *J. Mater. Chem.* **2010**, *20*, 3563–3578.

[17] E.-K. Schillinger, M. Kümin, A. Digennaro, E. Mena-Osteritz, S. Schmid, H. Wennemers, P. Bäuerle, *Chem. Mater.* **2013**, *25*, 4511–4521.

Chapter 2

State of the Art

2.1 Oligothiophene

2.1.1 Introduction

Oligothiophenes have attracted huge interest among researchers all over the world enough to become the most frequently used π-conjugated materials, in particular as active components in organic electronics.[1-3] Five main reasons count for this:

1) Thiophenes are ideal building blocks in transition metal-catalyzed cross-coupling reactions such as Kumada-,[4] Suzuki-,[5,6] Sonogashira-,[7] Stille-,[8] and Negishi-[9]type reactions, which are well known to offer the basis for the synthesis of most π-conjugated systems.[10,11]

2) Oligothiophenes have an enormous potential of structural variation which allows the tuning of the electronic properties.

3) They are typically stable in various oxidation states and can be characterized by many methods.

4) Their unique electronic, optical, and redox properties are intriguing, as well as their self-assembling properties on solid surfaces or in the bulk.

5) The high polarizability of sulfur atoms in thiophene rings leads to the stabilization of the conjugated chain and to excellent charge transport properties, which are one of the most crucial assets for applications in organic and molecular electronics.

In 1989, Garnier and Fichou contributed to the oligothiophenes´ renaissance by realizing that also shorter conjugated oligomers such as α-sexithiophene (**2.1.2**) can be used as an active semiconductor materials in organic field-effect transistors (OFETs).[12,13] In 1993 and in 1995, respectively, the employment of structurally defined end-capped oligothiophenes (**2.1.4**) in OLEDs[14], and of α-quinquethiophene (**2.1.1**) and α-octathiophene (**2.1.3**) in OSCs[15] was demonstrated (**Chart 2.1.1**).

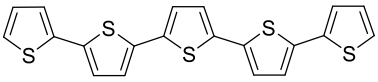

2.1.1

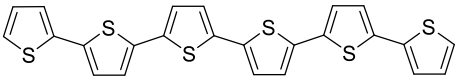

2.1.2

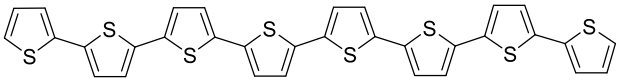

2.1.3

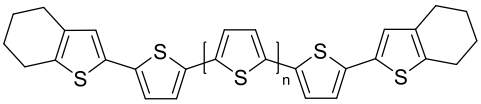

2.1.4 n = 1-3

Chart 2.1.1. *Molecular structures of α-quinquethiophene* ***2.1.1****, α-sexithiophene* ***2.1.2****, α-octathiophene* ***2.1.3****, and end-capped oligothiophene* ***2.1.4****.*

2.1.2 Synthesis of Oligothiophenes

Today, most of the oligothiophene syntheses provide methods for the isolation of short oligothiophenes (less than 8 units).[16,17] Fortunately, the recent development of effective catalysts and versatile building blocks have resulted in a wide variety of defect-free, monodisperse, and long oligothiophenes.

2.1.2.1 Oxidative Coupling

Oligothiophenes can be either oxidized in the presence of certain oxidizing agents, such as ferric chloride, or deprotonated and dimerized by $CuCl_2$ to form a mixture of short α-conjugated oligomers (***Scheme 2.1.1***).[18,19]

This method takes advantage of the varying electron density at different positions of the thiophene monomer; the coupling mainly occurs at the highest electron density positions.[20]

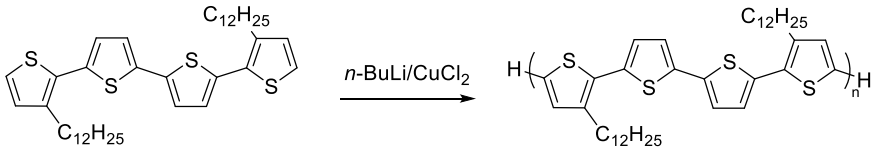

2.1.5 **2.1.6** n = 2, 3, 4

Scheme 2.1.1. *Synthesis of long oligothiophenes via oxidative coupling.*

Nevertheless, a major problem occurs: the oligomers produced contain considerable amounts of undesirable α−β couplings and regioirregularity.[21] Furthermore, it should also be taken into account that an increase of conjugation in the precursor molecule causes a loss of reactivity of the corresponding cation radical, resulting in short oligomers.[18] Another consistent problem is the purification of the materials: repeated sublimation and chromatographic separation are needed to purify the desired product because of metal residues that are often present in the desired products.

In 2007, Bäuerle and co-workers described a new “metal template approach” to synthesize oligothiophenes. The preparation of the oligothiophenes involved a reaction between lithiated shorter oligothiophenes and $dppfPtCl_2$ or $dpppPtCl_2$ to afford an oligothiophene-based Pt-complex, which was then oxidized to the longer oligothiophenes by treatment with silver triflate.[22]

2.1.2.2 Palladium-Catalyzed C−H Homocoupling

Transition metal-catalyzed cross-couplings have been proven to proceed by chain growth mechanism making the synthesis of monodisperse oligomers with precise molecular weight difficult.[23]

Mori and co-workers developed a new synthetic strategy involving the palladium-catalyzed C−H homocoupling of bromothiophene in the presence of a silver reagent as an activator.[24,25] This technique results in oligothiophenes with C−Br bonds at the terminal rings, which can be further functionalized. More recently, the same authors reported an improved procedure for the synthesis of oligothiophenes: treatment of 3-alkylthiophene with Knochel−Hauser base (TMPMgCl·LiCl) induces metalation at the 5-position selectively. Subsequent addition of 2-bromo-3-alkylthiophene and a nickel catalyst leads to the corresponding bithiophene (***Scheme 2.1.2***).[26] The obtained bithiophene is converted to the terthiophene and then to the quaterthiophene by repeating the protocol.

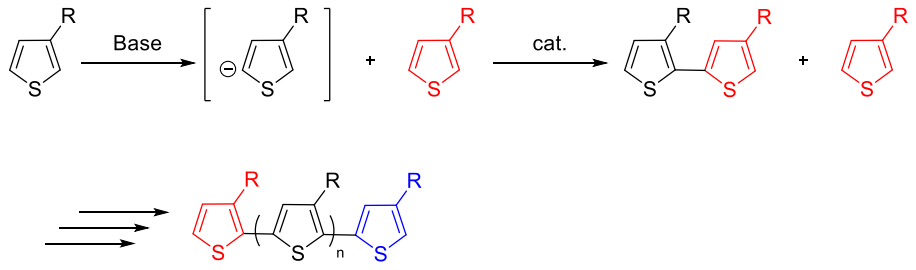

Scheme 2.1.2. *Synthesis of long oligothiophenes via palladium-catalyzed C–H homocoupling.*

2.1.2.3 Palladium-Catalyzed Cross-Coupling

This synthetic strategy allows the synthesis of monodisperse molecular systems with relatively facile isolation and purification. Typically, long oligothiophenes are prepared by the successive addition of bromine, tin, and/or boronic acid groups to thiophene intermediates for palladium catalyzed cross-coupling, such as Stille or Suzuki reactions.[3,17] Recently, Briseno and coworkers prepared a series of didodecylquaterthiophene oligomers with up to 24 thiophene units via Pd-catalyzed Stille coupling reactions.[27] In recent papers, regioregular head-to-head oligothiophenes have been efficiently prepared by combining Pd-catalyzed Stille coupling reactions with microwave radiation.[28] To get longer homologues, oligothiophenes need to be selectively functionalized at the terminal α-positions. However, the reactivity at α-positions of long oligothiophenes decreases and the possibility of reaction at β-positions increases due to the increase of the number of β-positions relative to α-positions with increased chain length.[29] This becomes a big problem, as the α-linked products could not be separated from the β-linked products. To avoid the undesirable β-reactions, the use of substituents to block the β-positions is a possible solution.

2.1.3 Crystal Packing in the Solid Sate

Unsubstituted oligothiophenes crystallize in the monoclinic space group and display 2D herringbone arrangement due to strong edge-to-face interactions.[30] This configuration limits the electronic overlap between π orbitals.[31-34] As a result, higher performance may be achieved in crystal structures, which exhibit more "π-stacking" because of the strong electronic coupling.[33]

2.1.3.1 α-Substituted Oligothiophenes

The incorporation of substituents along the backbone has a strong influence on the crystal packing of the oligothiophenes.[35] However, it is surprising to see that substitution at the high electron density (α-) positions with linear alkyl chains or less bulky substituents does not significantly alter the molecular packing motif.[36] Bao and co-workers observed that the crystal packing of quaterthiophene terminated with different alkyl chains and different number of trimethylsilyl (TMS) groups (***Chart 2.1.2***) adopt the same layer-by-layer herringbone motif, but diverse tilt angle within the crystallographic *bc* plane by varying with the terminal substitution.[37]

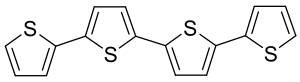

2.1.7

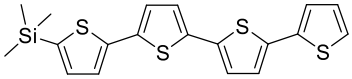

2.1.8

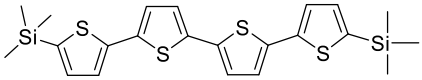

2.1.9

Chart 2.1.2. *Molecular structures of quaterthiophene* ***2.1.7****, mono-TMS-substituted quaterthiophene* ***2.1.8****, and bis-TMS-substitute quaterthiophene* ***2.1.9****.*

This indicates that in addition to enhanced chemical stability and solubility, the end-substitution does not induce inter-ring torsion and the dominant force dictating the crystal packing is the interaction between aromatic cores. On the other hand, branched alkyl chains or bulky substituents at the α-positions reduce the relative density of the thiophene cores causing the deviation from the herringbone arrangement.[35]

2.1.3.2 β-Substituted Oligothiophenes

In contrast to substitutions at the α-positions, functionalisation at the low electron-density positions (β-) have a great effect on the backbone planarity and thiophene conformation.[38] This influence is clearly seen in many β-substituted oligothiophenes,

which crystallize to form π-π stacks instead of following the herringbone motif which is typical for the unsubstituted oligothiophenes.[39] The crystal packing behaviour of substituted oligothiophenes arises not only from the backbone organization, but also from the side chain conformation. The chain length, position, and concentration of the substituents play all important roles in the crystal packing.

In general, the difference in the crystal structures derives from the alkyl side chains: hexyl and dodecyl chains are sufficiently long to provide hydrophobic alkyl-alkyl interactions with neighbouring chains, while propyl chains are too short to maintain the hydrophobic interactions between each other.[40,41] In particular, oligothiophene derivatives with longer alkyl chains, such as 9 and 14, form lamellar packing motifs by self-assembly through π-π interactions between co-facial thiophene units and intermolecular dispersive interactions between the alkyl chains which are perpendicular to the backbones (***Figure 2.1.1***).

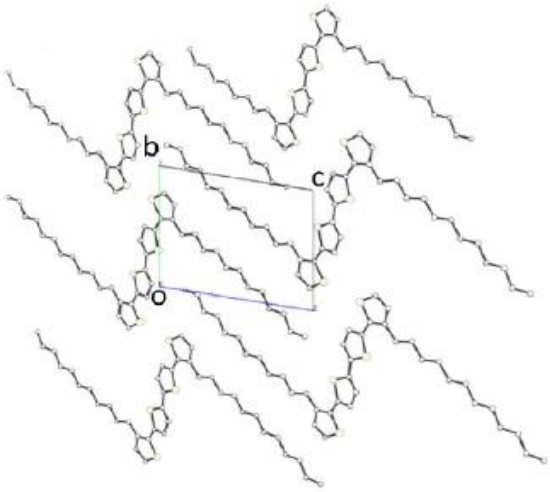

Figure 2.1.1. *Representative lamellar packing model of ß-substituted oligothiophenes. Adapted with permission from* ACS Appl. Mater. Interfaces ***2014****,* 6*, 5327-5343. Copyright 2014 American Chemical Society.*

References

[1] D. Fichou in *Handbook of Oligo- and Polythiophenes*, (Ed.: D. Fichou), Wiley-VCH, Weinheim, **1999**.

[2] K. Müllen and G. Wegner in *Electronic Materials: The Oligomer Approach* (Eds.: K. Müllen and G. Wegner), Wiley-VCH, Weinheim, **1998**.

[3] A. Mishra, C.-Q. Ma, P. Bäuerle, *Chem. Rev.* **2009,** *109,* 1141–1276

[4] K. Tamao, K. Sumitani, Y. Kiso, M. Zembayashi, A. Fujioka, S. Kodama, I. Nakajima, A. Minato, M. Kumada, *Bull. Chem. Soc. Jpn.* **1976**, *49*, 1958–1969.

[5] A. Suzuki, *Pure Appl. Chem.* **1991**, *63*, 419–422.

[6] S. Kotha, K., Lahiri, D., Kashinath, *Tetrahedron* **2002**, *58*, 9633–9695.

[7] K. Sonogashira, Y. Tohda, N. Hagihara, *Tetrahedron Lett.* **1975**, *16*, 4467–4470.

[8] J. K. Stille, *Angew. Chem., Int. Ed.* **1986**, *25*, 508–524.

[9] M. Miyasaka, A. Rajca, *Synlett.* **2004**, 177-181.

[10] R. Chinchilla, C. Nájera, M. Yus, *Chem. Rev.* **2004**, *104*, 2667-2722.

[11] F. Diedrich and P. J. Stang in *Metal Catalyzed Cross-Coupling Reactions,* (Eds.: F. Diedrich and P. J. Stang), Wiley-VCH, Weinheim, **1998** and **2006**.

[12] G. Horowitz, D. Fichou, X. Peng, Z. Xu, F. Garnier, Solid State Commun. **1989**, 72, 381-384.

[13] F. Garnier, G. Horowitz, X. Peng, D. Fichou, Adv. Mater. **1990**, 2, 592-594.

[14] F. Geiger, M. Stoldt, H. Schweizer, P. Bäuerle, E. Umbach, Adv. Mater. **1993**, 5, 922-925.

[15] N. Noma, T. Tsuzuki, Y. Shirota, Adv. Mater. **1995**, 7, 647-648.

[16] H. Katz, Z. Bao, S. L. Gilat, *Acc. Chem. Res.* **2001**, *34*, 359-369.

[17] S. Allard, M. Forster, B. Souharce, H. Thiem, U. Scherf, *Angew. Chem.* **2008**, *120*, 4138-4167; *Angew. Chem., Int. Ed.* **2008**, *47*, 4070-4098.

[18] G. Barbarella, M. Zambianchi, R. Di Toro, M. Colonna, D. Iarossi, F. Goldoni, A. Bongini, *J. Org. Chem.* **1996**, *61*, 8285-8292.

[19] Y. Wei, C. Chan, J. Tian, G. Jang, K. Hsueh, *Chem. Mater.* **1991**, *3*, 888-897.

[20] J. Roncali, *Chem. Rev.* **1997**, *97*, 173-206.

[21] G. Engelmann, W. Jugelt, G. Kossmehl, H. Welzel, P. Tschuncky, J. Heinze, *Macromolecules* **1996**, *29*, 3370-3375.

[22] F. Zhang, P. Bäuerle, *J. Am. Chem. Soc.* **2007**, *129*, 3090-3091.

[23] I. Osaka, R. McCullough, *Acc. Chem. Res.* **2008**, *41*, 1202−1214.

[24] M. Takahashi, K. Masui, H. Sekiguchi, N. Kobayashi, A. Mori, M. Funahashi, N. Tamaoki, *J. Am. Chem. Soc.* **2006**, *128*, 10930-10933.

[25] N. Masuda, S. Tanba, A. Sugie, D. Monguchi, N. Koumura, K. Hara, A. Mori, *Org. Lett.* **2009**, *11*, 2297-2300.

[26] S. Tanaka, S. Tamba, D. Tanaka, A. Sugie, A. Mori, *J. Am. Chem. Soc.* **2011**, *133*, 16734-16737.

[27] L. Zhang, N. Colella, F. Liu, S. Trahan, J. Baral, H. Winter, S. Mannsfeld, A. Briseno, *J. Am. Chem. Soc.* **2013**, *135*, 844-854.

[28] F. Di Maria, P. Olivelli, M. Gazzano, A. Zanelli, G. Biasiucci, G. Gigli, D. Gentili, P. D'Angelo, M. Cavallini, G. Barbarella, *J. Am. Chem. Soc.* **2011**, *133*, 8654-8661.

[29] R. Rieke, S. Kim, X. W, *J. Org. Chem.* **1997**, *62*, 6921-6927.

[30] D. Fichou, *J. Mater. Chem.* **2000**, *10*, 571-588.

[31] L. Tan, L. Zhang, X. Jiang, X. Yang, L. Wang, Z. Wang, L. Li, W. Hu, Z. Shuai, L. Li, D. Zhu, *Adv. Funct. Mater.* **2009**, *19*, 272-276.

[32] L. Zhang, L. Tan, Z. Wang, W. Hu, D. Zhu, *Chem. Mater.* **2009**, *21*, 1993-1999.

[33] V. Coropceanu, J. Cornil, D. A. Da Silva Filho, Y. Olivier, R. Silbey, J. L. Brédas, *Chem. Rev.* **2007**, *107*, 926-952.

[34] C. Wang, H. Dong, W. Hu, Y. Liu, D. Zhu ,*Chem. Rev.* **2012**, *112*, 2208-2267.

[35] H. Usta, A. Facchetti, T. J. Marks, *Acc. Chem. Res.* **2011**, *44*, 501-510.

[36] H. B. Akkerman, S. C. B. Mannsfeld, A. P. Kaushik, E. Verploegen, L. Burnier, A. P. Zoombelt, J. D. Saathoff, S. Hong, S. Atahan-Evrenk, X. Liu, A. Aspurn-Guzik, M. F. Toney, P. Clancy, Z. Bao, *J. Am. Chem. Soc.* **2013**, *135*, 11006-11014.

[37] C. Reese, M. Roberts, S. P. Parkin, Z. Bao, *Adv. Mater.* **2009**, *21*, 3678-3681.

[38] G. Barbarella, M. Zamhianchi, R. Di Toro, M. Colonna, L. Antolini, A. Bongini, *Adv. Mater.* **1996**, *8*, 327−331.

[39] R. Azumi, E. Mena-Osteritz, R. Boese, J. Benet-Buchholz, P. Bäuerle, *J. Mater. Chem.* **2006**, *16*, 728-735.

[40] R. Azumi, G. Götz, T. Debaerdemaeker, P. Bäuerle, *Chem.Eur. J.* **2000**, *6*, 735-744.

[41] L. Zhang, N. S. Colella, B. P. Cherniawski, S. C. B. Mannsfeld, A. L. Briseno, *ACS Appl. Mater. Interfaces* **2014**, *6*, 5327-5343.

2.2 Click Chemistry

2.2.1 Introduction

"Click chemistry is not limited to a specific type of reaction, but stands for a synthetic philosophy that comprises of a range of reactions, with different reaction mechanisms but common reaction trajectories."[1]

In the last decades, the need for defined structural materials and surfaces has been increasingly popular. The controlled synthesis of such materials, however, imposes major challenges. In this direction, well-defined *ligation strategies* that can be effectively used in the presence of a wide range of different functional groups were continuously explored. First of all, it has to be taken into account that the key requirements for successful ligation strategies include high selectivity, orthogonality to other functional groups, compatibility with water and other protic solvents, and close-to-quantitative yields. In addition, such an approach should also make use of readily available starting materials and should avoid chromatography isolations.[2]

Few synthetically useful reactions were found to fulfil such criteria: opening of strained rings such as epoxides and aziridines,[3] oxygen additions to carbon-carbon double bonds (epoxidation),[4] oxime reactions, Staudinger reactions, hydrazone reactions, thiol-ene reactions, Aza-Wittig reactions, 1,3 dipolar[5] and Diels-Alder[6] cycloadditions. Such reactions can be gathered under the name of "click chemistry".

The concept of "click chemistry" was established by Sharpless *et al.* in term of a "set of powerful, highly reliable, and selective reactions for the rapid synthesis of useful new compounds and combinatorial libraries".[2]

"Click chemistry" has been especially successful in the preparation of 1,2,3-triazoles by 1,3-dipolar cycloaddition between azides and alkynes.[2,7] The original reaction, known as Huisgen cyclization, involved a thermal treatment of both reagents and afforded the corresponding triazoles with a complete lack of regioselectivity, yielding a 1:1 mixture of the 4- and 5-substituted derivatives.[6] Nevertheless, the discovery that this reaction can be efficiently catalyzed by copper(I)-salts to give exclusively the 4-substituted regioisomer and that the reaction times could be improved to almost 10^7 times than the non-catalyzed one, resulted in an excellent procedure for the preparation of such heterocycles.[2] Furthermore, the triazole ring was shown to be compatible with a plethora of functional groups, as well as exhibiting good stability under

several reaction conditions. Fortunately, this modified triazole synthesis has become the paradigm of “click chemistry” in modern chemistry and both terms are now associated[8] (***Figure 2.2.1***).

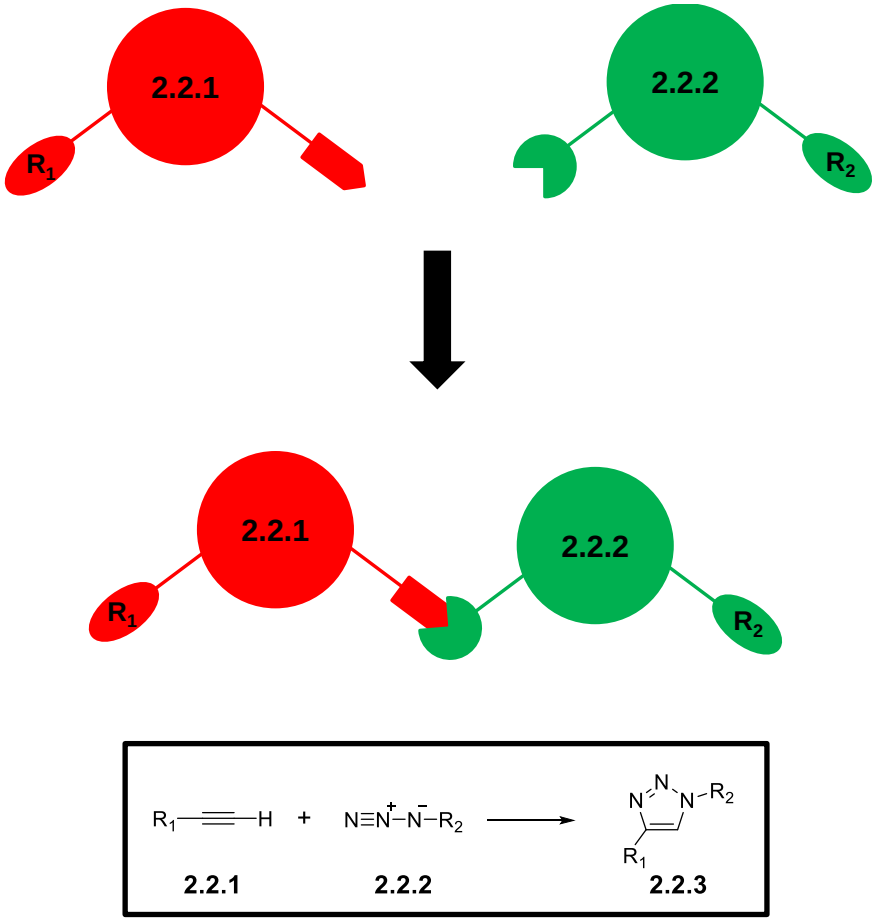

Figure 2.2.1. *Simplification of a click reaction between alkyne* ***2.2.1*** *and azide* ***2.2.2****.*

Moreover, 1,2,3-triazole is an intriguing heterocycle offering various supramolecular interactions,[9] ranging from anion complexation *via* (charge-assisted) hydrogen and halogen bonds to metal coordination by anionic, neutral, or cationic nitrogen donors as well as carbanionic and mesoionic carbene donors (***Chart 2.2.1***).

Some of these diverse functions can even be employed simultaneously resulting in virtually unlimited applications in supramolecular and coordination chemistry.

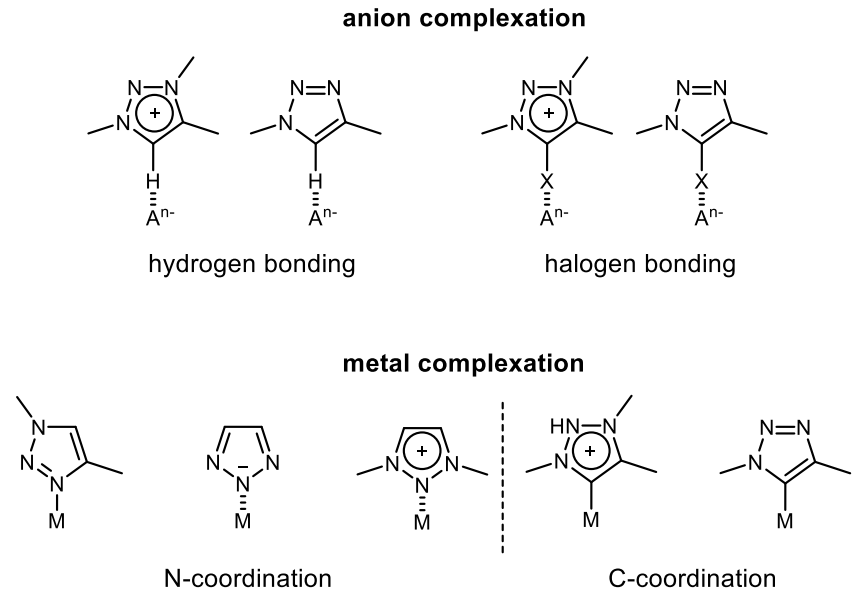

Chart 2.2.1. *Selected supramolecular interactions of 1,2,3-triazoles and their derivatives.*[10] Adapted from *Chem. Soc. Rev.* **2014**, *43, 2522-2571* with permission of The Royal Society of Chemistry.

The similarity of the triazole moiety to the amide bond is interesting in terms of molecular dimension (***Chart 2.2.2***). Although the 1,2,3-triazolyl ring extends the distance between R_1 and R_2 by approximately 1.1 Å compared to the amide bond, topology and electron-distribution resemble each other. Both moieties are configured rather planar and rigid. The triazolyl rest possesses a larger dipole moment than an amide bond (~5 Debye vs. 3.7–4.0 Debye for an amide bond).[11,12] This might enhance the mimicry of amide bonds by triazoles, since, besides having hydrogen bond acceptor at N_2 and N_3 in the ring, the dipole may polarize the C-H bond at the 5-position to the extent that it acts as hydrogen-bond donor.[13,14]

Additionally, the hydrogen-bond accepting and donating pattern of the amide bond is also mimicked by the triazole.

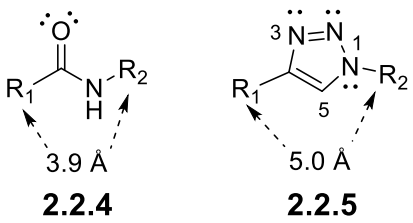

Chart 2.2.2. *Steric and electronic similarities between an amide **2.2.4** and a 1,2,3-triazole **2.2.5**.*

2.2.2 1,3-Dipolar Cycloaddition (without Cu-Catalysis)[10]

Already in 1893, Michael discovered a synthesis of 1,2,3-triazoles (also *v*-triazole for vicinal)[15-17] by reacting phenyl azide with dimethyl acetylenedicarboxylate.[18] This type of reaction was later classified by Huisgen as either (3+2)- or 1,3-dipolar-cycloaddition, *i.e.*, the concerted addition of a 1,3-dipole to a multiple bond.[19-21] The 1,3-dipole is characterized by the presence of an electrophilic atom having an electron sextet and a formal positive charge, as well as a nucleophilic atom, having an electron octet and a formal negative charge, with one in the 1-position and the other on the 3-position (**2.2.6c**, ***Chart 2.2.3***).[19a]

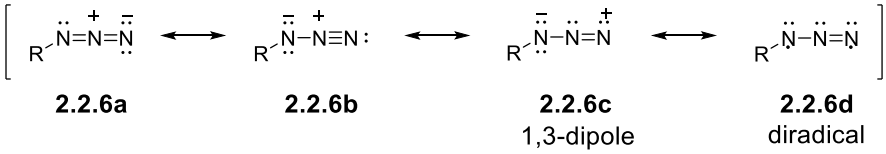

Chart 2.2.3. *Mesomeric selected contributing structures of an organic azide.*[10] Adapted from *Chem. Soc. Rev.* **2014**, *43, 2522-2571* with permission of The Royal Society of Chemistry.

Azides belong to the propargyl-allenyl type of 1,3-dipoles and are thus almost linear.[19f] Woodward and Hoffmann in turn classified the 1,3-dipolar cycloaddition as an example of pericyclic reactions which is thermally allowed due to symmetrically and geometrically favourable [$_{\pi}4_s$ + $_{\pi}2_s$] interactions.[22] Nevertheless, reaction rates and regioselectivity remained unexplained until Sustmann *et al.*[23] and Houk *et al.*[24] applied the frontier molecular orbital (FMO) model to the reaction.[25] This model is based on perturbation theory[26-29] and implies that the reaction between the 1,3-dipole and the 1,3-dipolarophile proceeds essentially *via* interaction of the highest occupied molecular orbital (HOMO) of one reactant and the lowest unoccupied molecular orbital (LUMO) of the other reactant. The reaction rate depends on the corresponding energy gap. Therefore, a HOMO-rising electron-donating group (EDG) as well as a LUMO-lowering electron-withdrawing group (EWG) will increase the reaction rate.[23b,c] Additionally, EDGs and EWGs will particularly polarize the π-system which influences the regioselectivity. The interaction occurs in such a way that the orbitals with larger orbital coefficients overlap (***Figure 2.2.2***).

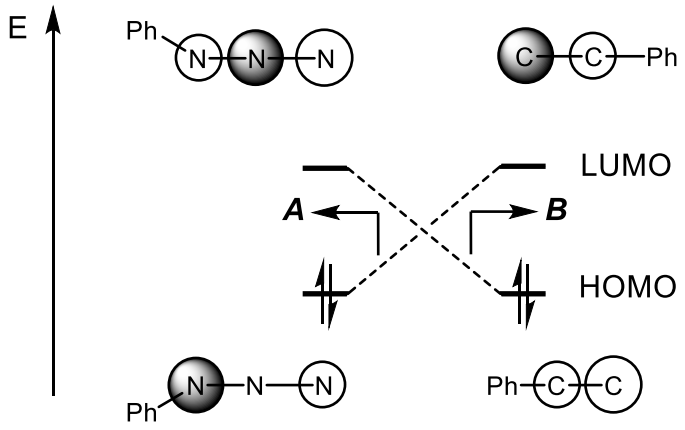

Figure 2.2.2. *FMO interactions between azide and alkyne.*[10,23c,30] Adapted from *Chem. Soc. Rev.* **2014***, 43, 2522-2571* with permission of The Royal Society of Chemistry.

The cycloaddition of phenyl azide and phenylacetylene yields the 1,4- and the 1,5-substituted 1,2,3-triazoles in roughly a 1:1-ratio,[24a] while electron-deficient and electron-excessive alkynes favour the formation of the 1,4-regioisomer (dipole-HOMO control, ***A***) and the 1,5-regioisomer (dipole-LUMO control, ***B***), respectively.[16,19f,24b-35] Houk *et al.* recently proposed a distortion/interaction model as alternative to the FMO model based on high-accuracy quantum chemical methods (***Figure 2.2.3***).[36]

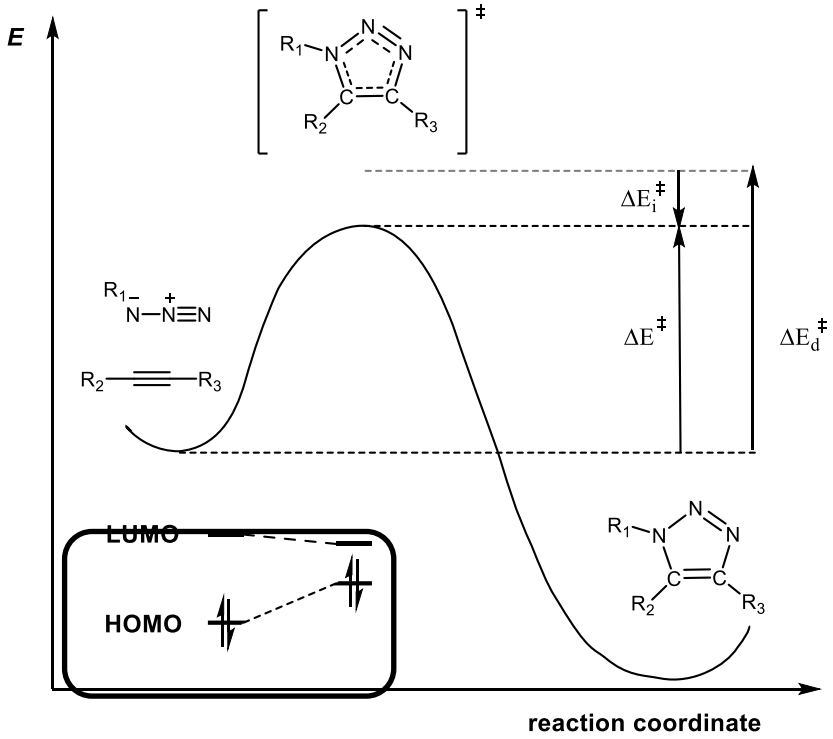

Figure 2.2.3. *The distortion/interaction model.*[10,36b] Adapted from *Chem. Soc. Rev.* **2014***, 43, 2522-2571* with permission of The Royal Society of Chemistry.

The activation energy ($\Delta E^{\neq}$) of the reaction is mainly determined by the energy required to transform the reactants into their transition-state geometries meaning that the reactivity is controlled by the stability of the dipolarophile and, in particular, of the 1,3-dipole. The introduction of strain to the alkyne ground state (e.g. cyclooctyne, benzyne) causes a rate enhancement in 1,3-dipolar cycloadditions (strain-promoted azide-alkyne cycloaddition). This allows an easy linking in the original sense of "click-chemistry": the alkyne building blocks induce only low regioselectivities, their synthesis is rather demanding, and their substitution pattern is fixed.

In contrast to terminal alkynes, the cycloaddition of organic azides **2.2.7** with trimethylsilyl-substituted alkynes **2.2.8** generally shows a very high selectivity for the 4-silylated 1,5-regioisomer **2.2.9**.[34,16,37-40] The trimethylsilyl group is a common protecting group for the introduction of alkynes *via* Sonogashira cross-coupling and it can be cleaved off after the triazole synthesis. Like other thermal cycloadditions, the reaction requires elevated temperature (85 to 110 °C) and prolonged reaction times, but affords high yields and is ideally conducted in water (***Scheme 2.2.1***).[40,41]

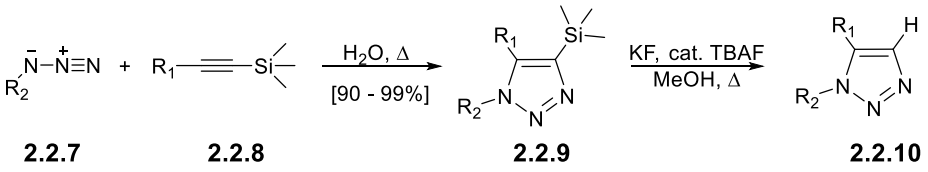

2.2.7 **2.2.8** **2.2.9** **2.2.10**

Scheme 2.2.1. *Trimethylsilyl-directed azide-alkyne cycloaddition.*[10,34] Adapted from *Chem. Soc. Rev.* **2014***, 43, 2522-2571* with permission of The Royal Society of Chemistry.

Indeed, the trimethylsilyl group causes a total destabilization of the transition state for the 1,4-attack by about 15 to 25 kJ mol^{-1}, while the transition state for the 1,5-attack is similar in energy to the one of the cycloaddition with the corresponding terminal alkyne. In line with the distortion/interaction model, this is mainly due to an increased distortion energy of the alkyne for the 1,4-attack and electronic effects of the substituents have less influence.[35a] Consequently, the trimethylsilyl-directed azide-alkyne cycloaddition (SiAAC) represents an elegant method to selectively synthesize 1,5-disubstituted triazoles by using the distortion energy and screening out electronic influence, which offers variable substitution patterns.

2.2.3 Copper-Catalyzed Azide-Alkyne Cycloaddition

The prominent Cu(I)-catalyzed azide-alkyne cycloaddition (CuAAC) discovered independently by Medal *et al.*[7] and Sharpless *et al.*[42] yields 1,2,3-triazoles most efficiently with a very high regioselectivity for the 1,4-regioisomer.[43-46] A collection of mechanistic key aspects based on computational[47-49] and experimental studies[50-52] is represented in ***Scheme 2.2.2***.

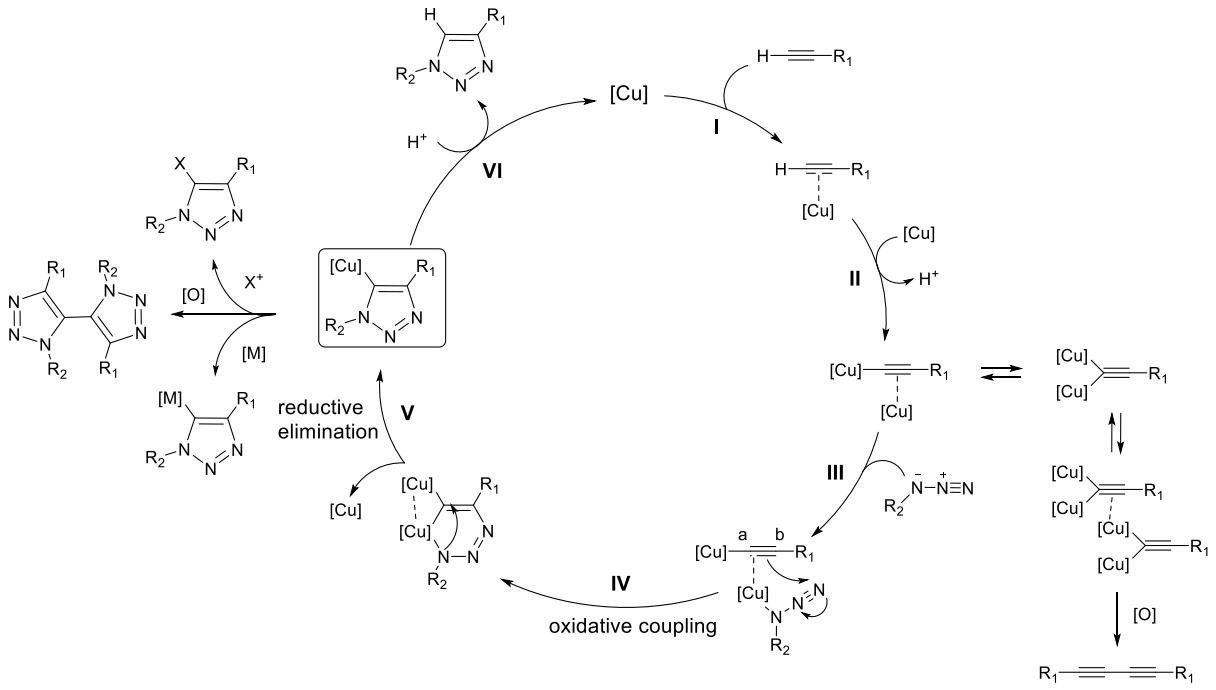

Scheme 2.2.2. *Proposed mechanism of the CuAAC ([Cu] denotes a copper fragment that varies in the number of ligands and in the formal oxidation state).* [10,43,45,52,53] Adapted from *Chem. Soc. Rev.* **2014**, *43, 2522-2571* with permission of The Royal Society of Chemistry.

Firstly, a Cu(I) species undergoes π-coordination of an alkyne (**I**), which greatly increases the CH-acidity of the terminal alkyne (pK_a drops from ~25 to ~15) and allows the subsequent formation of a σ-coordinated Cu(I) acetylide with activated alkyne (**II**) in aqueous media, without an addition of an amine base.[48] DFT calculations suggest that a second Cu(I) remains π-coordinated at the α-carbon of the σ-bound acetylide resembling the μ-coordination mode of Cu(I) acetylides.[47,54] In the next step, coordination of an azide at the π-coordinated Cu(I) centre occurs (**III**). In principle, the coordination of the organic azide can occur *via* both the substituted or the terminal nitrogen, but, in contrast to the π-accepting terminal nitrogen, the π-donating substituted nitrogen is expected to increase the electron density on the metal center[55] which

would facilitate the subsequent oxidative coupling (**IV**). The observed selectivity for the 1,4-regioisomer may be explained by the preference for Cu(I) π–coordination at the α-carbon of the acetylide,[47,54] which directs a nucleophilic attack of the β-carbon at the terminal, electrophilic nitrogen[21] of the coordinated azide upon oxidative coupling.[56] As a result of the latter, in the rate-limiting step[43,44,47-49] a six-membered metallacycle is formed including a μ-alkenylidene.[49] According to computational methods, this intermediate is stabilized by a geminal bimetallic coordination,[47,48,57,58] while a potential monometallic cupra-cycle, which was postulated earlier, would represent an unfavourably strained structure having excessive electron density.[59]

It should be noted that the formal oxidation states of the two Cu centres are not given as it remains unclear, whether Cu(III)[59] is intermediately formed or if both metal centers cooperate in the oxidation step. Furthermore, improved activity has been observed when using a bimetallic, mixed-valent Cu(II)/Cu(I) catalytic system.[60] Ultimately, ring contraction and Cu(I) extrusion *via* reductive elimination (**V**) affords the Cu(I)-bound triazolide in a highly exothermic process.[49,51] In aqueous media, the Cu(I)-triazolide then undergoes protonolysis (**VI**) liberating the free triazole and allowing the Cu(I) to re-enter the catalytic cycle.

The most important factor in such a process seems to be the maintenance of [Cu(I)] at a high level during reaction. This is the reason why the use of a Cu(II)-source in the presence of a large excess reducing agent has been one of the preferred methods. In the presence of a reducing agent the reaction is much less susceptible to oxygen, and such reactions have often been carried out under air.[45]

The most used conditions for the click-reaction are aqueous conditions employing $CuSO_4$ and a reducing agent. Other frequently used Cu(I) sources are CuI or CuBr, which is often preferred in polymer-analogous reactions.

Aqueous conditions introduced originally by Rostovtsev *et al.*[47] are extremely useful in biochemical conjugation, where it is the most used procedure. They ensure easy isolation and high purity of the products. Conditions utilizing a mixture of Cu(0) in form of wire, turning, powder, or nanoparticles[61] with or without the addition of a Cu(II)-source such as $CuSO_4$, are also quite useful in the aqueous environment although there seems to be a latency period for the active catalytic species to form.[62]

Finally, there is a range of other Cu(I)-sources that have been introduced for several reasons, *e.g.*, for increased solubility in organic solvents such as ($[Cu(CH_3CN)_4]PF_6$,

$(EtO)_3PCuI$, $Cu(CH_3CN)_4OTf$) or $Cu(OAc)_2$ in order to improve reactivity in comparison to $CuSO_4$.[63,44]

$Cu(CH_3CN)_4OTf$ was found to be particularly reactive when used with a bathophenanthroline ligand for *in vivo* surface conjugation of molecular probes onto viral particles.[64] $Cu(OAc)_2$ has been reported to catalyse the formation of triazole from alkyne and azide almost as effectively as Cu(I) salts.[65]

Since the formation of Cu(I) is essential for catalysis and Cu(I) efficiently catalyses the reaction at less than 0.01 eq., it is attempting to ascribe catalysis to small amounts of Cu(I) present in the reaction mixture.

Except for decomposition due to substrate instability, triazole formation is essentially insensitive to steric bulk and electronic properties of the alkyne and azide, although the rates may differ and conditions may have to be optimized in particular cases.[10]

An example of steric factor and complexation influencing the triazole formation was described in the synthesis of rotaxanes,[66] where it was found that the counter ion in the Cu(I) source had a major influence on the outcome. In nonpolar solvents, $[Cu(CH_3CN)_4]PF_6$ was found to be better than other copper salts such as CuOTf or CuI leading to excellent yields of rotaxanes.

2.2.4 General Examples of Click Reaction in Material Science

Several recent reviews have described the use of the Cu-catalyzed azide-alkyne cycloaddition (CuAAC) for the synthesis of dendritic, branched, linear, and cyclic copolymers.[10] For example, one of the biggest strength of “click-chemistry” is its utility in conjunction with polymerization methods to offer a facile access to a broad range of polymeric materials that would be otherwise difficult to prepare.[67-69]

A very interesting example is the application of the CuAAC reaction towards chemical functionalization of nanomaterials such as single-walled carbon nanotubes (SWNTs). In this case, alkyne groups introduced onto the surface of the SWNTs offered a route towards highly specific post-modification. This method granted a greater amount of control on the orientation and the density of the polymer attached to the surface of the nanotube while reducing the risk of side reactions.[70]

The high efficiency of “click-chemistry” was also demonstrated by Hawker, Sharpless *et al*. by coupling dendritic units together **2.2.11** (***Chart 2.2.4***).[71] The tolerance of “click-chemistry” to a wide variety of functional groups allowed the introduction of reactive units at the periphery without the use of protecting groups.[72-75]

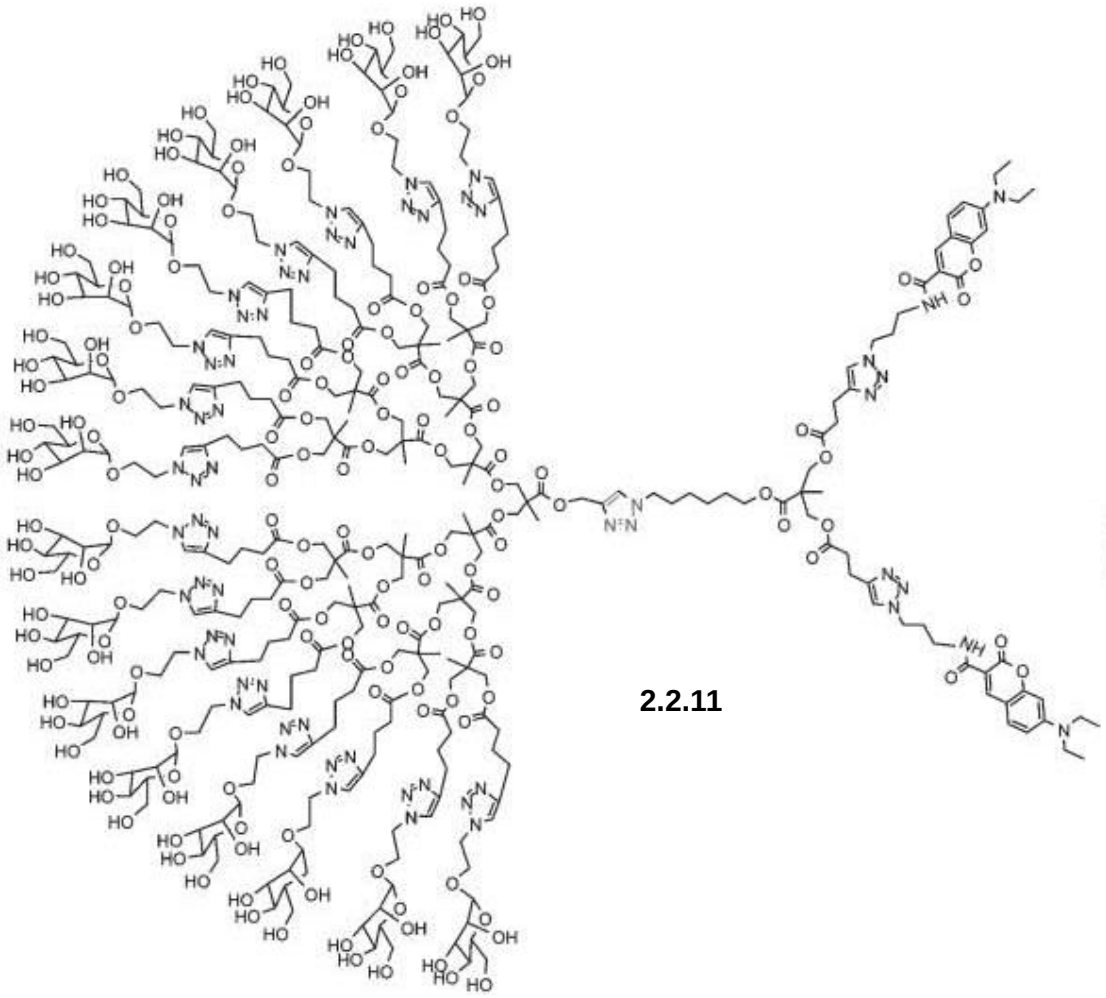

2.2.11

Chart 2.2.4. *Mannose-decorated unsymmetrical dendrimer by Hawker, Sharpless et al.*[79] Reprinted from *Chem. Commun.* **2005**, 5775–5777 with permission of The Royal Society of Chemistry.

Click-reactions have been recently proposed for covalent labelling in living systems, such as cells or tissues. If biomolecules expressed within cells could be fluorescently labelled, their destiny could be tracked in real time. Moreover, important metabolic studies could be conducted *in vitro* and even *in vivo*. The reactions used for covalent labelling must not only fulfil the criteria of an efficient click-reaction such as high yields, selectivity, and compatibility with aqueous environment, but has to be also bio-orthogonal. This means that interactions towards functionalities present in biological systems have to be avoided.[84,76,77]

While other reactions include the use of nucleophiles or electrophiles, the components of a click-reaction do not react in an undesirable way within biological systems and even in living cells.

For this reason, the click-reaction is used as an alternative to other established methods described in literature for the preparation of biomolecules[78,79] (for example,

olefin metathesis of glycosides, intermolecular enyne metathesis of alkynyl and alkenyl glycosides).

Wennemers and co-workers presented oligoproline **2.2.12** post-functionalized by CuAAC on a solid substrate (***Chart 2.2.5***).[80] The synthesis was accomplished by stepwise coupling of tripeptide fragments, alternate with click-reactions of the azide positions at C_4 of the residual proline ring. Thus, an oligoproline comprising a different triazolyl moieties in every third position was obtained.

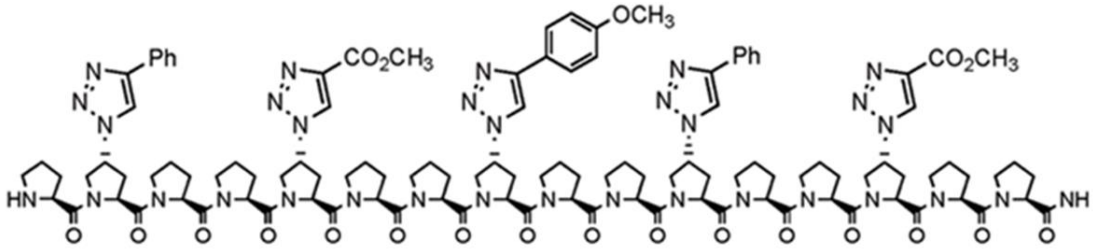

2.2.12

Chart 2.2.5. *Oligoproline post-functionalized by CuAAC on solid substrate.*[80] Reprinted with permission from *J. Am. Chem. Soc.* **2007***, 129,* 466-467. Copyright 2007 American Chemical Society.

Guan and Oh proposed that cycloaddition between peptide strands derivatized with azides **2.2.13** and terminal alkynes **2.2.14** may provide an efficient convergent synthesis of β-turn units based on the triazole ring (***Scheme 2.2.3***).[81]

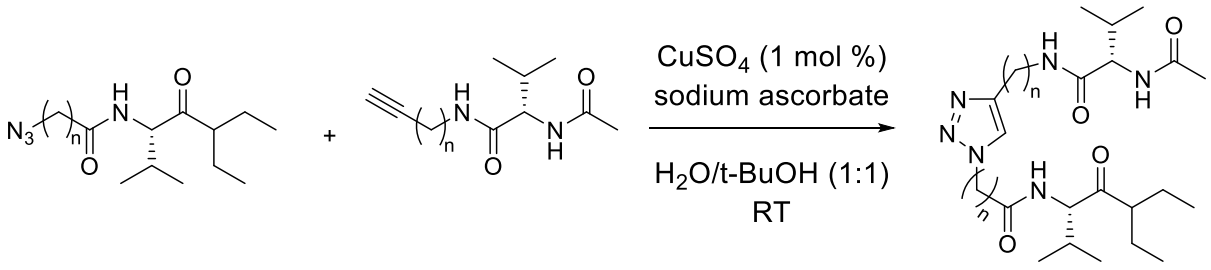

2.2.13 **2.2.14** **2.2.15**

Scheme 2.2.3. *Example of "click chemistry" on peptides.*[81] Adapted from *Chem. Commun.* 2006, 3069-3071 with permission of The Royal Society of Chemistry.

In our group, Jatsch presented an approach to the synthesis of complementary 2´-deoxyadenosine- and thymidine-functionalized quaterthiophenes **2.2.16**. The application of "click-chemistry" allowed for the effective linkage of the oligothiophene and the nucleoside moieties despite their rather different polarities (***Chart 2.2.6***).[82]

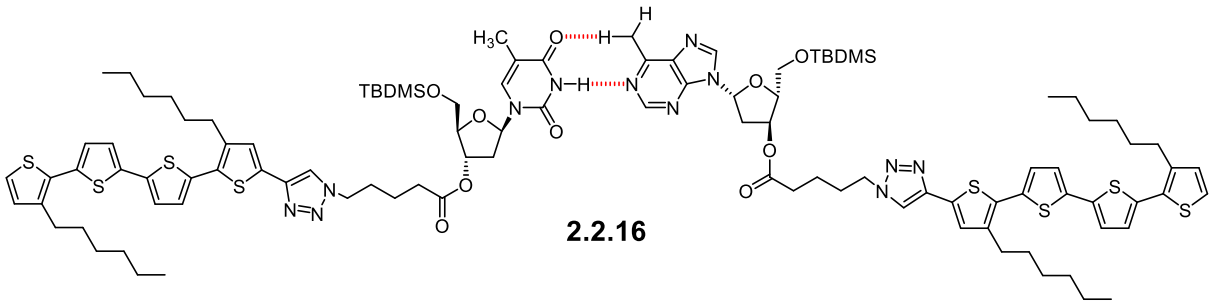

Chart 2.2.6. *Example of "click chemistry" on nucleosides. Product of click reaction between nucleoside and quaterthiophene performed with $Cu(CH_3CN)_4PF_6$-Cu(0), THF.*[82]

Recently, Schillinger published quaterthiophenes decorated with only a single triazolylproline as an amino acid containing two stereocenters. Three "bioinspired" oligothiophene-amino acid hybrids with (2*R*,4*R*)-, (2*S*,4*S*)-, or (2*S*,4*R*)-configuration of the proline residue were prepared (**Scheme 2.2.4**).[83] Quaterthiophene alkyne **2.2.17** was reacted with Boc-protected (2*S*,4*R*)-azidoproline methyl ester **2.2.18a** *via* click-reaction[2,7] to yield hybrid **2.2.19a** after saponification of the fully protected quaterthiophene-amino acid intermediate.

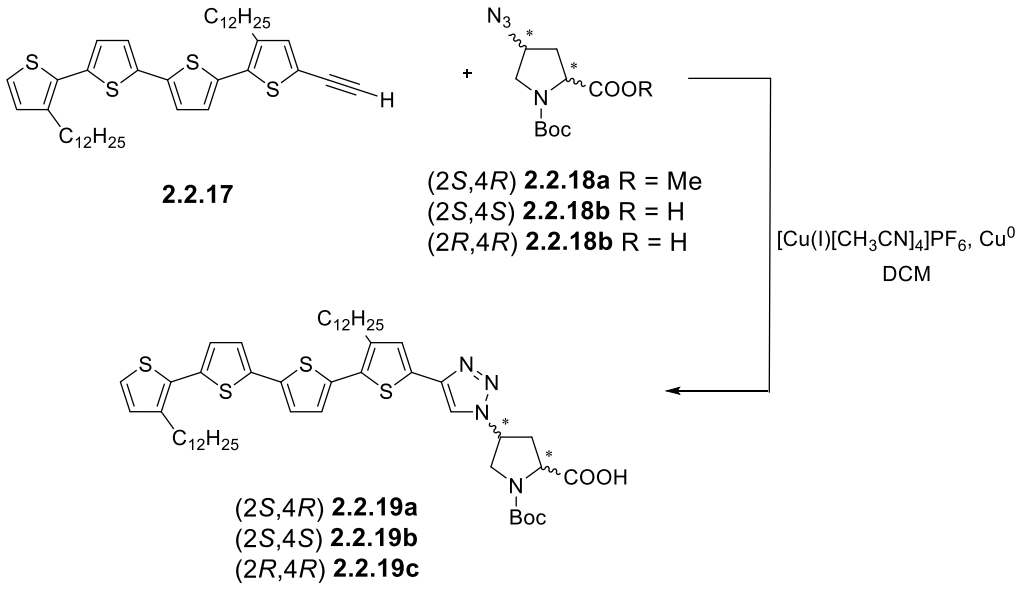

Scheme 2.2.4. *Synthesis of quaterthiophene−amino acid hybrids **2.2.18a−2.2.18b**.*

The same synthetic route was not possible for enantiomers **2.2.19b** and **2.2.19c**. Saponification of the corresponding fully protected hybrids of **2.2.19b** and **2.2.19c** caused a partial epimerization at the stereocenter at C4 of the proline ring. The epimerization could not be avoided by employing different bases and reaction tempera-

tures either. Therefore, quaterthiophene **2.2.17** was reacted with Boc-protected azidoprolines **2.2.18b** and **2.2.18c** *via* click-reaction.[83]

Seela *et al.* demonstrated the applicability of "click-chemistry" on duplex DNA (***Scheme 2.2.5***).[84]

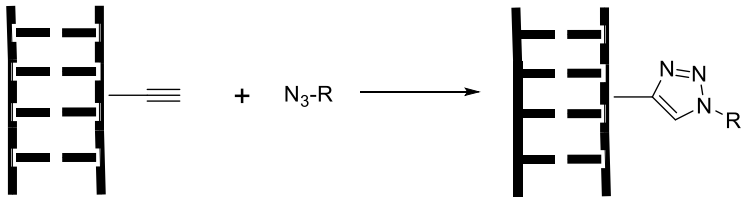

2.2.20 **2.2.21** **2.2.22**

Scheme 2.2.5. *Example of "click chemistry" on duplex DNA*.[84] Reused from *Chem. Biodiv.* **2006***, 3, 509-514* with permission of John Wiley and Sons.

In spite of the great success of the concept of "click-chemistry", there are still few limitations associated with the concept. As a matter of fact, the CuAAC reaction is still by far the most used click-reaction. However, copper is believed to be cytotoxic and demonstrated side effects associated with excessive copper intake including hepatitis, Alzheimer's disease and neurological disorders.[85] For click-reactions, which should be used in contact with living systems, the copper catalyst must be completely removed. Azides are sometimes explosive and also associated with potential toxic side effects.[86]

References

[1] J. Lahann in *Click chemistry for Biotechnology and Material Science*, (Ed.: J. Lahann), Wiley & Sons, Ltd, **2009.**

[2] H. C. Kolb, M. G. Finn, K. B. Sharpless, *Angew. Chem.* **2001**, *113*, 2056–2073; *Angew. Chem., Int. Ed.* **2001**, *40*, 2004–2021.

[3] I. M. Pastor, M. Yus, *Curr. Org. Chem.* **2005**, *9*, 1–29.

[4] T. Siu, A. K. Yudin, *J. Am. Chem. Soc.* **2002**, *124*, 530–531.

[5] J. G. Fernández-Bolaños, Ó. López in *Carbohydrates in Heterocyclic Chemistry,* (Ed.: E. S. H. El Ashry), Springer, Berlin, **2007**, 351.

[6] B. Gacal, H. Durmaz, M. A. Tasdelen, G. Hizal, U. Tunca, Y. Yagci, A. L. Demirel, *Macromolecules* **2006**, *39*, 5330–5336.

[7] C. W. Tornøe, C. Christensen, M. Meldal, *J. Org. Chem.* **2002**, *67*, 3057–3064.

[8] M. V. Gil, M. J. Arévalo, O. Lòpez, *Synthesis* **2008**, *11*, 1589–1620.

[9] J. M. Lehn, *Science* **1993**, *260*, 1762–1763.

[10] B. Schulze, U. S. Schubert, *Chem. Soc. Rev.* **2014**, *43*, 2522–2571.

[11] H. C. Kolb, K. B. Sharpless, *Drug Discov. Today* **2003**, *8*, 1128–1137.

[12] W. P. Purcell, J. A. Singer, *J. Phys. Chem.* **1967**, *71*, 4316–4319.

[13] M. H. Palmer, R. H. Findlay, A. J. Gaskeil, *J. Chem. Soc., Perkin Trans. 2* **1974**, *4*, 420–428.

[14] W. S. Horne, M. K. Yadav, C. D. Stout, M. R. Ghadiri, *J. Am. Chem. Soc.* **2004**, *126*, 15366–15367.

[15] F. R. Benson, W. L. Savell, *Chem. Rev.* **1950**, *46*, 1–68.

[16] T. L. Gilchrist, G. E. Gymer in *Advances in Heterocyclic Chemistry* (Eds.: A. R. Katritzky and A. J. Boulton), Academic Press, **1974**, 33–85.

[17] S. Rachwal, A. R. Katritzky in *Comprehensive Heterocyclic Chemistry III*, (Eds.: A. R. Katritzky, C. A. Ramsden, E. F. V. Scriven and R. J. K. Taylor), Elsevier, Oxford, **2008**, 1–158.

[18] A. Michael, *J. Prakt. Chem.* **1893**, *48*, 94–95.

[19] a) R. Huisgen, G. Szeimies, L. Möbius, *Chem. Ber.* **1967**, *100*, 2494–2507; b) R. Huisgen, *Angew. Chem.* **1963**, *75*, 604–637; *Angew. Chem., Int. Ed.* **1963**, *2*, 565–598; c) R. Huisgen, *Angew. Chem.* **1963**, *75*, 742-754; *Angew. Chem., Int. Ed.* **1963**, *2*, 633–645; d) R. Huisgen, Angew. Chem. **1968**, *80*,

329; *Angew. Chem., Int. Ed.* **1968**, *7*, 321–328; e) R. Huisgen, *J. Org. Chem.* **1968**, *33*, 2291–2297; f) R. Huisgen, *J. Org. Chem.* **1976**, *41*, 403–419.

[20] K. N. Houk, J. Gonzalez, Y. Li, *Acc. Chem. Res.* **1995**, *28*, 81–90.

[21] S. Bräse, C. Gil, K. Knepper, V. Zimmermann, *Angew. Chem.* **2005**, *117*, 5320–5374; *Angew. Chem., Int. Ed.* **2005**, *44*, 5188–5240.

[22] R. B. Woodward, R. Hoffmann, *Angew. Chem.* **1969**, *81*, 797–869; *Angew. Chem., Int. Ed.* **1969**, *8*, 781–853.

[23] a) R. Sustmann, *Tetrahedron Lett.* **1971**, *12*, 2717–2720; b) R. Sustmann, H. Trill, *Angew. Chem., Int. Ed.* **1972**, *11*, 838–840; c) R. Sustmann, *Pure Appl. Chem.* **1974**, *40*, 569–593.

[24] a) K. N. Houk, *Acc. Chem. Res.* **1975**, *8*, 361–369; b) K. N. Houk, J. Sims, R. E. Duke, R. W. Strozier, J. K. George, *J. Am. Chem. Soc.* **1973**, *95*, 7287–7301; c) K. N. Houk, J. Sims, C. R. Watts, L. J. Luskus, *J. Am. Chem. Soc.* **1973**, *95*, 7301–7315.

[25] a) K. Fukui, *Science* **1982**, *218*, 747–754; b) K. Fukui, T. Yonezawa, H. Shingu, *J. Chem. Phys.* **1952**, *20*, 722–725.

[26] W. C. Herndon, *Chem. Rev.* **1972**, *72*, 157–179.

[27] R. F. Hudson, *Angew. Chem.* **1973**, *85*, 63–84; *Angew. Chem., Int. Ed.* **1973**, *12*, 36–56.

[28] G. Klopman, *J. Am. Chem. Soc.* **1968**, *90*, 223–234.

[29] L. Salem, *J. Am. Chem. Soc.* **1968**, *90*, 553–566.

[30] I. Fleming in *Frontier Orbitals and Organic Chemical Reactions*, (Ed.: I. Fleming), Wiley & Sons, Chichester, **1976**.

[31] M. J. S. Dewar *J. Mol. Struc.(Theochem)* **1989**, *200*, 301–323.

[32] W. Kirmse, L. Horner, *Liebigs Ann. Chem.* **1958**, *614*, 1–3.

[33] Z. Li, T. S. Seo, J. Ju, *Tetrahedron Lett.* **2004**, *45*, 3143–3146.

[34] F. Kloss, U. Köhn, B. O. Jahn, M. D. Hager, H. Görls, U. S. Schubert, *Chem. Asian J.* **2011**, *6*, 2816–2824.

[35] a) G. Molteni, A. Ponti, *Chem. Eur. J.* **2003**, *9*, 2770–2774; b) G. Molteni, A. Ponti, *Arkivoc* **2006** (*xvi)* 49–55.

[36] a) D. H. Ess, K. N. Houk, *J. Am. Chem. Soc.* **2008**, *130*, 10187–10198; b) D. H. Ess, K. N. Houk, *J. Am. Chem. Soc.* **2007**, *129*, 10646–10647.

[37] G. Himbert, D. Frank, M. Regitz, *Chem. Ber.* **1976**, *109*, 370–394.

[38] S. J. Coats, J. S. Link, G. Gauthier, D. J. Hlasta, *Org. Lett.* **2005**, *7*, 1469–1472.

[39] L. Birkofer, A. Ritter, H. Uhlenbrauck, *Chem. Ber.* **1963**, *96*, 3280–3288.

[40] R. Breslow, *Acc. Chem. Res.* **1991**, *24*, 159–164.

[41] U. M. Lindström, *Chem. Rev.* **2002**, *102*, 2751–2772.

[42] V. V. Rostovtsev, L. G. Green, V. V. Fokin, K. B. Sharpless, *Angew. Chem.* **2002**, *114*, 2708–2711; *Angew. Chem., Int. Ed.* **2002**, *41*, 2596–2599.

[43] J. E. Hein, V. V. Fokin, *Chem. Soc. Rev.* **2010**, *39*, 1302–1315.

[44] S. Dìez-Gonzàlez, *Catal. Sci. Technol.* **2011**, *1*, 166–178.

[45] M. Meldal, C. W. Tornoe, *Chem. Rev.* **2008**, *108*, 2952–3015.

[46] V. D. Bock, H. Hiemstra, J. H. van Maarseveen, *Eur. J. Org. Chem.* **2006**, 51–68.

[47] F. Himo, T. Lovell, R. Hilgraf, V. V. Rostovtsev, L. Noodleman, K. B. Sharpless, V. V. Fokin, *J. Am. Chem. Soc.* **2005**, *127*, 210–216.

[48] M. Ahlquist, V. V. Fokin, *Organometallics* **2007**, *26*, 4389–4391.

[49] B. F. Straub, *Chem. Commun.* **2007**, 3868–3870.

[50] V. O. Rodionov, V. V. Fokin, M. G. Finn, *Angew.Chem.* **2005**, *117*, 2250–2255; *Angew. Chem., Int. Ed.* **2005**, *44*, 2210–2215.

[51] C. Nolte, P. Mayer, B. F. Straub, *Angew.Chem*. **2007**, *119*, 2147–2149; *Angew. Chem., Int. Ed.* **2007**, *46*, 2101–2103.

[52] B. T. Worrell, J. A. Malik, V. V. Fokin, *Science* **2013**, *340*, 457–460.

[53] J. E. Hein, J. C. Tripp, L. B. Krasnova, K. B. Sharpless, V. V. Fokin, *Angew. Chem.* **2009**, *121*, 8162–8165; *Angew. Chem., Int. Ed.* **2009**, *48*, 8018–8021.

[54] J. J. Eisch, H. Gopal, S. G. Rhee, *J. Org. Chem.* **1975**, *40*, 2064–2069.

[55] H. V. R. Dias, S. A. Polach, S. K. Goh, E. F. Archibong, D. S. Marynick, *Inorg. Chem.* **2000**, *39*, 3894–3901.

[56] J. P. Selegue, *Coord. Chem. Rev.* **2004**, *248*, 1543–1563.

[57] M. Böhme, T. Wagener, G. Frenking, *J. Organomet. Chem.* **1996**, *520*, 31–43.

[58] I. Marek, *Chem. Rev.* **2000**, *100*, 2887–2900.

[59] E. Sperotto, G. P. M. van Klink, G. van Koten, J. G. de Vries, *Dalton Trans.* **2010**, *39*, 10338–10351.

[60] G. C. Kuang, P. M. Guha, W. S. Brotherton, J. T. Simmons, L. A. Stankee, B. T. Nguyen, R. J. Clark, L. Zhu, *J. Am. Chem. Soc.* **2011**, *133*, 13984–14001.

[61] A. J. Link, M. K. S. Vink, D. A. Tirrell, *J. Am. Chem. Soc.* **2004**, *126*, 10598–10602.

[62] G. Molteni, C. L. Bianchi, G. Marinoni, N. Santo, A. Ponti, *New J. Chem.* **2006**, *30*, 1137–1139.

[63] L. D. Pachòn, J. H. Van Maarseveen, G. Rothenberg, *Adv. Synth.Catal.* **2005**, *347*, 811–815.

[64] L. Zhu, V. M. Lynch, E. V. Anslyn, *Tetrahedron* **2004**, *60*, 7267–7275.

[65] S. S. Gupta, J. Kuzelka, P. Singh, W. G. Lewis, M. Manchester, M. G. Finn, *Bioconjugate Chem.* **2005**, *16*, 1572–1579.

[66] R. Guezguez, K. Bougrin, K. El Akri, R. Benhida, *Tetrahedron Lett.* **2006**, *47*, 4807–4811.

[67] R. K. O'Reilly, M. J. Joralemon, C.J. Hawker, K.L. Woole, *J. Polym. Sci. A Polym. Chem.* **2006**, *44*, 5203–5217.

[68] H. Gao, G. Louche, B. S. Sumerlin, N. Jahed, P. Golas, K. Matyjaszewski, *Macromolecules* **2005,** *38*, 8979–8982.

[69] J. F. Lutz, H. G. Borner, K. Weichenhan, *Macromol. Rapid Commun.* **2005**, *26*, 514–518.

[70] H. Li, F. Cheng, A. M. Duft, A. Androv, *J. Am. Chem. Soc.* **2005**, *127*, 14518–14524.

[71] P. Wu, M. Malkoch, J. N. Hunt, R. Vestberg, E. Kaltgrad, M. G. Finn, V. V. Fokin, K. B. Sharpless, C. J. Hawker, *Chem. Commun*. **2005**, 5775–5777.

[72] J. A. Opsteenand, J. C. M. VanHest, *Chem. Commun*. **2005**, 57–59.

[73] M. Malkoch, K. Schleicher, E. Drockenmuller, C. J. Hawker, T. P. Russell, P. Wu, V. V. Fokin, *Macromolecules* **2005**, *38*, 3663–3678.

[74] N. V. Tsarevsky, B. S. Sumerlin, K. Matyjaszewski, *Macromolecules* **2005**, *38*, 3558–3561.

[75] B. Parrish, R. B. Breitenkamp, T. Emrick, *J. Am. Chem. Soc.* **2005**, *127*, 7404–7410.

[76] S. T. Laughlin, J. M. Baskin, S. L. Amacher, C. R. Bertozzi, *Science* **2008**, *320*, 664–667.

[77] J. A. Prescher, C. R. Bertozzi, *Nat. Chem. Biol.* **2005**, *1*, 13–21.

[78] S. Hotha, S. Kashyap *J. Org. Chem.* **2006**, *71*, 364-367.

[79] B. S. Arora, S. Shafi, S. Singh, T. Ismail, H. M. Sampath Kumar, *Carbohydr. Res.* **2008**, *343*, 139–144.

[80] M. Kümin, L. S. Sonntag, H. Wennemers, *J. Am. Chem. Soc.* **2007**, *129*, 466–467.

[81] K. Oh, Z. Guan, *Chem. Commun.* **2006**, 3069–3071.

[82] A. Jatsch, A. Kopyshev, E. Mena-Osteritz, P. Bäuerle, *Org. Lett.* **2008**, *10*, 961–964.

[83] E.-K. Schillinger, M. Kümin, A. Digennaro, E. Mena-Osteritz, S. Schmid, H. Wennemers, P. Bäuerle, *Chem. Mater.* **2013**, *25*, 4511–4521.

[84] F. Seela, V. R. Sirivolu, *Chem. Biodiv.* **2006**, *3*, 509–514.

[85] J. M. Baskin, C. R. Bertozzi, *QSAR Comb Sci.* **2007**, *26*, 1211–1219.

[86] T. Wang, Z. Guo, *J. Curr. Med. Chem.* **2006**, *13*, 525–537.

2.3 Self-Assembly

2.3.1 Introduction

"Put the different parts of a car in a big box, and shake the whole, will you get a car? This image is often used to express what self-assembly (SA) can achieve."[1]

Self-assembly is clearly a process of construction, "in which humans are not actively involved, in which atoms, molecules, aggregates of molecules and components arrange themselves into ordered, functioning entities without human intervention".[2]
More precisely, self-assembly can be defined as type of process, in which a disordered system of pre-existing components forms an organized structure as a consequence of specific, local interactions among the components themselves, without guidance or management from an outside source. When the constitutive components are molecules, one can talk about *molecular self-assembly*.
There are two types of molecular self-assembly: *intramolecular* and *intermolecular*. Commonly, the term molecular self-assembly refers to the intermolecular one, while the intramolecular analogue is more commonly called folding.
Furthermore, self-assembly can be classified as either *static or dynamic*: in static self-assembly, the ordered state forms as a system approaches equilibrium reducing its free energy, whereas dynamic self-assembly involves structures whose existence depends on the dissipation of energy. In the latter case, one will not talk about "self-assembly" but "self-organization".[3]
In general, three distinctive features are used to describe self-assembled systems:

Order: the self-assembled structures must have a higher order than the isolated components.

Interactions: non-covalent interactions such as Van der Waals, capillary, π-π, or hydrogen bonds have a key role with respect to more 'traditional' covalent, ionic, or metallic bonds. Although typically less energetic by a factor of 10, these weak interactions play an important role in materials, especially in biological systems.

Building blocks: not only atoms and molecules, but a wide range of nano- and mesoscopic structures, with different chemical compositions, shapes and functionalities, can be considered as building blocks.[4,5]

Molecular self-assembly is also of practical interest for disciplines connected to "making" molecules and molecular materials;[6,7] examples include non-covalent synthesis,[8,9] crystallization,[10] micelle formation,[11] and phase-separation in block copolymers.[12,13]

2.3.2 Self-Assembly of π-Conjugated Systems

Recently, great attention was focused on molecular self-assembly of π-conjugated materials, and in particular of small molecules and oligomers.[14] Because they typically possess more defined chemical structures than polymers, the study of their self-assembling behaviour in water and other organic solvents as well as in solid state is of great importance and worth to be investigated. The self-assembling ability of π-conjugated oligomers is usually controlled by two secondary interactions, such as π-π intractions and hydrogen bonding.[15] The strength as well the causes of π-π interactions vary strongly: in water, for example, the stack between aromatic molecules is mainly caused by the hydrophobic effect. Water molecules, solvating the aromatic surface, have higher energy than bulk water resulting in stacking of the aromatic surfaces, which reduces the total surface exposed to the solvent. In solvents other than water, the interactions between solvent molecules are weaker, and therefore, solvophobic forces play a minor role. Hydrogen bonds are ideal to construct supramolecular architectures due to their highly selectivity and directionality. These interactions are formed when a donor (D) with an acidic hydrogen atom is in close proximity to an acceptor (A) carrying non-bonding electron lone pairs; the strength of this kind of forces depends mainly on the solvent.[16]

This possibility to control the self-assembly of π-conjugated oligomers have attracted a growing number of research investigations in the field of electronic devices, such as organic field-effector transistors (OFETs), organic light-emitting diodes (OLEDs), and organic solar cells (OSCs).[17-19] In particular, the prospect of improving electronic properties by providing long-range ordering and additional tuning parameters for the control of the devices' properties, is of great interest.

Nowadays, the most frequent systems found in literature are the one which have a basic structure of alternating conjugated double and triple bonds; some parent structures are shown in ***Chart 2.3.1***.[20]

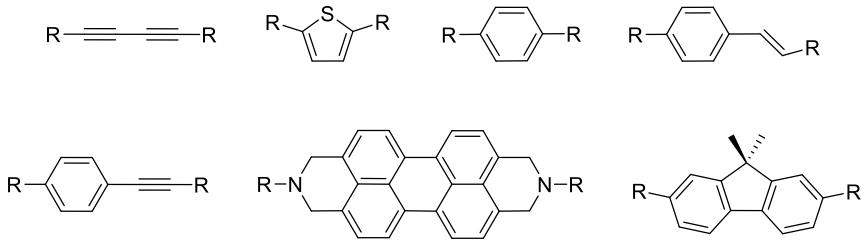

Chart 2.3.1*. The most frequent systems found in literature having a basic structure of alternating conjugated double and triple bonds.*[20]

Giuseppone and co-workers have reported the synthesis of an entirely new class of nanostructures based on oxidized triarylamine **2.3.1** stacks, as well as their addressable self-organization between two electrodes which represents a major progress towards the control of supramolecular electroactive materials at 100 nm length scale (***Figure 2.3.1***). With these structures it is possible to spatially address the localization and directionality of the fibres' elongation by applying an electric field directly between electrodes. A channel conductivity exceeding 5 x 10^{-3} S/cm was measured for this device.[22]

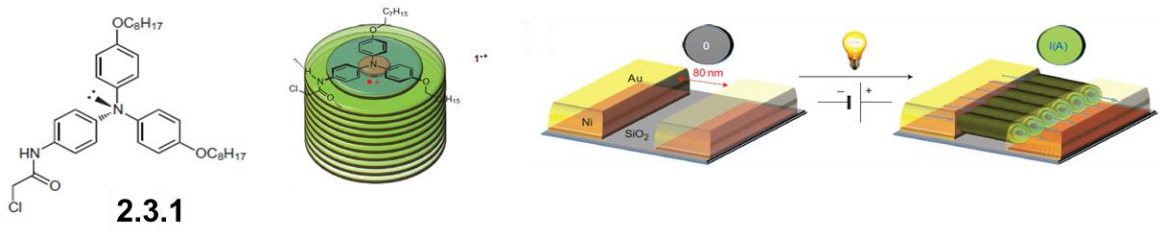

Figure 2.3.1. *Electrically conducting self-assembled nanofibre.*[22b] Reprinted by permission from Macmillan Publishers Ltd: *Nat. Chem.* **2012***, 4,* 485–490, copyright 2012.

On the other hand, Würthner and co-workers studied bacteriochlorophyll c (BChl c) derivatives equipped with hydrophilic wedges **2.3.2** which self-assemble in water to produce well-defined nanotubes having a diameter of 6 nm (***Figure 2.3.2***). These nanostructures have shown conductivities up to 0.48 S/cm and charge-carrier mobilities of 0.03 $cm^2\ V^{-1}\ s^{-1}$.[23]

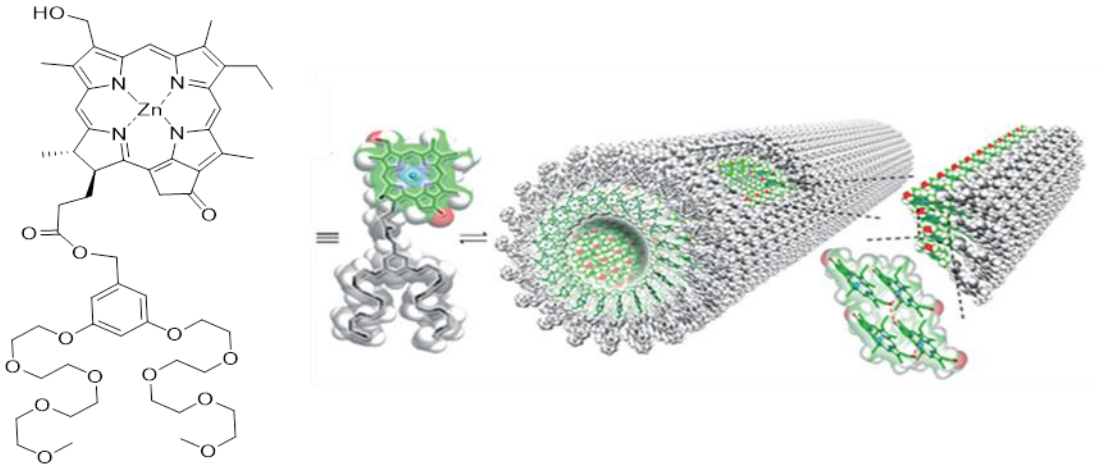

2.3.2

Figure 2.3.2. *Chemical structure of a zinc chlorin derivative, the corresponding space-filling model and a schematic model of self-assembled nanotubes.*[23] Reproduced with permission from ref. 23.

Regarding the area of organic field-effect transistors (OFETs), fabrication of film and single-nanofibre OFETs from organogels based on anthracene derivative **2.3.3** has been described by Lee *et al.* (***Figure 2.3.3***).[24]

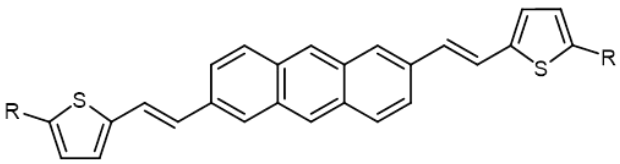

2.3.3 (R = dodecyl)

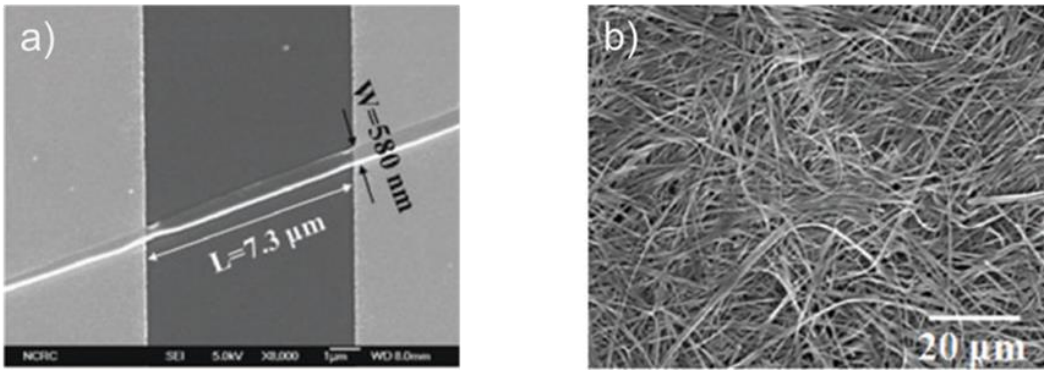

Figure 2.3.3. *Molecular structure of anthracene derivative **2.3.3**; (a) The bottom-contact single-nanofibre transistor of **2.3.3**, and (b) SEM images of its xerogel.* [24] Adapted from *Chem. Commun.* **2009**, 310–312 with permission of The Royal Society of Chemistry.

The supramolecular organization of **2.3.3** into fibres led to higher performance (field-effect mobility 0.48 $cm^2\ V^{-1}\ s^{-1}$; on-off ratio 10^5) compared to the film-casted versions.

In 2009, Bao and co-workers have described the fabrication of single-crystalline wire OFETs from perylene tetracarboxydiimide.[25] In this study, the nanowires showed a mobility as high as 1.4 cm^2 V^{-1} s^{-1}. In 2012, Samori and co-workers demonstrated that not only the processing techniques, but also side chains have strong influence on the morphology of perylene tetracarboxydiimide (PTCI) nanofibres and consequently on the characteristic parameters of field-effect transistors.[26]

In the OLED field, Del Guerzo *et al.* have described the self-assembly of blends of tetracene derivatives **2.3.4**-**2.3.6** leading to color-tunable organogels constituted of fluorescent nanofibres (***Figure 2.3.4***).[27]

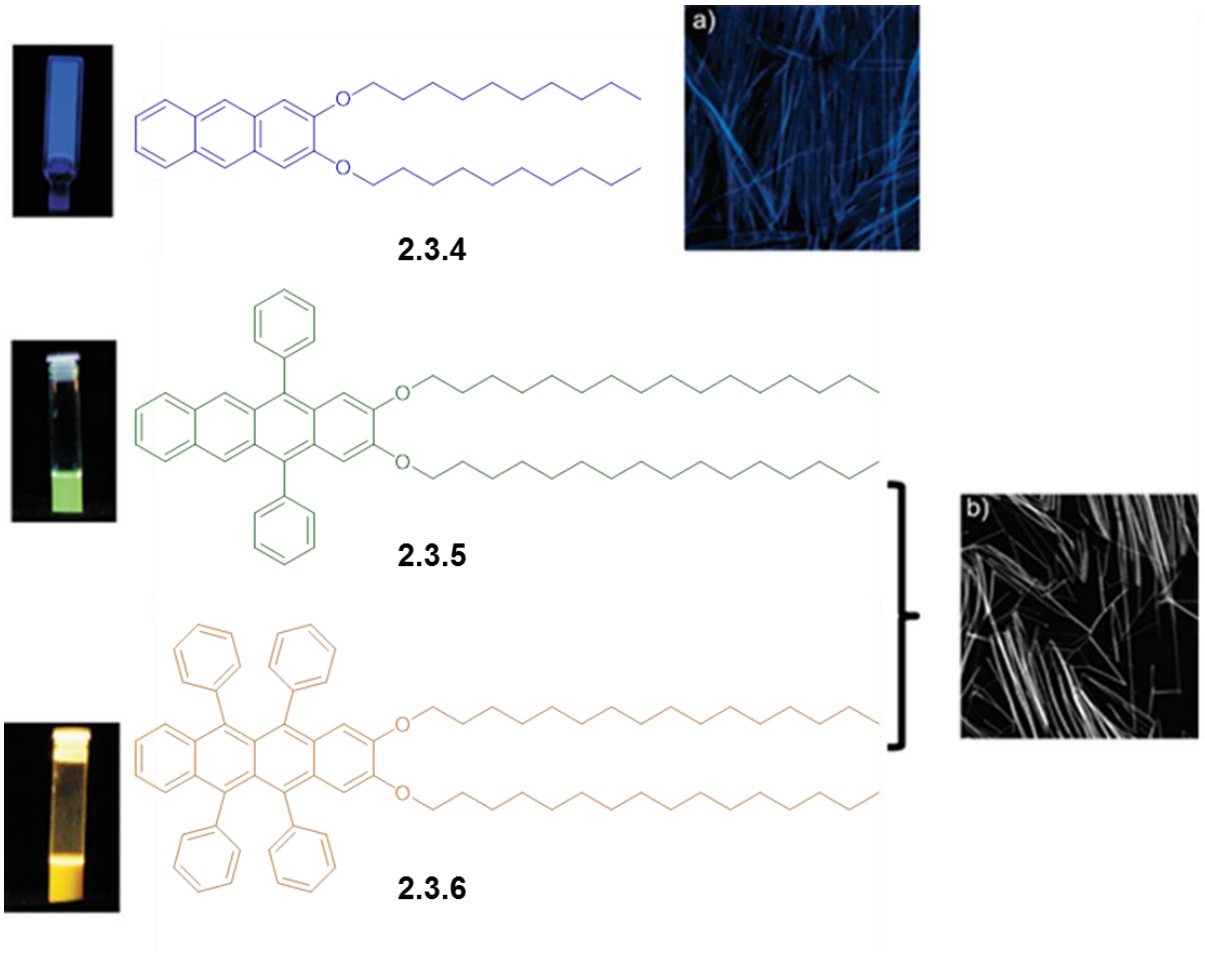

Figure 2.3.4. *Molecular structures of* ***2.3.4-2.3.6****; pictures of a 2 µM* ***2.3.4*** *gel in DMSO, 10 µM* ***2.3.5*** *solution in THF, and 10 µM* ***2.3.6*** *solution in THF under UV light (λ_{ex} = 365 nm) and the fluorescence intensity confocal microscopy images (30 × 30 µm, 80 × 80 nm/pixel) of (a) a* ***2.3.4*** *gel and (b) a* ***2.3.5+2.3.6****-gel of DMSO at 22 °C.*[27] Reprented with permission from *J. Am. Chem. Soc.* ***2011****, 133, 316-325.* Copyright 2011 American Chemical Society.

Under near UV light excitation, both organogels and dry films of nanofibres emit white light, which is polarized in the blue spectral region. Additional confocal fluorescence microscopy experiments showed that white light is emitted by each individual nanofibre. De Cola and co-workers have reported the use of platinium(II) complexes, which self-assemble in bright gelating nanofibres as dopant for solution-processed OLEDs.[28]

Intensive research is currently being carried out in the field of organic photovoltaic devices,[29-38] because of their lower cost compared to silicon-based materials and easy processing in devices. The prospective morphology of the active layer plays a critical role in the device performance and a lot of attention was devoted to its ordering.[3,29-38]

In 2004, Würthner and co-workers have described the use of triaminotriazine-substituted oligo(phenylene vinylenes) to bind perylene bisimides under the formation of hydrogen bonded trimers.[32] The trimers self-assemble into right-handed supercoils. Organic photovoltaic (OPV) devices of the trimers showed only poor diode behaviour (open circuit voltage of 0.74 V and a low current density of 2.6 μA cm^{-2}) due to the lateral organization of the supercoils at the surface. In 2006, Kamat and co-workers have used stacked-cup carbon nanotubes (SCCNTs) in a photoelectrochemical cell.[33] A maximum photoconversion efficiency of 17% was reached that is lower than that of dye-sensitized solar cells, but comparable to that of nanostructured semiconductor films (TiO_2, ZnO, etc.).

In 2008, Shinkai *et al.* have described the self-assembly of electron-rich quaterthiophenes **2.3.7**, **2.3.8**, and electron-poor perylene bisimide **2.3.9** and obtained n–p heterojunction nodes (***Figure 2.3.5***).[34] Interestingly, a sorted formation of a pure oligothiophene nanofibres and of pure perylene bismide nanofibres was observed from a 1:1-mixture of both compounds and a bulk heterojunction solar cell was made using a cast film of this organogel.

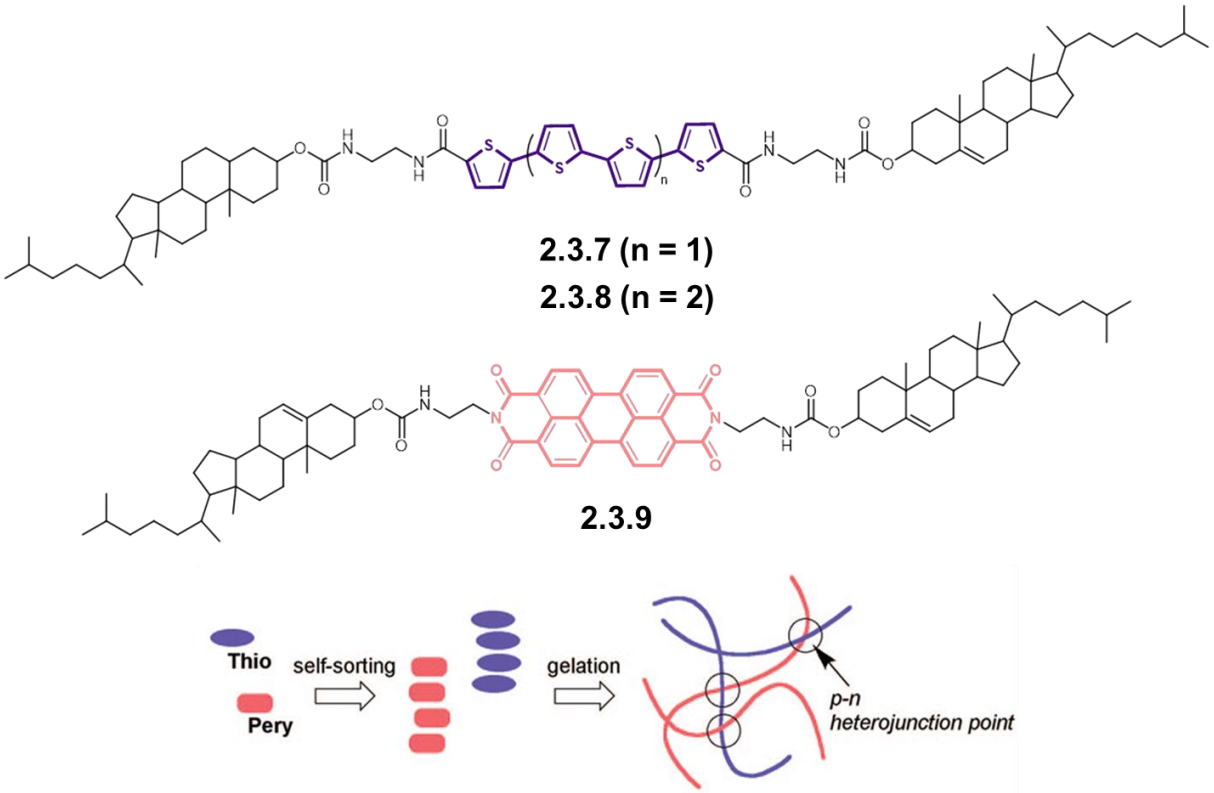

Figure 2.3.5. *Molecular structures of oligothiophenes* ***2.3.7****,* ***2.3.8*** *and perylene* ***2.3.9*** *organogelators with a schematic representation of their self-sorting organogel formation yielding p–n heterojunction points.*[34] Reproduced with permission from *Chem. Mater*. **2008**, *20*, 2863–2865. Copyright 2008 American Chemical Society.

In 2010, Nuckolls *et al.* have reported solar cell devices based on fullerene C_{60} and dibenzotetrathienocoronene (6-DBTTC), which self-assembles in a network of cables after thermal annealing.[35] As well in 2010, Aida and co-workers have reported different self-assembly modes between enantiopure and racemic forms of porphyrin–fullerene dyads.[36] The racemate generated nanometric spheres with a mean diameter of 300 nm, whereas the enantiopure compound gave nanofibres up to 10 mm in length. A cast film of the spherical assemblies showed only a relatively small hole mobility of 1.5 x 10^{-4} cm^2 V^{-1} s^{-1} and no electron mobility by the time-of-flight method. Matile *et al.* have introduced the programmed self-assembly of interdigitating intra- and interlayer recognition motifs on conducting surfaces, using *p*-oligophenyl, *p*-oligophenylethynyl chromophores, and naphthalenediimides (***Figure 2.3.6***). These self-assembled zippers allowed access to supramolecular coaxial n–p-heterojunctions with good photocurrents, which were measured by carrying out cyclic voltammetry experiments.[37]

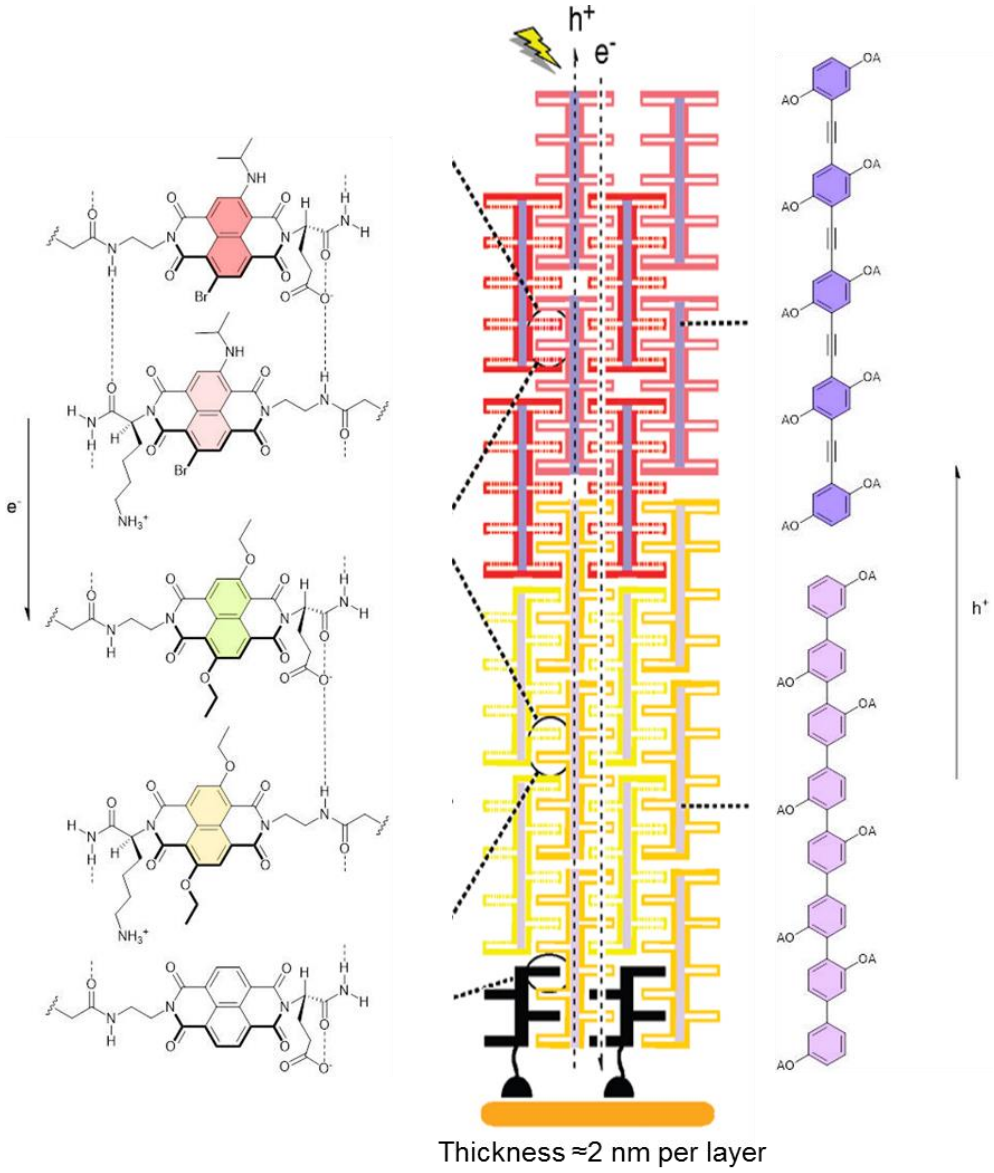

Figure 2.3.6. *Molecular structures of p-oligophenyl, p-oligophenylethynyl chromophores, and naphthalenediimides, together with their corresponding supramolecular heterojunction architectures.*[37a] Reproduced with permission from *J. Am. Chem. Soc*. **2010**, *132*, 6923–6925.Copyright 2010 American Chemical Society.

Wong and co-workers described the use of a difluorenyl-substituted hexabenzocoronene (HBC) which self-assembles into columnar discotic liquid crystals.[38] Solar cell devices based on the blend of the previous compound with $PC_{60}BM$ (1:2) generated a short circuit current (J_{SC}) of 2.68 mA cm^{-2} and *PCE* of 1.46% after thermal annealing (150 °C). The same authors also modified the latter compounds by attaching oligothiophenes to the difluorenyl-substituted HBC.[39] Devices based on blends of this compound and $PC_{70}BM$ (1:2) gave a J_{SC} of 2.53 mA cm^{-2} and *PCE* of 1%. Finally,

diketopyrrolopyrrole units were attached to the HBC derivative and blends with $PC_{70}BM$ showed a *JSC* of 3.96 mA cm^{-2}, a V_{OC} of 0.86 V, and a *PCE* of 1.59%.[40]
In 2014, Stupp and co-workers reported that the introduction of a hairpin-shaped molecules based on trans-diamidocyclohexane (DACH) as a self-assembly motif through hydrogen bonds and sexithiophene as a donor moiety resulted in a 23% increase of the device efficiency compared to the sexithiophene alone. Their idea was to test the ability of non-linearly shaped nanowires of donor molecules with cavities as a strategy to create better interfaces between donors and acceptors in OPV devices. Afterwards, they report the use of a different hairpin-shaped molecule **2.3.10** based on thiophene-capped diketopyrrolopyrrole units and the self-assembly motif DACH (***Figure 2.3.7***). Thiophene-capped diketopyrrolopyrrole was selected as light harvesting motif because of its high extinction coefficient, its absorption in a broad region of the solar spectrum, and its high hole mobility. This characteristics render it a more powerful chromophore than sexithiophene.

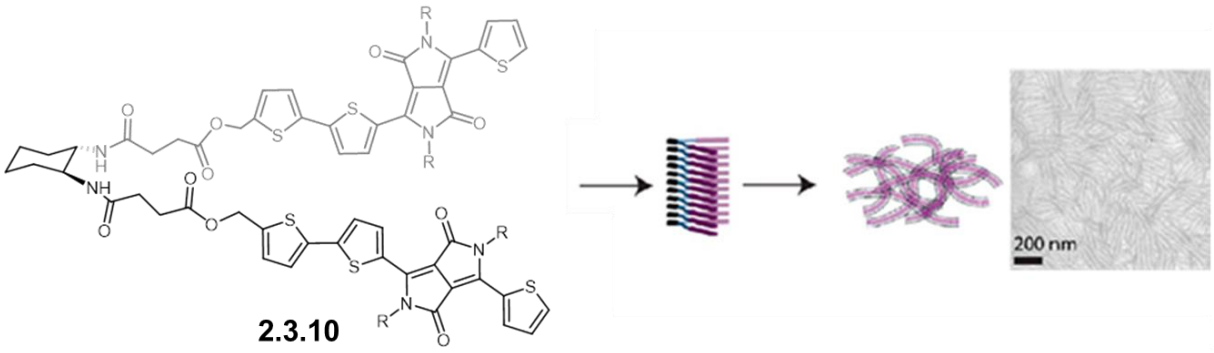

Figure 2.3.7. *Hairpin-shaped molecule* ***2.3.10*** *based on thiophene-capped diketopyrrolopyrrole units and trans-diamidocyclohexane.*[41a] Adapted from *J. Mater. Chem. A* **2013**, *1*, 11674-11681 with permission of The Royal Society of Chemistry.

In this paragraph, it was shown how in the last years the researchers have acquired a high control of objects at the supramolecular level. They were able to apply their knowledge and experiences towards the construction of functional nanomaterials with novel properties related to the sizes, structures, and dynamics of the implemented systems. Anyway, it is true that there is still plenty of room for improvements in this field which will certainly produce even more sophisticated nanomaterials in the future. In particular, the main challenge remains the deep and complete understanding of self-organization at the nanoscale.

2.3.3 Self-Assembly of Peptides

Biological systems such as proteins, DNA, cellular organelles, or microorganisms are submicron-sized objects. Thus, they can be considered as 'biological nanostructures' when compared to synthetic nanostructures. In particular, peptides are highly versatile structural building blocks and can generate supramolecular architectures including sheets, spheres, fibres, tapes, and tubes. Peptides are able to self-assemble through various types of interactions such as electrostatic, hydrophobic, and hydrogen bonding.[42] More studies are required in rational peptide design to investigate systematically the role of these forces in pattern formation and to examine the effects on morphologies, and to elucidate the fundamental physical interactions that drive their self-assembly. These investigations will help in determining the guiding principles in terms of roles of size, charge, and hydrophobicity for self-assembly into specific structures. The control of the size of peptide nanostructures is especially crucial in its applications such as drug delivery systems and biosensors and can be controlled with external stimuli such as pH, ionic strength, solvent, chemical additives, or temperature. For example, an optimal balance of hydrophobicity and charge could generate self-assembled nanostructures in aqueous solution by intramolecular and/or intermolecular interactions, minimizing aggregation through hydrophobic groups.[42] Ghadiri and co-workers were able to rationally design cyclic peptide structures with alternating D- and L-amino acids which adopted flat ring-shaped conformations and assembled into ordered parallel arrays of solid-state nanotubes (***Figure 2.3.8***).[42,43]

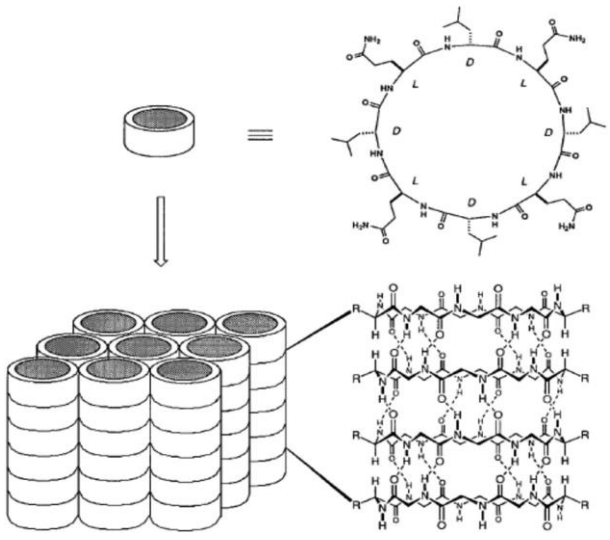

Figure 2.3.8. *Cyclic peptide structures with alternating D- and L-amino acids .* [43c] Reprinted with permission from *J. Am. Chem. Soc.* **1996**, *118 (***1***)*, 443-50. Copyright 1996 American Chemical Society.

Some nanotubular structures are also formed by self-assembly of peptide amphiphiles (PAs).[44] The tails of PAs are normally composed of non-polar amino acid residues (Gly, Ala, Val, Ile, Leu, Pro, o Phe) or of a combination of hydrocarbon chain and non-polar amino acids. Positively charged amino acids (His, Lys, or Arg) and/or negatively charged residues (Asp or Glu) have been found applicable in heads. Interestingly, peptides containing alanine and valine tails have been found to form more stable structures than those of glycine, isoleucine, and leucine.[42]

Sometimes the molecular geometry also effects the formation of nanostructures. For example, cone-shaped PA, Ac-Gly-Ala-Va-IIle-Leu-Arg-Arg-NH_2, which has a hydrophobic tail and a large cationic head group composed of two arginine residues led to formation of the simultaneous shapes of nano-sphere and nano-doughnut structures (***Figure 2.3.9***).[42,45] At low concentrations' peptides are randomly oriented and distributed (***Figure 2.3.9A***); above the critical aggregation concentration (CAC) peptides form micelles (***Figure 2.3.9B***), which fuse or elongate by forming a nanopipe (***Figure 2.3.9C***). The bending of the nanopipe leads to the formation of a nano-doughnut structure (***Figure 2.3.9C***).

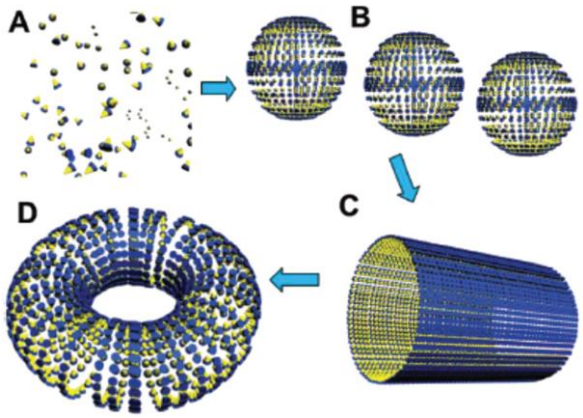

Figure 2.3.9. *Proposed self-assembling process of the nano-doughnut structure.*[42] Reprinted with permission from *Langmuir* **2009***, 25, 4111–4114.* Copyright 2009 American Chemical Society.

PAs are also able to self-assemble into nano-belts under specific conditions. For instance, Stupp and his group synthesized peptides containing alternating hydrophilic and hydrophobic amino acid residues, which are known to have a strong tendency to generate β-sheet structures, one of the major secondary structural elements in proteins along with the α-helix.[46] The template consisted of hydrophobic and negatively

charged residues (Val and Glu) and an alkyl side chain with 16 carbons ($C_{16}H_{31}O$Val-Glu-Val-Glu) **2.3.11** (***Figure 2.3.10***).

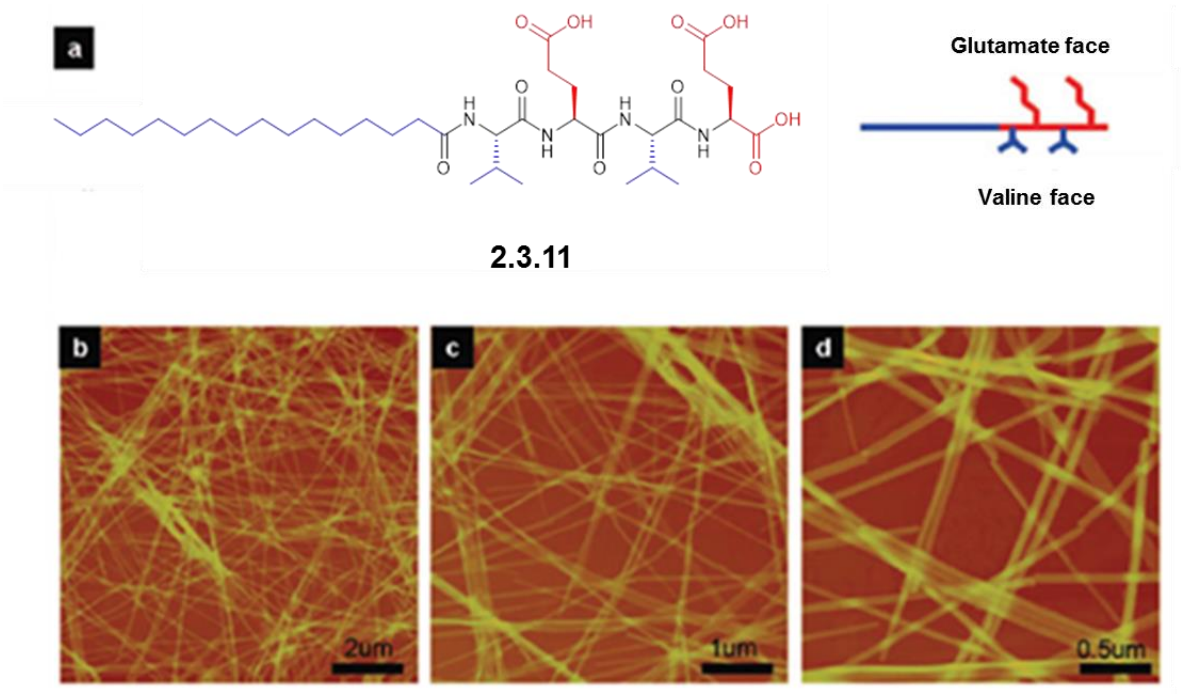

Figure 2.3.10. *a) Chemical structure of the PA; b–d) AFM images of* ***2.3.11*** *at different scanning sizes.*[46] *Reprinted with permission from Nano Lett.* **2009**, *9*, 945–951. Copyright 2009 American Chemical Society.

The investigators assumed that the Val-Glu-Val-Glu sequence flips the hydrophilic and hydrophobic side chains to the opposite sides of the peptide amide backbone when adopting an extended β-strand conformation leading to a more effective chain packing within the peptide region and to the formation of nano-belts morphology.[46]
Additionally, amphiphilic oligopeptides consisting of various ratios of hydrophilic to hydrophobic block length, such as proline-rich peptides, and cyclic peptides, are also able to self-assemble into vesicular structures.
The self-assembly of proline-rich peptides was explored by Lee and his group.[47] Among the 20 naturally amino acids, proline is the only one, in which the side chain atoms form a pyrrolidine ring with the backbone atoms. Because the cyclic structure of proline causes conformational constraints among the atoms in the pyrrolidine ring, the proline-rich peptide tends to form stiff helical rod structure, the so called polyproline II (PPII). Even if proline itself as an isolated amino acid has a small hydrophobicity, the three non-polar methylene groups, which are aligned at the outer part of the

PPII helix give a hydrophobic character to the helical rod structure. Based on these facts, Lee hypothesized that the stiff rod character and the non-polar nature of the outer surface of PPII helix might impart microphase-separation characteristics to the rod–coil of a PPII rod and a hydrophilic coil leading to self-assembly. Having in mind this idea, a block polypeptide of polyproline and an arginine oligomer **2.3.12** was synthesized and the self-assembly process was investigated. The secondary structure of **2.3.12** consisting of 10 proline and 3 arginine residues showed characteristics of a PPII helix in solution and microscopy data suggested the formation of vesicles (***Figure 2.3.11***).[47a]

Finally, one could state that peptides are highly versatile structural building blocks and can generate supramolecular architectures such as sheets, spheres, fibres, and tubes. Self-assembled peptides are able to form numerous nanostructures through various types of interactions, such as electrostatic, hydrophobic, and H-bonding. In any case, more studies are required in order to design rational peptide and to investigate the role of hydrophobicity, electrostatics, and to examine the sequence effects on morphologies, and clarify the fundamental physical interactions that drive their self-assembly.

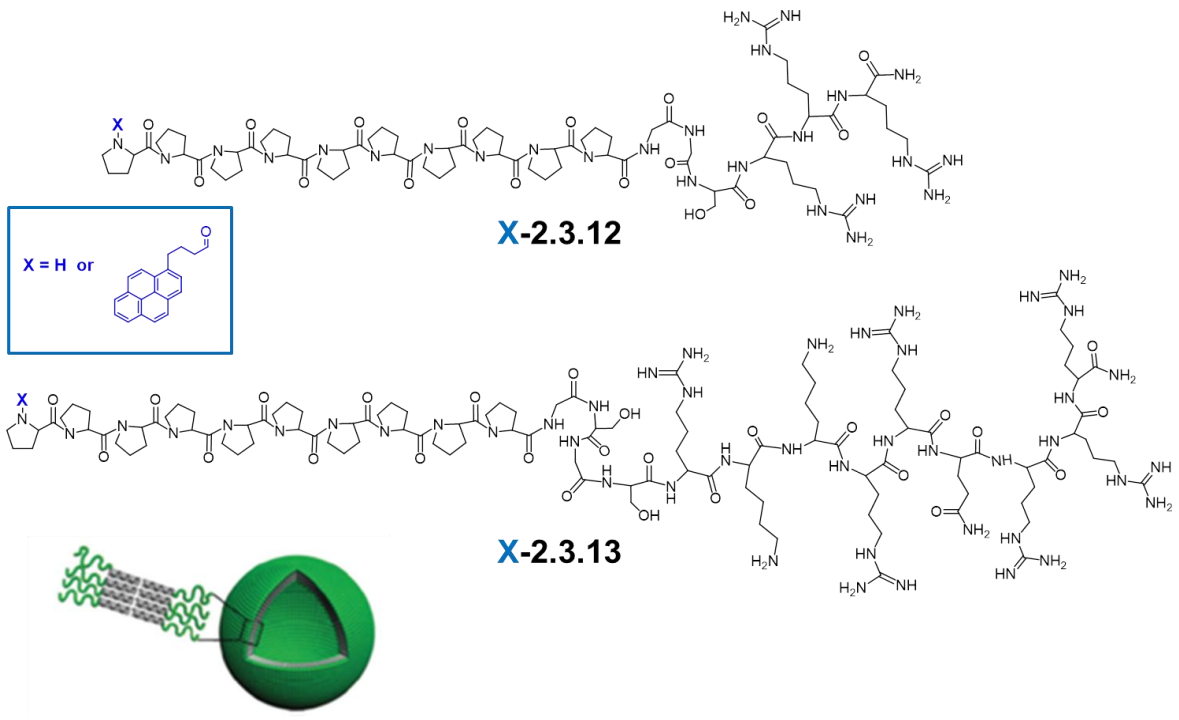

Figure 2.3.11. *Molecular structures of peptide rod–coil building blocks and their self-assembly into nanocapsule structures.*[47a] Reprinted from *Chem. Commun.* **2008**, 1892–1894 with permission of The Royal Society of Chemistry.

2.3.4 Peptide-Guided Self-Assembly of π-Conjugated Systems

As previously discussed, organic semiconducting materials composed of π-conjugated systems have shown great potential in organic electronic devices such as OFETs, OLEDs, or OSCs. For the performance of these devices, the organization of the molecules on surface or in the bulk into ordered suprastructures is of high importance and several strategies have been employed in order to obtain control over the self-assembly of π-conjugated systems into regular patterns.[48-52] In the last decade, the most fashionable approach consisted in the combination of π-systems with biomolecules such as carbohydrates, nucleic acids, or peptides having the inherent ability to self-assemble into well-defined suprastructures.[53]

Peptides and proteins, in particular, represent an interesting class of biomolecules for the enhanced self-assembly of oligomeric semiconducting materials. Due to the possible dihedral angles of the amide bond and the amino acids' ability of hydrogen bonding, several secondary structural motifs such as α-helices, β-sheet, or β-turns, can be exploited in order to guide supramolecular self-organization by choosing an appropriate sequence of amino acids (***Figure 2.3.12***)

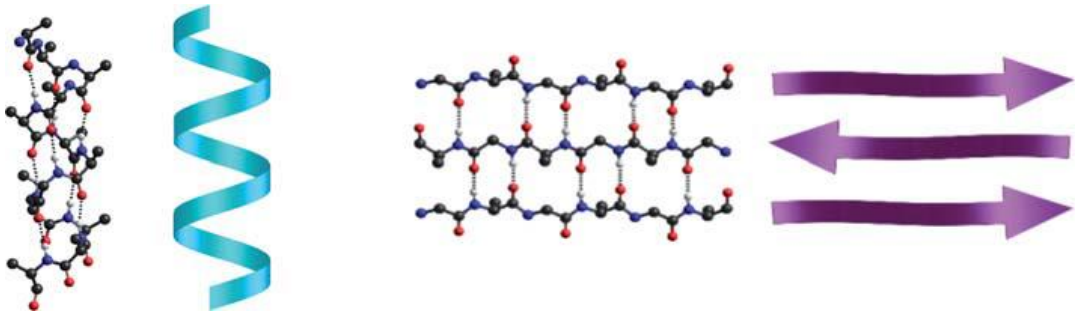

Figure 2.3.12. *Examples of peptide secondary structure motifs: left: α–helical backbone (here: polyalanine); right: antiparallel β–sheet (here: a glycinealanine sequence)*[53]*.* Reproduced from *J. Mater. Chem.* **2010***, 20,* 3563-3578 with permission of The Royal Society of Chemistry.

In 2004, our group presented the first example of an oligothiophene as potential semiconductor, which was directly conjugated to a β-sheet peptide.[54] The pentapeptide sequence glycine-(L-alanine)-glycine-(L-alanine)-glycine (GAGAG) was inspired by Bombyx mori (silk-worm) silk, and the regioregularly hexyl-substituted quaterthiophene represents a structurally defined oligomeric model of the well-known regioregular poly(3-hexylthiophene) (P3HT) (***Chart 2.3.2***).

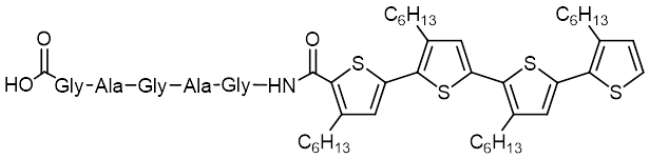

2.3.14

Chart 2.3.2. *Molecular structure of GlyAlaGlyAlaGly-4T* ***2.3.14****.*[54]

The hybrid GlyAlaGlyAlaGly-4T **2.3.14** showed an antiparallel orientation of the pentapeptide sequence on surface confirming the retention of the peptide secondary structure (β-sheets) in the hybrid.[54]

In 2008, Schenning and colleagues presented conjugates, in which oligo(*p*-phenylenevinylene)s (OPVs) were combined with GlyAlaGlyAlaGly **2.3.15** and GlyAlaAspProAspAlaAlaGly **2.3.16** peptide sequences which typically arrange in β-sheets (***Figure 2.3.13***).[55] In particular, **2.3.15** showed very regular domains at the liquid-solid interface (1-octanoic acid/highly oriented pyrolytic graphite (HOPG)) (***Figure 2.3.13***). The suprastructures formed are reminiscent of bilayers. Hybrid **2.3.16** did not show any regular superstructure in STM, probably due to aggregation in 1-octanoic acid.

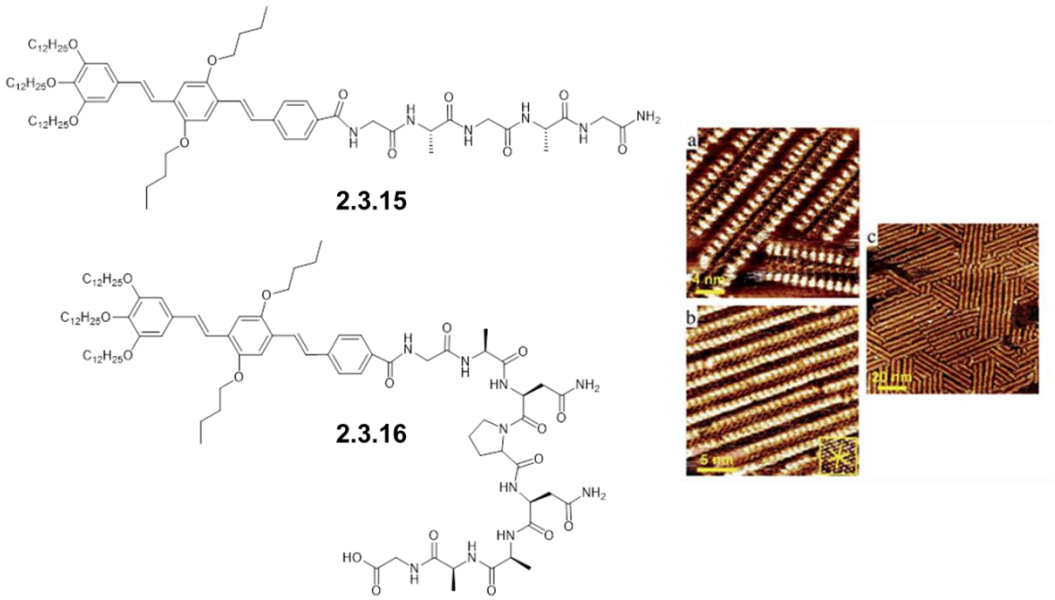

Figure 2.3.13. *Molecular structure of oligo(p-phenylenevinylenes) substitituted with a β–sheet forming peptide GlyAlaGlyAlaGly (****2.3.15****) and a GlyAlaaAspProAspAlaAlaGly octapeptide sequence (****2.3.16****). a)–c) STM images of* ***2.3.16*** *at the 1-octanoic acid/HOPG interface.*[55] Adapted with permission from *J. Am. Chem. Soc.* **2008***, 130,* 14576–14583. Copyright 2008 American Chemical Society.

A more elaborate example was introduced by Börner, Bäuerle, and co-workers in 2009: a symmetric conjugate (A-B-A-type) consisting of a semiconducting quaterthiophene and a PEO-β-sheet peptide sequence containing three repeat units of the dipeptide L-valine-L-threonine **2.3.17** (***Figure 2.3.14***).[56]

Surprisingly, experiments evidenced that hybrid **3.17** self-assembles into left-handed helical suprastructures instead of forming extended secondary β-sheet structures (***Figure 2.3.14***). In fact, from the solution of **2.3.17** in a dichloromethane/methanol mixture, well-defined microstructures could be observed after 2 days by means of atomic force microscopy (AFM) on mica substrate (***Figure 2.3.15a***). By adding a base (0.001 M NaOH), the formation of fibrous structures were detected in AFM and TEM.

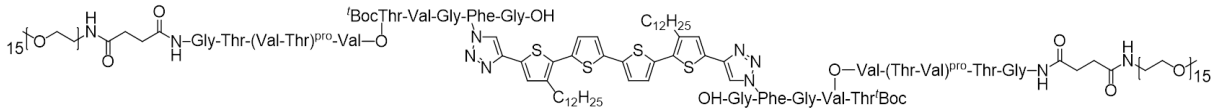

2.3.17

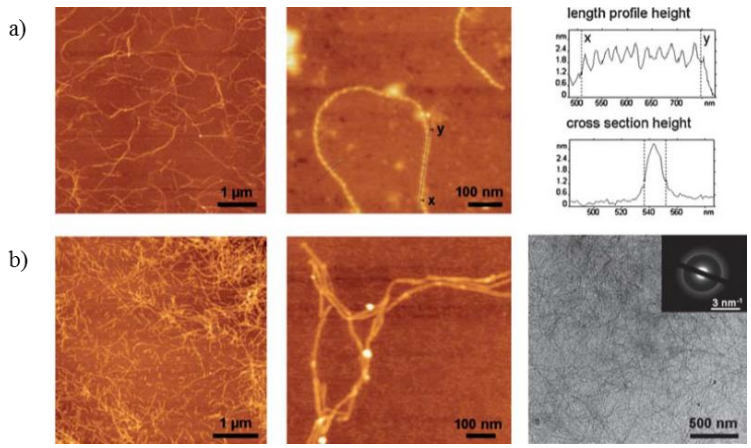

Figure 2.3.15*. Molecular structure of symmetrically substituted quaterthiophene-peptide conjugate* ***2.3.17*** *(A-B-A); a) AFM images and height and length profiles of* ***2.3.17****; b) AFM and TEM images of* ***2.3.17*** *after addition a base.*[56] Adapted with permission from ref. 56.

In 2011, Holmes and co-workers reported the attachment of an oligothiophene to L-lysine and subsequent polymerization to the corresponding poly(L-lysine) (**2.3.20**, ***Chart 2.3.3***). Polymer **2.3.20** was found to form a R-helical secondary structure, which underwent hierarchical self-assembly in a variety of solvents.

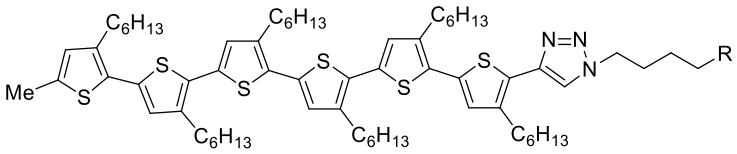

2.3.18 (R = -CH_3)

2.3.19 (R = -CH(NHBoc)COOMe)

2.3.20 (R = 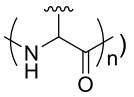)

Chart 2.3.3. *Molecular structure of oligothiophenes derivatives* ***2.3.18****-****2.3.20****.*

Furthermore, in solar cell devices, blends of the polypeptide and PCBM showed an improvement of *PCE* (0.2%) compared to reference compounds **2.3.18** (0.14%) and **2.3.19** (0.12%), which do not produce any helical arrangement of the chromophore, due to the missing amide group.[57]

In 2013, Frauenrath and co-workers found that oligopeptide (L-Ala)-substituted perylene bisimide **2.3.21** and quaterthiophene **2.3.22** (***Chart 2.3.4***) give rise to nanowires allowing the detection of photoinduced polaron generation and transport.

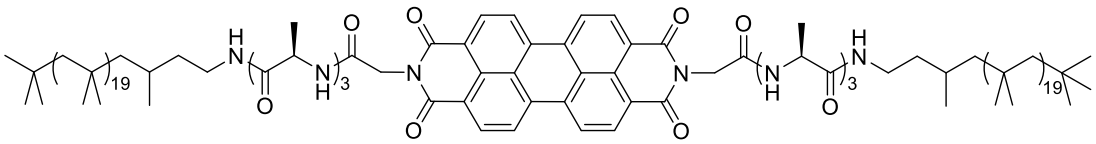

2.3.21

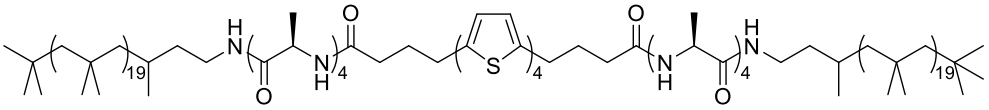

2.3.22

Chart 2.3.4. *Oligo(L-alanine)-poly(isobutylene)-substituted perylene bisimide* ***2.3.21*** *and quaterthiophene* ***2.3.22****.*

Self-assembly of the π-conjugated cores into nanofibrils with excellent π-π overlap was achieved by using oligopeptide-polymer substituents to promote one-dimensional aggregation by β-sheet-like hydrogen-bonding, while supramolecular helicity and polymer attachment served to suppress lateral aggregation.[58] Moreover, these molecules were proven to show a very tight π-π stacking promoted by the

strong hydrogen-bonding of the oligopeptide substituents in a hydrophobic environment and the inclusion of conformational flexibility in the molecular design.

Recently, Ulijn and co-workers identified optimized peptide sequences for the formation of hydrogen-donor (dihydroxy-naphatelene (DHN) **2.3.23**)/hydrogen-acceptor (dialkoxynaphtalene (DAN) **2.3.24**-**2.3.27**) peptide nanostructures by using a non-selective protease and a small library of amino acid building blocks; in this way, various peptide sequences are produced and their thermodynamic selection is possible whereby the most stable peptide structure is preferentially formed.[59] They investigated and demonstrated that enzymatic condensation and self-assembly can be used to produce energy-minimized peptide-based NDI structures and as well co-assemblies with dialkoxy/ hydroxy naphthalene donors in water (***Figure 2.3.16***).

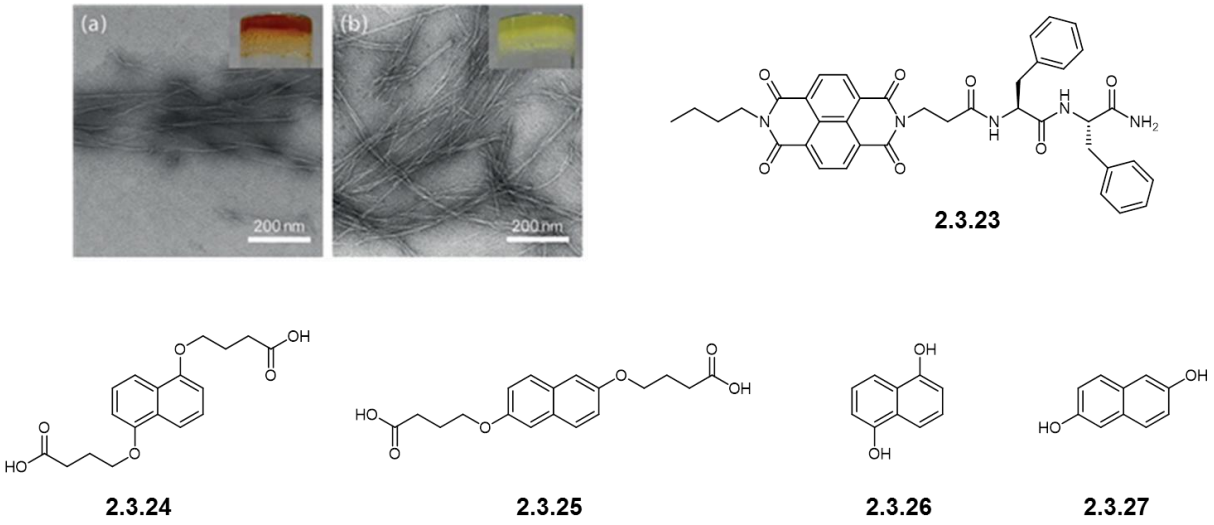

Figure 2.3.16. *Molecular structures of various di-alkoxy/hydroxy-naphthalene (DAN/DHN) donors* ***2.3.23-2.3.27****; TEM images of hydrogels before a) and after b) the addition of thermolysin.*[60] Adapted with permission from ref. 60.

In 2013, Schillinger *et al.* published three stereoisomeric hybrid materials consisting of a π-conjugated oligothiophene backbone and a proline **2.3.28a-c** (***Chart 2.3.5***).[60] The hybrids were in particular investigated regarding their self-assembling behaviour in solution. From optical investigations, including circular dichroism spectroscopy, the formation of chiral suprastructures could be deduced and correlated with the stereochemistry of the proline residue.

.

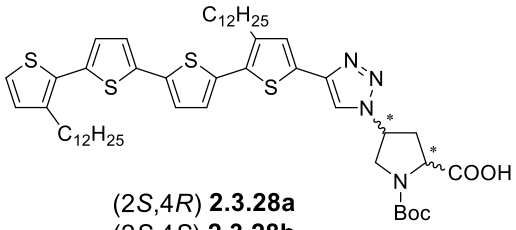

(2*S*,4*R*) **2.3.28a**
(2*S*,4*S*) **2.3.28b**
(2*R*,4*R*) **2.3.28c**

Chart 2.3.5. *Molecular structures of oligothiophenes-proline hybrids* ***2.3.28a-c****.*

Their self-assembling behaviour in solution accounted for left- and right-handed chiral aggregates in the case of the enantiomeric pure hybrids **2.3.28b** and **2.3.28c**, respectively, and non-chiral aggregation in the case of diastereomer **2.3.28a** (***Figure 2.3.17***).

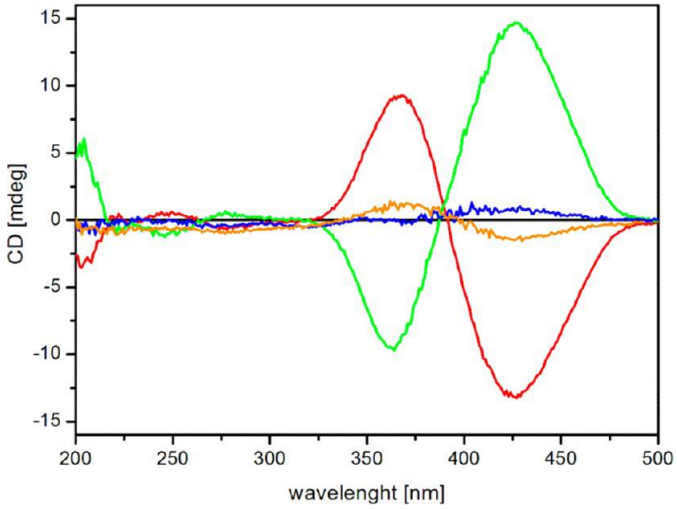

Figure 2.3.17. *Circular dichroism spectra of (2S,4R)-hybrid* ***2.3.28a*** *(blue), (2S,4S)-compound* ***2.3.28b*** *(red), (2R,4R)-compound* ***2.3.28c*** *(green), and a 1:1 mixture of* ***2.3.28b*** *and* ***2.3.28c*** *(orange).*[60]

In order to elucidate the structure of the chiral aggregates in the solid phase, AFM investigations were performed for enantiomer **2.3.28b** on muscovite mica. The formation of fibres could be detected. In some cases, the fibers coalesce to bundles, in which the original chirality is preserved (***Figure 2.3.18a***). Additionally, the left-handed chirality of the aggregates could be observed (***Figure 2.3.18b***).

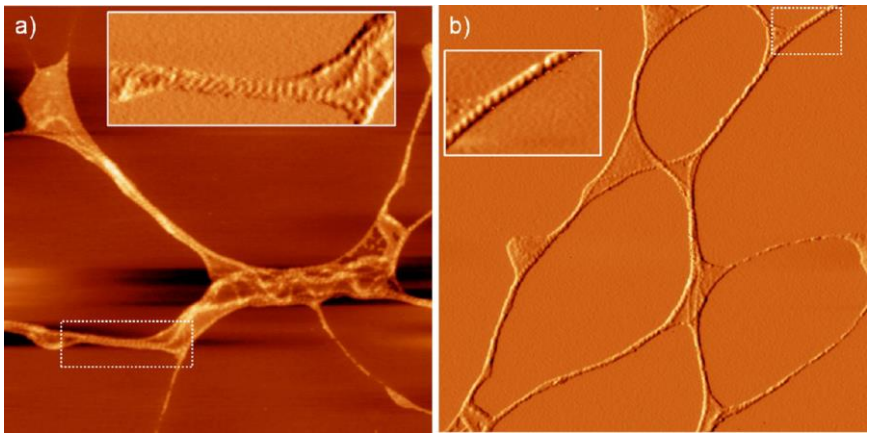

Figure 2.3.18. *AFM micrographs of superstructures of* ***2.3.28b*** *on mica substrates. (a) Topography image (2.3 × 2.3 μm); (b) Amplitude image (2.3 × 2.3 μm).*[60]

In this paragraph, the ability of combined semiconductor biomolecules, which self-assemble into well-defined suprastructures was shown. In summary, it can be sated that the research in this field is going into the right direction, but a deep understanding of the suprastructure formation of the hybrids in order to achieve the establishment of more universally valid design principles, is extremely important. Once this goal will be reached, we will be able to successfully proceed to the next step: the application of bio-hybrids in nanoelectronic devices.

References

[1] K. E. Drexler, *Engines of Creation, The Coming Era of Nanotechnology* Anchor Books, **1986**, 2.

[2] G. M. Whitesides, *Scientific American*, **1995**, *273*, 146–149.

[3] Y. Yamamoto, *Sci. Technol. Adv. Mater.* **2012**, *13*, 33001–33015.

[4] P. F. Damasceno, M. Engel, S. C. Glotzer, *Cond-Mat.Soft* **2012**.

[5] P. Gale, J. Steed in *Supramolecular Chemistry: From Molecules to Nanomaterials; Eds.:* P. Gale, J. Steed, Wiley-VCH, Weinheim, **2012**.

[6] A. P. Alivisatos, P. F. Barbara, A. W. Castelman, J. Chang, D. A. Dixon, M. L. Klein, G. L. McLend, J. S. Miller, M. A. Ratner, P. J. Rossky, S. I. Stupp, M. E. Thompson, *Adv. Mater.* **1998**, *10*, 1297–1394.

[7] S. I. Stupp, V. LeBonheur, K. Walker, L. S. Li, K. E. Huggins, M. Keser, A. Amstutz, *Science* **1997**, *276*, 384–389.

[8] J. D. Hartgerink, E. Beniash, S. I. Stupp, *Science* **2001**, *294*, 1684–1688.

[9] J.-M. Lehn, P. Ball in *The New Chemistry*, Ed.: N. Hall, Cambridge University Press, Cambridge, UK, **2000**.

[10] M. D. Hollingsworth, *Science* **2002**, *295*, 2410–2413.

[11] M. N. Jones, D. Chapman in *Micelles, Monolayers and Biomembranes*, Wiley-Liss, New York, **1995**.

[12] J.-W. Park, E. L. Thomas, *Polym. Prepr.* **2002**, *43*, 360–361.

[13] E. L. Thomas, *Science* **1999**, *286*, 1307–1308.

[14] F. J. M. Hoeben, P. Jonkheijm, E. W. Meijer, A. P. H. J. Schenning, *Chem. Rev.* **2005**, *105*, 1491–1546.

[15] J.-M. Lehn, *Science* **2002**, *295,* 2400–2403.

[16] L. J. Prins, D. N. Reinhoudt, P. Timmerman, *Angew. Chem., Int. Ed.* **2001**, *40*, 2382–2426.

[17] E. Moulin, J. J. Cid, N. Giuseppone, *Adv. Mater.* **2013**, *25*, 477–487.

[18] S. S. Babu, S. Prasanthkumar, A. Ajayaghosh, *Angew. Chem.* **2012**, *124*, 1800 – 1810; *Angew. Chem., Int. Ed.* **2012**, *51*, 1766–1776.

[19] M. Hasegawa, M. Iyoda, *Chem. Soc. Rev.* **2010**, *39*, 2420–2427.

[20] A. O. Patil, A. J. Heeger, F. Wudl, *Chem. Rev.* **1988**, *88*, 183–200.

[21] E. Busseron, Y. Ruff, E. Moulin, N. Giuseppone, *Nanoscale* **2013**, *5*, 7098–7140.

[22] a) E. Moulin, F. Niess, M. Maaloum, E. Buhler, I. Nyrkova, N. Giuseppone, *Angew. Chem.* **2010**, *122*, 7128–7132; *Angew. Chem., Int. Ed.* **2010**, *49*, 6974–6978; b) V. Faramarzi, F. Niess, E. Moulin, M. Maaloum, J. F. Dayen, J. B. Beaufrand, S. Zanettini, B. Doudin, N. Giuseppone, *Nat. Chem.* **2012**, *4*, 485–490; c) E. Moulin, F. Niess, G. Fuks, N. Jouault, E. Buhler, N. Giuseppone, *Nanoscale* **2012**, *4*, 6748–6751; d) N. Giuseppone, *Acc. Chem. Res.* **2012**, *45*, 2178–2188.

[23] S. Sengupta, D. Ebeling, S. Patwardhan, X. Zhang, H. von Berlepsch, C. Böttcher, V. Stepanenko, S. Uemura, C. Hentschel, H. Fuchs, F. C. Grozema, L. D. A. Siebbeles, A. R. Holzwarth, L. Chi, F. Würthner, *Angew. Chem.* **2012**, *124*, 6484–6488; *Angew. Chem., Int. Ed.* **2012**, *51*, 6378–6382.

[24] J. P. Hong, M. C. Um, S. R. Nam, J. I. Hong, S. Lee, *Chem. Commun.* **2009**, 310–312.

[25] J. H. Oh, H. W. Lee, S. Mannsfeld, R. M. Stoltenberg, E. Jung, Y. W. Jin, J. M. Kim, J. B. Yoo, Z. Bao, *Proc. Natl. Acad. Sci. U. S. A.* **2009**, *106*, 6065–6070.

[26] R. C. Savage, E. Orgiu, J. M. Mativetsky, W. Pisula, T. Schnitzler, C. L. Eversloh, C. Li, K. Müllen, P. Samorì, *Nanoscale* **2012**, *4*, 2387–2393.

[27] C. Giansante, G. Raffy, C. Schäfer, H. Rahma, M.-T. Kao, A. G. L. Olive, A. Del Guerzo, *J. Am. Chem. Soc.* **2011**, *133*, 316–325.

[28] C. A. Strassert, C. H. Chien, M. D. Galvez Lopez, D. Kourkoulos, D. Hertel, K. Meerholz, L. De Cola, *Angew. Chem.* **2011**, *123*, 976–980; *Angew. Chem., Int. Ed.* **2011**, *50*, 946–950.

[29] D. Gonzàlez-Rodrìguez, A. P. H. J. Schenning, *Chem. Mater.* **2011**, *23*, 310–325.

[30] G. Bottari, O. Trukhina, M. Ince, T. Torres, *Coord. Chem. Rev.* **2012**, *256*, 2453–2477.

[31] M. Wang, F. Wudl, *J. Mater. Chem.* **2012**, *22*, 24297–24314.

[32] F. Würthner, Z. Chen, F. J. M. Hoeben, P. Osswald, C. C. You, P. Jonkheijm, J. V. Herrikhuyzen, A. P. H. J. Schenning, P. P. A. van der Schoot, E. W. Meijer, E. H. A. Beckers, S. C. J. Meskers, R. A. J. Janssen, *J. Am. Chem. Soc.* **2004**, *126*, 10611–10618.

[33] T. Hasobe, S. Fukuzumi, P. V. Kamat, *Angew. Chem.* **2006**, *118*, 769–773; *Angew. Chem., Int. Ed.* **2006**, *45*, 755–759.

[34] K. Sugiyasu, S. I. Kawano, N. Fujita, S. Shinkai, *Chem. Mater.* **2008**, *20*, 2863–2865.

[35] A. A. Gorodetsky, C. Y. Chiu, T. Schiros, M. Palma, M. Cox, Z. Jia, W. Sattler, I. Kymissis, M. Steigerwald, C. Nuckolls, *Angew. Chem.* **2010**, *122*, 8081–8084; *Angew. Chem., Int. Ed.* **2010**, *49*, 7909–7912.

[36] a) Y. Hizume, K. Tashiro, R. Charvet, Y. Yamamoto, A. Saeki, S. Seki, T. Aida, *J. Am. Chem. Soc.* **2010**, *132*, 6628–6629; b) W. Zhang, W. Jin, T. Fukushima, A. Saeki, S. Seki, T. Aida, *Science* **2011**, *334*, 340–343.

[37] a) N. Sakai, R. Bhosale, D. Emery, J. Mareda, S. Matile, *J. Am. Chem. Soc.* **2010**, *132*, 6923–6925; b) R. Bhosale, A. Perez-Velasco, V. Ravikumar, R. S. K. Kishore, O. Kel, A. Gomez-Casado, P. Jonkheijm, J. Huskens, P. Maroni, M. Borkovec, T. Sawada, E. Vauthey, N. Sakai, S. Matile, *Angew. Chem.* **2009**, *121*, 6583–6586; *Angew. Chem., Int. Ed.* **2009**, *48*, 6461–6464; c) R. Bhosale, J. Míšek, N. Sakai, S. Matile, *Chem. Soc. Rev.* **2010**, *39*, 138–149.

[38] W. W. H. Wong, T. B. Singh, D. Vak, W. Pisula, C. Yan, X. Feng, E. L. Williams, K. L. Chan, Q. Mao, D. J. Jones, C.-Q. Ma, K. Müllen, P. Bäuerle, A. B. Holmes, *Adv. Funct. Mater.* **2010**, *20*, 927–938.

[39] W. W. H. Wong, C.-Q. Ma, W. Pisula, A. Mavrinskiy, X. Feng, H. Seyler, D. J. Jones, K. Müllen, P. Bäuerle, A. B. Holmes, *Chem. Eur. J.* **2011**, *17*, 5549–5560.

[40] W. W. H. Wong, J. Subbiah, S. R. Puniredd, B. Purushothaman, W. Pisula, N. Kirby, K. Müllen, D. J. Jones, A. B. Holmes, *J. Mater. Chem.* **2012**, *22*, 21131–21137.

[41] a) A. Ruiz-Carretero, T. Aytun, C. J. Bruns, C. J. Newcomb, W.-W. Tsai, S. I. Stupp, *J. Mater. Chem. A* **2013**, *1*, 11674–11681; b) S. I. Stupp, L. C. Palmer, *Chem. Mater.* **2014**, *26*, 507–518.

[42] D. Mandal, A. N. Shirazi, K. Parang, *Org. Biomol. Chem.* **2014**, *12*, 3544–3561.

[43] a) M. R. Ghadiri, J. R. Granja, R. A. Milligan, D. E. McRee, N. Khazanovich, *Nature* **1993**, *366*, 324–327; b) M. R. Ghadiri, J. R. Granja, L. K. Buehler, *Nature* **1994**, *369*, 301–304; c) J. D. Hartgerink, J. R. Granja, R. A. Milligan, M. R. Ghadiri, *J. Am. Chem. Soc.* **1996**, *118*, 443–450.

[44] H. Cui, M. J. Webber, S. I. Stupp, *Biopolymers* **2010**, *94*, 1–18.

[45] U. Khoe, Y. Yang, S. Zhang, *Langmuir* **2009**, *25*, 4111–4114.

[46] H. Cui, T. Muraoka, A. G. Cheetham, S. I. Stupp, *Nano Lett.* **2009**, *9*, 945–951.

[47] a) Y.-R. Yoon, Y.-B. Lim, E. Lee, M. Lee, *Chem. Commun.* **2008**, 1892–1894; b) Y.-B. Lim, E. Lee, M. Lee, *Angew. Chem., Int. Ed.* **2007**, *46*, 9011–9014.

[48] H. Sirringhaus, J. P. Brown, R. H. Friend, M. M. Nielsen, K. Beechgard, B. M. W. Langeveld-Voss, A. J. H. Spiering, R. A. J. Janssen, E. W. Meijer, P. Herwig, D. M. deLeeuw, *Nature* **1999**, *401*, 685–688.

[49] R. J. O. M. Hoofman, M. de Haas, L. D. A. Siebbeles, J. M. Warmann, *Nature* **1998**, *392*, 54–56.

[50] R. D. McCullough, *Adv. Mater.* **1998**, *10*, 93–116.

[51] A. P. H. J. Schenning, E. W. Meijer, *Chem. Commun.* **2005**, *26*, 3245–3258.

[52] W. Hamley, *Angew. Chem.* **2003**, *115*, 173 –1752; *Angew. Chem., Int. Ed.* **2003**, *42*, 1692–1712.

[53] A. Jatsch, E.-K. Schillinger, S. Schmid, P. Bäuerle, *J. Mater. Chem.* **2010**, *20*, 3563–3578.

[54] H.-A. Klok, A. Rösler, G. Götz, E. Mena-Osteritz, P. Bäuerle, *Org. Biomol. Chem.* **2004**, *2*, 3541–3544.

[55] R. Matmour, I. De Cat, S. J. George, W. Adriaens, P. Leclère, P. H. H. Bomans, N. A. J. M. Sommerdijk, J. C. Gielen, P. C. M. Christianen, J. T. Heldens, J. C. M. Van Hest, D. W. P. M. Löwik, S. De Feyter, E. W. Meijer , A. P. H. J. Schenning, *J. Am. Chem. Soc.* **2008**, *130*, 14576–14583.

[56] E.-K. Schillinger, E. Mena-Osteritz, J. Hentschel, H. G. Börner, P. Bäuerle, *Adv. Mater.* **2009**, *21*, 1562–1567.

[57] R. J. Kumar, J. M. MacDonald, T. B. Singh, L. J. Waddington, A. B. Holmes, *J. Am. Chem. Soc.* **2011**, *133*, 8564–8573.

[58] a) R. Marty, R. Szilluweit, A. Sánchez-Ferrer, S. Bolisetty, J. Adamcik, R. Mezzenga, E.-C. Spitzner, M. Feifer, S. N. Steinmann, C. Corminboeuf, H. Frauenrath, *ASC Nano* **2013**, *7*, 8498–8508; b) L. Tian, R. Szilluweit, R. Marty, L. Bertschi, M. Zerson, E.-C. Spitzner, R. Magerle, H. Frauenrath, *Chem. Sci.* **2012**, *3*, 1512–1521.

[59] S. K. M. Nalluri, C. Berdugo, N. Javid, P. W. J. M. Frederix, R. V. Ulijn, *Angew. Chem.* **2014**, *126*, 5992–5997; *Angew. Chem., Int. Ed.* **2014**, *53*, 5882–5887.

[60] E.-K. Schillinger, M. Kümin, A. Digennaro, E. Mena-Osteritz, S. Schmid, H. Wennemers, P. Bäuerle, *Chem. Mater.* **2013**, *25*, 4511–4521.

Chapter 3

Own Work: Syntheses of Quaterthiophene-Proline Hybrids

3.1 Introduction

On the base of the overview given so far and the promising results related to hybrids **3.1a-c** (***Chart 3.1***), published by my former colleague Dr. E.-K. Schillinger,[1] I decided to focus my research on the further development of this molecule by doing diverse structural changes. These should allow the achievement of highly ordered self-assembled suprastructures, which could be finally tested as donor in solar cell devices.

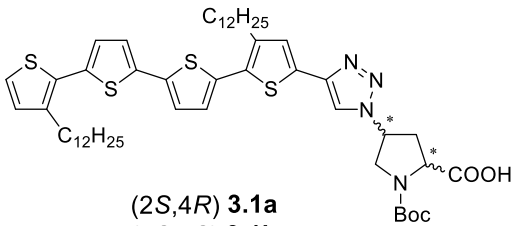

(2*S*,4*R*) **3.1a**
(2*S*,4*S*) **3.1b**
(2*R*,4*R*) **3.1c**

Chart 3.1. *Molecular structure of oligothiophene-proline hybrids* ***3.1a-c****.*

To do so, I designed the new molecules **3.2-3.9** (***Chart 3.2***) characterized by the same backbone of **3.1** (quaterthiophene-triazolylproline), but different functionalization on the π-conjugated core.

In general, the strategy followed for the synthesis of the target hybrids ends with a click reaction for all molecules. As already reported, click-reactions can be considered as a simple and effective method to introduce biological moieties into π-conjugated systems. Since the aim of my work is to prepare hybrids by connecting a quaterthiophene derivative with a monoproline, such an approach was thought to be the most suitable one.

Because 2-azidothiophene has been shown to be instable,[2,3] whereas acetylene groups are easier to introduce into thiophenic building blocks and azido amino acids are easier to synthesize or even commercially available, I decided to use an acetylene-quaterthiophene derivative and azido-proline as reactants in order to obtain target hybrids **3.2-3.9**.

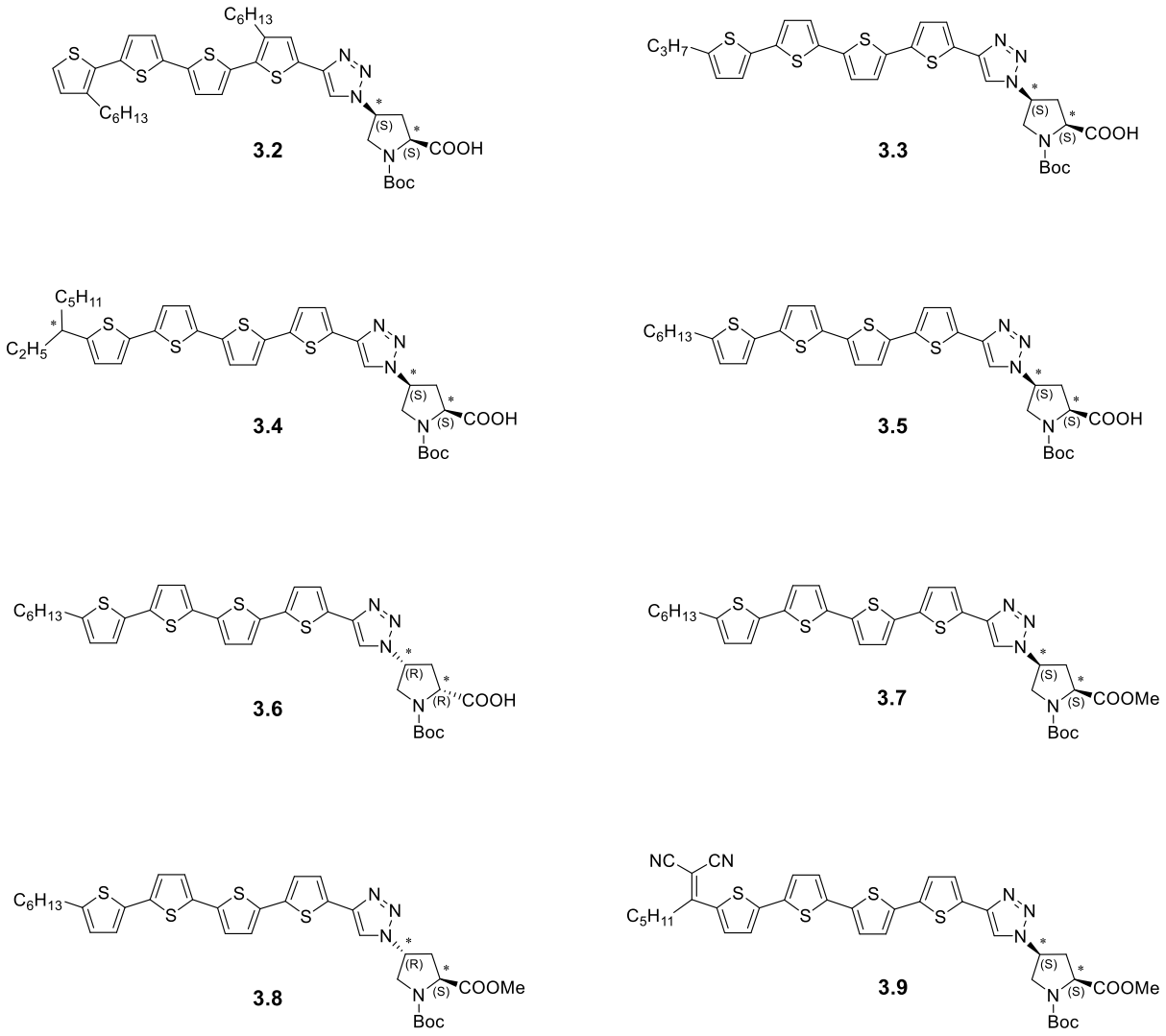

Chart 3.2. *Newly synthesized target quaterthiophene-proline hybrids* ***3.2-3.9****.*

In general, in order to verify the stereochemistry of the azidoproline, circular dichroism experiments were carried out before their implementation in the click reaction.

3.2 Synthesis of β-Substituted Quaterthiophene-Proline Hybrid 3.2

The first step in the synthetic plan was to replace the long lateral dodecyl chains of hybrid **3.1** by hexyl rests. This structural change should allow the π-conjugated backbones to get closer to each other during the self-assembling process. In fact, dodecyl chains are too long and prevent a closer π-π stacking of the quaterthiophenes in the supramolecuar structures.[4]

The synthesis of the new proline-quaterthiophene **3.2** follows the procedures shown by Schillinger and Jatsch in their PhD thesis.[5,6] A Kumada-type cross-coupling of 3-bromothiophene **3.10** and the Grignard reagent of 1-bromohexane **3.11** gave 3-hexylthiophene **3.12** in 68% yield.[7] After the bromination of **3.12** with *N*-bromosuccinimide in acetic acid,[8] 2-bromo-3-hexylthiophene **3.13** was isolated in 67% yield. Another Kumada coupling was carried out by reacting the Grignard reagent **3.14** and 5,5'-dibromo-2,2-bithiophene **3.15** to give the desired 3,3'''-dihexyl-2,2';5',2'';5'',2'''-quaterthiophene **3.16** in 66% yield (***Scheme 3.1***).[9]

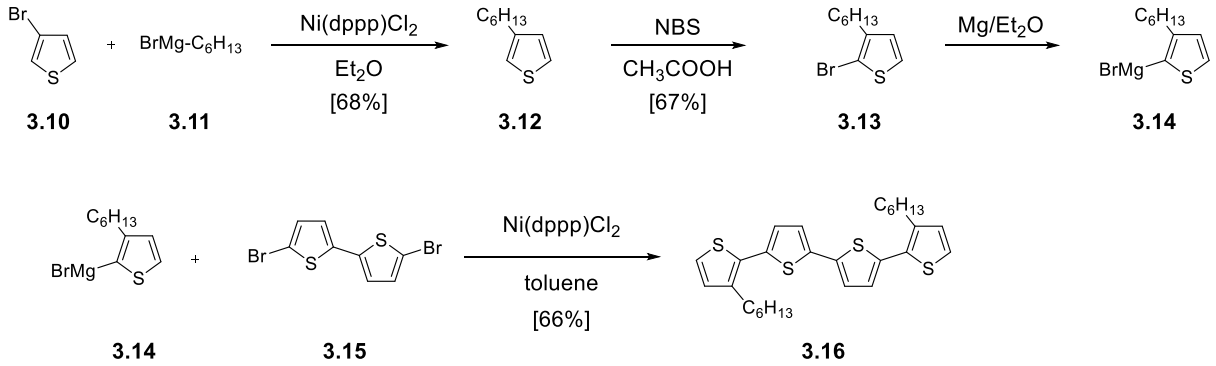

Scheme 3.1. *Synthesis of 3,3'''-dihexyl-2,2';5',2'';5'',2'''-quaterthiophene* ***3.16****.*

In order to synthesize a mono-functionalized quaterthiophene, a desymmetrization had to be performed. However, the regioselectivity of suitable reactions generally decreases with increasing chain length of the oligomer and leads to a mixture of all possible products.[10] Formylation of quaterthiophene **3.16** by Vilsmeier-Haack reaction yielded a mixture of corresponding monoaldehyde **3.17** and dialdehyde **3.18** (***Scheme 3.2***).

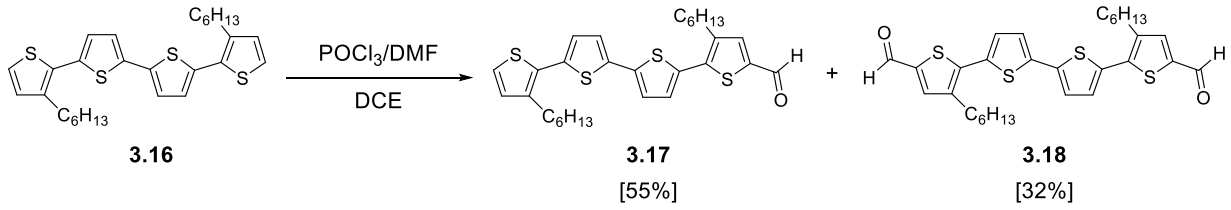

Scheme 3.2. *Vilsmeier-Haack formylation of* 3,3'''*-dihexyl-2,2';5',2'';5'',2'''-quaterthiophene* ***3.16****.*

The product mixture exhibited different polarities and could be purified by column chromatography giving *3,3'''*-dihexyl-2,2';5',2'';5'',2'''-quaterthiophene **3.17** in 55% yield and quaterthiophene dialdehyde in 32% yield (***Scheme 3.2***).[6]

Subsequent introduction of the ethynyl moiety into the oligothiophene core of **3.17** was achieved by Ohira-Bestmann homologation utilizing dimethyl-1-diazo-2-oxopropyl-phosphonate **3.21** in a Horner-Wadsworth-Emmons-type reaction (***Scheme 3.3***).[11-13] This method allows the introduction of ethynyl moieties under very mild reaction conditions without strong bases such as *n*-butyl lithium. The active reagent **3.21** was directly synthesized before performing the Ohira-Bestmann reaction. Its synthesis started by deprotonating the dimethyl-(2-oxopropyl)-phosphonate **3.19** at its C-H acidic position C_1 with sodium hydride (***Scheme 3.3***).[11,13] The formed anion of **3.19** reacted with tosylazide in an aza-group transfer according to *Regitz* to give dimethyl-1-diazo-2-oxopropyl-phosphonate **3.21**.[14]

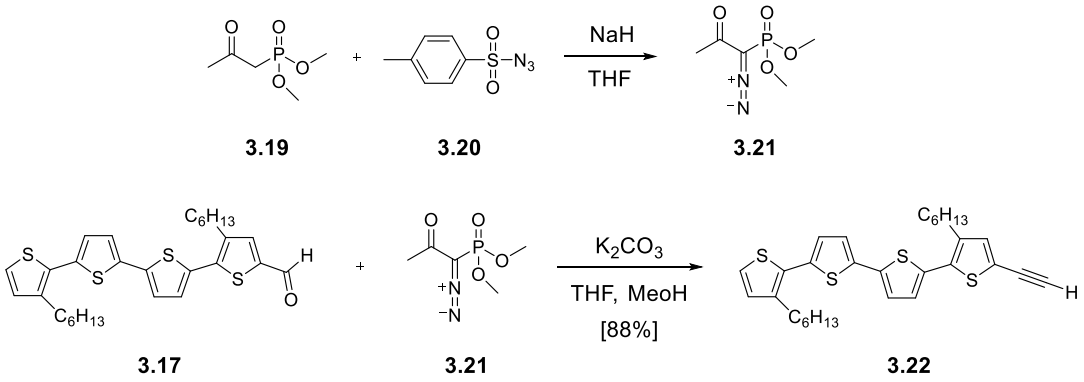

Scheme 3.3. *Synthesis of 3,3'''-dihexyl-5-ethynyl-2,2';5',2'';5'',2'''-quaterthiophene* ***3.22****.*

Ten equivalents of dimethyl-1-diazo-2-oxopropylphosphonate **3.21** were necessary for the Ohira-Bestmann reaction of 3,3'''-dihexyl-2,2';5',2'';5'',2'''-quaterthiophene-5-carbaldehyde **3.17**, because lower ratios led to poor conversion rates and longer reaction times. Therefore, in a one-pot procedure, a solution of **3.17** in dry THF was added to a mixture of phosphonate **3.21** and potassium carbonate in dry methanol. The reaction was stirred for 24 hours at room temperature and the crude product was purified by column chromatography to yield 88% of 3,3'''-dihexyl-5-ethynyl-2,2';5',2'';5'',2'''-quaterthiophene **3.22**.[6]

Proline-quaterthiophene hybrid **3.2** was synthesized via click reaction of 3,3'''-dihexyl-5-ethynyl-2,2';5',2'';5'',2'''-quaterthiophene **3.22** and the commercially available (2*S*, 4*S*)-azido proline cyclohexyl ammonium salt **3.23** (***Scheme 3.4***). Therefore, (2*S*, 4*S*)-azido proline cyclohexylammonium salt was added to a solution of ethynyl quaterthiophene **3.22,** tetrakis(acetonitrile)copper(I) and elemental copper powder in a dry mixture of THF-dichloromethane. The Cu(I) complex is not used as a catalyst

here, but in stoichiometric amounts due to the possible complex formation of Cu(I) by the carboxylic acid group. Oligothiophene **3.2** was isolated in 90% yield.

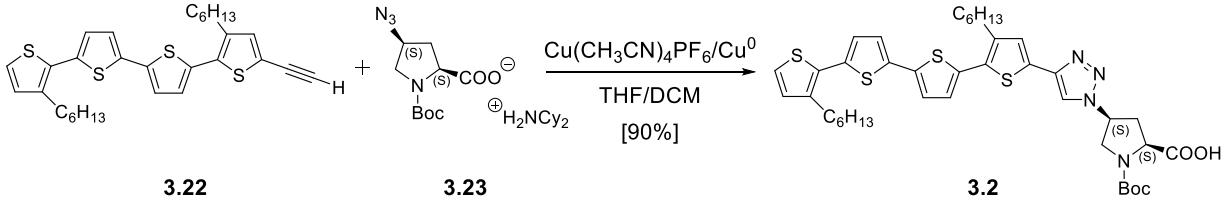

3.22 **3.23** **3.2**

Scheme 3.4. *Synthesis of proline-quaterthiophene hybrid* ***3.2****.*

The formation of the desired proline-quaterthiophene hybrid **3.2** was confirmed by ^{1}H-NMR spectroscopy (***Figure 3.1***).

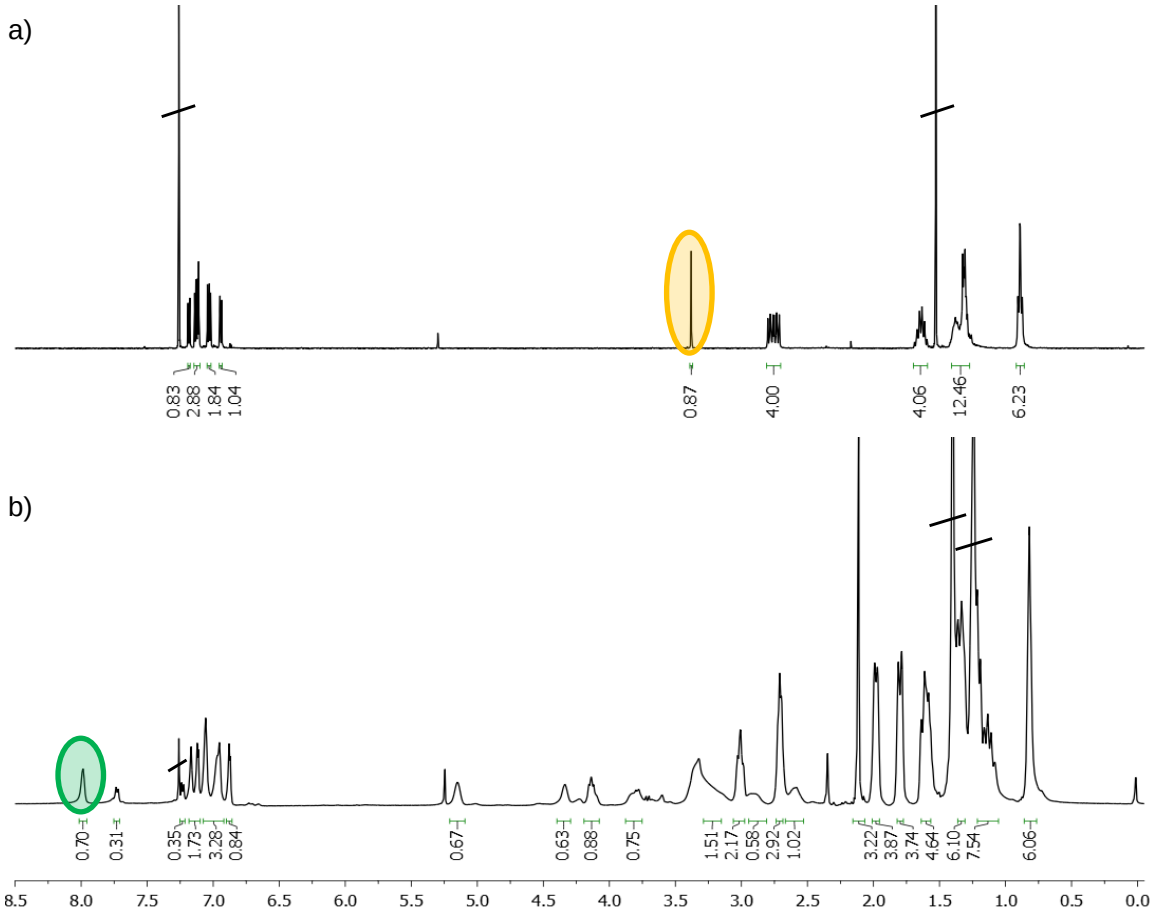

Figure 3.1. Comparison of a *^{1}H-NMR spectrum of a) 3,3'''-dihexyl-5-ethynyl-2,2';5',2'';5'',2'''-quaterthiophene* ***3.22*** *and b)* proline-quaterthiophene hybrid **3.2** measured in $CDCl_3$, 400 MHz.

By comparison of the ^{1}H-NMR spectra of 3,3'''-dihexyl-5-ethynyl-2,2';5',2'';5'',2'''-quaterthiophene **3.22** (***Figure 3.1***,***a***) and proline-quaterthiophene **3.2** (***Figure 3.1***,***b***), it was observed that the singlet related to the ethynyl function at 3.38 ppm (**orange**) disappeared after the click reaction and a singlet appeared instead at 7.98 ppm (**green**) characteristic for the triazole moiety.

Purity of hybrid **3.2** was verified with high resolution mass spectrometry (HRMS-MALDI). Only one peak could be detected and it matches with the mass calculated for hybrid **3.2** (**Figure 3.2**).

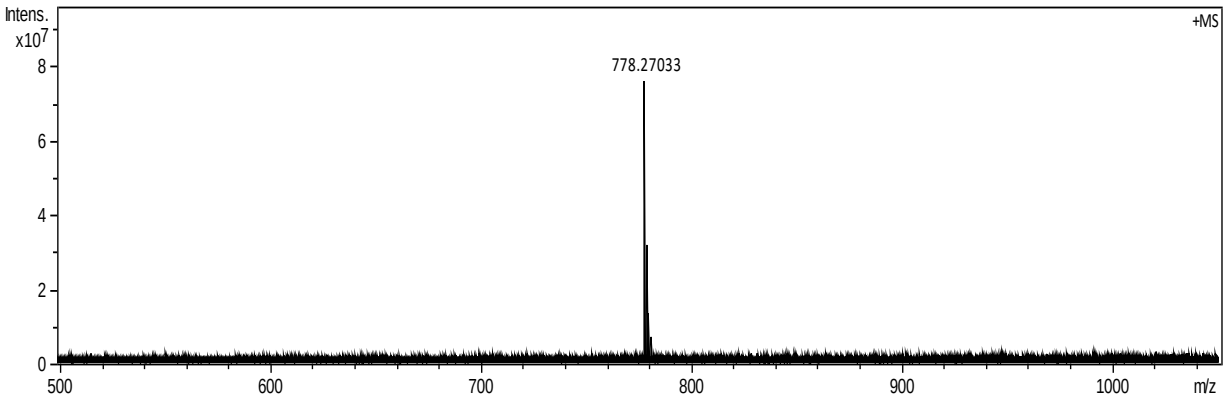

Figure 3.2. *HRMS (MALDI, (DCTB)) spectrum of proline-quaterthiophene hybrid* ***3.2****.*

3.3 Synthesis of α-Substituted Quaterthiophene-Proline Hybrids 3.3-3.9

To further improve the amphiphilic character of the quaterthiophene-proline hybrid, an ulterior step was to remove the lateral hexyl chains and to introduce diverse alkyl moieties at the 5'''-position of the quaterthiophene. Additionally, this modification was thought in order to prevent the oxidation of the oligothiophene at this position.

*3.3.1 Quaterthiophene-Proline Hybrid **3.3***

The first α-substituted quaterthiophene-proline hybrid synthesized was 5'''-propyl-2,2';5',2'';5'',2'''-quaterthiophene-proline **3.3** (***Chart 3.3***).

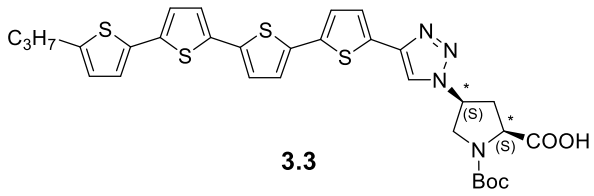

3.3

Chart 3.3. *Molecular structure of new 5-ethynyl-5'''-propyl-2,2';5',2'';5'',2'''-quaterthiophene-proline hybrid* ***3.3****.*

The choice of a propyl chain as substituent in 5'''-position was guided by the need to reach a better π-π stacking distance between quaterthiophenes in the self-organization process.

The synthetic strategy employed for the synthesis of target hybrid **3.3** is similar to the one shown for hybrid **3.2**; but, instead of utilizing Kumada-type cross-coupling reactions for the synthesis of the quaterthiophene core, Stille-type cross-coupling reactions were implemented. Firstly, a Stille cross-coupling reaction was carried out between stannyl **3.25** and 2-iodothiophene **3.26** in dry DMF and in the presence of tetrakis(triphenylphosphine)- palladium(0) as catalyst in order to obtain 5-propyl-2,2'-bithiophene **3.27** in 86% yield (***Scheme 3.5***).[15]

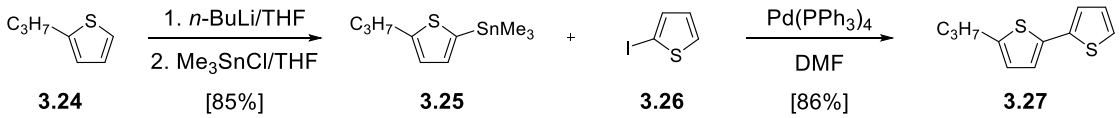

3.24 [85%] **3.25** **3.26** [86%] **3.27**

Scheme 3.5. *Synthesis of 5-propyl-2,2'-bithiophene* ***3.27****.*

Subsequent Stille reaction of stannyl **3.28** and 5-bromo-2,2′-bithiophene **3.29** allowed the isolation of 5'''-propyl-2,2';5',2'';5'',2'''-quaterthiophene **3.30** in 85% yield (***Scheme 3.6***).

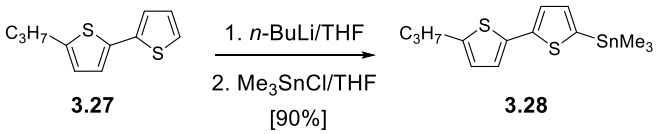

3.27 **3.28**

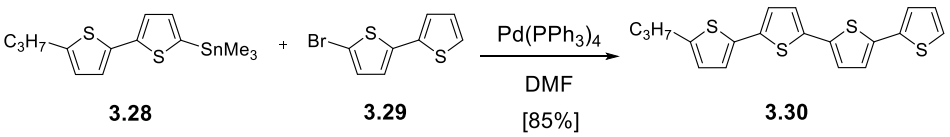

3.28 **3.29** **3.30**

Scheme 3.6. *Synthesis of 5''''-propyl-2,2';5',2'';5'',2'''-quaterthiophene* ***3.30****.*

5-Ethynyl-5'''-propyl-2,2';5',2'';5'',2'''-quaterthiophene **3.32** was gained after Vilsmeier-Haack reaction of 5'''-propyl-2,2';5',2'';5'',2'''-quaterthiophene **3.30** and following Ohira-Bestmann reaction of aldehyde **3.31** (***Scheme 3.7***).

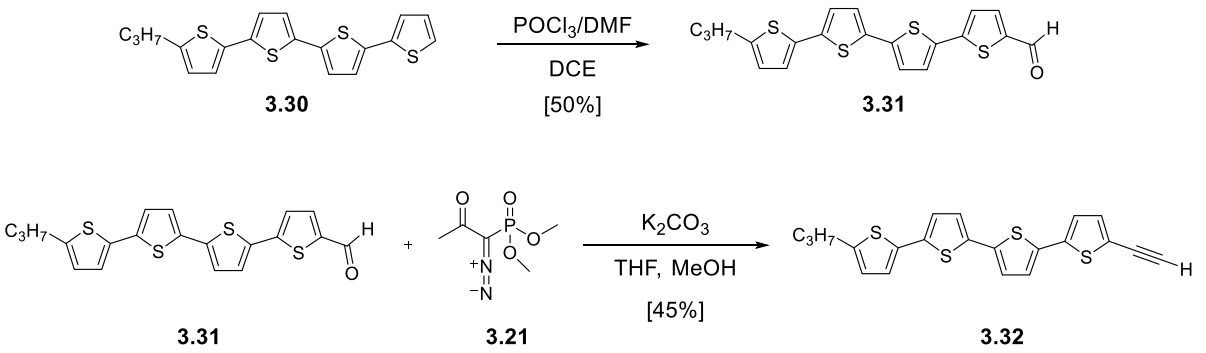

Scheme 3.7. *Synthesis of 5-ethynyl-5'''-propyl-2,2';5',2'';5'',2'''-quaterthiophene* ***3.32****.*

In both reactions, the yield of the isolated quaterthiophenes was mediocre. Concerning the Vilsmeier-Haack reaction, the reason could be the incomplete hydrolysis of the iminium salt, which was formed during the reaction, whereas the low yield of quaterthiophene **3.32** was caused by polymerization of the ethynyl functionality, when the solvent was removed under vacuum at 40 °C.

Quaterthiophenes **3.30**, **3.31**, and **3.32** are new molecules, which are not known in literature and they were completely analytically characterized.

The new 5'''-propyl-2,2';5',2'';5'',2'''-quaterthiophene-proline **3.3** was then synthesized via click reaction and obtained in 30% yield (***Scheme 3.8***). Because of its low solubility, 5-ethynyl-5'''-propyl-2,2';5',2'';5'',2'''-quaterthiophene **3.32** could not be brought entirely in solution and consequently it could not completely react. This could explain the low yield of quaterthiophene-proline hybrid **3.3**. This problem could not be overcome by rising the reaction temperature. In fact, high temperatures are not allowed during click chemistry, otherwise the 1,4-regioselectivity would be lost and a mixture of 1,4- and 1,5-regioisomers would be obtained instead.[16]

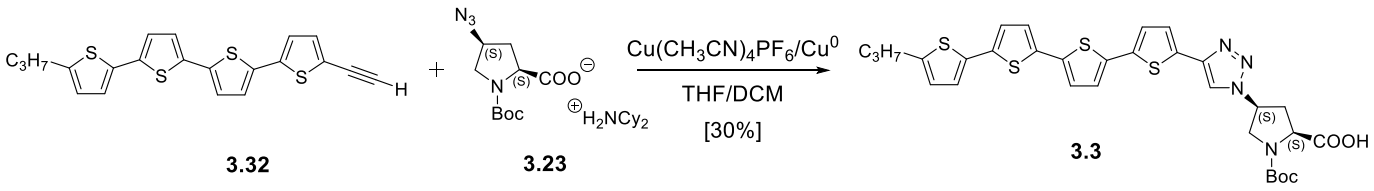

Scheme 3.8. *Synthesis of 5'''-propyl-2,2';5',2'';5'',2'''-quaterthiophene-proline* ***3.3****.*

Because of the extremely low solubility of the target proline-quaterthiophene **3.3**, it was not possible to record a well resolved ^{1}H-NMR spectrum. In order to prove the formation of the new molecule and its purity, HRMS-MALDI was carried out (***Figure 3.3***).

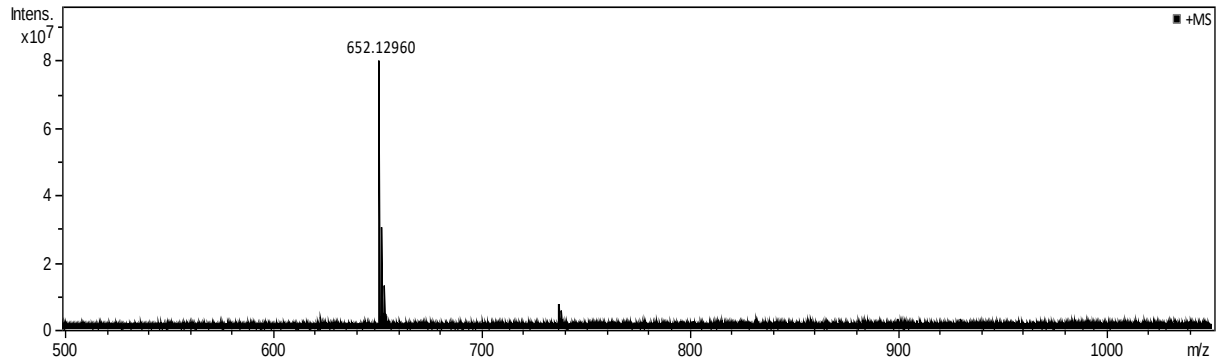

Figure 3.3. *HRMS (MALDI, DCTB) spectrum of proline-quaterthiophene hybrid* ***3.3****.*

3.3.2 Quaterthiophene-Proline Hybrid ***3.4***

In order to solve the solubility problem faced in the case of 5'''-propyl-2,2';5',2'';5'',2'''-quaterthiophene-proline **3.3**, it was thought to replace the propyl chain by the branched ethylhexyl moiety. In this respect, the new 5'''-(2-ethylhexyl)-2,2';5',2'';5'',2'''-quaterthiophene-proline hybrid **3.4** was synthesized (***Chart 3.4***).

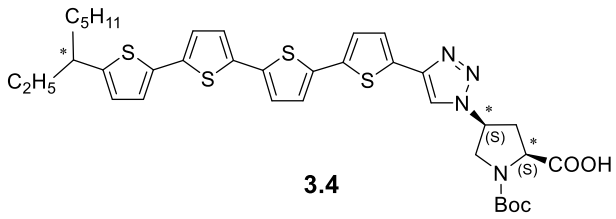

3.4

Chart 3.4. *Molecular structure of the new 5'''-(2-ethylhexyl)-2,2';5',2'';5'',2'''-quaterthiophene-proline hybrid* ***3.4****.*

The synthetic strategy planned to gain quaterthiophene-proline hybrid **3.4** proceeded slightly differently to the one previously shown in order to achieve higher yield.

First of all, 2-(2-ethylhexyl)-thiophene **3.34** was synthesized by reacting thiophene **3.33** and the commercially available racemic mixture of 1-bromo-2-ethylhexane (***Scheme 3.9***). [17] In parallel, **3.37** was synthesized following a standard procedure established in our group: the starting material 2,2'-bithiophene **3.36** was treated with

1 equivalent of $Hg(OAc)_2$; subsequently, iodine was added to yield a mixture of 5-iodo-2,2'-bithiophene **3.37**(48%), corresponding diiodo bithiophene **3.38** (50%), and starting material **3.36** (1%) (***Scheme 3.9***).[18] Because the by-products exhibited the same polarity as the desired bithiophene **3.37**, crystallization in *n*-hexane was preferred in order to separate bithiophenes **3.37** and **3.38**.

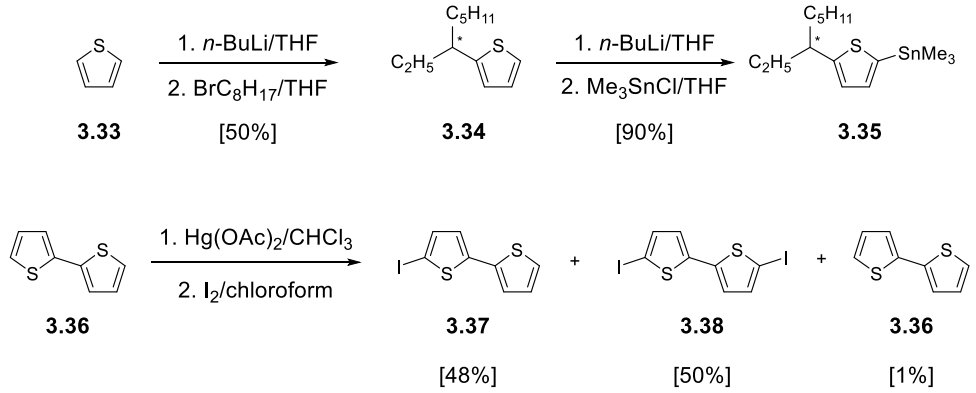

Scheme 3.9. *Synthesis of stannyl **3.35** and 5-iodo-2,2'-bithiophene **3.37**.*

In order to obtain 5'''-(2-ethylhexyl)-2,2';5',2'';5'',2'''-quaterthiophene **3.42** two Stille cross-coupling reactions were performed. Firstly, 5-iodo-2,2'-bithiophene **3.37** and stannyl **3.35** were reacted to yield 5''-(2-ethylhexyl)-2,2';5',2''-terthiophene **3.39** in 49% (***Scheme 3.10***).[19] Subsequently, Stille cross-coupling reaction of 5-bromo-5''-(2-ethylhexyl)-2,2';5',2''-terthiophene **3.40** and stannyl **3.41** gave 5'''-(2-ethylhexyl)-2,2';5',2'';5'',2'''-quaterthiophene **3.42** in 85% yield (***Scheme 3.10***).

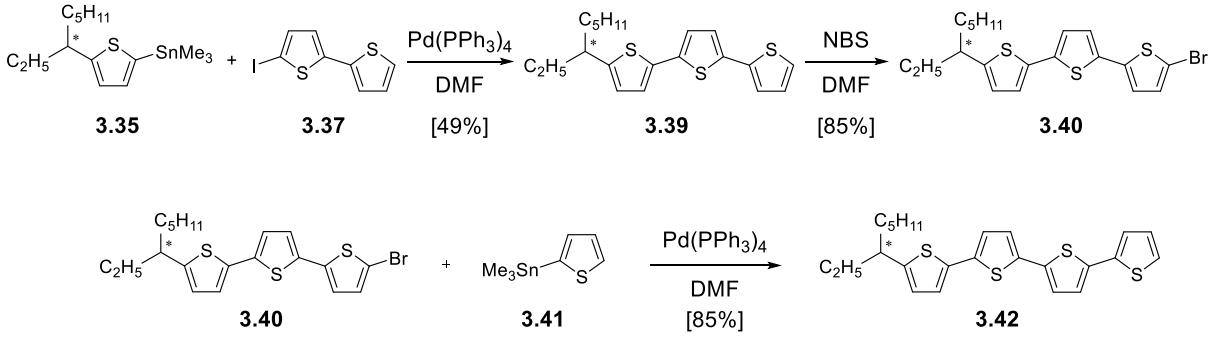

Scheme 3.10. *Synthesis of 5'''-(2-ethylhexyl)-2,2';5',2'';5'',2'''-quaterthiophene **3.42**.*

Instead of the usual combination of Vilsmeier-Haack and Ohira-Bestmann reactions, a new approach was necessary in order to obtain the more stable trimethylsilyl (TMS)-protected ethynyl quaterthiophene **3.45**, which is not known in literature.

5'''-(2-Ethylhexyl)-2,2';5',2'';5'',2'''-quaterthiophene **3.42** was reacted with N-bromosuccinimide to yield 92% of 5-bromo-5'''-(2-ethylhexyl)-2,2';5',2'';5'',2'''-quaterthiophene **3.43** (***Scheme 3.11***). Subsequent introduction of trimethylsilyl acetylene to quaterthiophene **3.43** was carried out via Sonogashira cross-coupling reaction: trimethylsilyl acetylene **3.44** was added to a solution of 5-bromo-5'''-(2-ethylhexyl)-2,2';5',2'';5'',2'''-quaterthiophene **3.43**, $Pd(PPh_3)_2Cl_2$, and CuI to give 5-([trimethylsilyl]ethynyl)-5'''-(2-ethylhexyl)-2,2';5',2'';5'',2'''-quaterthiophene **3.45** in 75% yield (***Scheme 3.11***).

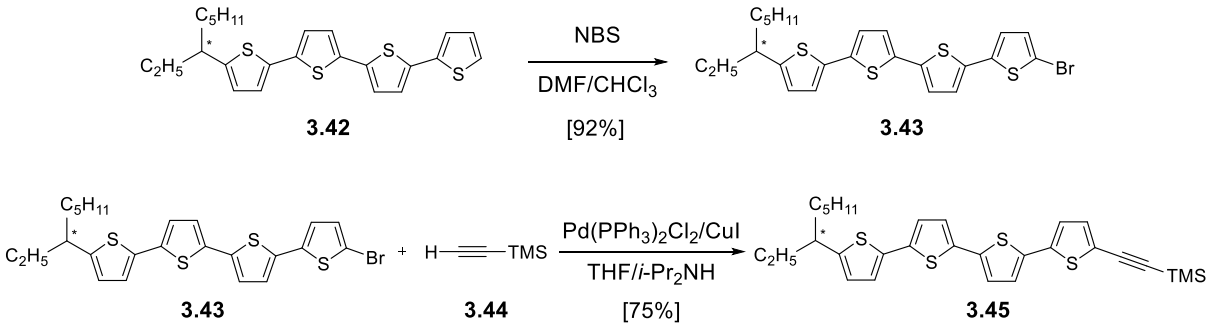

Scheme 3.11. *Synthesis of 5-([trimethylsilyl]ethynyl)-5'''-(2-ethylhexyl)-2,2';5',2'';5'',2'''-quaterthiophene* ***3.45****.*

The new quaterthiophene-proline hybrid **3.4** was synthesized via click reaction (***Scheme 3.12***). Potassium fluoride is first needed to cleave off the TMS-protecting group *in situ*. Subsequently, the reaction proceeds as always in the presence of *N*-Boc–cis-4-azido-L-proline (dicyclohexylammonium)salt **3.23**, copper powder, and tetrakis(acetonitrile) copper(I) hexafluorophosphate to give quaterthiophene-proline hybrid **3.4** in 90% yield (***Scheme 3.12***). Methanol was added to the solution in order to dissolve potassium fluoride.

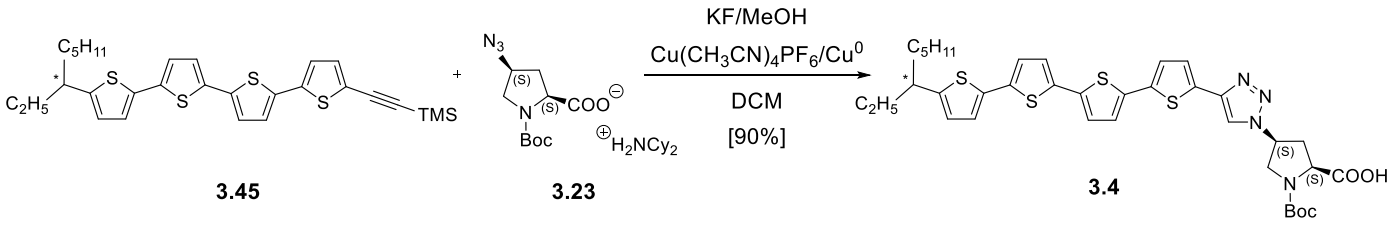

Scheme 3.12. *Synthesis of 5'''-(2-ethylhexyl)-2,2';5',2'';5'',2'''-quaterthiophene -proline* ***3.4****.*

The success of the click-reaction could be followed easily by ^{1}H-NMR spectroscopy. In fact, by comparing the ^{1}H-NMR spectra of 5-([trimethylsilyl]ethynyl)-5'''-(2-

ethylhexyl)-2,2';5',2'';5'',2'''-quaterthiophene **3.45** (**Figure 3.4a**) and of proline-quaterthiophene hybrid **3.4** (**Figure 3.4b**), it is evident that the peak at 0.24 ppm representative for the TMS-group (**turquoise**) disappears after the click reaction and the singlet characteristic for the trizole moiety appears at 8.29 ppm (**green**) (***Figure 3.4***). Due to the enhanced solubility of proline-quaterthiophene **3.4**, achieved by introducing the branched ethylhexyl chain as substutuient, recording of a well-resolved NMR-spectrum was possible.

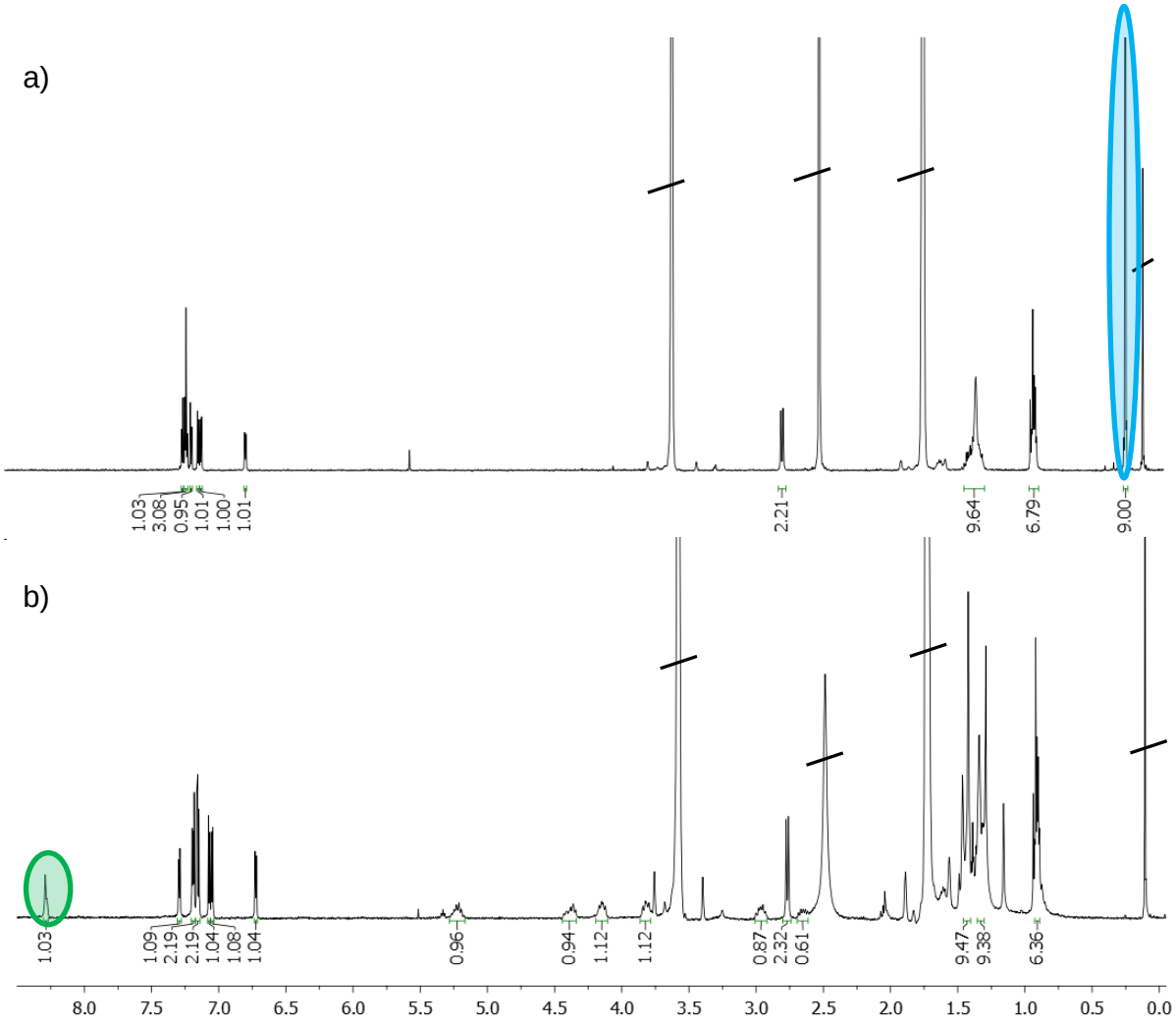

Figure 3.4. *Comparison between ^{1}H-NMR spectra of a) 5-([trimethylsilyl]ethynyl)-5'''-(2-ethylhexyl)-2,2';5',2'';5'',2'''-quaterthiophene **3.45** and b) proline-quaterthiophene hybrid **3.4**, measured in THF-d_8, 400 MHz.*

Additionally, the purity of the new hybrid was further verified via HRMS-MALDI (***Figure 3.5***).

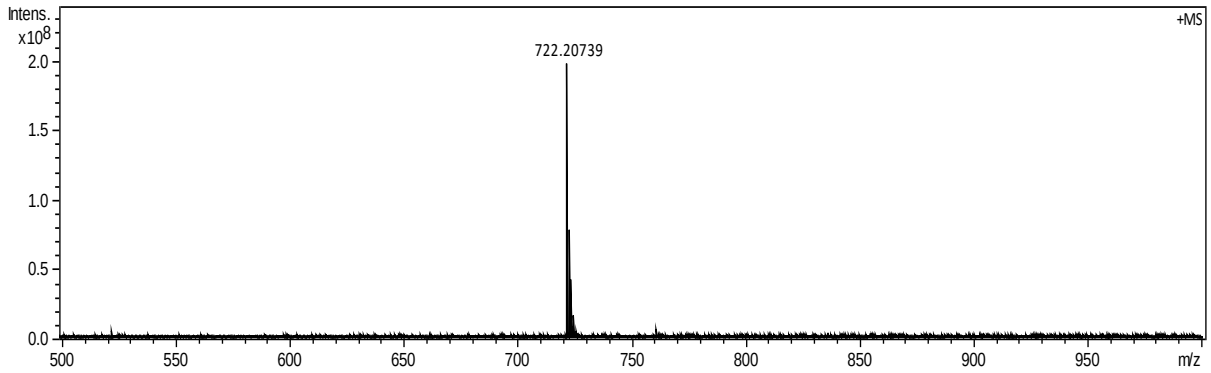

Figure 3.5. *HRMS-MALDI, (DCTB) spectrum of proline-quaterthiophene hybrid* ***3.4****.*

3.3.3 Quaterthiophene-Proline Hybrids ***3.5-3.8***

The new quaterthiophene-proline hybrid **3.5** was synthesized (***Chart 3.5***).

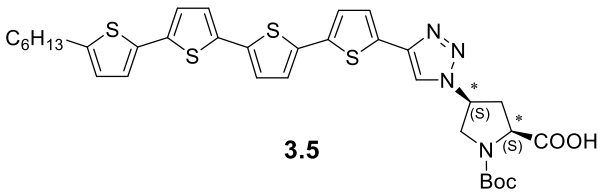

3.5

Chart 3.5. *Molecular structure of 5'''-hexyl-2,2';5',2'';5'',2'''-quaterthiophene-proline hybrid* ***3.5****.*

Here, the 2-ethylhexyl rest was replaced by hexyl chain. Even if the introduction of the branched substituent at the quaterthiophene 5'''-position enhanced the solubility of the hybrid, it brought a new complication: an additional stereocentre into the molecular structure. In fact, this new stereogenic centre could alo influence the self-assembling process of the new 4T which should be normally guided only by the biological moiety. For this reason, a linear hexyl chain was chosen instead which should be also long enough to preserve the gained solubility of the target quaterthiophene-proline. Additionally, (2*R*,4*R*)-proline-quaterthiophene **3.6** was synthesized in order to have a comparison of the optical and chiroptical properties of the enantiomeric pair (***Chart 3.6***).

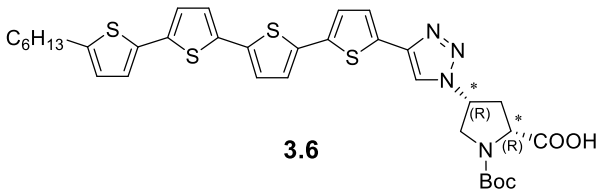

3.6

Chart 3.6. *Molecular structure of 5'''-hexyl-2,2';5',2'';5'',2'''- quaterthiophene-(2R,4R)-proline hybrid* ***3.6****.*

An ulterior change was the replacement of the free carboxylic acid with an ester function; in this way, the formation of H-bond interactions is prevented and the molecular solubility should further increase. In this respect, quaterthiophene-proline hybrids **3.7** and **3.8** were synthesized.

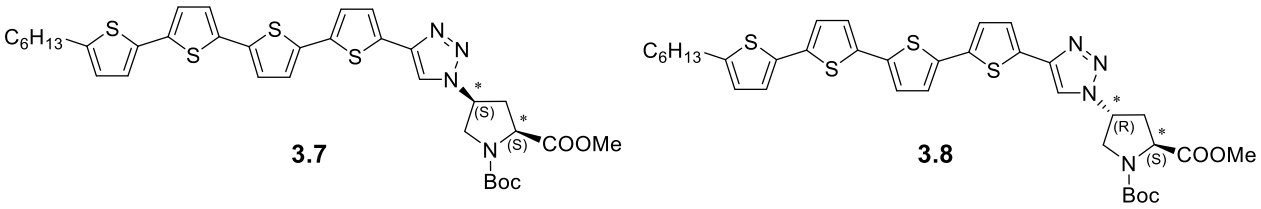

3.7 **3.8**

Chart 3.7. *Molecular structure of 5'''-hexyl-2,2';5',2'';5'',2'''-quaterthiophene-proline hybrids* ***3.7*** *and* ***3.8****.*

The same synthetic strategy was employed for hybrids **3.5-3.8**. Firstly, a Stille-type cross-coupling reaction of 5-bromo-2,2'-bithiophene **3.29**[20] and stannyl **3.47**[21] gave 5'''-hexyl-2,2';5',2'';5'',2'''- quaterthiophene **3.48** in 86% yield (***Scheme 3.13***). [22,23]

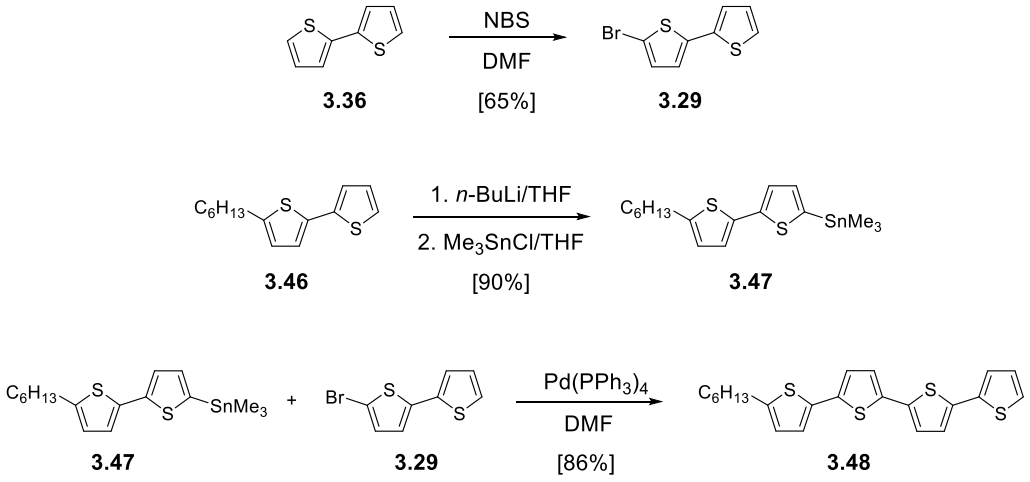

Scheme 3.13. *Synthesis of* 5'''*-hexyl-2,2';5',2'';5'',2'''*-quaterthiophene ***3.48****.*

Subsequently, Vilsmeier-Haack formylation of 5'''-hexyl-2,2';5',2'';5'',2'''-quaterthiophene **3.48** and subsequent Ohira-Bestmann reaction of aldehyde **3.49** and dimethyl-1-diazo-2-oxopropyl-phosphonate **3.21** allowed the isolation of 5-ethynyl-5'''-hexyl-2,2';5',2'';5'',2'''-quaterthiophene **3.50** in 70% yield (***Scheme 3.14***).[23,24]

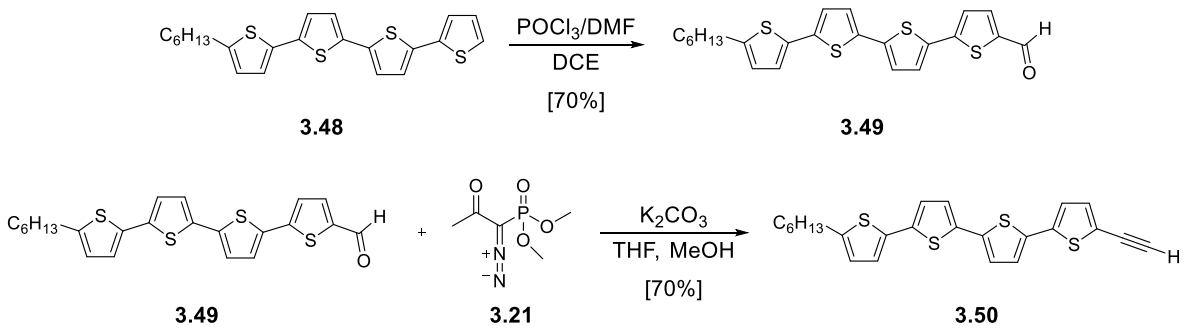

Scheme 3.14. *Synthesis of 5-ethynyl-5'''-hexyl-2,2';5',2'';5'',2'''-quaterthiophene* ***3.50****.*

Quaterthiophene-proline hybrid **3.5** was synthesized via click reaction of 5-ethynyl-5'''-hexyl-2,2';5',2'';5'',2'''-quaterthiophene **3.50** and *N*-Boc–cis-4-azido-L-proline (di-cyclohexylammonium)salt **3.23** and isolated in 90% yield (***Scheme 3.15***).

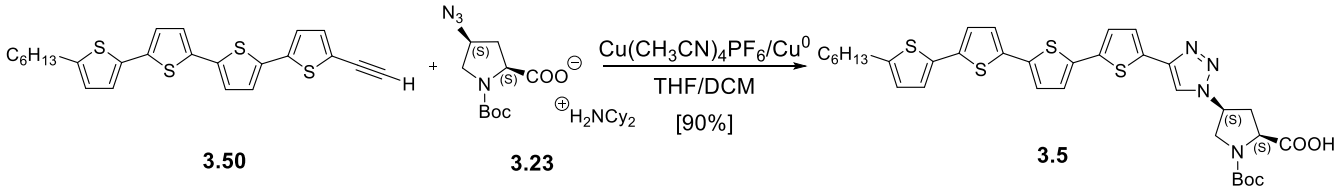

Scheme 3.15. *Synthesis of 5-ethynyl-5'''-hexyl-2,2';5',2'';5'',2'''-quaterthiophene-proline hybrid* ***3.5****.*

The enantiomeric (2*R*,4*R*)-proline quaterthiophene **3.6** was analogously synthetized. Here, (2*R*,4*R*)-azido proline **3.51** was implemented instead (***Scheme 3.16***). This biological moiety was synthesized by the Wennemers group at ETH Zürich.

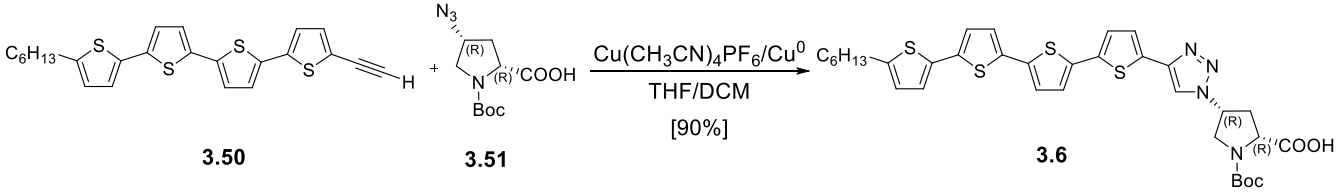

Scheme 3.16. *Synthesis of 5-ethynyl-5'''-hexyl-2,2';5',2'';5'',2'''-quaterthiophene-proline hybrid* ***3.6****.*

For the synthesis of methyl ester-substituted proline-quaterthiophene hybrid **3.7**, the azido-functionalized (2*S*, 2*S*)-proline ester had to be synthesized (**Scheme 3.17**).
The activation of the hydroxyl group was carried out via a mild Mitsunobu reaction of proline **3.52** with methane sulfonic acid and a subsequent S_N2 reaction with sodium azide gave the desired proline **3.54** in 85% yield.[23]

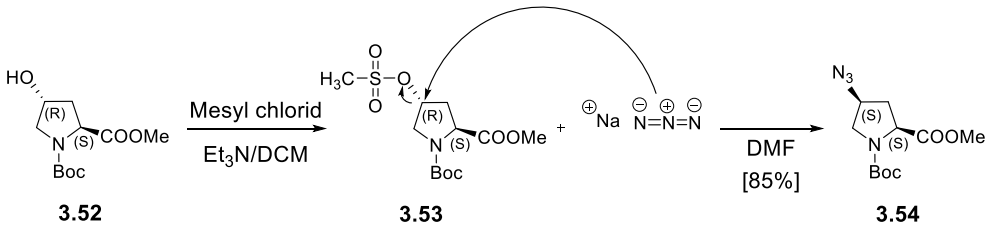

3.52 **3.53** **3.54**

Scheme 3.17. *Synthesis of (2S,2S)-proline ester **3.53**.*

The purity of (2*S*, 2*S*)-proline ester **3.54** was verified via ^{1}H-NMR spectroscopy. From the ^{1}H-NMR spectrum shown in ***Figure 3.6*** it was evident that the starting hydroxyl proline had completely reacted and that the desired azido proline **3.54** could be detected. The purity was additionally verified by electrospray ionisation **(**ESI) mass spectrometry.

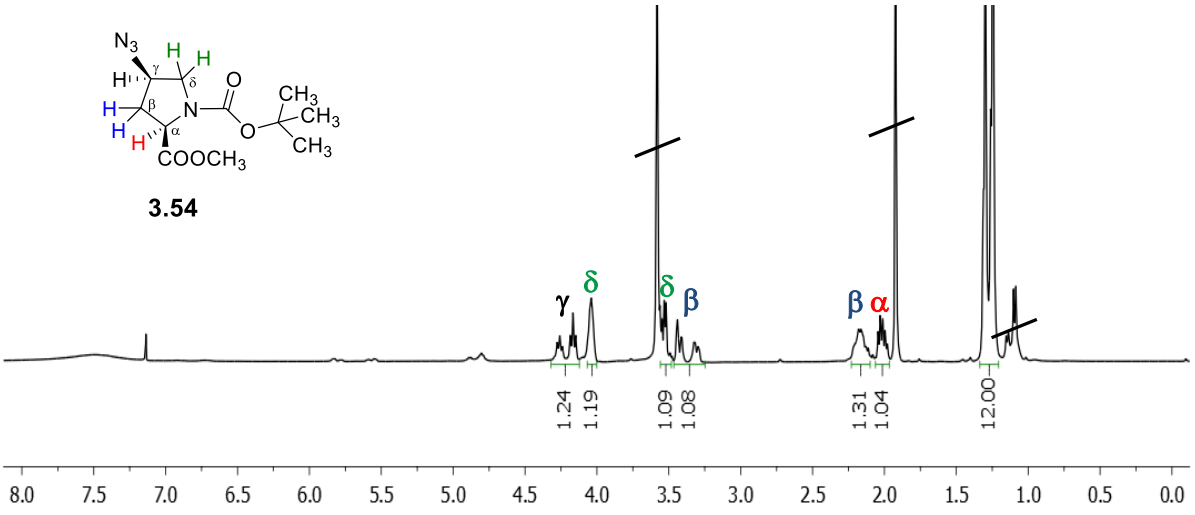

3.54

Figure 3.6. *^{1}H-NMR spectrum of methyl ester-azido proline **3.53**, measured in THF-d_8, 400 MHz.*

Subsequently, click reaction of 5-ethynyl-5'''-hexyl-2,2';5',2'';5'',2'''-quaterthiophene **3.50** and methyl ester azido proline **3.54** gave quaterthiophene-proline hybrid **3.7** (***Scheme 3.18***).

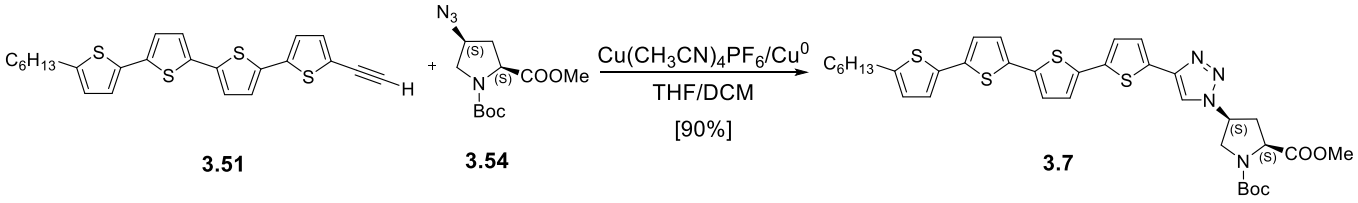

Scheme 3.18. *Synthesis of 5-ethynyl-5'''-hexyl-2,2';5',2'';5'',2'''-quaterthiophene-proline hybrid* ***3.7****.*

.

The isolation of diastereomer-(2*R*,4*S*)-proline quaterthiophene **3.8** was possible via click reaction of 5-ethynyl-5'''-hexyl-2,2';5',2'';5'',2'''-quaterthiophene **3.50** and (2*R*,4*S*)-azido proline **3.54** which was synthesized by the Wennemers group (***Scheme 3.19***).

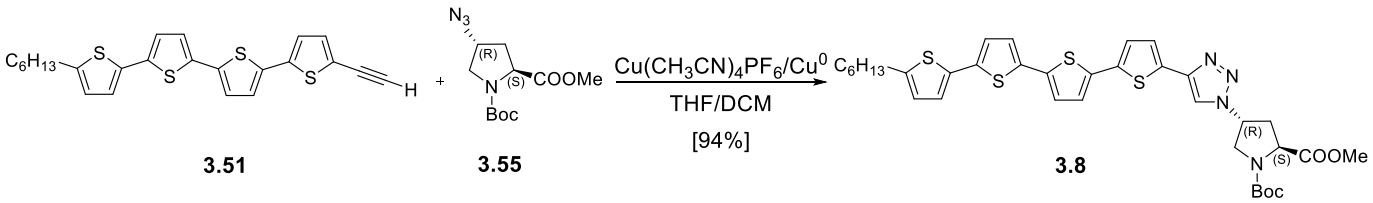

Scheme 3.19. *Synthesis of 5-ethynyl-5'''-hexyl-2,2';5',2'';5'',2'''-quaterthiophene-proline hybrid* ***3.8****.*

New quaterthiophene-proline hybrids **3.5**-**3.8** were fully characterized and, in particular, the presence of the methyl ester function could be proven by comparing the HRMS (MALDI) mass spectra of the free carboxylic acid proline-quaterthiophene **3.5** (***Figure 3.7****,* **black**) with methyl ester proline-quaterthiophene hybrid **3.7** (***Figure 3.7****,* ***red***).

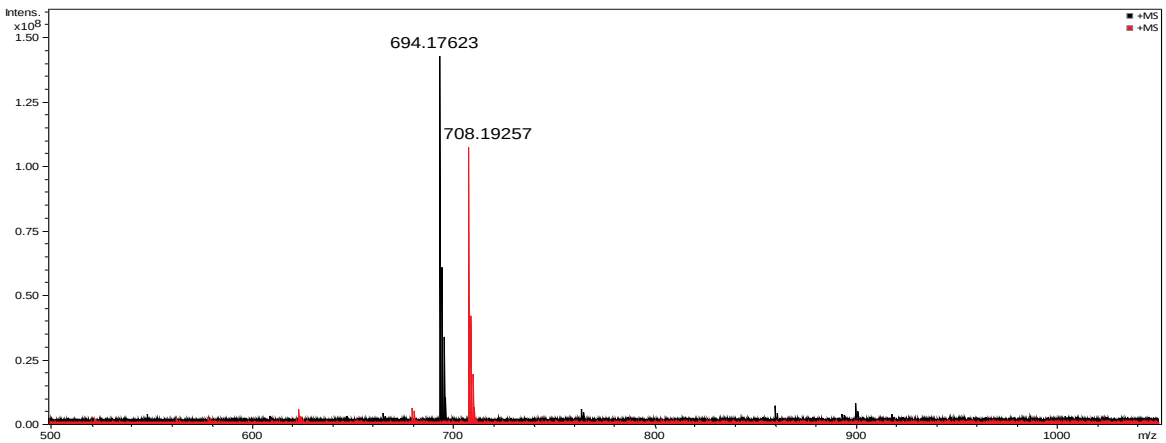

Figure 3.7. *Comparison between* HRMS *(MALDI, (DCTB))* spectra of *proline-quaterthiophene* ***3.5*** (**black**) and *of methyl ester proline-quaterthiophene hybrid* ***3.7*** (**red**)*.*

3.3.4 Quaterthiophene-Proline Hybrid ***3.9***

One of the aims of my research was the application of newly synthesized hybrids in organic solar cell devices. To do so, it was necessary to bring a new modification into the molecular structure: an acceptor function such as a dicyanovinyl group. For this reason, new DCV-quaterthiophene-proline hybrid **3.9** was synthesized (***Chart 3.8***).

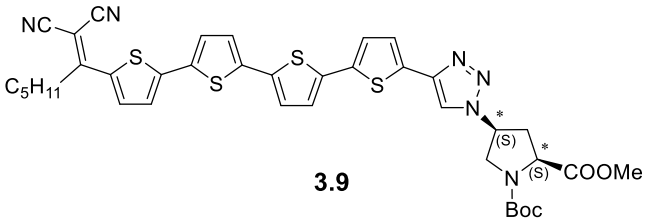

Chart 3.8. *Molecular structure of 2-{1-(5'''ethynyl-[2,2';5',2'';5'',2'''-quaterthien]-5-yl)-hexylidene}-propanedinitril-proline hybrid* ***3.9****.*

The procedure started with the synthesis of the Weinreb amide **3.56**: the reaction consisted in a nucleophilic acyl substitution, in which the acid chloride **3.56** was converted into *N,O*-dimethylhydroxyamide **3.57**, in the presence of *N*,*O*-dimethylhydroxylamine hydrochloride (***Scheme 3.20***).[25]

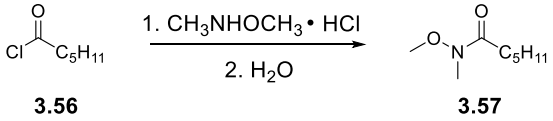

Scheme 3.20. *Synthesis of Weinreb amide* ***3.57****.*

After the reaction of Weinreb amide **3.57** and 2,2'-bithiophene **3.36**, and the subsequent bromination of the gained (2,2'-bithien-5-yl)-1-hexanone **3.59**, the new (5'-bromo-[2,2'-bithien)]-5-yl)-1-hexanone **3.60** was isolated in quantitative yield (***Scheme 3.21***). [26] Subsequent Knoevenagel condensation of hexanone **3.60** with malononitrile in the presence of ammonium acetate as a base, was carried out. New 2-[1-(5'-bromo[2, 2'-bithien]-5-yl)hexylidene]-propanedinitrile **3.62** could be isolated in 87% yield (***Scheme 3.21***).[26]

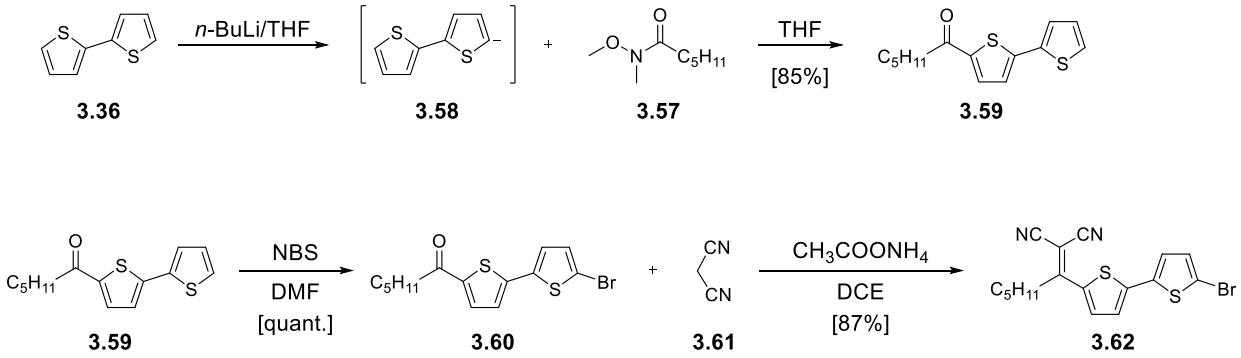

Scheme 3.21. *Synthesis of 2-[1-(5'-bromo[2, 2'-bithien]-5-yl)hexylidene]-propanedinitrile* ***3.61****.*

The formation of DCV-bithiophene **3.62** was checked via ^{1}H-NMR spectroscopy. By comparing the ^{1}H-NMR spectra of hexanone bithiophene **3.60** (***Figure 3.8***,***a***) and DCV-bithiophene **3.62** (***Figure 3.8***,***b***) a shift to higher ppm of the duplet characteristic for the proton at the 3,3'-position could be observed (***Figure 3.8***).

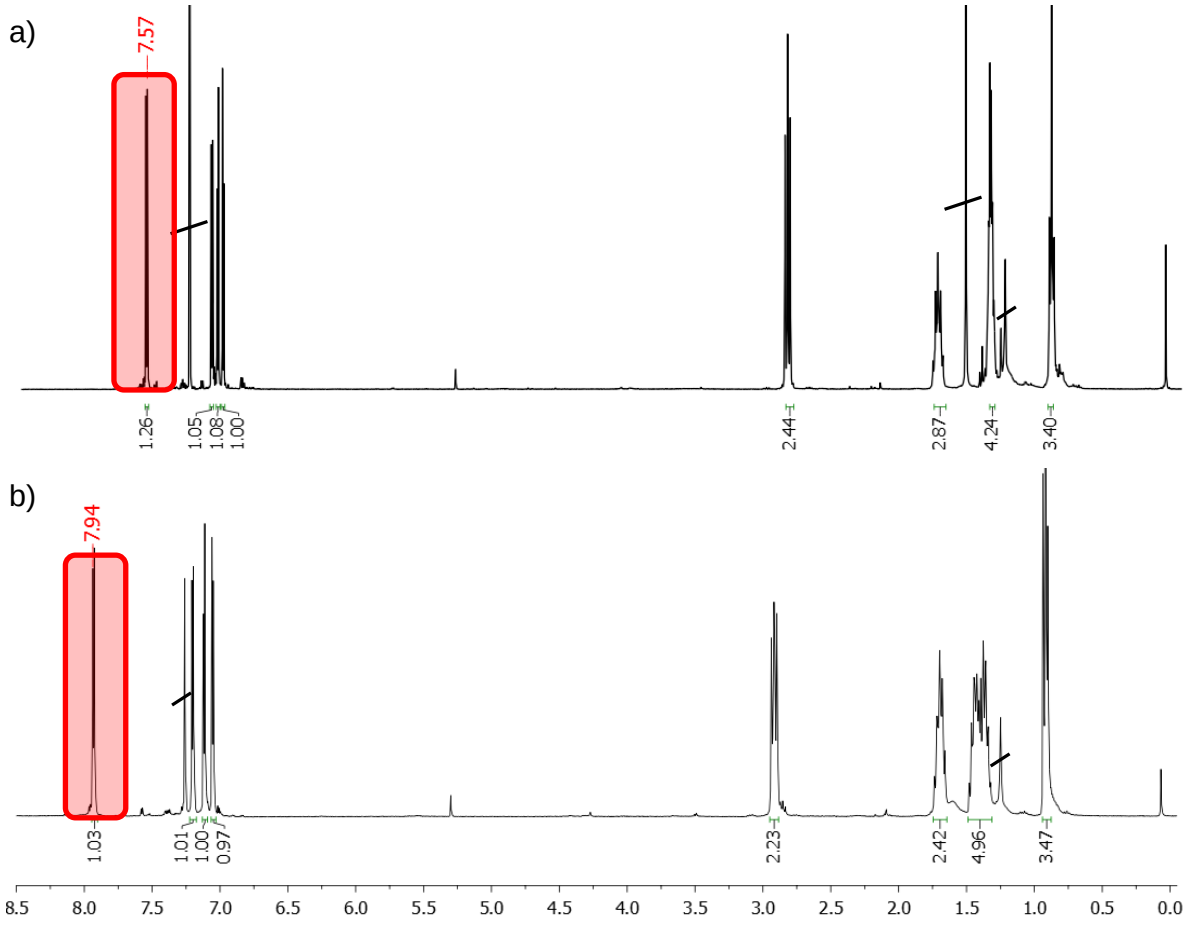

Figure 3.8. *Comparison between ^{1}H-NMR spectra of a) hexanone bithiophene* ***3.60*** *and b) DCV-bithiophene* ***3.62****, measured in $CDCl_3$, 400 MHz.*

In parallel, a Sonogashira cross-coupling reaction of 2,2'-bithiophene **3.36** and TMS-protected acetylene **3.44** gave ethynyl bithiophene **3.63** in 70% yield, which was subsequently stannylated to yield a mixture of TMS-protected bithiophene **3.64** and deprotected bithiophene **3.65** (***Scheme 3.22***).[27] The TMS group was partially cleaved off during the lithiation reaction. The mixture was used without further purification in the next step.

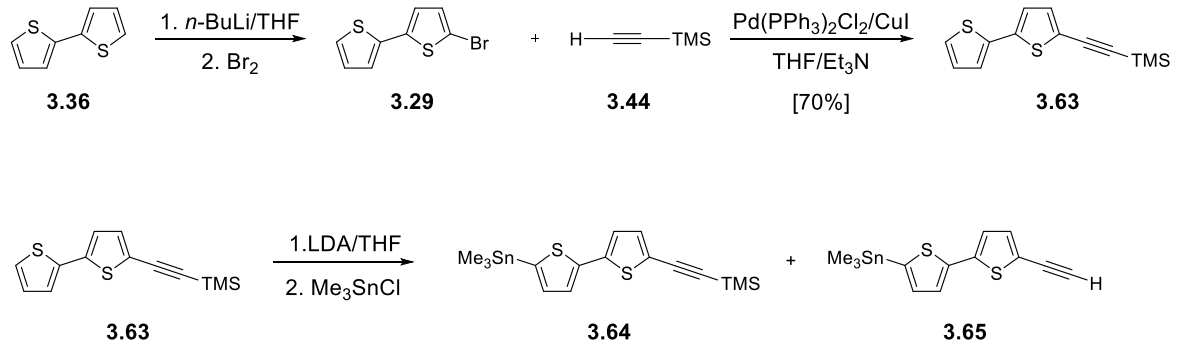

Scheme 3.22. *Synthesis of {5'-([trimethylsilyl]ethynyl)[2,2'-bithien]-5-yl}trimethyl-stannane* ***3.64****.*

A Stille cross-coupling reaction of 2-[1-(5'-bromo[2,2'-bithien]-5-yl)hexylidene]-propanedinitrile **3.62** and stannyl **3.64** was carried out in order to obtain TMS-protected 2-{1-(5'''-ethynyl-[2,2';5',2'';5'',2'''-quaterthien]-5-yl)-hexylidene}-propanedinitrile **3.66** (***Scheme 3.23***).

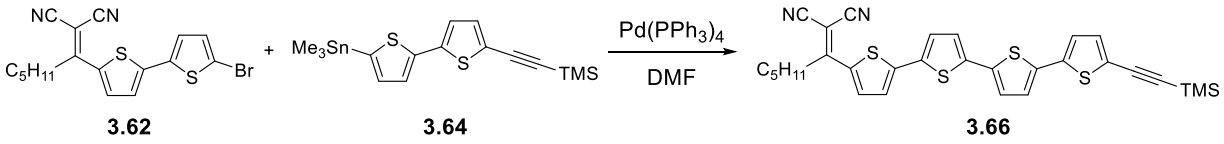

Scheme 3.23. *Synthesis of TMS-protected 2-{1-(5'''-ethynyl-[2,2';5',2'';5'',2'''-quaterthien]-5-yl)-hexylidene}-propanedinitrile* ***3.66****.*

Because this strategic procedure exhibited diverse problems, mainly due to the synthesis of stannyl **3.64**, an alternative synthetic path was instead implemented. A Stille-type cross-coupling reaction of stannyl bithiophene **3.67** and hexanoylbithiophene **3.60** yielded 83% of the desired hexanoylquaterthiophene **3.68** (***Scheme 3.24***).

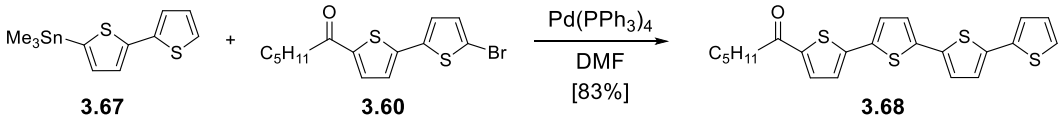

Scheme 3.24. *Synthesis of 1-(2,2';5',2'';5'',2'''-quaterthien-5-yl)-1-hexanone* ***3.68****.*

After bromination of hexanoylquaterthiophene **3.68** with NBS and subsequent Sonogashira cross-coupling reaction of the gained 1-(5'''-bromo-[2,2';5',2'';5'',2'''-quaterthien]-5-yl)-1-hexanone **3.69** and trimethylsilyl acetylene **3.44**, TMS-protected ethynyl quaterthiophene **3.70** was isolated in 72% yield (***Scheme 3.25***).

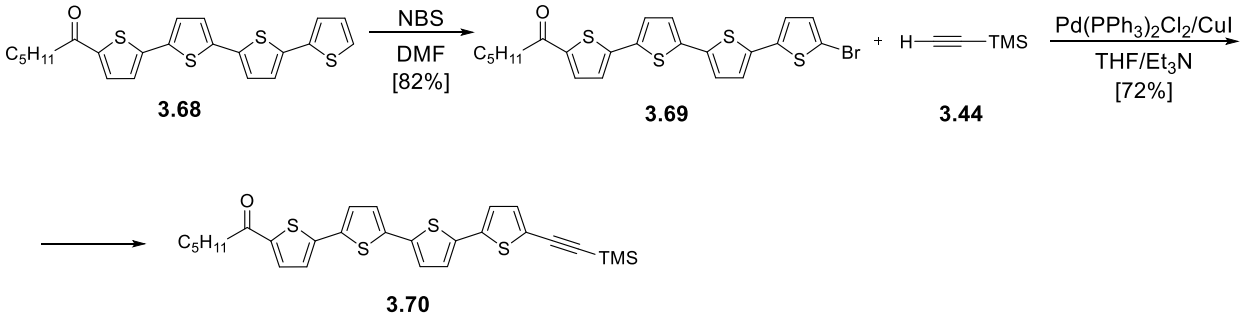

Scheme 3.25. *Synthesis of the TMS-protected ethynyl quaterthiophene* ***3.70****.*

Knoevenagel condensation of TMS-protected ethynyl quaterthiophene **3.70** and malononitrile in the presence of titanium isopropoxide as a Lewis acid gave the deprotected 2-{1-(5'''-ethynyl-[2,2';5',2'';5'',2'''-quaterthien]-5-yl)-hexylidene}-propane-dinitrile **3.71** in 75% yield (***Scheme 3.26***).[28] Titanium isopropoxide was needed for the activation of the low reactive keto group.

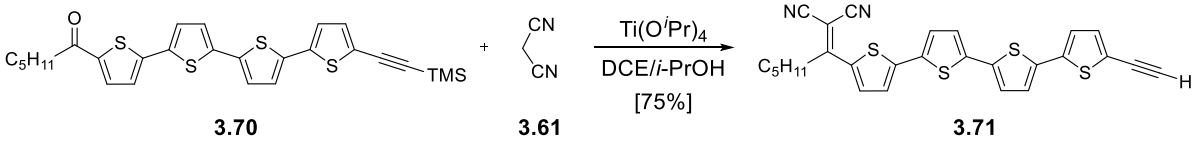

Scheme 3.26. *Synthesis of the 2-{1-(5'''-ethynyl-[2,2';5',2'';5'',2'''-quaterthien]-5-yl)-hexylidene}-propane-dinitrile* ***3.70****.*

DCV-quaterthiophene-proline hybrid **3.9** was synthesized via click reaction of (2*S*, 4*S*)-azido proline ester **3.54** and ethynyl quaterthiophene **3.71** (***Scheme 3.27***).

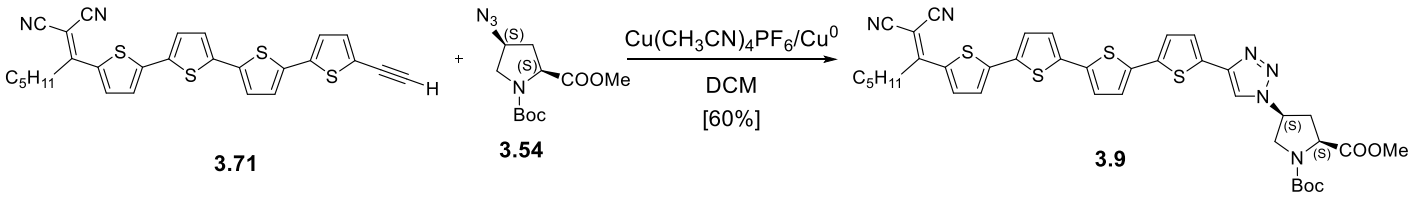

Scheme 3.27. *Synthesis of (4S)-1-tert-butoxycarbonyl-{2-[(1-[2,2';5',2'';5'',2'''-quaterthien]-5-yl)-hexylidene]-propanedinitrile}-1*H*-1,2,3-triazol-1yl}-proline* ***3.9****.*

Quaterthiophenes **3.68**-**3.71** and proline-quaterthiophene hybrid **3.9** are new and were fully characterized.

Because of the strong aggregation in solution of proline-quaterthiophene hybrid **3.9** in solution, the record of ^{1}H-NMR and ^{13}C-NMR spectra was not possible even at high temperature. The formation and purity of the new acceptor-donor-proline hybrid **3.9** could by verified by HRMS (MALDI) (**Figure 3.9**). The signal at 722 m/z has to be attributed to the presence of the starting material **3.70**.

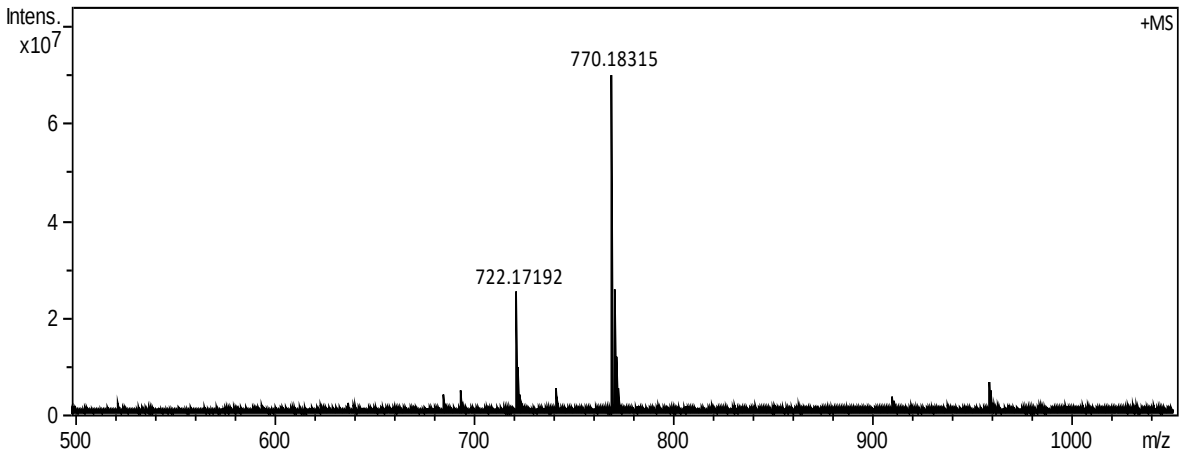

Figure 3.9. *HRMS (MALDI, (DCTB)) spectrum of 5-([trimethylsilyl]ethynyl)-5'''-(2-ethylhexyl)-2,2';5',2'';5'',2'''-quaterthiophene* ***3.9.***

3.4 Summary

In this chapter, the synthesis of a new series of quaterthiophene-proline hybrids was shown. The aim of my research was the synthesis of hybrids capable to self-organize in ordered supramolecular structures. To reach this purpose, it was firstly necessary to test diverse alkyl substituents in different positions (3,3'''- or 5'''-positions) of the quaterthiophene core (***Chart 3.8***).

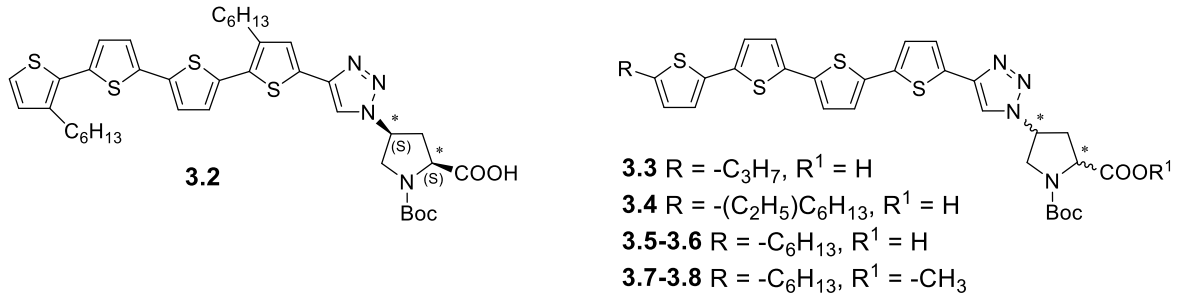

Chart 3.8. *Molecular structures of* 3,3'''*-alkyl substituted quaterthiophene-proline hybrid* ***3.2*** *and* 5'''-alkyl substituted *quaterthiophene-proline hybrids* ***3.3-3.8****.*

5'''-Hexyl-substituted quaterthiophene-proline hybrids **3.5-3.8** were judged as the best in term of combination of good solubility and self-assembly behaviour. This will be investigated in the next chapter.

Additionally, a new donor-acceptor was synthesized (***Chart 3.9***) in order to accomplish first tests in OSC devices.

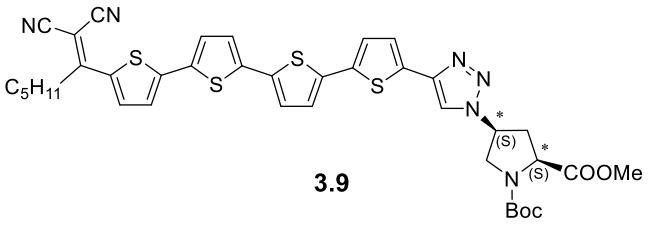

Chart 3.9. *Molecular structure of 2-{1-(5'''ethynyl-[2,2';5',2'';5'',2'''-quaterthien]-5-yl)-hexylidene}-propanedinitrile-proline hybrid* ***3.9****.*

References

[1] E.-K. Schillinger, M. Kümin, A. Digennaro, E. Mena-Osteritz, S. Schmid, H. Wennemers, P. Bäuerle, *Chem. Mater.* **2013**, *25*, 4511–4521.

[2] F. Valenti, P. Zanirato, *J. Chem. Soc., Perkin Trans. 2* **1999**, 623–627.

[3] D. Spinelli, P. Zanirato, *J. Chem. Soc., Perkin Trans. 2* **1993**, 1129–1133.

[4] R. Azumi, G. Götz, T. Debaerdemaeker, P. Bäuerle, *Chem.Eur. J.* **2000**, *6*, 735-744.

[5] E.-K. Schillinger, *PhD Thesis*, University of Ulm, **2010**.

[6] A. Jatsch, *PhD Thesis*, University of Ulm, **2010**.

[7] C. Van Pham, H. B. Mark Jr., H. Zimmer, *Synth. Commun.* **1986**, *16*, 689–696.

[8] D. J. Turner, R. Anémian, P. R. Mackie, D. C. Cupertino, S. G. Yeates, M. L. Turner, A. C. Spivey, *Org. Biomol. Chem.* **2007**, *5*, 1752–1763.

[9] H. Kanato , K Takimiya , T. Otsubo , Y. Aso , T. Nakamura , Y.Araki , O. Ito, *J. Org. Chem.* **2004**, *69*, 7183–7189.

[10] B. Nessakh, G. Horowitz, F. Gamier, F. Deloffre, P. Srivastava, A. Yassar, *J. Electroan. Chem.* **1995**, *399*, 97–103.

[11] S. Müller, B. Liepold, G. J. Roth, H. J. Bestmann, *Syntlett.* **1996**, 521–522.

[12] G. J. Roth, B. Liepold, S. G. Müller, H. J. Bestmann, *Synthesis* **2004**, 59–62.

[13] S. Ohira, *Synth. Commun.* **1989**, *19*, 561–564.

[14] M. Regitz *Ann.* **1964**, *676*, 101–109.

[15] M. Funahashi, J.-I. Hanna *Mol. Cryst. Liq. Cryst.* **2004**, *410*, 1–12.

[16] G. Molteni, A. Ponti, *Chem. Eur. J.* **2003**, *9*, 2770–2774.

[17] J.-Y. Li, C.-Y. Chen, C.-P. Lee, S.-C. Chen, T.-H. Lin, H.-H. Tsai, K.-C. Ho, C.-G. Wu, *Org. Lett.* **2010**, *12*, 5454–5457.

[18] B. R. Kim, E. J. Kim, G. H. Sung, J.-J. Kim, D.-S. Shin, S.-G. Lee, Y.-J. Yoon, *Eur. J. Org. Chem*. **2013**, 2788–2791.

[19] E. A. Kleymyuk, P. A. Troshin, E. A. Khakina,Y. N. Luponosov, Y. L. Moskvin, S. M. Peregudova, S. D. Babenko, T. Meyer-Friedrichsen, S. A. Ponomarenko, *Energy Environ. Sci.* **2010**, *3*, 1941–1948.

[20] J. P. Brand, J. Waserer, *Angew. Chem.* **2010**, *122*, 7462–7465; *Angew.Chem., Int. Ed.* **2010**, *49*, 7304–7307.

[21] K. Parab, K. Venkatasubbaiah, F. Jaekle, *J. Am. Chem. Soc.* **2006**, *128*, 12879-12885.

[22] Z. Hu, E. Reichmanis, *J. Polym. Sci. A Polym. Chem.* **2011***, 49,* 1155–1162*.*

[23] A. Digennaro, H. Wennemers, G. Joshi, S. Schmid, E. Mena-Osteritz, P. Bäuerle, *Chem. Commun.* **2013**, *49*, 10929–10931.

[24] M. Melucci, G. Barbarella, M. Zambianchi, M. Benzi, F. Biscarini, M. Cavallini, A. Bongini, S. Fabbroni, M. Mazzeo, M. Anni, G. Gigli, *Macromolecules* **2004**, *37*, 5692–5702.

[25] J. Verron, P. Malherbe, E. Prinssen, A. W. Thomas, N. Nock, R. Masciadri, *Tetrahedron Lett.* **2007**, *18*, 377–380.

[26] Q. Meng, J. Gao, R. Li, L. Jiang, C. Wang, H. Zhao, C. Liu, H. Li, W. Hu, *J. Mater. Chem.* **2009**, *19*, 1477–1482.

[27] M. Löbert, *PhD Thesis*, University of Ulm, **2014**.

[28] A. Mishra, C. Uhrich, E. Reinold, M. Pfeiffer, P. Bäuerle, *Adv. Energy Mater.* **2011**, *1*, 265–274.

Chapter 4

Own Work: Optical, Chiroptical, and Electrochemical Properties of Quaterthiophene-Proline Hybrids

4.1 Introduction

All proline-quaterthiophene hybrids synthesized so far were investigated with respect to their properties in absorption and emission in a “good solvent” such as THF, in which they are molecularly dissolved. Their electrochemical properties were examined using tetrabutylammonium hexafluorophosphae (TBAHFP) in dichloromethane as electrolyte.Furthermore, their self-assembly has been investigated by UV/Vis, fluorescence, and circular dichroism (CD) spectroscopy. The supramolecular structure formation was guided by titrating the oligomer containing THF solution with water. In all cases, the formation of suprastructures could be detected when the amount of water was higher than the amount of THF.

4.2 Optoelectronic Properties in the Dissolved State

*4.2.1 UV/Vis and Fluorescence Properties of Quaterthiophene-Proline Hybrids **3.2**-**3.5***

The optoelectronic properties of the *S*,*S*.quaterthiophene-proline hybrids **3.2**-**3.5** (***Chart 4.1***) were investigated with regard to structure–property relationships.

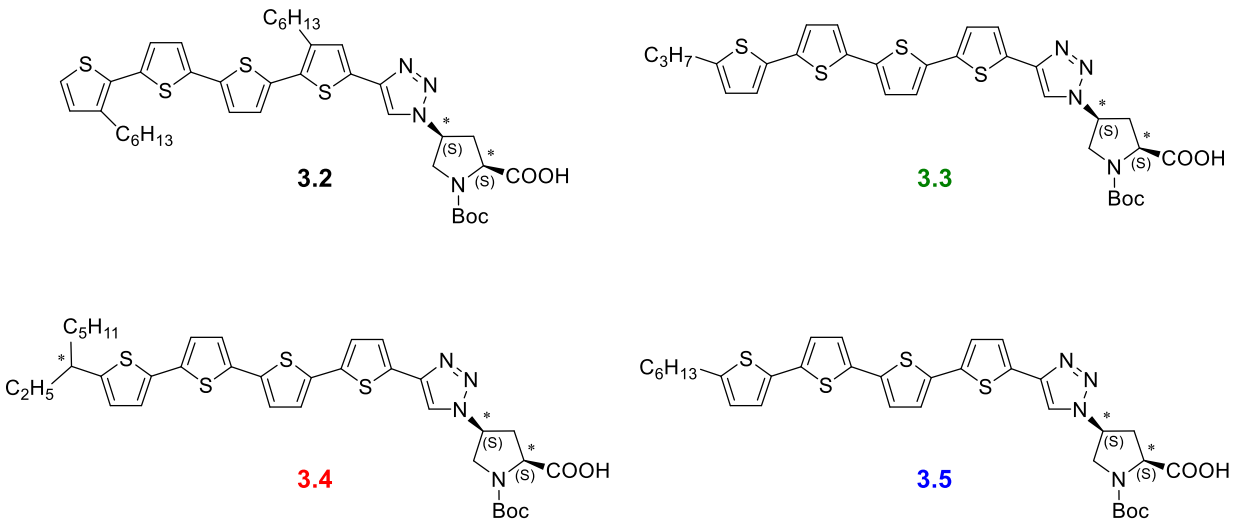

Chart 4.1. *Molecular structures of quaterthiophene-proline hybrids **3.2**-**3.5**.*

Going from 3,3’’’-dihexyl-substituted quaterthiophene **3.2** (λ_{max} = 392 nm) to 5’’’-alkyl quaterthiophene **3.4** and **3.5** (λ_{max} = 417 nm), a red-shift ($\Delta\lambda$= 25 nm) of the absorp-

tion maximum relative to the π-π* transition of the quaterthiophene moiety along the long axis of the molecule was observed (***Figure 4.1***). This bathochromic shift is a consequence of the better overlap of the π-π* orbitals of the α-alkyl-substituted molecules in comparison to the lateral-substituted ones. In fact, the suppression of the laterally hexyl chains allows the π-conjugated backbone to adopt a less distorted conformation. As further consequence, the molar extinction coefficient increases from 32000 L cm^{-1} mol^{-1} (**3.2**) to 37000 L cm^{-1} mol^{-1} (**3.4**, **3.5**). Another maximum can be observed at 260 nm. This band can be attributed to the absorption perpendicular to the long axis of the π-conjugated backbone and the absorption of the 1,2,3-triazole moiety.[1]

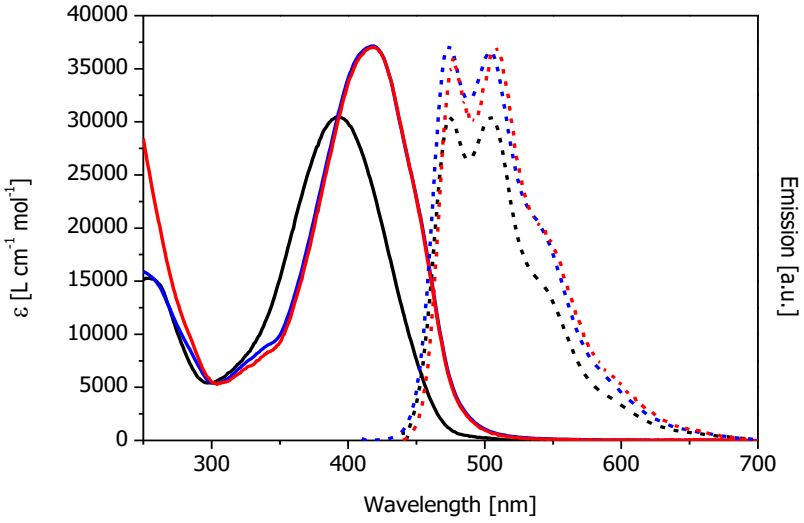

Figure 4.1. *Absorption ([c] = 10^{-5} M) and emission ([c] = 10^{-7} M, excitation at λ = 380 nm) spectra of (2S,4S)-proline quaterthiophene hybrids* ***3.2****,* ***3.4****, and* ***3.5*** *in THF.*

The emission spectra displayed a vibronic fine structure, which indicates rigidity of the π-conjugated backbone in the excited state due to the stronger quinoidal character of the quaterthiophene resulting in a planarization of the molecule. Emission maxima for quaterthiophene hybrids **3.2**, **3.4**, and **3.5** were located at λ_{max} = 474 nm, 476 nm and 476 nm each with a shoulder at 542 nm, 547 nm, and 541 nm (***Figure 4.1***). The vibronic transition from S_1 to S_0 (E_{00}) is not particularly affected by the presence of different substituents at diverse positions. This suggests a similar conformational geometry for S_1 for the three oligomers. On the contrary, the different substitution position influences the Stokes shift values. In fact, it is larger in case of 3,3'''-dihexyl-quaterthiophene-proline **3.2**. This indicates more significant structural differences in

the ground and in the first excited state in comparison to the α-substituted hybrids. By comparing the normalised absorption and emission spectra of 5'''-substituted quaterthiophene-proline hybrids **3.3**-**3.5**, it can be asserted that neither the optical properties nor the Stokes shift values of the three oligomers are particularly influenced by the diverse alkyl chains (***Figure 4.2***).

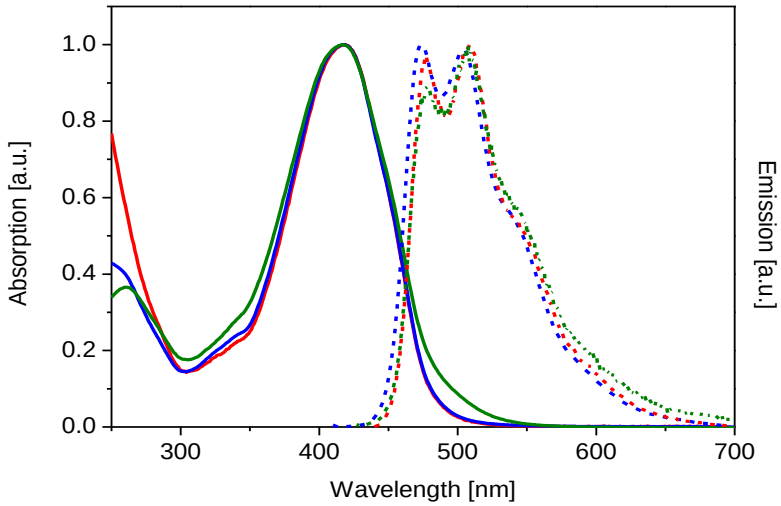

Figure 4.2. *Normalised absorption ([c] = 10^{-6} M) and emission ([c] = 10^{-7} M, excitation at λ = 380 nm) spectra of (2S,4S)-proline quaterthiophene hybrids **3.3**, **3.4**, and **3.5** in THF.*

However, hybrid **3.3** showed a very strong aggregation character even at low concentrations, when compared to the other oligomers. The presence of aggregates could be detected in the low energy region of the absorption spectrum between 467 nm and 550 nm. An additional hint is given by the quenching of the fluorescence transition at 477 nm which indicates that even in the 10^{-7} M solution the molecules are not completely dissolved (***Figure 4.2***). For this reason the molar extinction coefficient of quaterthiophene-proline **3.3** could be not determinated.

Absorption and emission maxima, Stokes shifts, optical gaps, and solubility of the quaterthiophene-proline hybrids are summarized in ***Table 4.1***.

Table 4.1. *Optical data and solubility of quaterthiophene-proline hybrids **3.1**-**3.5**.*

Hybrid	λ_{max}^{Abs} [nm]	ε_{max}^{Abs} [L cm^{-1} mol^{-1}]	Stokes shift [cm^{-1}]	λ_{max}^{Emiss} [nm]	$E_{g,opt}$ [eV]	Solubility[b] [mg mL^{-1}]
3.1[a][2]	389	35300	-	468,(498, 540)	-	-

3.2[b]	392	32000	4410	474 (506, 542)	2.40	19.8
3.3[b]	417	-	3010	(477) 507 (547)	2.30	6.4
3.4[b]	417	37000	2970	(476) 509 (547)	2.31	11.2
3.5[b]	417	37100	2880	474 (504, 541)	2.32	7.9

[a] Measured in n-propanol; [b] measured in THF.

In order to prove whether the triazolylproline moiety influences the optical properties of the π-conjugated backbone, proline-quaterthiophene hybrids **3.2**, **3.3**, **3.4**, and **3.5** were compared with the respective ethynyl-quaterthiophenes **3.22**, **3.32**, **3.45**, and **3.50** in pure THF. In general, no relevant effects on the absorption maximum and the shape of the absorption spectra were observed. All ethynyl quaterthiophenes showed higher molar extinction coefficients and larger Stokes shifts in comparison to the triazolylproline-quaterthiophenes. As an example, the comparison of the absorption and emission spectra of ethylhexyl-quaterthiophene alkyne **3.45** and the equivalent quaterthiophene hybrid **3.4** is shown in ***Figure 4.3***.

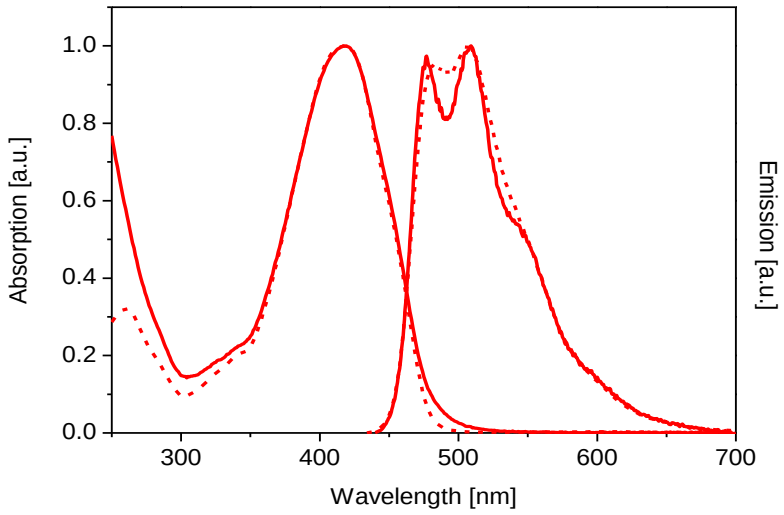

Figure 4.3. *Normalised absorption ([c] = 5 x 10^{-5} M) and emission ([c] = 10^{-7} M, excitation at λ = 380 nm) spectra of ethynyl quaterthiophene* ***3.45*** *(dotted curve) and (2S,4S)-proline quaterthiophene hybrids* ***3.4*** *(solid curve) in THF.*

With regard to the fluorescence properties, the emission spectrum became in all cases more structured after replacement of the alkyne moiety with the triazole. In particular, the fluorescence transition located at 474 nm increased (**Figure 4.3**). This alteration of the emission spectrum was more evident for 5'''-hexyl quaterthiophene **3.50**, as shown in ***Figure 4.4***. In fact, the electronic transition at 476 nm was strongly quenched in case of alkyne **3.50**, whereas it was recovered in case of the proline hybrid **3.5**.

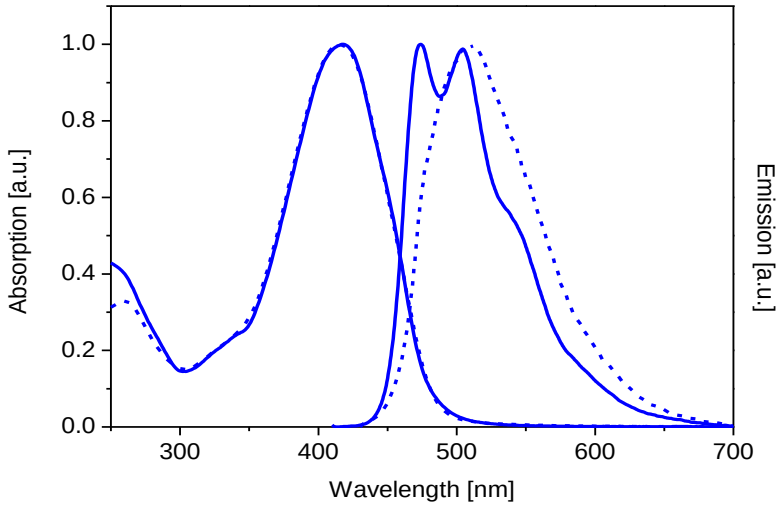

Figure 4.4. *Normalised absorption ([c] = 5 x 10^{-5} M) and emission ([c] = 10^{-7} M, excitation at λ = 380 nm) spectra of ethynyl quaterthiophene* ***3.50*** *(dotted curve) and (2S,4S)-proline quaterthiophene hybrid* ***3.5*** *(solid curve) in THF.*

The optical data for all the molecules are reported in **Table 4.2**.

Table 4.2. *Comparison of optical data of ethynyl quaterthiophenes* ***3.22***, ***3.32***, ***3.45***, ***3.50***, *and quaterthiophene-proline hybrids* ***3.2***-***3.5***.

Molecule	λ_{max}^{Abs} **[nm]**	ε_{max}^{Abs} **[L cm^{-1} mol^{-1}]**	**Stokes shift [cm^{-1}]**	λ_{max}^{Emiss} **[nm]**	$E_{g,opt}$ **[eV]**
3.22[a]	394	32800	4280	474,(500, 535)	2.43
3.2[a]	392	32000	4410	474 (506, 542)	2.40

3.35[a]	414	41000	3150	(476) 508 (542)	2.36
3.3[a]	417	-	3010	(477) 507 (547)	2.30
3.45[a]	418	45200	3130	(481) 508 (537)	2.34
3.4[a]	417	37000	2970	(476) 509 (547)	2.31
3.50[a]	415	43500	3090	(476) 509 (540)	2.32
3.5[a]	417	37100	2880	474 (504, 541)	2. 32

[a] Measured in THF.

*4.2.2 Electrochemical Properties of Quaterthiophene-Proline Hybrids **3.2**-**3.5***

Quaterthiophene-proline hybrids **3.2**-**3.5** were also investigated with respect to their redox properties with cyclic voltammetry (CV) using dichloromethane and tetrabutylammonium hexafluorophosphate (TBAHFP) as electrolyte (***Figure 4.5***).

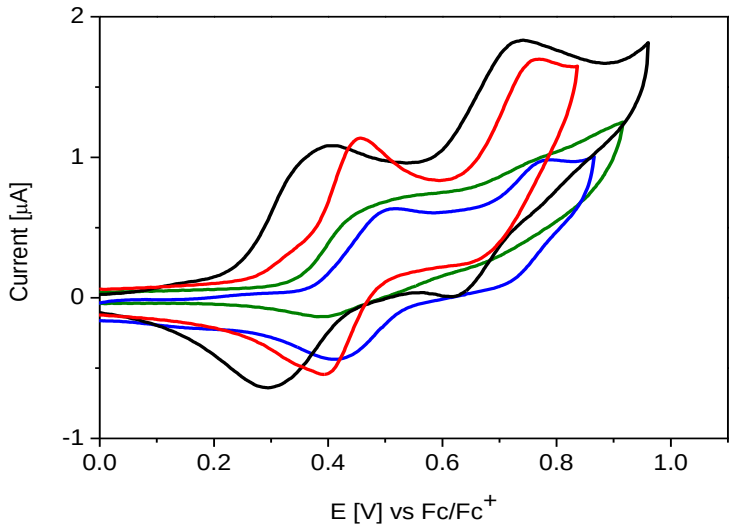

Figure 4.5. *Cyclic voltammograms of quaterthiophene-proline hybrids **3.2**-**3.5** ([c] = 10^{-3} M) in dichloromethane, TBAHFP ([c] = 0.1 M), v = 100 mV s^{-1}.*

The cyclic voltammograms in ***Figure 4.5*** displayed first reversible and second quasi-reversible oxidation waves for 3,3'''-dihexyl-substituted quaterthiophene **3.2** (black curve), 5'''-ethylhexyl quaterthiophene **3.4** (red curve) and 5'''-hexyl-quaterthiophene **3.5** (blue curve) which are characteristic for the formation of stable quaterthiophene radical cations and dications. The oxidation potentials of hybrids **3.2**, **3.4**, and **3.5** were E_{Ox1} = 0.34 V, 0.40 V, 0.42 V, and E_{Ox2} = 0.69 V, 0.70 V, 0.72 V, respectively. The cyclic voltammogram of quaterthiophene-proline **3.3** (green curve) is less structured because of the low solubility of the molecule. In fact, a first quasi-reversible oxidation wave was detectable at 0.46 V, whereas the formation of the radical dication species could not be observed due to the non-resolved second oxidation wave. In general, no signal was found in the reductive regime. All electrochemical data are summed up in ***Table 4.3***.

Table 4.3. *Electrochemical data of quaterthiophene-proline hybrids **3.1**-**3.5**.*

Hybrid	$E^{1/2}_{Ox1}$ [V]	$E^{1/2}_{Ox2}$ [V]	$E_{Ox1,onset}$ [V]	E_{HOMO} [eV]
3.1[a][2]	0.42	0.66	0.35	-5.45
3.2[a]	0.34	0.69	0.24	-5.34
3.3[a]	0.43	-	0.34	-5.44
3.4[a]	0.42	0.70	0.39	-5.49
3.5[a]	0.44	0.72	0.38	-5.48

[a] Measured in dichloromethane.

The electrochemical properties of the π-conjugated backbone seemed to be unaffected by the different alkyl chains in 5'''-position, whereas an influence on the first oxidation potential was observed by changing the substitution position. Surprisingly, 3,3'''-dihexyl-quaterthiophene **3.2** showed a first oxidation potential lower than those observed for the equivalent α-substituted quaterthiophene hybrids. In fact, the radical cation of the terminal-substituted 4Ts should be more stable and therefore the oxidation potential should be lowered. Less astonishing, quaterthiophene-proline **3.2** showed also a lower first oxidation wave in comparison to the dodecyl-substituted hybrid **3.1**.

The HOMO energy levels of all quaterthiophene-proline hybrids were calculated from the onset value of the first oxidation wave using the standard approximation that the Fc/Fc^+ HOMO energy level is -5.1 eV versus vacuum.[3] The estimated values were similar which indicates that the diverse substitution positions or the different alkyl chains do not affect the HOMO energy level.

4.2.3 UV/Vis and Fluorescence Properties of Quaterthiophene-Proline Hybrids ***3.5-3.8***

(2*S*,4*S*)-Proline-quaterthiophene hybrid **3.5** was compared with the (2*R*,4*R*) enantiomer **3.6**, (2*S*,4*S*)-methyl ester proline-quaterthiophene **3.7** and (2*R*,4*S*)-methyl ester proline-quaterthiophene **3.8** with respect to their optical properties (***Chart 4.2***).

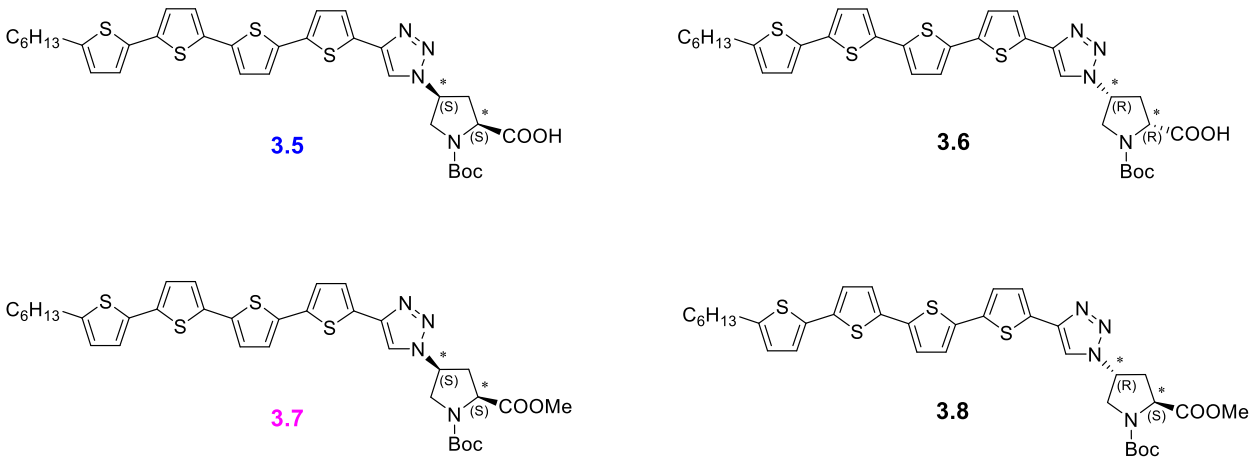

Chart 4.2. *Molecular structures of quaterthiophene-proline hybrids* ***3.5****-****3.8****.*

All four hybrids showed similar absorption and fluorescence maxima (***Figure 4.6***).This was expected because the stereochemistry of the triazolyl-proline moiety has not influence on the π-π* transition of the quaterthiophene moiety when the molecules are molecularly dissolved in a "good solvent" such as THF. The only difference was represented by the Stokes shifts. In fact, (2*S*,4*S*)-methyl ester proline-quaterthiophene **3.7** was characterized by a Stokes shift value bigger than those of quaterthiophene-proline hybrids **3.5**, **3.6**, and **3.8**. This indicates more structural differences for hybrid **3.7** in the ground and first excited state.

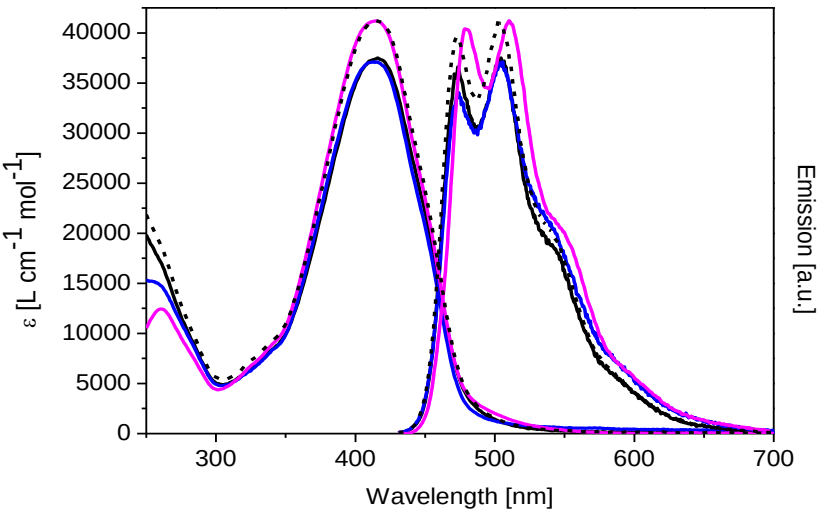

Figure 4.6. *Absorption ([c] = 10^{-5} M) and emission ([c] = 10^{-7} M, excitation at λ = 380 nm) spectra of (2S,4S)-proline quaterthiophenes* ***3.5****, (2R,4R) enantiomer* ***3.6****, (2S,4S)-methyl ester proline-quaterthiophene* ***3.7*** *and (2R,4S)-methyl ester proline-quaterthiophene* ***3.8****, in THF.*

All optical data were summed up in ***Table 4.4***.

Table 4.4. *Optical data and solubility of quaterthiophene-proline* ***3.5-3.8.***

Hybrid	λ_{max}^{Abs} [nm]	ε_{max}^{Abs} [L cm^{-1} mol^{-1}]	Stokes shift [cm^{-1}]	λ_{max}^{Emiss} [nm]	$E_{g,opt}$ [eV]	Solubility [mg mL^{-1}]
3.5[a]	417	37100	2280	474 (504, 541)	2.32	7.9
3.6[a]	417	37500	2280	474 (504, 541)	2.33	8.2
3.7[a]	415	41200	3210	(479) 511 (549)	2.32	24.2
3.8[a]	416	41300	2850	(472) 503 (542)	2.33	25

[a] Measured in THF.

4.2.4 Electrochemical Behaviour of Quaterthiophene-Proline Hybrids **3.5**-**3.7**

The redox properties of quaterthiophene-proline hybrids **3.5**-**3.7** were also investigated. The study of the electrochemical properties of diastereomer (2*R*,4*S*)-methyl ester proline-quaterthiophene **3.8** has not been carried out, because the amount isolated was not enough to effectuate all kind of analysis.

In **Figure 4.7** it is observed that the first oxidation potential is located for all hybrids at 0.44 V meaning that the stereochemistry of the molecules and the different substitution of the proline moiety do not influence the stability of the radical cation. Quaterthiophene hybrids **3.5** and **3.7**, which are characterized by the same stereochemistry, showed similar second oxidation potential, 0.72 V and 0.73 V, respectively, whereas the second oxidation wave of (2*R*,4*R*)-proline 4T is located at higher potential, 0.77 V. This stands for the easier formation of the radical dication species for (2*R*,4*R*)-quaterthiophene **3.6**.

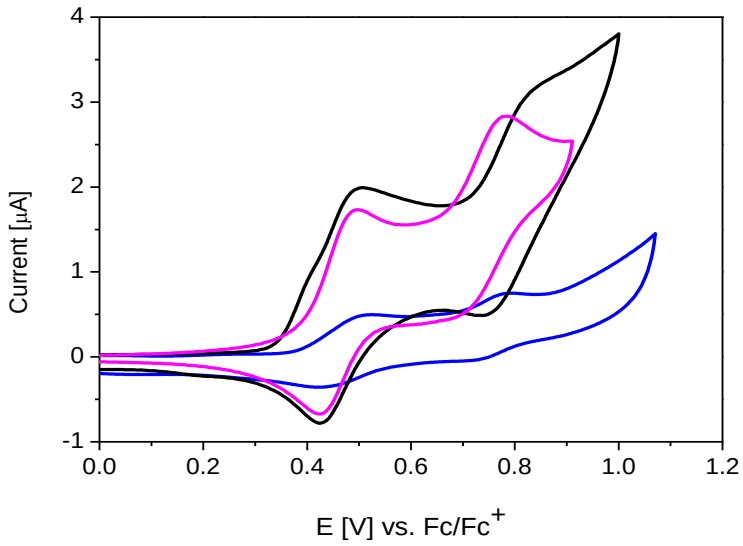

Figure 4.7. *Cyclic voltammograms of (2S,4S)-proline quaterthiophenes* ***3.5****, (2R,4R) enantiomer* ***3.6****, and (2S,4S)-methyl ester proline-quaterthiophene* ***3.7*** *([c] = 10^{-3} M) in dichloromethane, TBAHFP ([c] = 0.1 M), v = 100 mV s^{-1}.*

Additionally, the HOMO energy level calculated from the onset value of the first oxidation wave of (2*R*,4*R*)-hybrid **3.6** is slightly higher than the HOMO energy levels of (2*S*,4*S*)-proline-quaterthiophene **3.5** and **3.7**.

All electrochemical data are summarized in ***Table 4.5***.

Table 4.5. *Electrochemical data of quaterthiophene-proline* ***3.5***, ***3.6***, *and* ***3.7***.

Hybrid	$E^{1/2}_{Ox1}$ [V]	$E^{1/2}_{Ox2}$ [V]	$E_{Ox1,onset}$ [V]	E_{HOMO} [eV]
3.5[a]	0.44	0.72	0.38	-5.48
3.6[a]	0.44	0.77	0.34	-5.44
3.7[a]	0.44	0.73	0.38	-5.48

[a] Measured in dichloromethane.

*4.2.5 UV/Vis and Fluorescence Properties of Quaterthiophene-Proline Hybrid **3.9***

Quaterthiophene-proline hybrid **3.9** is characterized by the presence of an acceptor function such as a dicyanovinyl group (***Chart 4.3***).

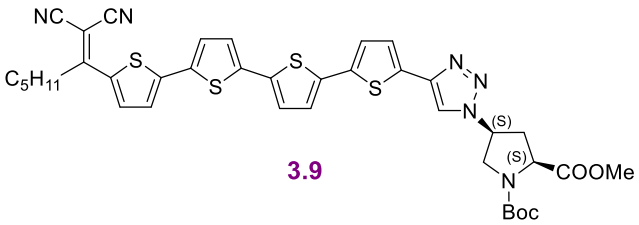

3.9

Chart 4.3. *Molecular structure of quaterthiophene-proline hybrid* ***3.9***.

The introduction of such electron-withdrawing group into the quaterthiophene-proline structure produced the emergence of a new transition band at 476 nm, which was assigned to the intramolecular charge transfer (ICT) from the quaterthiophene donor to the DCV acceptor (***Figure 4.8***). Additionally, the shoulder located at 396 nm is attributed to the $\pi-\pi^*$ transition of the oligothiophenes backbone. In fact, by comparing the absorption spectrum of (2*S*,4*S*)-methyl ester proline-quaterthiophene **3.7** and the shoulder at λ = 396 nm of (2*S*,4*S*)-methyl ester proline-DCV-quaterthiophene **3.9**, it could be indeed observed the correlation of the two bands (***Figure 4.8***). Additionally,

the optical gap decreases from 2.33 eV calculated for hybrid **3.7** to 1.94 eV in case of DCV-hybrid **3.9**.

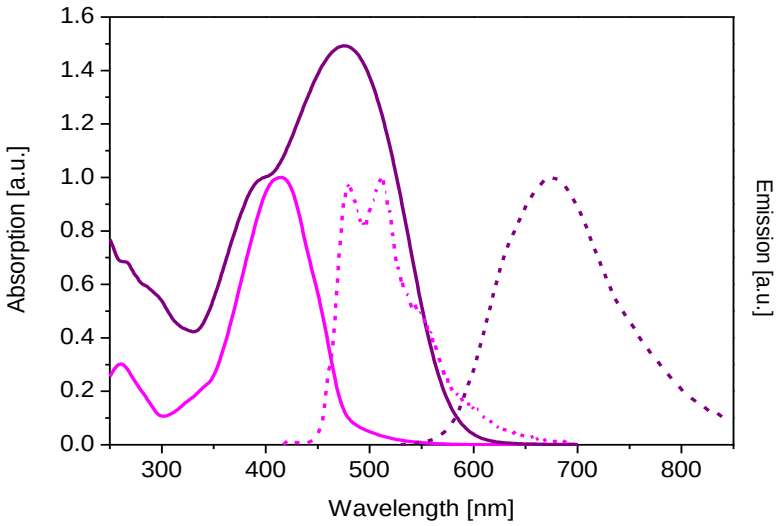

Figure 4.8. *Absorption ([c] = 10^{-5} M) and emission ([c] = 10^{-7} M, excitation at λ = 380 nm (magenta curve)and at λ = 490 nm (purple curve)) spectra of (2S,4S)-methyl ester proline-quaterthiophene **3.7** and (2S,4S)-methyl ester proline-DCV-quaterthiophene **3.9**, in THF.*

Looking at the emission spectra, DCV-4T **3.9** displayed a less structured emission spectrum and the maximum at lower energy than the one observed for quaterthiophene **3.7**. All these differences are just a further evidence of the strong influence of the DCV group on the optical properties of the π-conjugated core.

The optical and solubility data are summarized in ***Table 4.6***.

Table 4.6. *Optical data and solubility of quaterthiophene-proline **3.7** and **3.9.***

Hybrid	λ_{max}^{Abs} [nm]	ε_{max}^{Abs} [L cm^{-1} mol^{-1}]	Stokes shift [cm^{-1}]	λ_{max}^{Emiss} [nm]	$E_{g,opt}$ [eV]	Solubility [mg mL^{-1}]
3.7[a]	415	41200	3210	(479) 511 (549)	2.32	24.2
3.9[a]	476	-	5130	(630) 676	1.94	15

[a] Measured in THF.

4.2.6 Electrochemical Properties of Quaterthiophene-Proline Hybrid ***3.9***

The redox properties of **3.9** were measured and compared to those of hybrid **3.7** (***Figure 4.9***). In general, it was observed that by introducing the acceptor group a redox wave in the reduction regime was detected. Quaterthiophene-proline **3.9** showed one reversible oxidation wave at 0.50 V followed by a quasi-reversible oxidation wave at 0.88 V indicating the formation of stable quaterthiophene radical cations and dications, respectively. In the reductive regime, an irreversible reduction wave at -1.77 V was detected, which is assigned to the reduction of the electron-deficient DCV group. The HOMO and LUMO energy levels were calculated from the onset values of the first oxidation and reduction waves. The HOMO was located at -5.46 eV, whereas the LUMO was located at -3.54 eV resulting in an electrochemical gap of 1.9 eV. Once more, the influence of the DCV-group was evident: both HOMO and LUMO energy levels of DCV-4T **3.9** are lower than the HOMO (-5.44 V) and LUMO (-3.15 V) energy levels of quaterthiophene **3.7**.

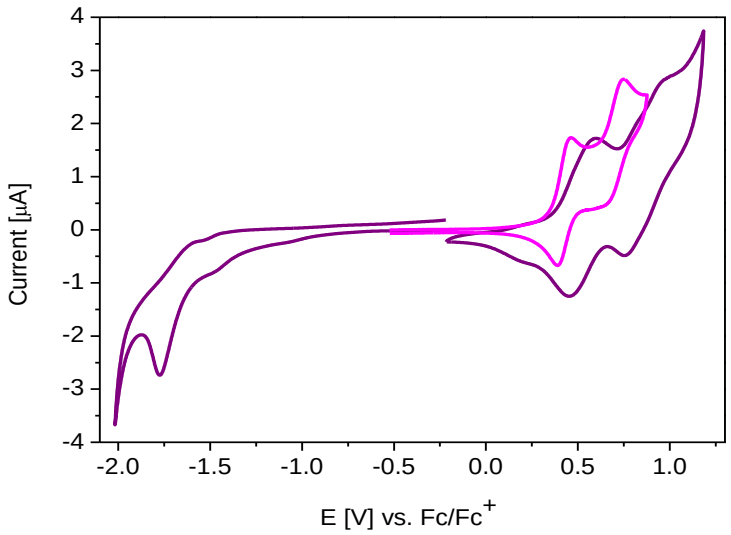

Figure 4.9. *Cyclic voltammograms of (2S,4S)-methyl ester proline-quaterthiophene **3.7** and (2S,4S)-methyl ester proline-DCV-quaterthiophene **3.9** ([c] = 10^{-3} M) in dichloromethane, TBAHFP ([c] = 0.1 M), v = 100 mV s^{-1}.*

4.2.7 Summary of the Structure-Property-Relationships of Quaterthiophene-Proline Hybrids **3.2**, **3.3**, **3.4**, **3.5**, **3.7**, and **3.9** in the Dissolved State

In the first part of ***Chapter 4*** the optoelectronic properties of all biohybrids in a "good solvent" such as THF were reported. It was observed that the β-functionalized quaterthiophene **3.2** and the α-substituted quaterthiophenes **3.3**, **3.4**, **3.5** and **3.7** displayed similar optical properties. In fact, all biosystems showed unstructured and broad absorption bands, whose maxima are located at similar wavelengths, except for **3.2**, whose maximum is hypsochromically shifted ($\Delta\lambda$ = 25 nm). This might be due to the slight twisting of the π-conjugated backbone caused by the β-hexyl substituents. Concerning the emission spectra, it was observed that all four hybrids showed a vibronic fine structure with very similar λ_{emiss}. The calculated spacings between the 1st-2nd and 2nd-3rd vibronic bands were calculated and are similar in all quaterthiophene-proline hybrids: 1295 cm^{-1} and 1450 cm^{-1}, respectively. This well correlates with the frequency of the structural modifications of the oligothiophene backbone: C=C stretching bond at 1450 cm^{-1} and C-H bending bond at 1295 cm^{-1} can be detected.[4,5] An example can be seen in ***Figure 4.10***: the vibronic bands of the emission spectrum of **3.5** are correlated with the vibration frequencies of the IR spectrum of the same oligomer.

By comparing the redox properties, the π-conjugated biohybrids showed first and second reversible/quasi-reversible oxidation waves, characteristic for the formation of stable quaterthiophene radical cations and dications, whereas no signal could be observed in the reductive regime. By introducing the DCV-group into the system (hybrid **3.9**), a change in optoelectronic properties was observed: a new band appeared in the UV/Vis absorption spectrum which corresponds to the ITC band of the quaterthiophene donor to the DCV acceptor, whereas the emission spectrum displayed an unstructured vibronic band and the λ^{em}_{max} was strongly bathochromically shifted in comparison to those of the other quaterthiophene-proline hybrids. In conclusion, DCV-quaterthiophene **3.9** showed lower HOMO and LUMO energy levels in comparison to the equivalent systems without acceptor group, and a lower optical gap, which is identical to the one calculated electrochemically.

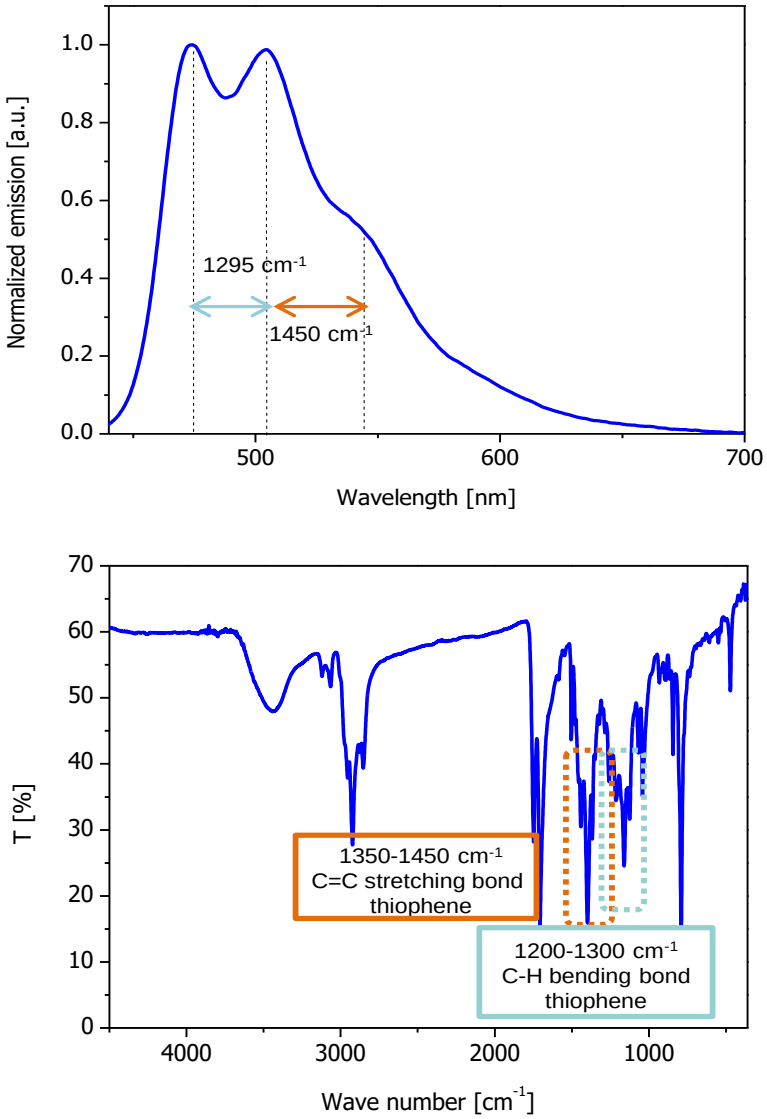

Figure 4.10. *Correlation of the vibronic bands of the emission spectrum (upper part) and the frequency area of the IR spectrum (bottom part) of* ***3.5****.*

4.3 Optical and Chiroptical Properties in the Aggregated State

4.3.1 Introduction to the Aggregate Formation

Self-assembly of molecules containing chromophores, such as the proline-quaterthiophene hybrids, is mainly studied by optical and chiroptical spectroscopy (UV/Vis, fluorescence, and CD). With these types of spectroscopy it is possible to say if and how the investigated molecules self-assemble. In fact, depending on the band shape and eventual shifts of band maxima, one can predict how the molecules interact with each other and how they arrange in solution.

When two or more chromophores are brought into proximity, the excitation of one of them can cause the interaction of the π-conjugated backbone of both. This phenomenon is called exciton coupling.[6] The electronic transition between energy levels in optical spectroscopy creates an instantaneous dipole or polarization of charge called electric transition dipole moment. If the electric transitions of two chromophores are similar in energy, the corresponding transition dipole moments can interact with one another forming a delocalized state of excitation energy (exciton) over two or more chromophores. This may result in a *Davydov splitting* of the locally excited states, which leads to spectral shifts or splitting of the absorption bands for the aggregated species.[7]

The *H*-type orientation of the transition dipoles leads to an exciton energy level diagram shown in ***Figure 4.11***, **a**.

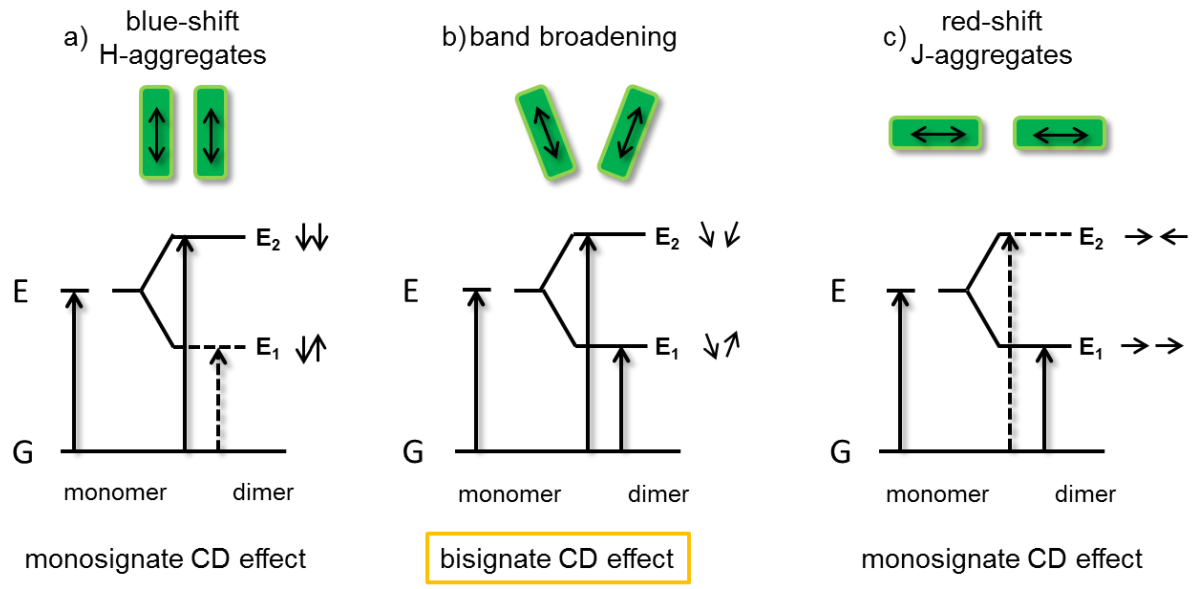

Figure 4.11. *Exciton band energy diagrams for a molecular dimer with a) parallel, b) oblique, and c) in-line arrangement of the transition dipoles. The double arrows represent the polarization axis of the molecular electronic transition; G = ground state, E = excited state.*

The transition moment is given by the vector sum of the transition dipoles of each molecule. Thus, transitions from the ground state (**G**) to excited state (**E**) E_1 are forbidden, while transitions to state E_2 are allowed, causing a blue-shift of the corresponding absorption maximum with respect to the monomeric species. The transition from ground state to E_1 is forbidden because the orbital wave functions which are involved in the transition have their overlap integral cancelled due to their symmetry.

The *J*-type arrangement of transition dipoles is displayed in ***Figure 4.11***, **c**.[7-9] The diagram shows that the in-phase alignment leads to an electrostatic attraction, which causes a lowering of the energy of the excited state E_1. The out-of-phase arrangement (energy level E_2) heads to an electrostatic repulsion which is the reason why this transition is forbidden. Here, the transition from ground state to excited state E_1 is allowed and a red-shift of the absorption maximum is observed for *J*-type aggregation.A third possibility for the alignment of the transition dipole moments is the oblique arrangement, which represents a combination of *H*- and *J*-type assemblies (***Figure 4.11***, **b**). In this case, the in-phase arrangement of the transition dipoles for the monomer is attractive and leads to a lowering of the energy E_1. The out-of-phase arrangement is repulsive and causes a rising of the excited state energy E_2 for the dimer. The transition moments from the ground state to the excited states are in both cases allowed and results in a broadening of the corresponding absorption bands.

For a system of molecules, in which chromophores are held in a chiral orientation, exciton coupling can be more easily and more clearly detected by CD-spectroscopy.[6] With this method the difference between absorption of left and right-handed circularly polarized light can be discriminated and it is possible to determine the absolute configuration of the stereocenters as well as the conformational features of the molecules, which are often completely obscured in ordinary absorption spectra.[10,11] In general, the CD spectra of chiral assemblies reveal two oppositely signed Cotton effects, which correspond to the UV/Vis absorption of the chromophore and the sign can be addressed with the relative orientation of the electric transition dipole moments. Harada and Nakanishi[12] established exciton chirality rules in a way that a negative torsion angle between the transition dipoles results in a negative long wavelength component of the associated exciton couplet and proves the left-handed helical arrangement of the chromophores (***Figure 4.12***). Vice versa a positive torsion angle accompanies a positive long-wavelength Cotton effect and mirrors a right-handed helicity.

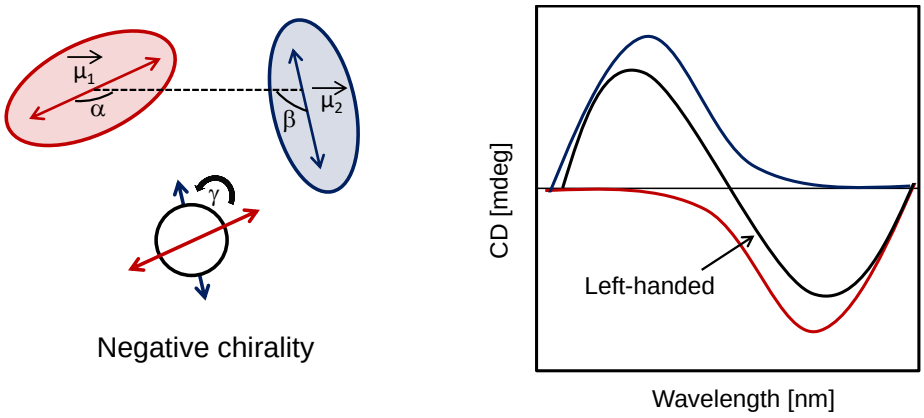

Figure 4.12. *Example of left-handed helicity due to a negative torsion angle.*

The exciton theory provides the fundamental basis for all investigations on optical properties of aggregated species and has been widely applied for the interpretation of various supramolecular structures.

4.3.2 Self-Assembly Investigation of Quaterthiophene-Proline Hybrids

As already explained in ***Chapter 2*** the self-assembling process of the amino acid conjugates should be directed by different intermolecular forces such as π-π stacking, van der Waals interactions or hydrogen bonding (***Figure 4.13***).

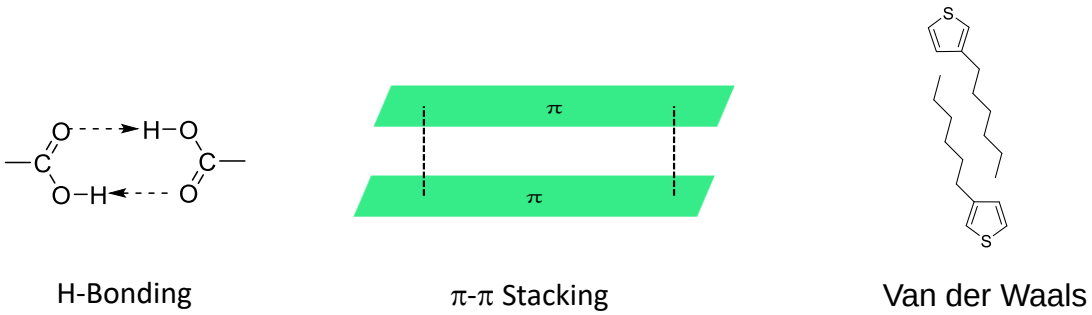

Figure 4.13. *Schematic representation of H-bonding, π-π stacking and van der Waals interactions.*

In particular, looking for example at quaterthiophene-proline hybrids **3.5** and **3.7** (***Chart 4.4***), in polar solvents such as water, π-π interactions are formed by the hydrophobic quaterthiophene part and the triazole moiety.

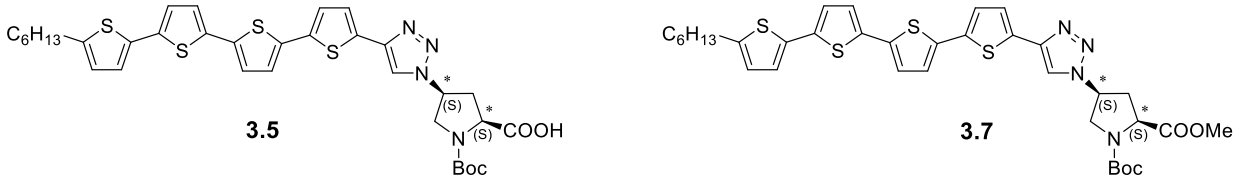

Chart 4.4. *Molecular structures of quaterthiophene-proline hybrids* ***3.5*** *and* ***3.7****.*

Furthermore, the terminal hexyl chain give rise to van der Waals interactions. Hybrid **3.5** includes a free carboxylic acid as hydrogen bonding donor site, whereas the hydrogen bonding source is supressed in quaterthiophene **3.7**, in which the proline is functionalized with the ester group. Additionally, both quaterthiophenes have the nitrogen of the triazole and the oxygen at the carbonyl group as hydrogen bond acceptor sites. Since all these interactions should contribute to the self-assembly process, the choice of the solvent is essential for the supramolecular organization. In fact, the interaction of the solvent molecules may compete with the intramolecular forces. If the solute-solvent bonds are stronger than the solute-solute bonds, the self-assembly process will not occur. This was the case shown in ***Chapter 4.2***, where THF was chosen as solvent for the study of the optoelectronic properties of quaterthiophene-proline hybrids. In order to fully understand the self-organization process, it will be also important to know the intrinsic properties of the chosen solvent such as dipole moment [*D*], Kamlet-Taft-Parameter ($\alpha =$ hydrogen bond donor, $\beta =$ hydrogen bond acceptor) and polarizability (***Table 4.7***).

Table 4.7. *Properties of the solvents utilized for the self-assembling investigation of quaterthiophene-proline* ***3.2****-****3.9****.*

	Water	**THF**	**Chloroform**	***n*-Hexane**
Dipole moment [D][6]	1.9	1.8	1.0	0.08
Kamlet-Taft-Parameter[6]				
α	1.17	0.00	0.20	0.00
β	0.47	0.55	0.10	0.00
Polarizability[6]	1.09	0.58	0.58	-0.04

In the next paragraphs, the aggregate formation will be investigated for all hybrids by UV/Vis-, fluorescence-, and CD-spectroscopy, and the sizes of the suprastructures will be analysed via Dynamic Light Scattering (DLS). The DLS measurements were carried out with the help of the Lindén group at the University of Ulm.

4.3.2.1 UV/Vis-, Fluorescence-, CD-Spectroscopy, and DLS Measurements of β-Hexyl Substituted Quaterthiophene-Proline **3.2**

The self-assembly properties of quaterthiophene-proline **3.2** (***Chart 4.5***) were investigated in different THF/water ratios. As already shown, no aggregate formation was detected in the pure THF solution.

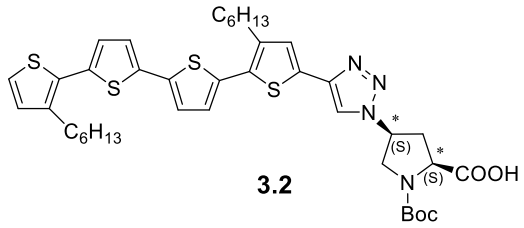

3.2

Chart 4.5. *Molecular structure of β-hexyl substituted quaterthiophene-proline hybrid* ***3.2****.*

By comparing the absorption spectra, it was observed that upon titration with water, the shape of the π-π* transition band remains the same until the THF/water (3:7) solution, whereas it differs when the ratio THF/water (1:9) is reached (***Figure 4.14***). In fact, for this solution the slope of the absorption band is less steep and the absorption onset is shifted towards higher wavelength in comparison to the other solvent mixtures. Keeping the previously explained exciton theory in mind, this slight broadening of the absorption band at low energy indicates that the arrangement of the chromophores is inclined to form *J*-like aggregates. Additionally, the absorption band with the λ_{max} located at 261 nm which corresponds to the absorption perpendicular to the long axis of the quaterthiophene together with the absorption of the 1,2,3-triazole moiety, increased in the aqueous solutions.

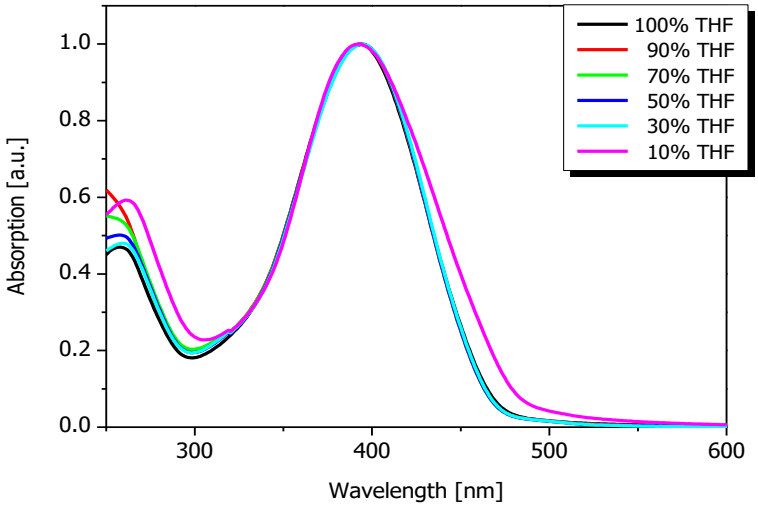

Figure 4.14. *Normalized absorption spectra of hybrid* ***3.2*** *upon titration of the THF solution with water. Black curve: absorption spectrum of the 100% THF solution; red curve: absorption spectrum of the THF/water (9:1) solution; green curve: absorption spectrum of the THF/water (7:3) solution; blue curve: absorption spectrum of the THF/water (1:1) solution; cyan curve: absorption spectrum of the THF/water (3:7) solution; magenta curve: absorption spectrum of the THF/water (1:9) solution.*

In order to study the stability of the formed suprastructures, temperature-dependent UV/Vis measurements were carried out. The THF/water (1:9) solution was investigated in a temperature range between 30 °C and 70 °C taking steps of 10 °C (***Figure 4.15***).

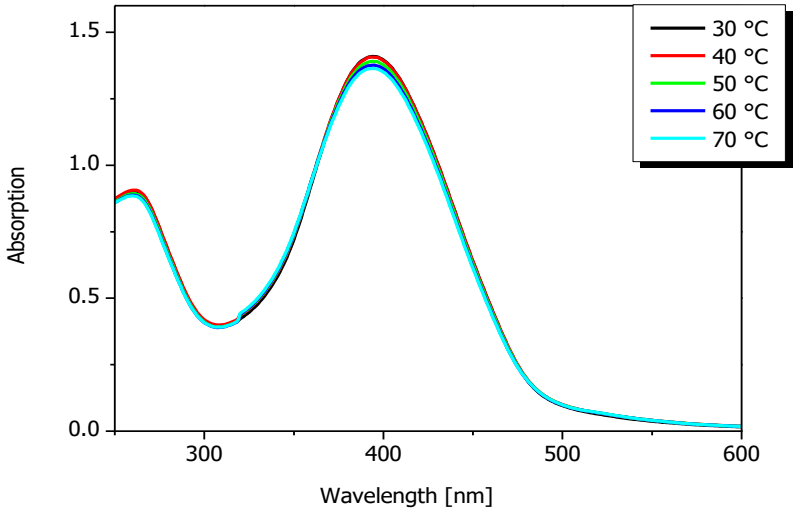

Figure 4.15. *Temperature-dependent absorption spectra of* ***3.2****, [c] = 5 x* 10^{-5} *M in THF/water (1:9 solution). Black curve: absorption spectrum at 30 °C; red curve: absorption spectrum at 40 °C; green curve: absorption spectrum at 50 °C; blue curve: absorption spectrum at 60 °C; cyan curve: absorption spectrum at 70 °C.*

The limit of 70 °C is imposed by the boiling point of THF. Upon increasing the temperature, small changes of the absorption bands could be just detected. This indicates that the aggregates, which were formed upon titration with water, are stable at high temperatures.

Looking at the fluorescence spectra of the THF and the THF/water (1:9) solutions of hybrid **3.2**, a strong quenching of the emission bands could be detected in the aqueous mixture (***Figure 4.16***). A decrease of the emission intensity of 95% compared to its previous emission intensity in pure THF (calculated from the areas of the emission bands) was observed.

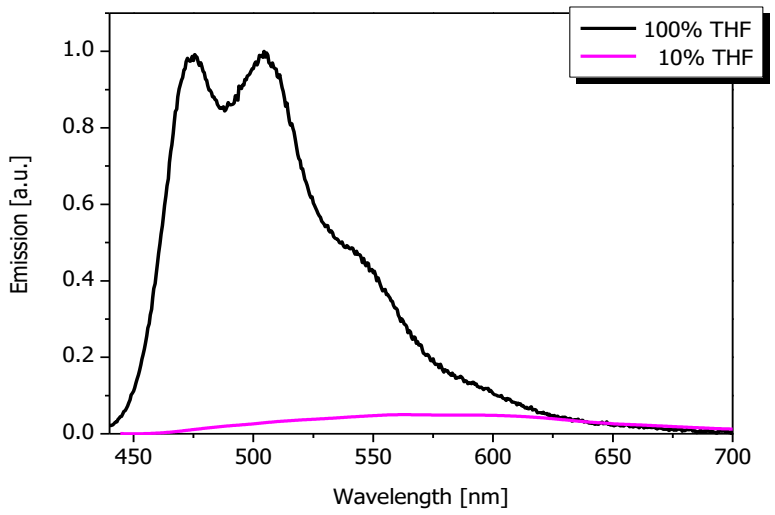

Figure 4.16. *Comparison of the normalized emission spectrum of hybrid **3.2**, [c] = 10^{-7} M in 100% THF (black curve) and the quenched emission spectrum inTHF/water (1:9) solution (magenta curve).*

Further investigations on the self-assembling process were accomplished by CD spectroscopy. As already described in ***Chapter 4.3.1***, CD spectroscopy can be used to determine whether the molecules, which aggregate in solution, form chiral supra-structures, and if so, in which manner they are arranged. Since the conjugated backbone is substituted with a proline containing two stereogenic centres, the formation of chiral arrangements is expected. The CD measurements were carried out in the same THF/water solutions, which were already investigated by UV/Vis- and fluorescence spectroscopy.

In pure THF no CD-signal could be detected in the wavelength range between 250 nm and 600 nm. This result is in agreement with the UV/Vis measurements, which indicated a molecularly dissolved and non-aggregated state of **3.2** in pure

THF. Upon titration with water, the formation of aggregates could be observed (***Figure 4.17***). A positive Cotton effect was observed for the THF/water (9:1), (7:3), (1:1), and (3:7) solutions indicating the presence of chiral suprastructures, in which the chromophores arrange in a right-handed helical way and are electronically-decoupled (***Figure 4.17***).

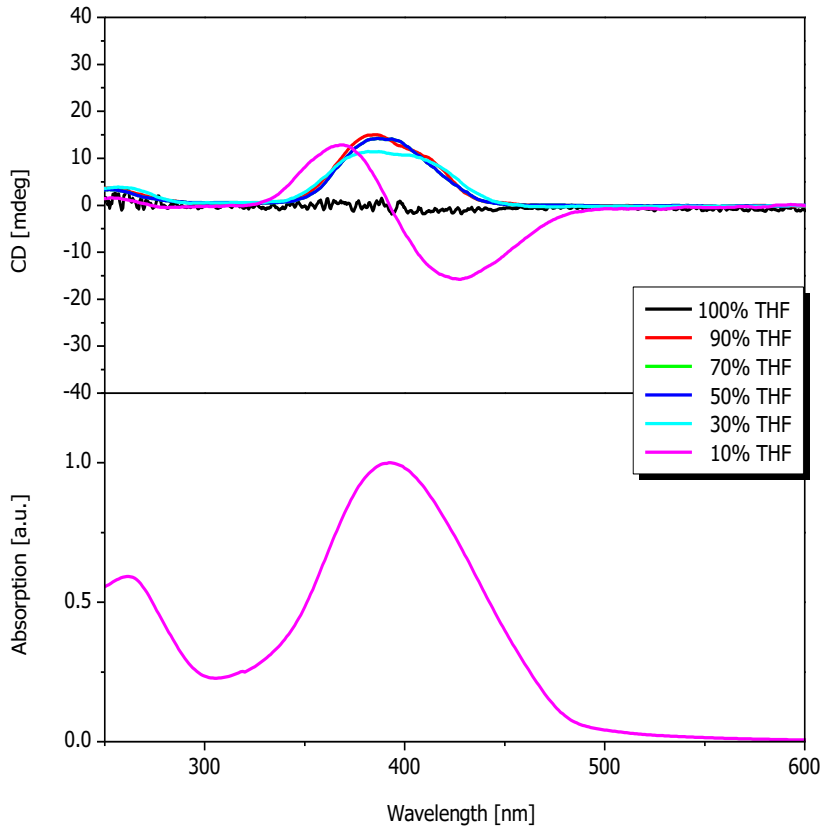

Figure 4.17. *CD-spectra of hybrid* ***3.2*** *upon titration of the THF solution with water (top), [c] = 5 x 10^{-5} M. Black curve: CD-spectrum of the 100% THF solution; red curve: CD- spectrum of the THF/water (9:1) solution; green curve: CD-spectrum of the THF/water (7:3) solution; blue curve: CD-spectrum of the THF/water (1:1) solution; cyan curve: CD-spectrum of the THF/water (3:7) solution; magenta curve: CD- (top) and absorption (bottom) spectra of the THF/water (1:9) solution.*

In the THF/water (1:9) solution quaterthiophene-proline **3.2** displayed a bisignate CD signal (the intensity of the signal is between -15 mdeg and +15 mdeg) consisting of a negative Cotton effect with a minimum located at 437 nm followed by a positive Cotton effect with the maximum situated at 362 nm. These findings stand for the formation of chiral suprastructures, in which the molecules are arranged in a left-handed helical fashion. Furthermore, the zero-crossing of the bisignate signal is located at 394 nm and correlates with the maximum of the absorption spectrum. This indicates

that the π-systems in the aggregates are electronically coupled. Additionally, a weaker positive Cotton effect with the maximum located at 260 nm was observed. This corresponds to the absorption band of the 1,2,3-triazole unit, whose λ_{max} is situated at 261 nm and indicates the supramolecular chirality of this part of the hybrid.

The stability of the aggregates was further verified by CD measurements. Firstly, the THF/water (1:9) solution was aged for one and two days, then CD spectra of the sample were recorded (***Figure 4.18***). No drastic changes in shape or in helicity could be observed. This trend suggests that the aggregates, which are formed in this mixture are thermodynamically stable. The decrease in intensity of the bisignate CD signal may be due to the precipitation in solution of aggregates, which became bigger after leaving the THF/water (1:9) mixture aging.

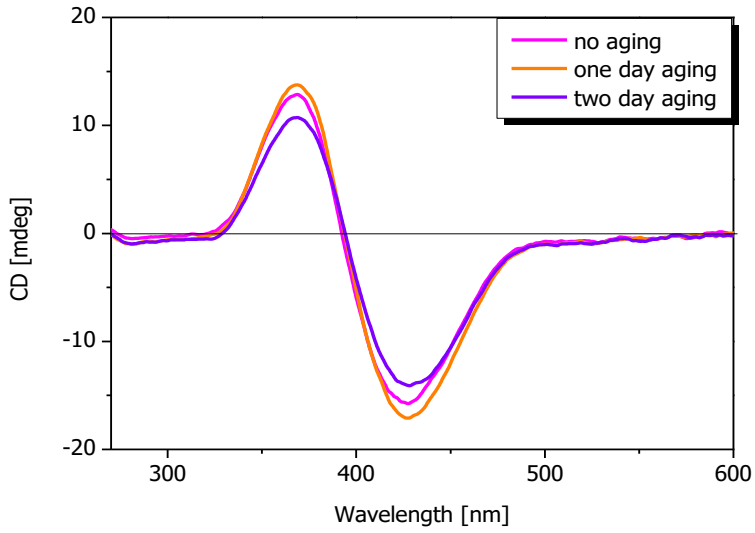

Figure 4.18. *CD-spectra of the THF/water (1:9) solution of hybrid* ***3.2****, [c] = 5 x 10 $^{-5}$ M. Magenta curve: before aging; light orange curve: after one day aging; violet curve: after two days aging.*

Additionally, the THF/water (1:9) solution was investigated at higher temperatures (***Figure 4.19***). The bisignate CD-signal lost initially its intensity going from 30 °C to 40 °C, whereas no additional changes could be detected up to 70 °C. This corroborates the hypothesis that the aggregates, which are built under aqueous conditions are stable.

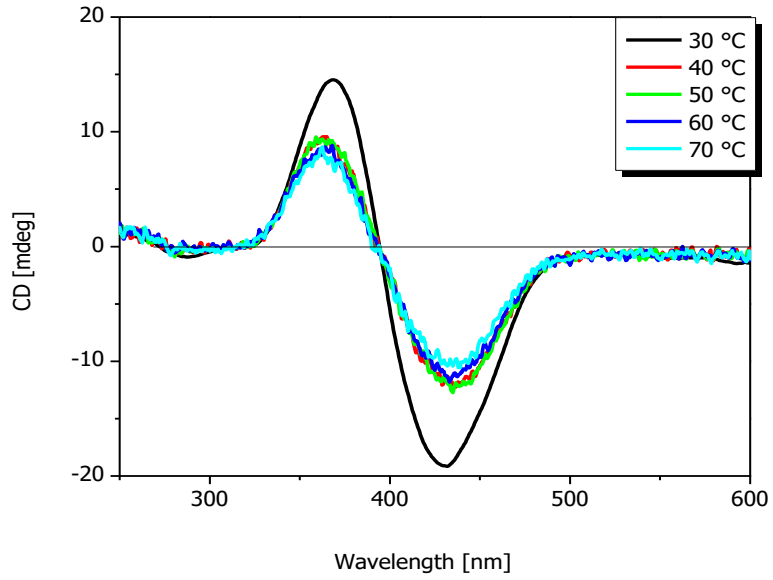

Figure 4.19. *Temperature-dependent CD-spectra of hybrid* ***3.2****, [c] = 5 x 10 $^{-5}$ M. Black curve: CD-spectrum at 30 °C; red curve: CD-spectrum at 40 °C; green curve: CD-spectrum at 50 °C; blue curve: CD-spectrum at 60 °C; cyan curve: CD-spectrum at 70 °C.*

The presence of aggregates in solution was further proven by carrying out dynamic light scattering (DLS) experiments (***Figure 4.20***). In particular, particles with an average thermodynamic radius of ca. 160 nm could be detected.

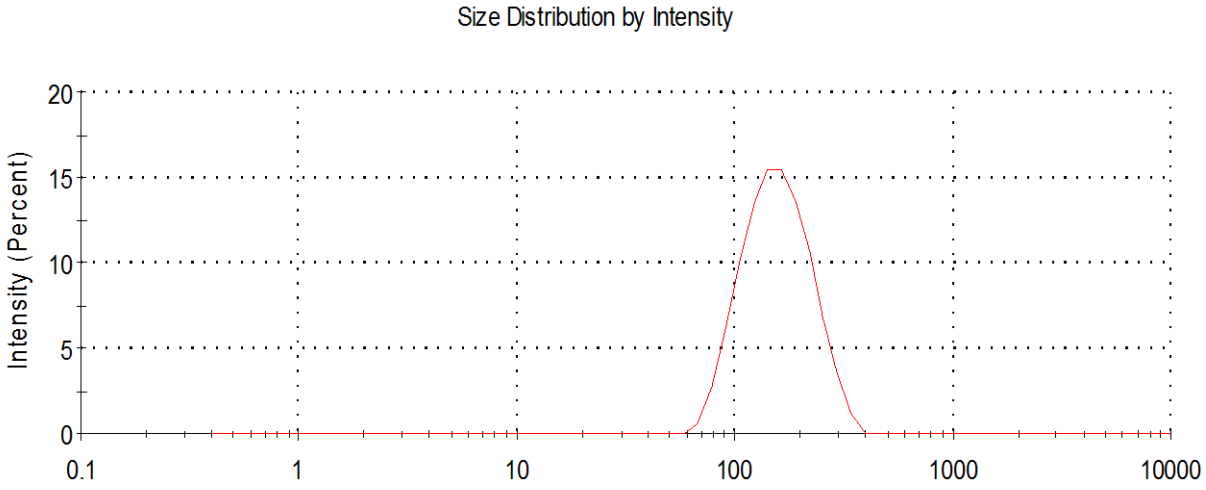

Figure 4.20. *DLS measurement of the aggregate size of hybrid* ***3.2*** *in the THF/water (1:9) solution, [c] = 5 x 10 $^{-5}$ M.*

4.3.2.2 UV/Vis-, Fluorescence-, CD-Spectroscopy, and DLS Measurements of α–Propyl Substituted Quaterthiophene-Proline **3.3**

Propyl-substituted quaterthiophene **3.3** (**Chart 4.6**) was studied with respect to its self-assembly behaviour in different THF/water solutions by UV/vis, fluorescence and CD- spectroscopy.

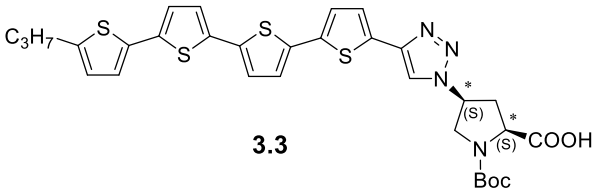

3.3

Chart 4.6. *Molecular structure of α-propyl substituted quaterthiophene-proline hybrid* ***3.3****.*

By comparing the absorption spectra, no differences could be observed for the 100%, 90%, 70% and 50% THF solutions. The aggregation process began in the THF/water (3:7) mixture, as an additional maximum at 350 nm appeared. In the THF/water (1:9) solution the absorption band with the maximum located at 416 nm was quenched, whereas the new absorption band at 350 nm increased in intesity (***Figure 4.21***). The loss of symmetrical shape of the absorption spectrum and the hypsochromic shift of the absorption maximum to higher energy account for the formation of *H*-type aggregates in the solvent mixture. As explained in the exciton theory, this type of aggregates are characterized by the parallel alignment of the transition dipoles which is responsible for the observed electronic transition, which in this case corresponds to the π–π* transition of the oligothiophene backbone. Additionally, it was observed that the absorption band of the 1,2,3-triazole moiety became more intense upon increasing the amount of water indicating the participation of this molecular part in the self-assembling process.

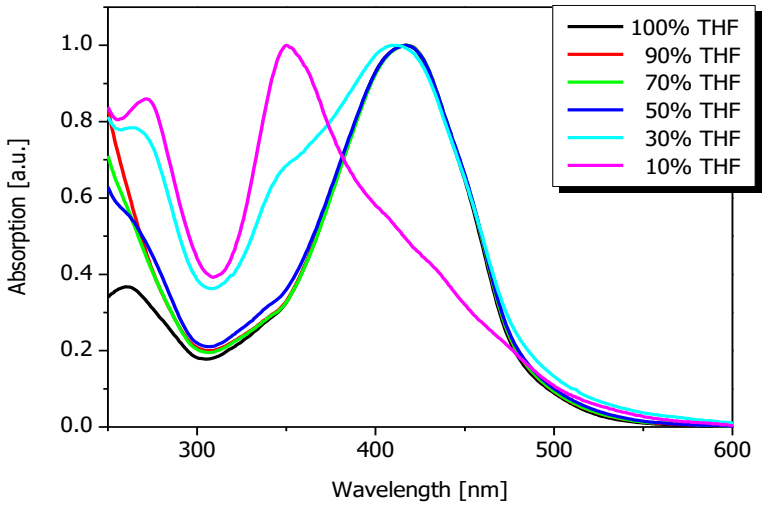

Figure 4.21. *Normalized absorption spectra of quaterthiophene-proline hybrid* ***3.3*** *upon titration of the THF solution with water. Black curve: absorption spectrum of the 100% THF solution; red curve: absorption spectrum of the THF/water (9:1) solution; green curve: absorption spectrum of the THF/water (7:3) solution; blue curve: absorption spectrum of the THF/water (1:1) solution; cyan curve: absorption spectrum of the THF/water (3:7) solution; magenta curve: absorption spectrum of the THF/water (1:9) solution.*

In order to study the stability of the formed suprastructures, temperature-dependent UV/Vis measurements were carried out on the THF/water (1:9) solution (***Figure 4.22***).

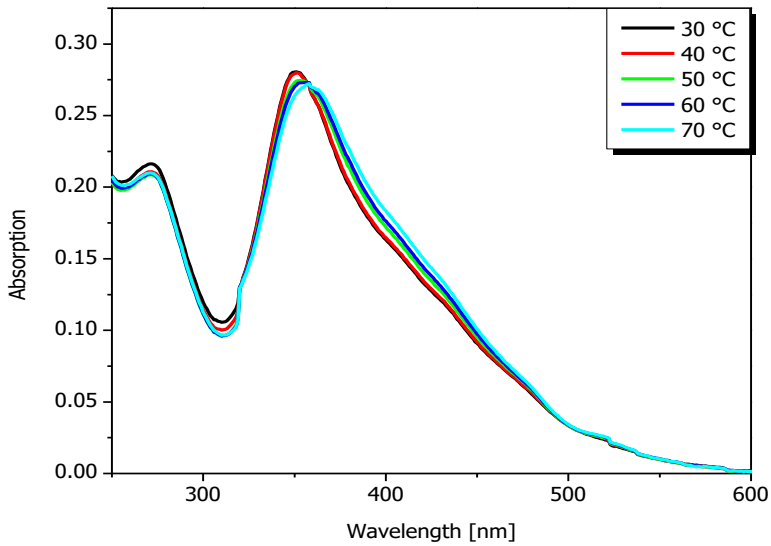

Figure 4.22. *Temperature-dependent absorption spectra of* ***3.3****, [c] = 5 x* 10^{-5} *M in THF/water (1:9). Black curve: absorption spectrum at 30 °C; red curve: absorption spectrum at 40 °C; green curve: absorption spectrum at 50 °C; blue curve: absorption spectrum at 60 °C; cyan curve: absorption spectrum at 70 °C.*

By increasing the temperature, the absorbance band at 350 nm slightly decreased, as shown in ***Figure 4.22***. This indicates that the aggregates which are formed in this aqueous solution are thermodynamically stable.

By comparing the emission spectra of the neat THF solution and the THF/water (1:9) mixture, a quenching of the emission transition bands of hybrid **3.3** in the aqueous solution was observed which corresponds to 9% of its previous emission intensity in pure THF (***Figure 4.23***).

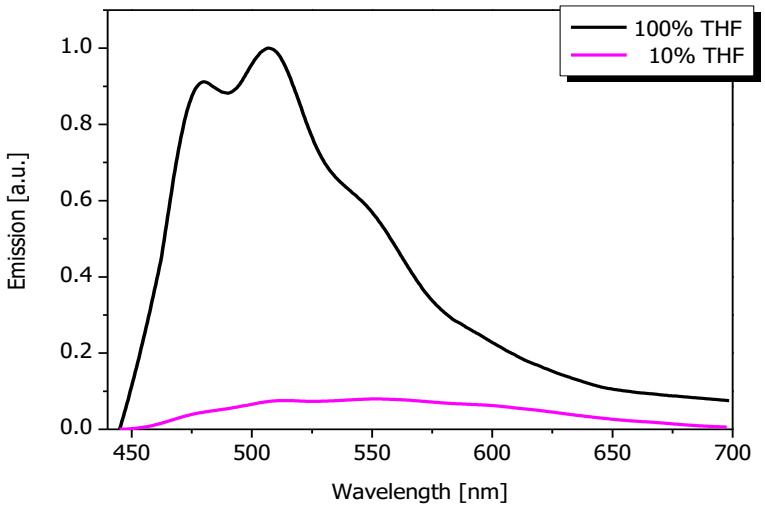

Figure 4.23. *Comparison of the normalized emission spectrum of* ***3.3****, [c] =* 10^{-7} *M in THF (black curve) and the quenched emission spectrum in THF/water (1:9)solution (magenta curve).*

The self-assembling behaviour was further studied by CD-measurements in different THF/water ratios. Until 50% water content in THF no signal could be detected in the wavelength range between 250 and 600 nm corroborating the UV/Vis results, which indicated no aggregation of **3.3** under these conditions. The aggregate formation was observed starting from the THF/water (3:7) solution, in which a negative Cotton-effect with the minimum located at 341 nm was observed (***Figure 4.24, cyan curve***). This indicates that in such solution the chromophores organize in a left-handed helical way, but they are electronically decoupled. In the THF/water (1:9) solution quaterthiophene-proline **3.3** disposed of a bisignate CD-signal consisting of a negative Cotton-effect with the minimum located at 364 nm and a positive Cotton-effect with the maximum situated at 332 nm.

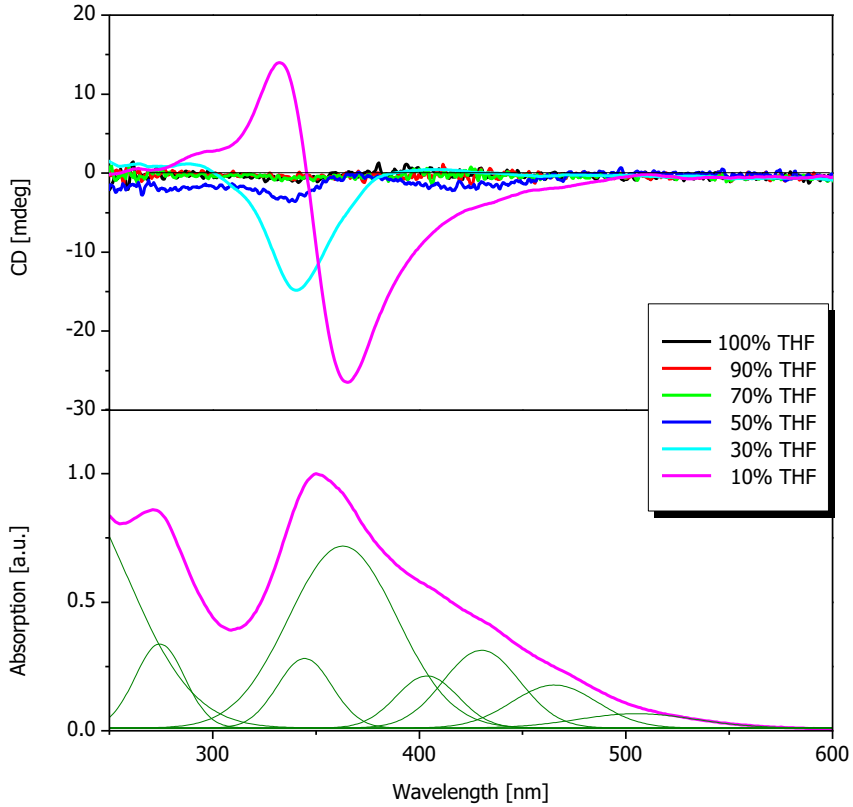

Figure 4.24. *CD-spectra of hybrid* ***3.3*** *upon titration of the THF solution with water (top), [c] = 5 x 10^{-5} M. Black curve: CD-spectrum of the 100% THF solution; red curve: CD- spectrum of the THF/water (9:1) solution; green curve: CD-spectrum of the THF/water (7:3) solution; blue curve: CD-spectrum of the THF/water (1:1) solution; cyan curve: CD-spectrum of the THF/water (3:7) solution; magenta curve: CD- (top) and absorption (bottom) spectra of the THF/water (1:9) solution; olive curves: deconvoluted absorption spectra.*

These findings point to the formation of left-handed supramolecular structures. The correlation between the zero-crossing of the bisignated signal and the maximum of the Gaussian curve deconvoluted from the absorption spectra in the solvent mixture evidences the exciton-coupled character of the transition. No CD-signal appeared in the triazole area (λ = 260 nm) indicating that the supramolecular chirality of this molecule part can be excluded.

Looking at the CD-spectra of the THF/water (1:9) solution after one and two days aging, neither drastic change in shape nor in helicity could be observed indicating that the aggregates have a thermodynamically stable nature (***Figure 4.25***). Nevertheless, the bisignate CD-signal lost intensity after one day (***Figure 4.25***, ***curve orange and violet***). This was due to the precipitation in solution of the aggregates which became bigger after leaving the THF/water (1:9) mixture aging, as was also observed in case of hybrid **3.2**.

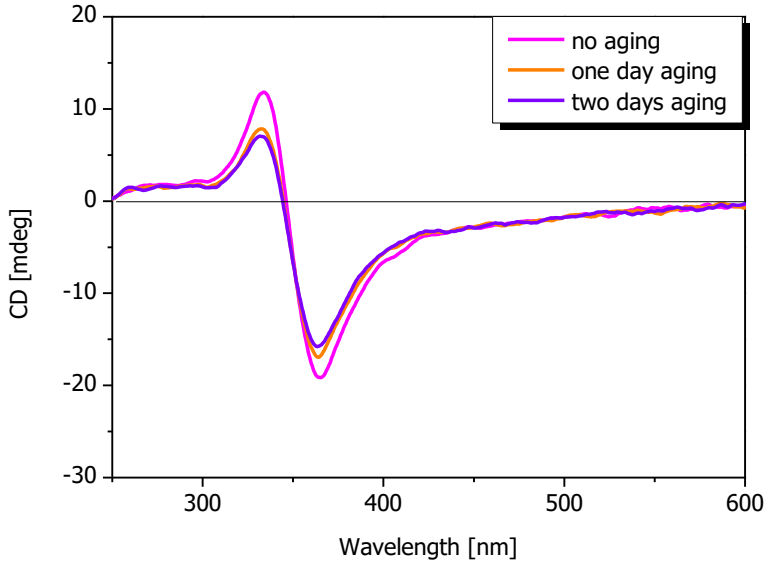

Figure 4.25. *CD-spectra of the THF/water (1:9) solution of hybrid* ***3.3****, [c] = 5 x 10 $^{-5}$ M. Magenta curve: before aging; light orange curve: after one day aging; violet curve: after two days aging.*

The stability of the supramolecular structures formed in the THF/water (1:9) solution was verified by temperature-dependent CD-spectroscopy (***Figure 4.26***).

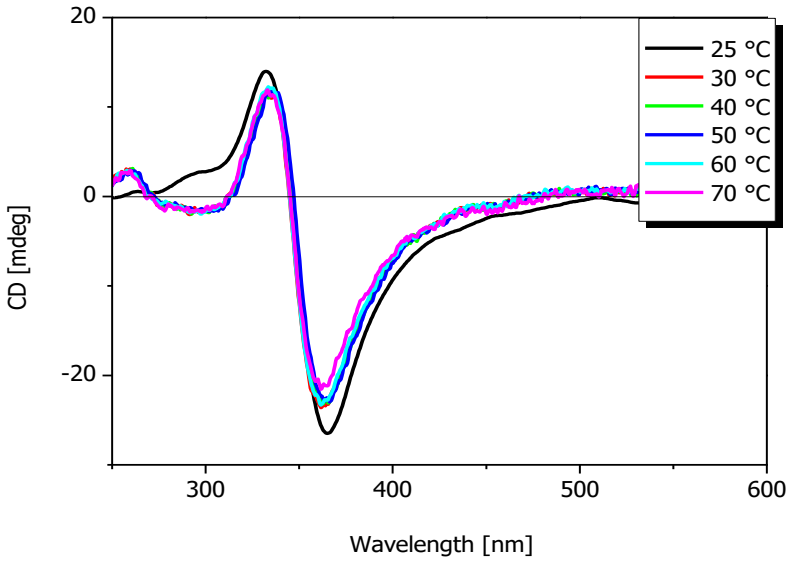

Figure 4.26*. Temperature-dependent CD-spectra of hybrid* ***3.3****, [c] = 5 x 10 $^{-5}$ M. Black curve: CD-spectrum at 30 °C; red curve: CD-spectrum at 40 °C; green curve: CD-spectrum at 50 °C; blue curve: CD-spectrum at 60 °C; cyan curve: CD-spectrum at 70 °C.*

Going from 25 °C to 30 °C the chromophores slightly rearranged into the supramolecular structures: a decrease of the intensity was observed. Additionally, a new signal at 270 nm appeared which correlates with the absorption region of the 1,2,3-

triazole unit. At higher temperatures no changes could be detected, meaning that the suprastructures are stable.

At room temperature, the presence of particles with an average thermodynamic radius of ca. 133 nm in the THF/water (1:9) solution could be detected carrying out DLS experiments (***Figure 4.27***).

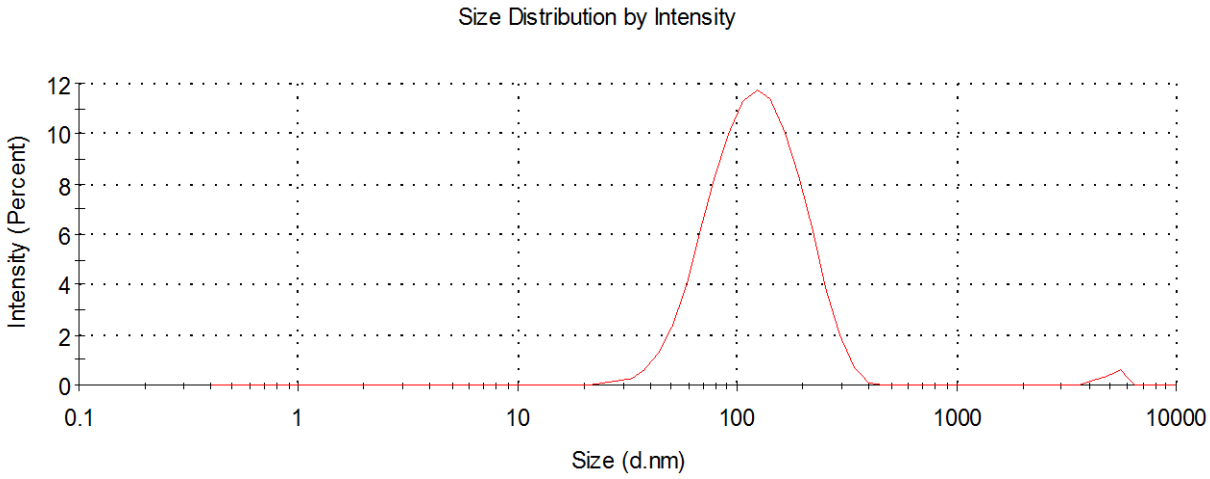

Figure 4.27. *DLS measurement of the aggregate size of hybrid* ***3.3*** *in the THF/water (1:9) solution, [c] = 5 x 10 $^{-5}$ M.*

4.3.2.3 UV/Vis-, Fluorescence-, CD-Spectroscopy, and DLS Measurements of α-Ethylhexyl Substituted Quaterthiophene-Proline ***3.4***

The self-assembly properties of ethylhexyl-substituted quaterthiophene **3.4** (***Chart 4.7***) were investigated in different THF/water ratios.

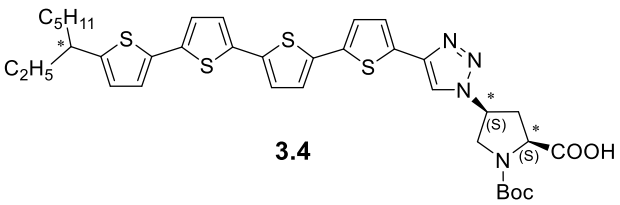

3.4

Chart 4.7. *Molecular structure of α-ethylhexyl substituted quaterthiophene-proline hybrid* ***3.4****.*

Looking at the normalized absorption spectra, it was observed that the aggregation process started in the THF/water (1:9) solution, as the absorption maximum relative

to the π-π* transition was hypsochromically shifted and the shape of the absorption band became asymmetric (***Figure 4.28***).

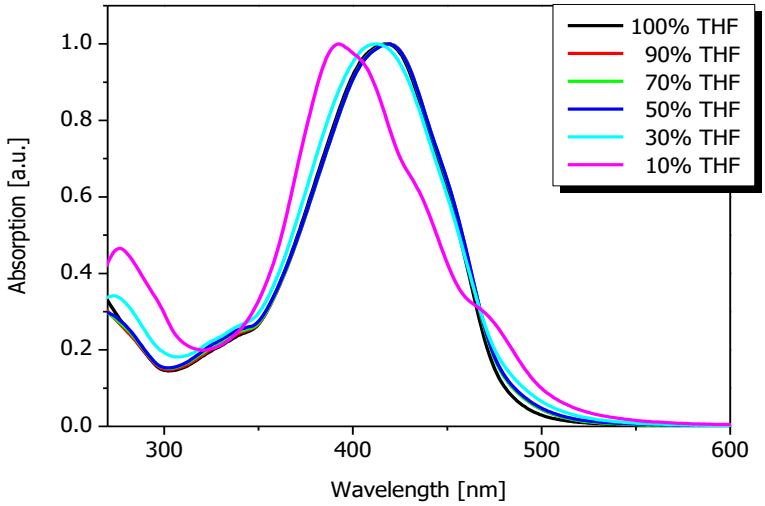

Figure 4.28. *Normalized absorption spectra of hybrid **3.4** upon titration of the THF solution with water. Black curve: absorption spectrum of the 100% THF solution; red curve: absorption spectrum of the THF/water (9:1) solution; green curve: absorption spectrum of the THF/water (7:3) solution; blue curve: absorption spectrum of the THF/water (1:1) solution; cyan curve: absorption spectrum of the THF/water (3:7) solution; magenta curve: absorption spectrum of the THF/water (1:9) solution.*

As assessed for hybrid **3.3**, it could be assumed that also quaterthiophene **3.4** assembles in *H*-type aggregates. However, the λ_{max} of the cyan curve is also slightly blue-shifted in comparison to the absorption spectra of **3.4** in the other solvent mixtures. This indicates that self-assembly is already occuring in the THF/water (3:7) solution. Besides, the weak transition band at low energy (λ > 450 nm) corresponds to the forbidden antiparallel alignment of the transition dipoles. The absorption band of the 1,2,3-triazole became more pronounced upon increasing the water amount. This indicates that this molecule unit participates in the self-assembling process.

The stability of the aggregates formed in the THF/water (1:9) solution was investigated by temperature-dependent UV/Vis spectroscopy. No alteration of the absorption band with the maximum located at 392 nm was detected at higher temperatureswas observed (***Figure 4.29***) indicating that the suprastructures are very stable.

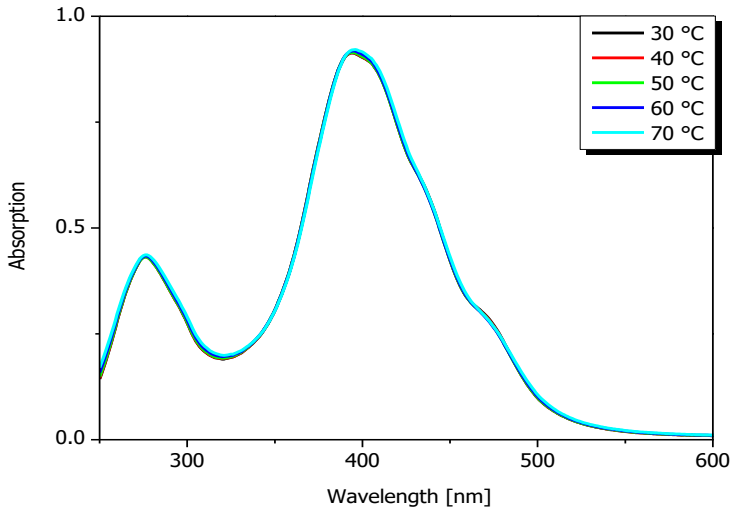

Figure 4.29. *Temperature-dependent absorption spectra of* ***3.4****, [c] = 5 x* 10^{-5} *M in THF/water (1:9) solution. Black curve: absorption spectrum at 30 °C; red curve: absorption spectrum at 40 °C; green curve: absorption spectrum at 50 °C; blue curve: absorption spectrum at 60 °C; cyan curve: absorption spectrum at 70 °C.*

The emission bands of hybrid **3.4** were strongly quenched in the THF/water (1:9) solution in comparison with the emission spectrum in pure THF (***Figure 4.30***, ***a***). In fact, the emission decreased to 96% of its previous emission intensity in pure THF. At the same time, in the THF/water (1:9) solution the emission maxima at 479 nm and 507 were quenched, whereas the transitions at 561 nm and 592 nm got more intense in comparison to the emission spectrum of quaterthiophene-proline **3.4** in pure THF (***Figure 4.30***, ***b***).

a)

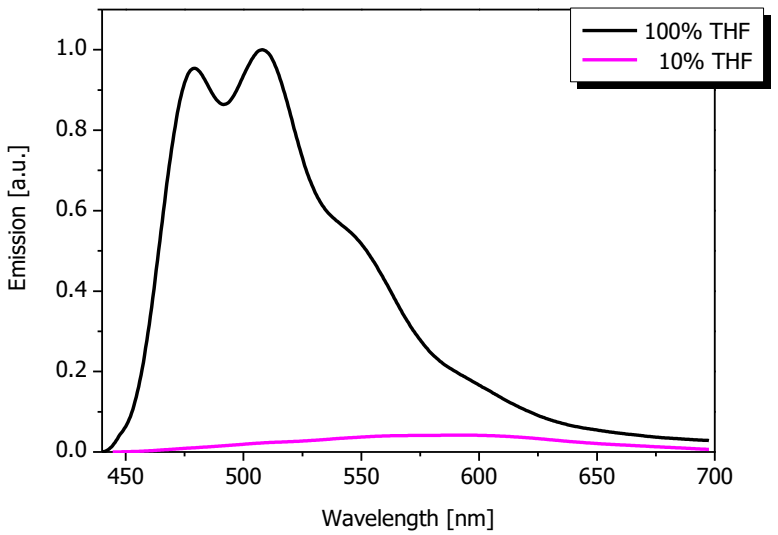

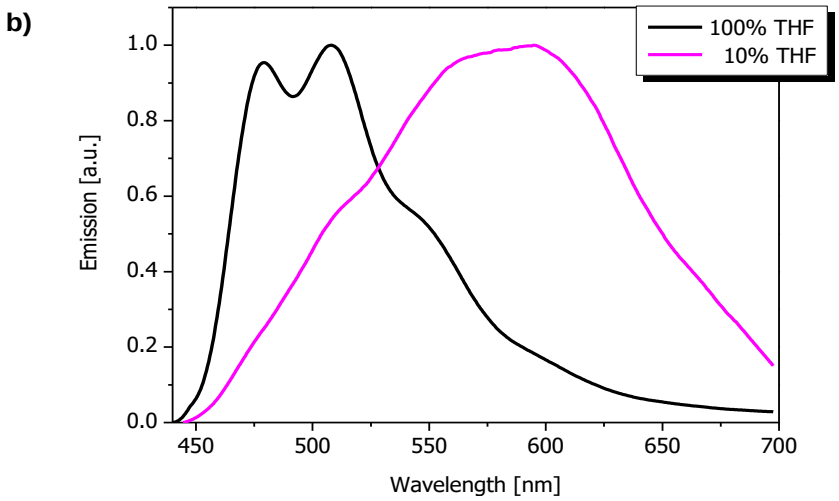

Figure 4.30. *a) Comparison of the emission spectrum of a)* ***3.4****, [c] =* 10^{-7} *M in THF (black curve) and the quenched emission spectrum inTHF/water (1:9) solution (magenta curve); b) comparison of the normalized emission spectra of* ***3.4****, [c] =* 10^{-7} *M in THF (black curve) and THF/water (1:9 solution) (magenta curve) (bottom).*

The aggregation process was further investigated by CD-spectroscopy. No chiral aggregates were detected in neat THF and in the THF/water (9:1), (7:3) and (1:1) solutions (***Figure 4.31***, ***top***). A CD-signal between 250 and 600 nm was detected starting from the THF/water (3:7) solution, reaching a maximum of intensity in the THF/water (1:9) solution (***Figure 4.31***, ***top***). Looking at both cyan and magenta curves, a negative Cotton-effect whose minimum was located at λ = 446 nm, was observed, followed by a positive Cotton-effect with the maximum at 392 nm and again a negative Cotton-effect with the minimum located at λ = 367 nm. The zero-crossing at higher wavelength coincides with the λ_{max} of the absorption band at 408 nm deconvoluted from the absorption spectrum of **3.4** in the THF/water (1:9) solution. The second zero-crossing (λ = 377 nm) corresponds almost exactly to the deconvoluted absorption band whose maximum is located at 479 nm. The UV/vis absorptions in the longer wavelength region at 435 nm and 470 nm are caused by *J*-type aggregates of the chromophores and their energies match almost those of the shoulders in the corresponding CD-spectrum. Due to the negative sign of the Cotton bands a left-handed helical arrangement of the quaterthiophenes in the *J*-type supramolecular packing of hybrid **3.4** can be concluded. Furthermore, the CD-spectrum revealed an almost complete absence of chirality below 300 nm. This indicates that supramolecular chirality of the 1,2,3-triazole unit can be excluded.

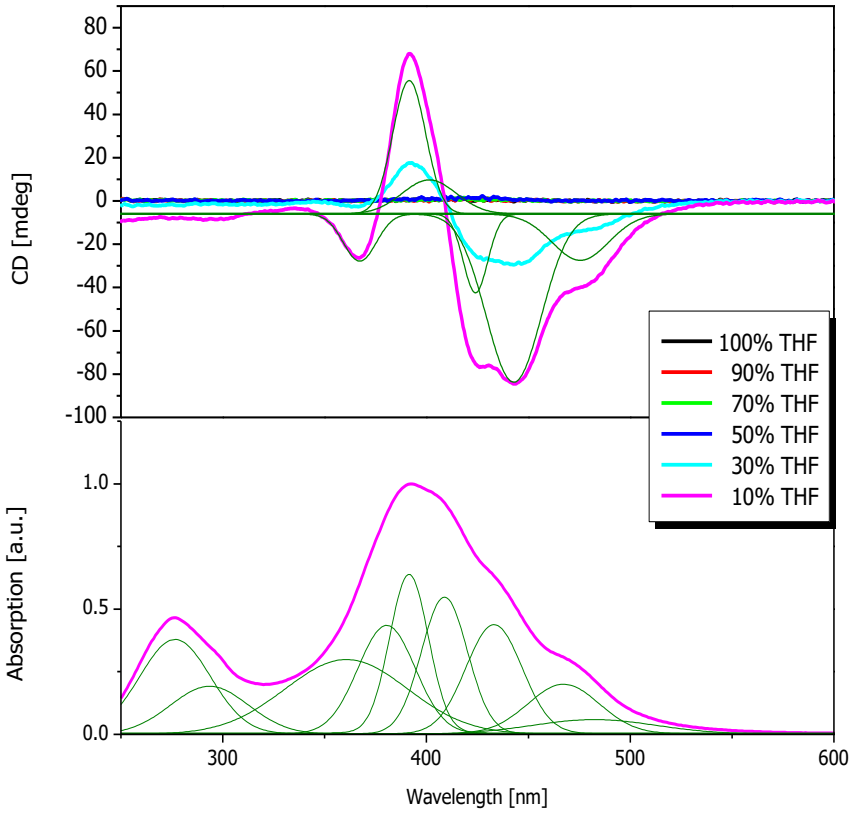

Figure 4.31. *CD-spectra of hybrid **3.4** upon titration of the THF solution with water (top), [c] = 5 x 10^{-5} M. Black curve: CD-spectrum of the 100% THF solution; red curve: CD-spectrum of the THF/water (9:1) solution; green curve: CD-spectrum of the THF/water (7:3) solution; blue curve: CD-spectrum of the THF/water (1:1) solution; cyan curve: CD-spectrum of the THF/water (3:7) solution; magenta curve: CD- (top) and absorption (bottom) spectra of the THF/water (1:9) solution; olive curves: deconvoluted CD- and absorption spectra.*

The THF/water (1:9) solution of hybrid **3.4** was additionally aged for two days (***Figure 4.32***). No changes were observed for the negative Cotton-effect located at higher wavelength, whereas the positive and negative CD-signals at higher energy increased in intensity after two days aging.

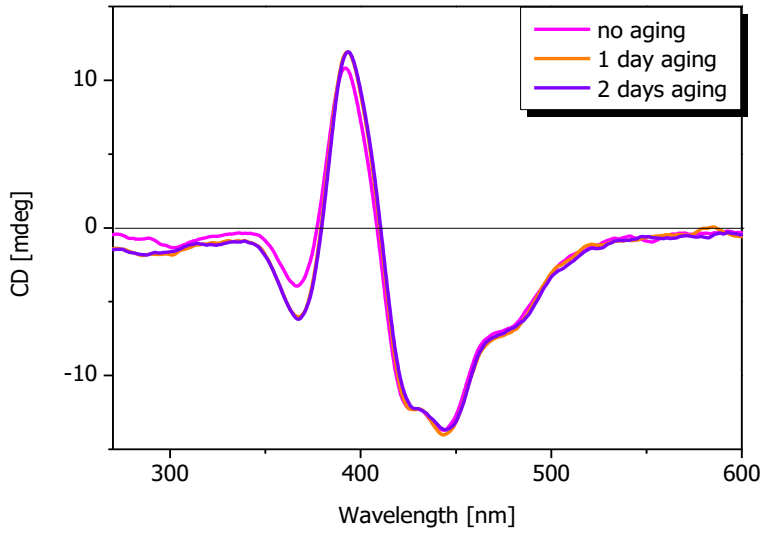

Figure 4.32. *CD-spectra of the THF/water (1:9) solution of hybrid* ***3.4****, [c] = 5 x 10^{-5} M. Magenta curve: before aging; light orange curve: after one day aging; violet curve: after two days aging.*

However, looking at the temperature-dependent CD-measurements of the THF/water (1:9) solution, it was observed that at high temperature the negative Cotton-effect located at 367 nm disappeared and the positive Cotton effect lost intensity (***Figure 4.33***).

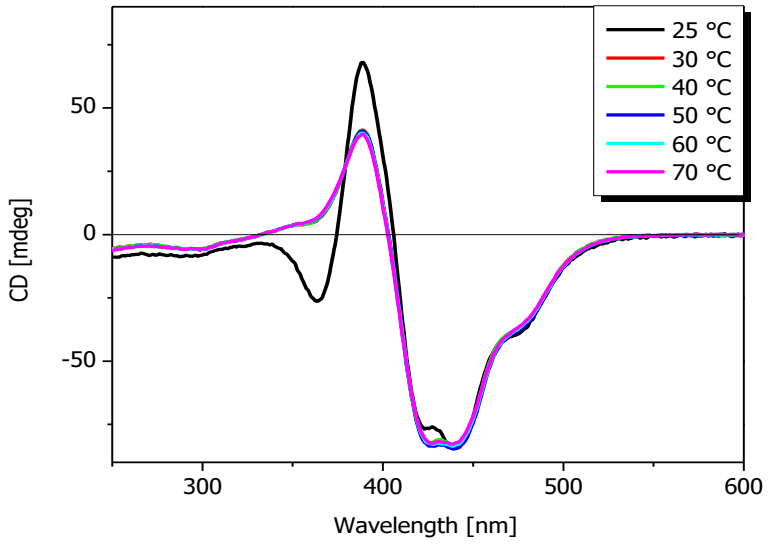

Figure 4.33. *Temperature-dependent CD-spectra of hybrid* ***3.4****, [c] = 5 x 10^{-5} M. Black curve: CD-spectrum at 30 °C; red curve: CD-spectrum at 40 °C; green curve: CD-spectrum at 50 °C; blue curve: CD-spectrum at 60 °C; cyan curve: CD-spectrum at 70 °C.*

This indicates that the interactions, which are involved in this supramolecular order are not strong. On the contrary, the negative CD-signal at higher wavelength was almost not affected by increasing temperature confirming the high stability of the suprastructures.

Furthermore, DLS measurements were carried out in the THF/water (1:9) solution: the presence of particles with an average thermodynamic radius of 136 nm could be detected (***Figure 4.34***).

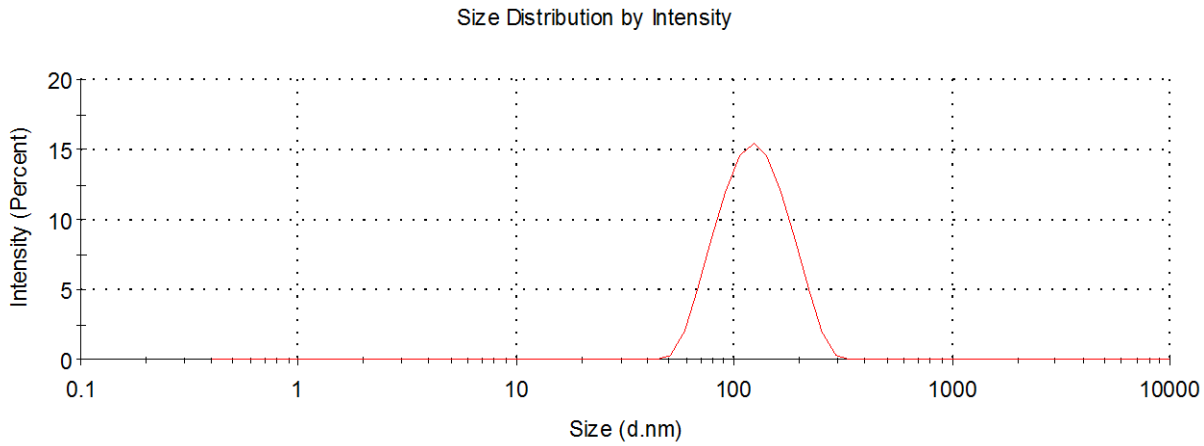

Figure 4.34. *DLS measurement of the aggregate size of hybrid* ***3.4*** *in the THF/water (1:9) solution, [c] = 5 x* 10^{-5} *M.*

4.3.2.4 UV/Vis-, Fluorescence-, CD-Spectroscopy, and DLS Measurements of α-Hexyl-Substituted Quaterthiophene-Proline Hybrids ***3.5*** *and* ***3.6*** *in Aqueous Solutions*

The self-assembly properties of the enantiomeric pair **3.5** and **3.6** were investigated in different THF/water ratios.

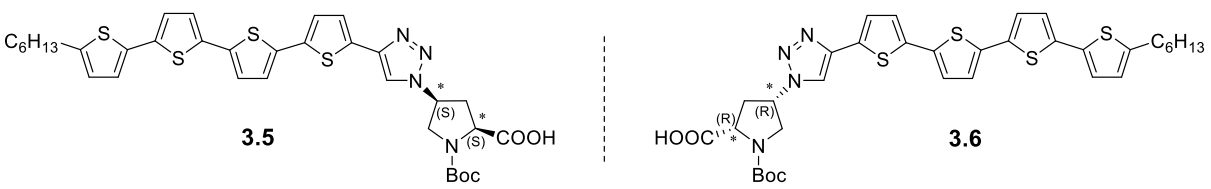

Chart 4.8. *Molecular structures of α-hexyl-substituted quaterthiophene-proline enantiomers* ***3.5*** *and* ***3.6****.*

No changes of the absorption spectra of the 100% THF and the THF/water (9:1), (7:3) and (1:1) solutions were observed (***Figure 4.35***). Starting from the THF/water (3:7) solution (***Figure 4.35***, ***cyan curve***), the formation of aggregates was detected. In fact, a hypsochromic shift of λ_{max} was observed reaching a maximum of $\Delta\lambda$ = 53 nm in case of the THF/water (1:9) solution. The evident asymmetrical shape of the absorption band and the strong blue-shifted component at λ_{max} = 363 nm account for the formation of *H*-type aggregates in the solvent mixture. The absorption band, whose maximum was located at 274 nm, became more intense in the THF/water (3:7) and (1:9) solutions. This indicates that the triazolyl moiety participates in the self-assembling process.

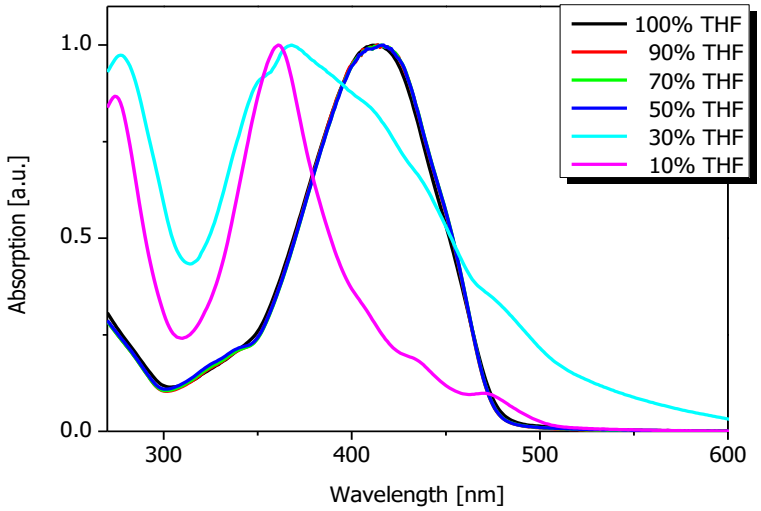

Figure 4.35. *Normalized absorption spectra of hybrid* ***3.5*** *upon titration of the THF solution with water. Black curve: absorption spectrum of the 100% THF solution; red curve: absorption spectrum of the THF/water (9:1) solution; green curve: absorption spectrum of the THF/water (7:3) solution; blue curve: absorption spectrum of the THF/water (1:1) solution; cyan curve: absorption spectrum of the THF/water (3:7) solution; magenta curve: absorption spectrum of the THF/water (1:9) solution.*

Because both enantiomers showed the same optical properties (***Figure 4.36***), I will mostly report on results obtained for (2*S*,4*S*)-hybrid **3.5**.

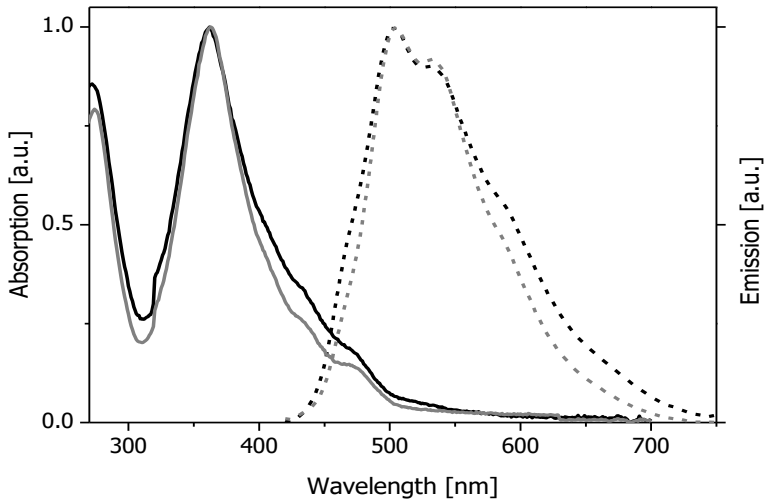

Figure 4.36. *Normalized UV/Vis and fluorescence spectra of (2S,4S)-hybrid* ***3.5*** *(black curve) and the (2R,4R)-hybrid* ***3.6*** *(grey curve), [c] = 5 x 10^{-5} M in THF/water (1:9) solution.*

The stability of the aggregates in the THF/water (1:9) (***Figure 4.37***) and (3:7) (***Figure 4.38***) solutions was investigated by temperature-dependent UV/Vis spectroscopy in a temperature range between 30 °C and 70 °C taking steps of 10 °C. At high temperatures, no relevant changes of the absorption bands in the THF/water (1:9) solution were detected (***Figure 4.37***), indicating that the suprastructures are extraordinary stable.

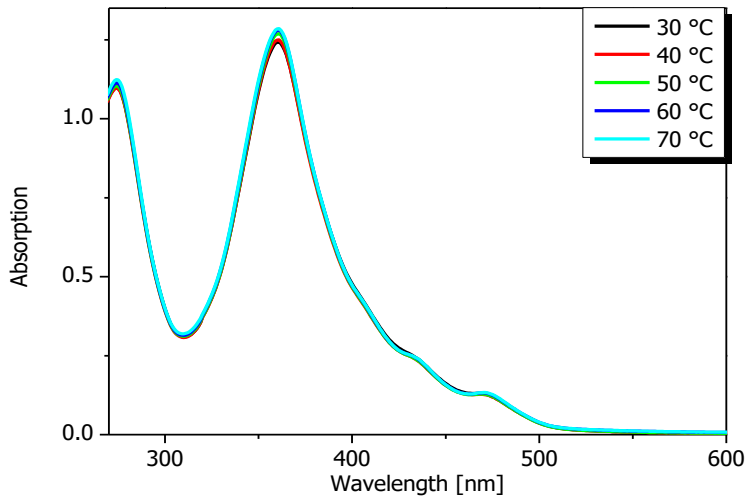

Figure 4.37. *Temperature-dependent absorption spectra of quaterthiophene-proline hybrid* ***3.5*** *in the THF/water (1:9) solution, [c] = 5 x 10^{-5} M. Black curve: absorption spectrum at 30 °C; red curve: absorption spectrum at 40 °C; green curve: absorption spectrum at 50 °C; blue curve: absorption spectrum at 60 °C; cyan curve: absorption spectrum at 70 °C.*

On the contrary, the supramolecular structures which are formed in the THF/water (3:7) solution are not thermodynamically stable. In fact, upon increasing temperature, the aggregates disassemble recovering the absorption spectrum observed in the case of the molecularly dissolved state (***Figure 4.38***, ***cyan curve***).

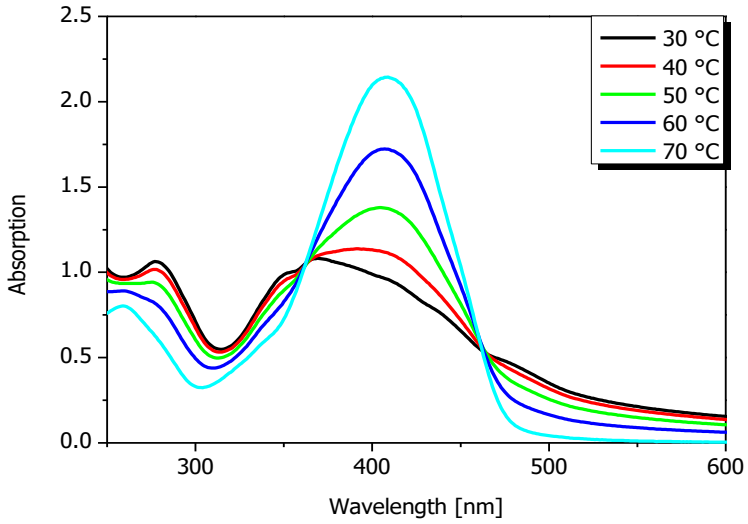

Figure 4.38. *Temperature-dependent absorption spectra of* ***3.5*** *in the THF/water (3:7) solution, [c] = 5 x 10^{-5} M. Black curve: absorption spectrum at 30 °C; red curve: absorption spectrum at 40 °C; green curve: absorption spectrum at 50 °C; blue curve: absorption spectrum at 60 °C; cyan curve: absorption spectrum at 70 °C.*

Because of the two isosbestic points located at 362 nm and 462 nm, respectively, it could be assessed that the species are in equilibrium between the molecularly dissolved and the aggregated states. In particular, it was interesting to analyse and to compare the three absorption components located at 348 nm, 412 nm, and 480 nm, respectively. In fact, plotting the percentage of absorption decrease/increase for each band against the temperature, it was observed that the band at 480 nm (***Figure 4.39***, ***blue curve***) decreased faster than the absorption band situated at 348 nm (***Figure 4.39***, ***black curve***). This may indicate that upon increasing temperature, the species absorbing at 480 nm are less stable than those absorbing at lower wavelength. Additionally, the intensity of the band at 413 nm increased rapidly going to higher temperatures. This confirmed that the aggregates formed in the THF/water (3:7) solution are not particularly stable and are quickly redissolved.

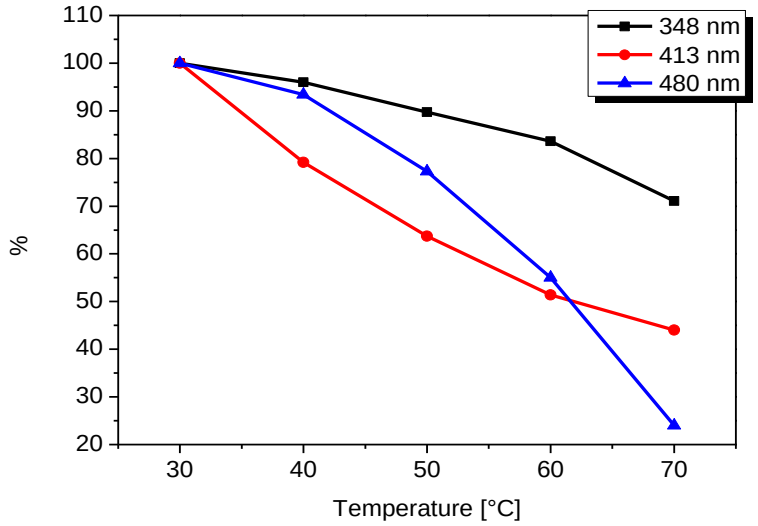

Figure 4.39. *Absorption decrease (in percent) for the maxima at 348 nm (black curve) and 480 nm (blue curve) and absorption increase (in percent) for the maximum at 413 nm, plotted against temperature.*

Looking at the fluorescence properties of hybrid **3.5** in pure THF and in THF/water (1:9) solution, a strong quenching of the emission band was observed (3% intensity of its previous emission intensity in pure THF) (***Figure 4.40***).

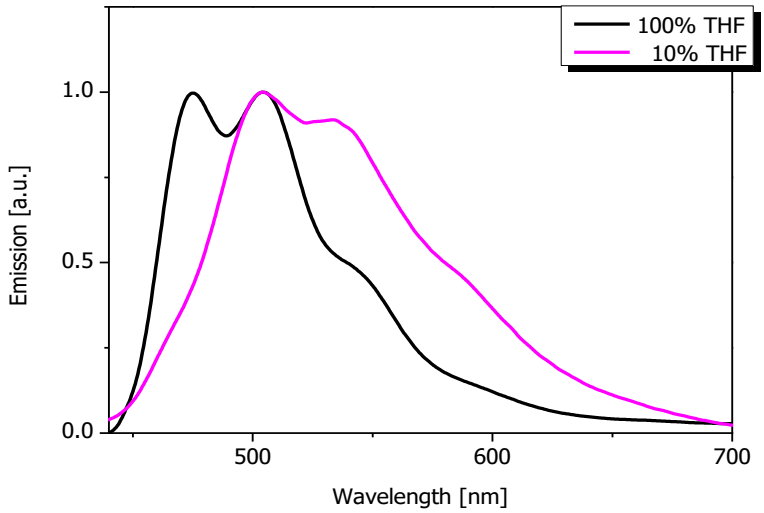

Figure 4.40. *Normalized emission spectra of **3.5**, [c] = 10^{-7} M in THF (black curve) and in THF/water (1:9) solution (magenta curve).*

Additionally, a quenching of the emission transition at 474 nm and, at the same time, an increase in intensity of the emission bands at 505 nm, 537 nm, and 594 nm were detected. Therefore, the formation of aggregates in the presence of water was as-

sessed. The self-assembly of quaterthiophene-proline **3.5** was further investigated by CD-spectroscopy. In the 100% THF solution a positive Cotton-effect with the maximum located at 378 nm and a weak negative Cotton-effect with the minimum at 342 nm were observed (***Figure 4.41***, ***black curve***). This indicates that chiral supramolecular structures are also present in the neat THF solution. In the THF/water (9:1), (7:3) and (1:1) mixtures no CD-signals were detected (***Figure 4.41***, ***red***, ***green***, ***blue curves***). This outcome is in agreement with the UV/Vis measurements, where no aggregation was observed (***Figure 4.35***).

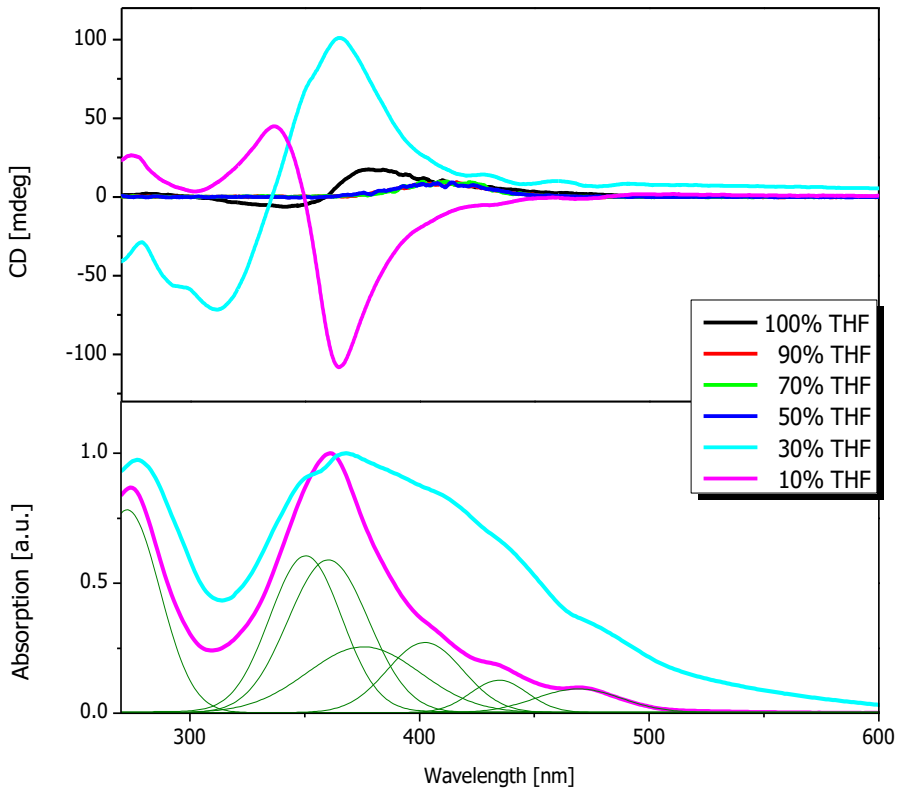

Figure 4.41. *CD-spectra of hybrid* ***3.5*** *upon titration of the THF solution with water (top), [c] = 5 x 10^{-5} M. Black curve: CD-spectrum of the 100% THF solution; red curve: CD-spectrum of the THF/water (9:1) solution; green curve: CD-spectrum of the THF/water (7:3) solution; blue curve: CD-spectrum of the THF/water (1:1) solution; cyan curve: CD-spectrum of the THF/water (3:7) solution; magenta curve: CD- (top) and absorption (bottom) spectra of the THF/water (1:9) solution; olive curves: deconvoluted CD- and absorption spectra.*

The appearance of a CD-signal in the wavelength range between 250 and 600 nm was again detected starting from the THF/water (3:7) solution (***Figure 4.41***, ***cyan curve***). A positive Cotton-effect (λ_{max} = 365 nm) was observed followed by a negative

Cotton-effect (λ_{min} = 319 nm); because the zero-crossing of the CD-signal ($\lambda_{zero\text{-}crossing}$ = 335 nm) was located at higher energy than the absorption maximum of **3.5** (λ = 363 nm) in the same THF/water solution, and, besides, the negative and positive bands are not symmetric to each other. It can be stated that the π-systems are electronically decoupled. In the THF/water (1:9) solution quaterthiophene **3.5** displayed a negative Cotton-effect, whose minimum was located at λ = 362 nm and a positive Cotton-effect with the maximum at 337 nm (***Figure 4.40***, ***top***, ***magenta curve***). The correlation between the zero-crossing (λ = 349 nm) of the bisignated bands and the maximum of the Gaussian curve deconvoluted from the absorption spectra of **3.5** in the solvent mixture (***Figure 4.41***, ***bottom***) evidences the exciton coupled character of the transition. The CD-spectrum revealed the presence of an additional positive Cotton-effect, whose maximum is located at 274 nm which corresponds to the absorption maximum of the 1,2,3-triazole. This indicates the supramolecular chirality of these molecule parts.

The self-assembled aggregates of the enantiomeric pair **3.5** and **3.6** formed in the THF/water (1:9) solvent mixture were compared by CD-spectroscopy (***Figure 4.42***).

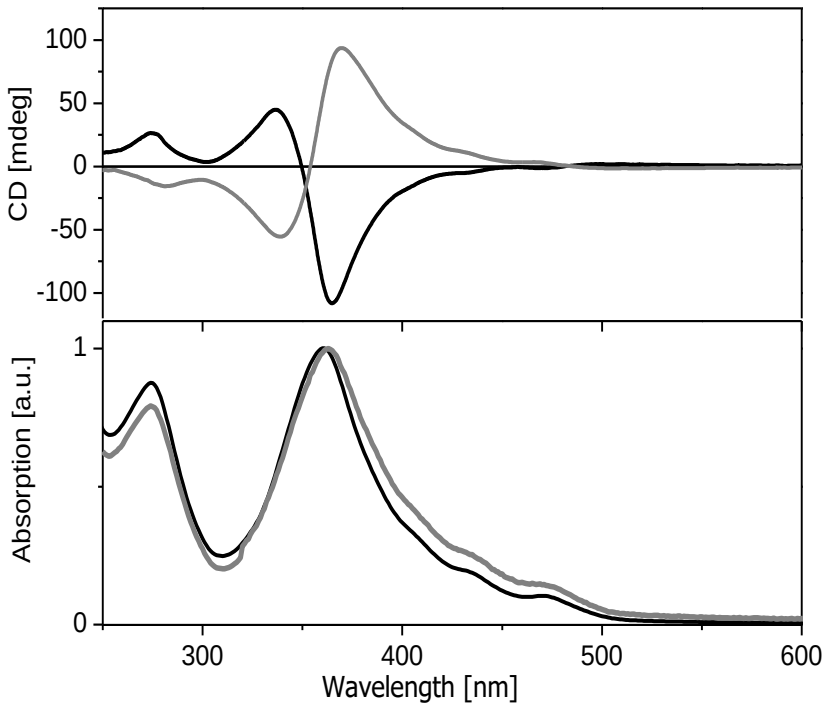

Figure 4.42. *Mirror-image CD-spectra (top) and UV/Vis curves (bottom) of quaterthiophene-proline hybrids **3.5** (black curve) and **3.6** (grey curve) in the THF/water (1:9) solution, [c] = 5 x 10^{-5} M.*

As expected, mirror-image CD-spectra were obtained (***Figure 4.42***, **top**). In fact, (2*R*,4*R*)-enantiomer **3.6** showed a positive couplet at 370 nm (+94 mdeg) and at 339 nm (-55 mdeg) (***Figure 4.42***, ***top***, ***grey curve***) corresponding to a right-handed helical arrangement of the chromophoric segments.

As additional experiment, the THF/water (1:9) solution of hybrid **3.5** was aged for two days (***Figure 4.43***). After one day, it was observed that the zero-crossing of the bisignate Cotton-effect and the minimum of the negative CD signal were hypsochromically shifted by 4 nm and 10 nm, respectively, and the intensity of the two CD-signals varied slightly. This indicates that the supramolecular structures formed in such THF/water mixture need one day to stabilize. In fact, it was observed that afterwards, no more changes occurred (***Figure 4.43***).

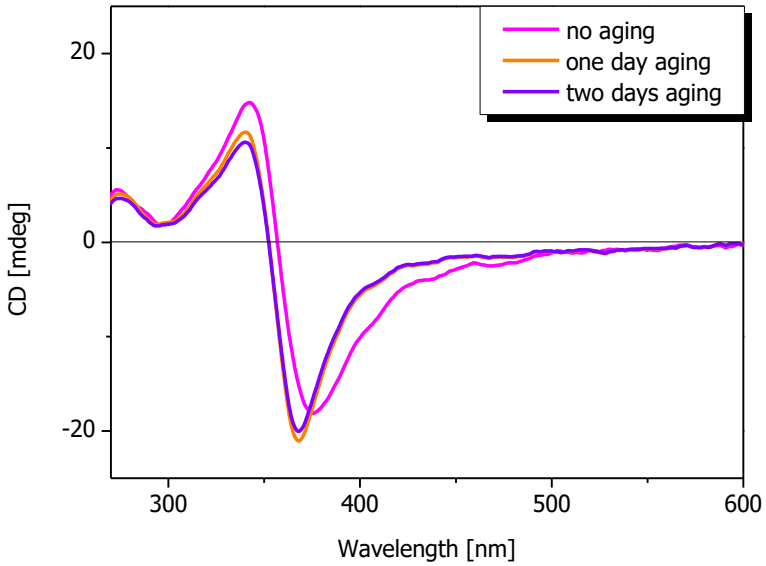

Figure 4.43. *CD-spectra of the THF/water (1:9) solution of hybrid* ***3.5****, [c] = 5 x 10^{-5} M. Magenta curve: before aging; light orange curve: after one day aging; violet curve: after two days aging.*

The stability of the suprastructures of hybrid **3.5** in the THF/water (1:9) (***Figure 4.44***) and in the THF/water (3:7) (***Figure 4.45***) mixtures was also investigated at high temperatures. Upon increasing temperature until 70 °C, the chiral aggregates in 90% aqueous solution were very stable.

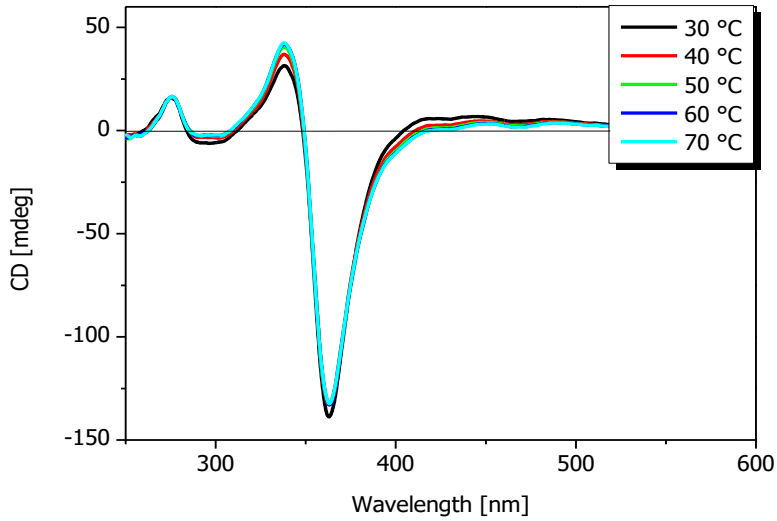

Figure 4.44. *Temperature-depending CD-spectra of hybrid* ***3.5*** *in the THF/water (1:9) solution, [c] = 5 x 10^{-5} M. Black curve: CD-spectrum at 30 °C; red curve: CD-spectrum at 40 °C; green curve: CD-spectrum at 50 °C; blue curve: CD-spectrum at 60 °C; cyan curve: CD-spectrum at 70 °C.*

In the case of the THF/water (3:7) solution, it was observed that upon increasing temperature the aggregates disassembled (***Figure 4.45***).

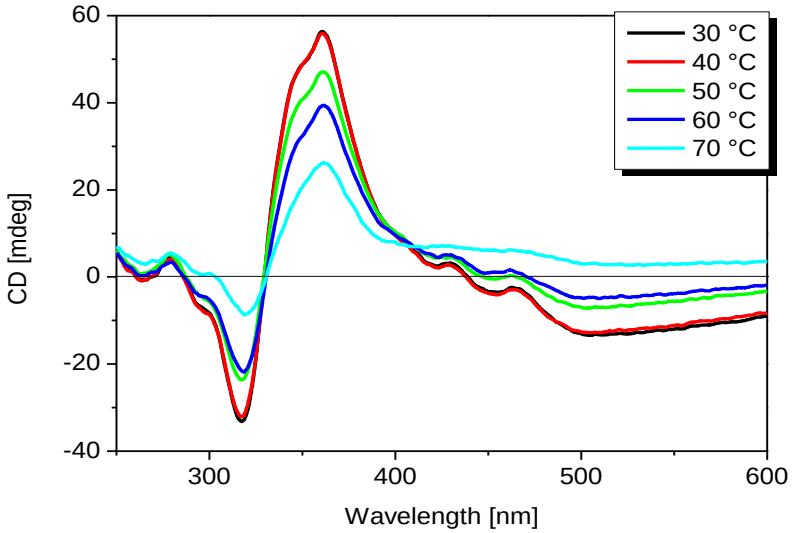

Figure 4.45. *Temperature-depending CD-spectra of hybrid* ***3.5*** *in the THF/water (3:7) solution, [c] = 5 x 10^{-5} M. Black curve: CD-spectrum at 30 °C; red curve: CD-spectrum at 40 °C; green curve: CD-spectrum at 50 °C; blue curve: CD-spectrum at 60 °C; cyan curve: CD-spectrum at 70 °C.*

The quenching in percent of the positive and negative Cotton-effect in correspondence to their maximum (360 nm) and minimum (317 nm), respectively, plotted

against the temperature is reported in ***Figure 4.46***. It was observed that both CD-signals are quenched almost with the same velocity upon increasing the temperature.

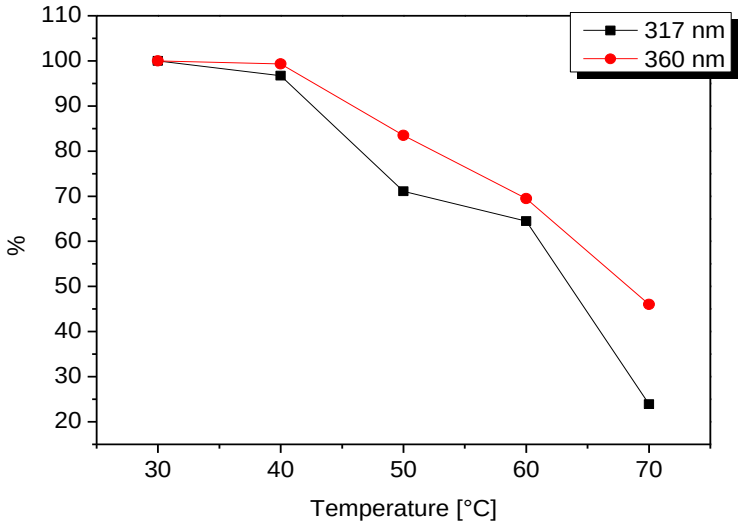

Figure 4.46. *Intensity quenching in percent of the Cotton-effects at 317 nm (black curve) and 360 nm (red curve) against the temperature.*

DLS measurements were performed with the THF/water (1:9) solution of hybrid **3.5**. Particles of 20 nm and 70 nm in diameter were detected, whereas only few bigger aggregates (~1.8 µm) were also observed (***Figure 4.47***).

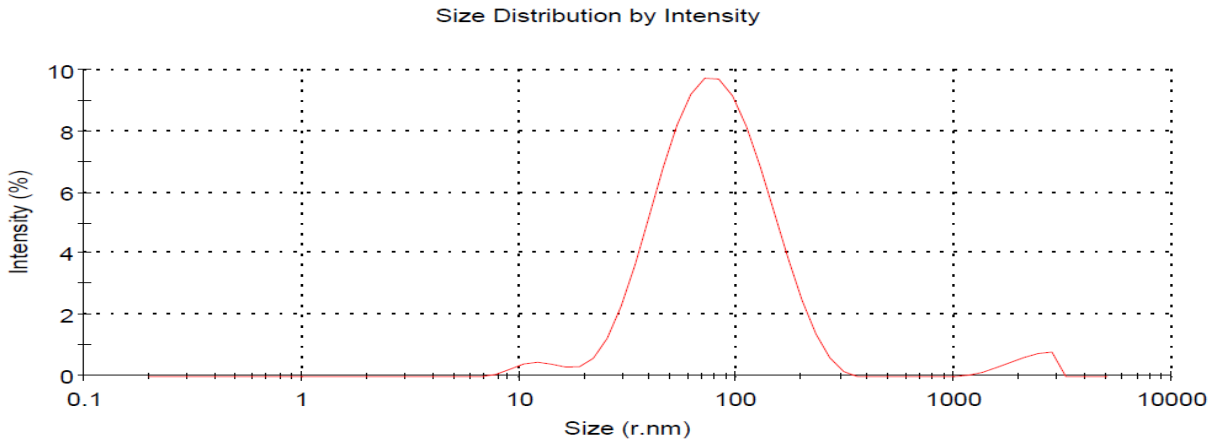

Figure 4.47. *DLS measurement of the aggregate size of hybrid **3.5** in THF/water (1:9) solution at room temperature, [c] = 5 x 10 -5 M.*

4.3.2.5 UV/Vis-, Fluorescence-, CD-Spectroscopy, and DLS Measurements of α-Hexyl-substituted Quaterthiophene-Proline Hybrid **3.5** in Apolar Solutions

The self-assembly of biohybrid **3.5** was also studied in an apolar solvent mixture such as chloroform/*n*-hexane. This study should help to analyse more deeply the formation of the supramolecular structures and the forces involved during the self-assembly. In this case, the self-organizing process should be guided more by the hydrophilic forces such as *H*-bond interactions than the hydrophobic forces like π-π stacking and van der Waals interactions. Firstly, the aggregation process was investigated by UV/Vis spectroscopy (***Figure 4.48***).

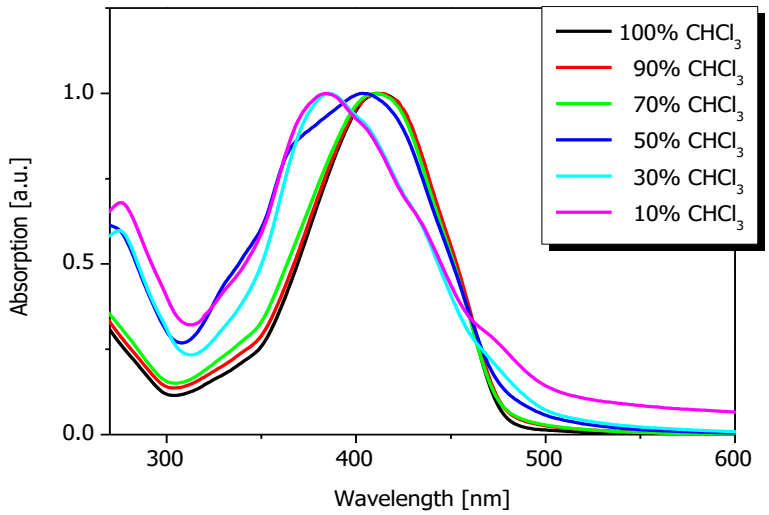

Figure 4.48. *Normalized absorption spectra of hybrid **3.5** upon titration of the chloroform solution with n-hexane. Black curve: absorption spectrum of the 100% chloroform solution; red curve: absorption spectrum of the chloroform/n-hexane (9:1) solution; green curve: absorption spectrum of the chloroform/n-hexane (7:3) solution; blue curve: absorption spectrum of the chloroform/n-hexane (1:1) solution; cyan curve: absorption spectrum of the chloroform/n-hexane (3:7) solution; magenta curve: absorption spectrum of the chloroform/n-hexane (1:9) solution.*

Upon titration of the chloroform solution with *n*-hexane a blue-shift of the absorption band was observed reaching a maximum in the chloroform/*n*-hexane (1:9) solution ($\Delta\lambda$ = 29 nm). The asymmetry of the shape of the absorption band together with the blue-shifted component at λ_{max} = 384 nm accounts for the formation of *H*-type aggre-

gates in the solvent mixture. It is interesting to see that in apolar environments the formation of supramolecular structures occurs already in the chloroform/*n*-hexane (1:1) solution (***Figure 4.48***, ***blue curve***).

In order to study the stability of the aggregates formed in the chloroform/*n*-hexane (1:9) solution, temperature-dependent UV/Vis measurements were carried out (***Figure 4.48***). In the apolar mixture the aggregates showed low thermodynamic stability. In fact, upon increasing the temperature a red shift of the absorption maximum was observed and, in particular, the absorption transition at 415 nm increased in intensity.

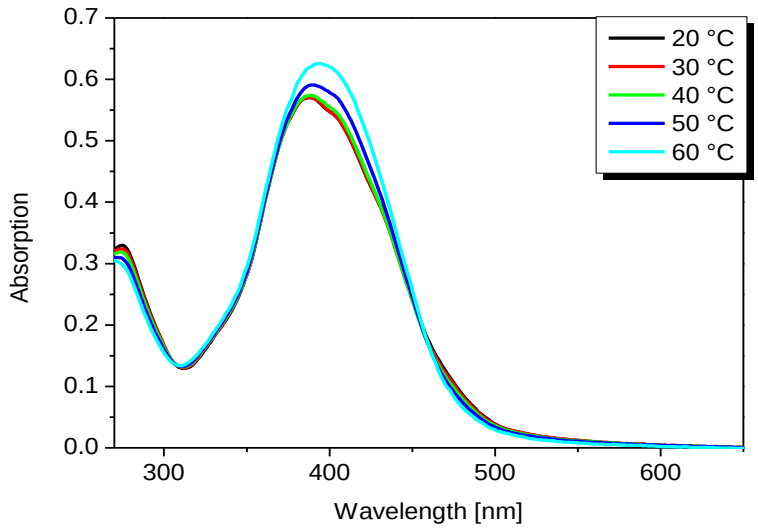

Figure 4.49. *Temperature-dependent absorption spectra of* ***3.5*** *in the chloroform/n-hexane (1:9) solution, [c] = 5 x 10^{-5} M. Black curve: absorption spectrum at 30 °C; red curve: absorption spectrum at 40 °C; green curve: absorption spectrum at 50 °C; blue curve: absorption spectrum at 60 °C; cyan curve: absorption spectrum at 70 °C.*

Looking at the fluorescence spectrum of the chloroform/*n*-hexane (1:9) solution (***Figure 4.50***, ***magenta curve***), the emission transitions located at 468 nm, 499 nm, and 538 nm are hypsochromically shifted ($\Delta\lambda$ = 10 nm) in comparison to the chloroform solution. This blue-shift may be due to the increased apolarity of the solvent mixture. Additionally, the intensity of the emission spectrum in the chloroform/*n*-hexane (1:9) solution decreased to 81% of the one in pure chloroform. This confirms for the formation of aggregates.

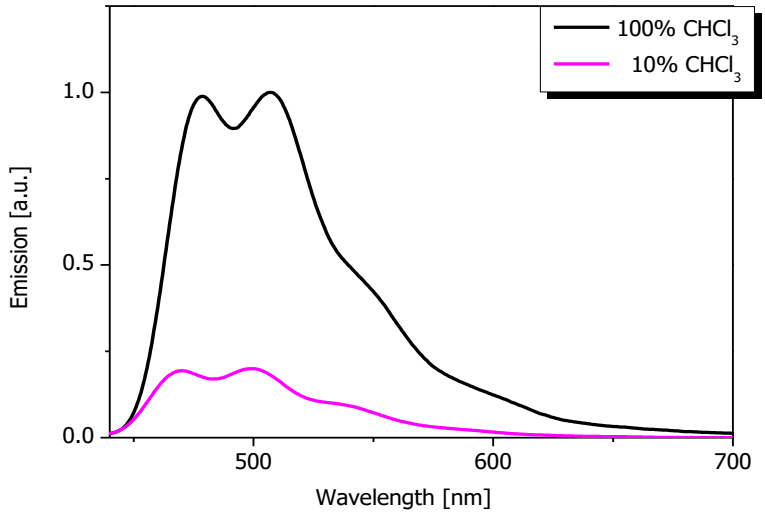

Figure 4.50. *Comparison of the normalized emission spectrum of* ***3.5****, [c] = 10^{-7} M in chloroform (black curve) and the quenched emission spectrum in chloroform/n-hexane (1:9) solution (magenta curve).*

The self-assembling behaviour of hybrid **3.5** was further investigated via CD-spectroscopy (***Figure 4.51***). In pure chloroform solution and in the chloroform/*n*-hexane (9:1) and (7:3) solutions no CD-signals were detected. This indicates that in such mixtures no chiral supramolecular self-assemblies are present. The chloroform/*n*-hexane (1:1) solution displayed a positive Cotton-effect with the maximum located at 370 nm, corresponding to a right-handed helical arrangement of the chromophores. Looking at the CD spectra of the chloroform/*n*-hexane (3:7) (***Figure 4.51***, ***cyan curve***) and (1:9) (***Figure 4.51***, ***magenta curve***) solutions, a positive Cotton-effect (λ_{max} = 395 nm) and a negative Cotton-effect (λ_{min} = 364 nm) were observed. Additionally, the zero-crossing at λ = 379 nm correlates almost exactly with the λ_{max} of the absorption band deconvoluted from the absorption spectrum of **3.5** in the chloroform/*n*-hexane (1:9) solution. This indicates the presence of right-handed helical superstructures, in which the π-systems are electronically coupled. The UV/vis absorptions in the longer wavelength region at 407 nm, 434 nm, and 468 nm are caused by *J*-type aggregates of the chromophores and their energies match those of the shoulders in the corresponding CD-spectrum. Due to the positive sign of the Cotton signals a right-handed helical arrangement of the quaterthiophenes in the *J*-type aggregates can be assessed.

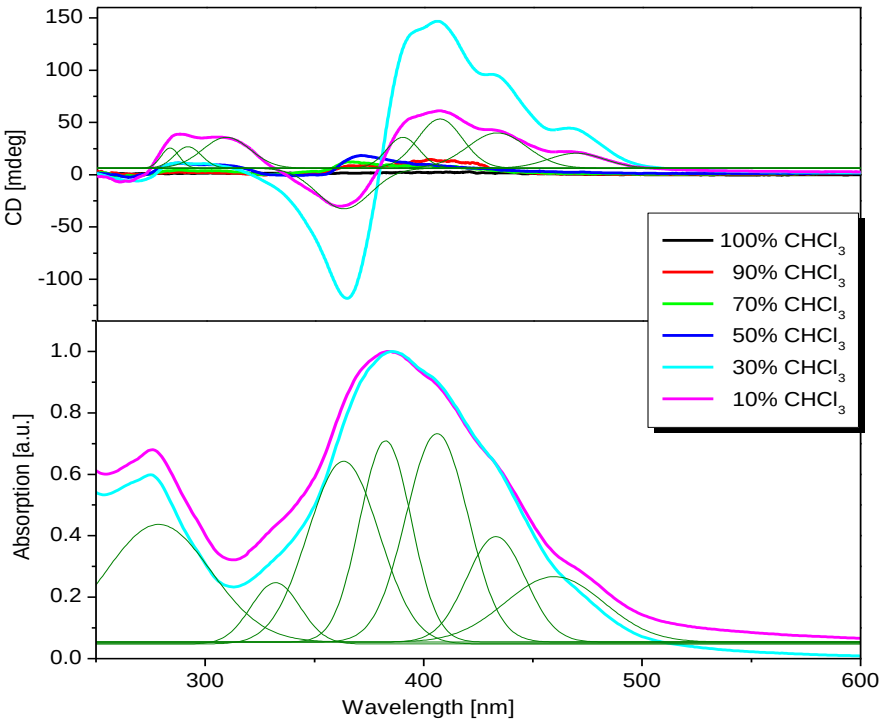

Figure 4.51. *CD-spectra of hybrid* ***3.5*** *upon titration of the chloroform solution with n-hexane (top), [c] = 5 x 10^{-5} M. Black curve: CD-spectrum of the 100% chloroform solution; red curve: CD-spectrum of the chloroform/n-hexane (9:1) solution; green curve: CD-spectrum of the chloroform/n-hexane (7:3) solution; blue curve: CD-spectrum of the chloroform/n-hexane (1:1) solution; cyan curve: CD- (top) and absorption (bottom) spectra of the chloroform/n-hexane (3:7) solution; magenta curve: CD- (top) and absorption (bottom) spectra of the chloroform/n-hexane (1:9) solution; olive curves: deconvoluted CD- and absorption spectra.*

Furthermore, it was observed that the intensity of the positive and the negative CD signals change similarly upon increasing the *n*-hexane content (***Figure 4.52***).

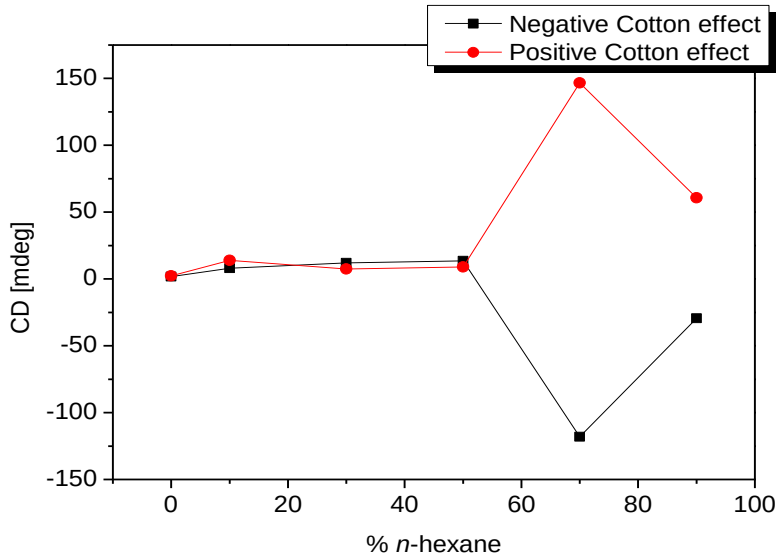

Figure 4.52. *CD-intensity of the negative (black curve) and positive (red curve) Cotton effects upon increasing of the n-hexane content.*

Temperature-dependent CD-measurements were also carried out for the chloroform/*n*-hexane (1:9) solution of hybrid **3.5** in order to study the stability of the chiral supramolecular structures (***Figure 4.53***). A loss of intensity of both positive and negative Cotton effects was detected upon increasing the temperature. This trend indicates that the chiral aggregates are not thermodynamically stable.

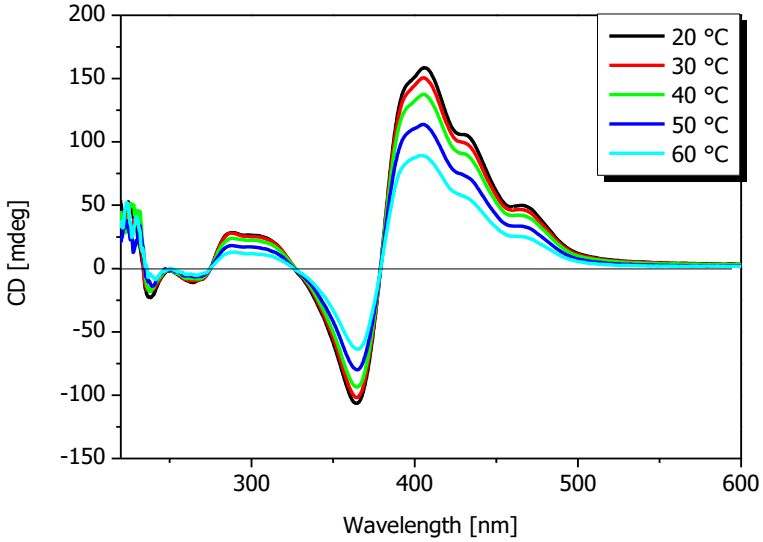

Figure 4.53. *Temperature-dependent CD-spectra of **3.5** in the chloroform/n-hexane (3:7) solution, [c] = 5 x 10^{-5} M. Black curve: CD-spectrum at 30 °C; red curve: CD-spectrum at 40 °C; green curve: CD-spectrum at 50 °C; blue curve: CD-spectrum at 60 °C; cyan curve: CD-spectrum at 70 °C.*

The quenching in percent of the positive and negative Cotton effects at their maximum (405 nm) and minimum (363 nm), respectively, was plotted against the temperature (***Figure 4.54***). Both CD signals lost their intensity with the same velocity upon increasing the temperature.

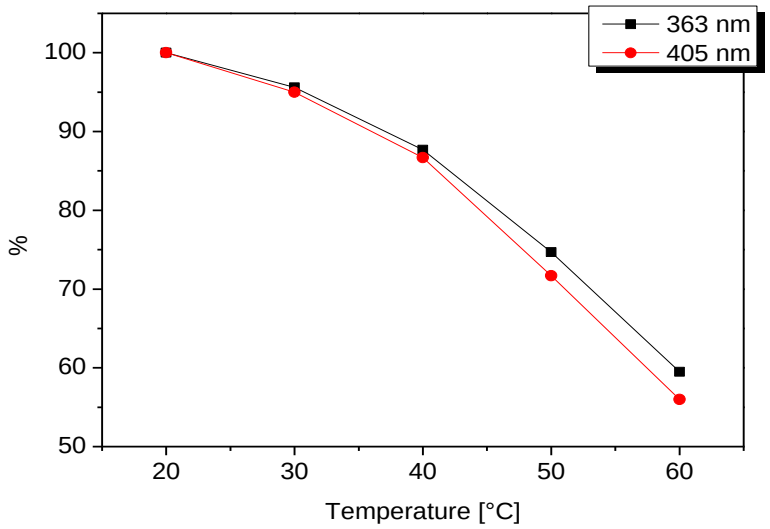

Figure 4.54. *Intensity quenching in percent of the Cotton-effects at 363 nm (black curve) and 405 nm (red curve) against the temperature.*

*4.3.2.6 UV/Vis-, Fluorescence-, CD-Spectroscopy, and DLS Measurements of Methyl Ester-Proline α-Hexyl-Substituted Quarterthiophene **3.7***

The self-assembly properties of hybrid **3.7** (***Chart 4.9***) were investigated in different THF/water solutions.

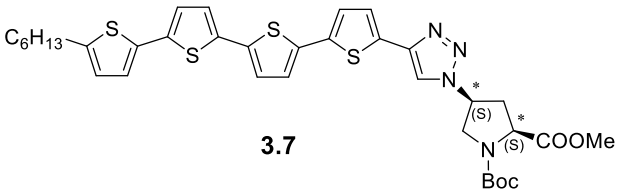

3.7

Chart 4.9. *Molecular structure of α-hexyl substituted quaterthiophene-methyl ester proline hybrid **3.7**.*

In this case, the *H*-bond interactions are suppressed because of the presence of the methyl ester group instead of the free carboxylic acid in the proline part of hybrids **3.5** and **3.6**. Therefore, it is expected that upon increasing the polarity of the solvent mixture the hydrophobic interactions will be the only forces responsible for aggregates

formation. The aggregation process was investigated by UV/Vis spectroscopy (***Figure 4.55***). The THF (100%) and the THF/water (9:1), (7:3) and (1:1) solutions displayed similar absorption spectra indicating that no self-assembly occurs in these mixtures. On the contrary, both THF/water (3:7) and (1:9) solutions are characterized by a hypsochromic shift of the λ_{max} and loss of the symmetrical shape of the absorption band. This suggests that in such mixtures the chromophores organize in *H*-like aggregates. Additionally, the band in the region below 300 nm which corresponds to the absorption band of the 1,2,3-triazole unit, increased strongly in the THF/water (1:9) solution.

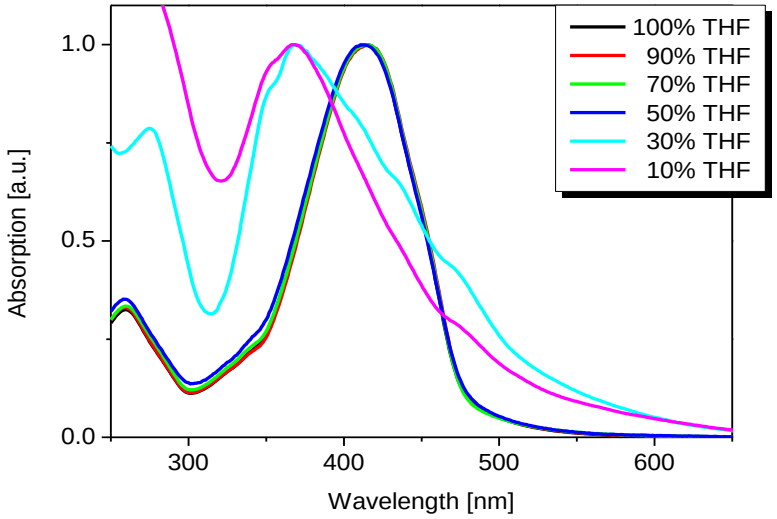

Figure 4.55. *Normalized absorption spectra of hybrid* ***3.7*** *upon titration of the THF solution with water, [c] = 10^{-5} M. Black curve: absorption spectrum of the 100% THF solution; red curve: absorption spectrum of the THF/water (9:1) solution; green curve: absorption spectrum of the THF/water (7:3) solution; blue curve: absorption spectrum of the THF/water (1:1) solution; cyan curve: absorption spectrum of the THF/water (3:7) solution; magenta curve: absorption spectrum of the THF/water (1:9) solution.*

The stability of the aggregates formed in the THF/water (1:9) solution was investigated by temperature dependent UV/Vis spectroscopy (***Figure 4.56***). The absorption spectra displayed similar intensity and shape upon increasing of the temperature until 70 °C. This behaviour points to a high stability of the supramolecular structures and stressed the extraordinary strength of the hydrophobic forces which are responsible for the self-assembling process.

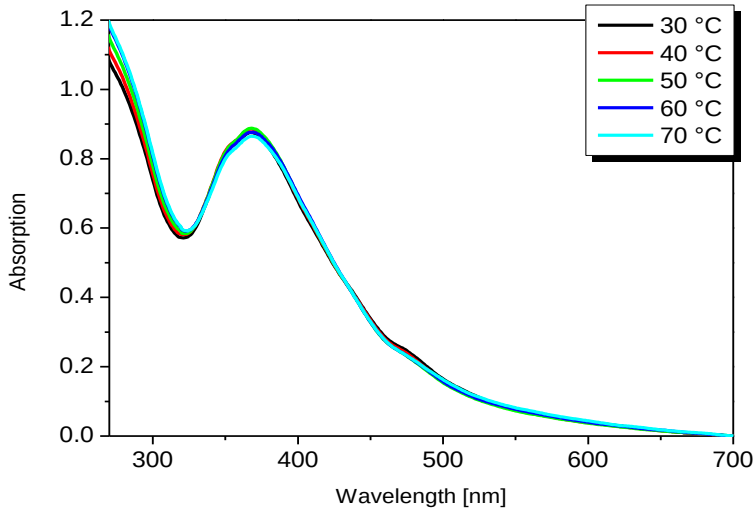

Figure 4.56. *Temperature-dependent absorption spectra of quaterthiophene-proline hybrid* ***3.7*** *in the THF/water (1:9) solution, [c] = 10^{-5} M. Black curve: absorption spectrum at 30 °C; red curve: absorption spectrum at 40 °C; green curve: absorption spectrum at 50 °C; blue curve: absorption spectrum at 60 °C; cyan curve: absorption spectrum at 70 °C.*

Looking at the fluorescence spectra of quaterthiophene-methyl ester proline **3.7** in pure THF and in the THF/water (1:9) solution, a strong quenching (92%) of the emission transitions was observed in the THF/water (1:9) solution, confirming the formation of aggregates in the aqueous environment (***Figure 4.57***).

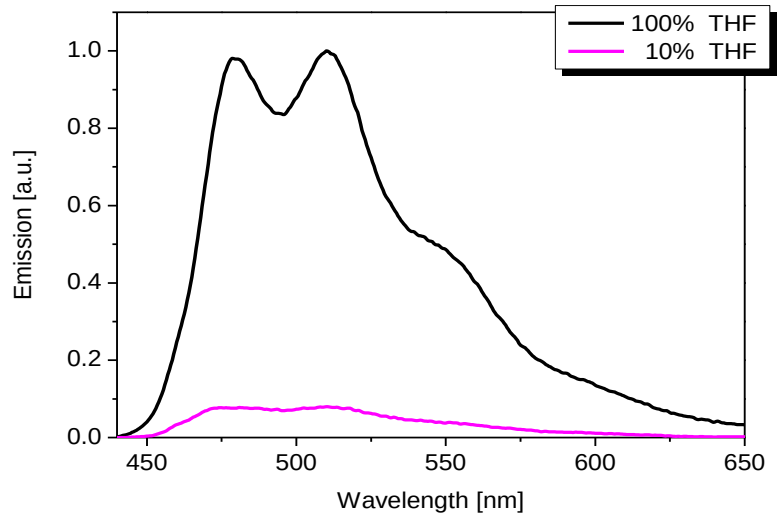

Figure 4.57. *Comparison of the normalized emission spectrum of* ***3.7****, [c] = 10^{-7} M in THF (black curve) and the quenched emission spectrum in THF/water (1:9) solution (magenta curve).*

The self-assembly process of hybrid **3.7** was investigated by CD-spectroscopy (**Figure 4.58**). No CD-signal could be detected in the THF (100%) solution and in the THF/water (9:1), (7:3) and (1:1) mixtures. A positive Cotton-effect (λ_{max} = 388 nm) and a negative Cotton-effect (λ_{min} = 339 nm) were observed starting from the THF/water (3:7) solution, which indicate the formation of suprastructures in which the chomophores are arranged in a right-handed helical fashion. The correlation between the zero-crossing of the bisignate band and the maximum of the Gaussian curve deconvoluted from the absorption spectra of **3.7** in the solvent mixture (λ = 363 nm) evidences the exciton coupled character of the transition.

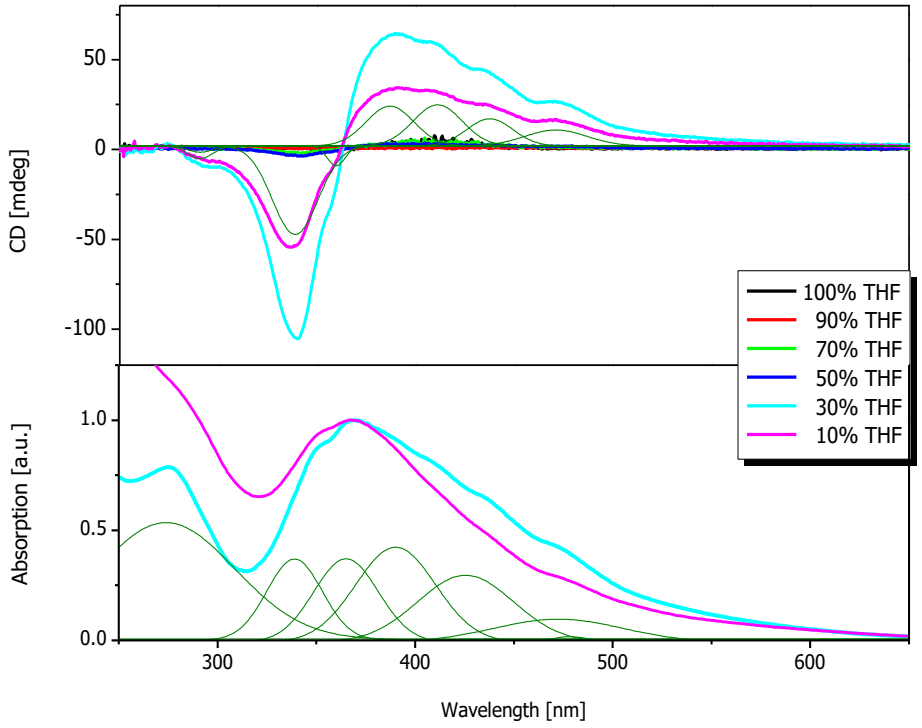

Figure 4.58. *CD-spectra of hybrid **3.7** upon titration of the THF solution with water (top), [c] = 10^{-5} M. Black curve: CD-spectrum of the 100% THF solution; red curve: CD-spectrum of the THF/water (9:1) solution; green curve: CD-spectrum of the THF/water (7:3) solution; blue curve: CD-spectrum of the THF/water (1:1) solution; cyan curve: CD-spectrum of the THF/water (3:7) solution; magenta curve: CD- (top) and absorption (bottom) spectra of the THF/water (1:9) solution; olive curves: deconvoluted CD- and absorption spectra.*

Three additional CD bands at 408 nm, 435 nm, and 476 nm could be detected and are caused by *J*-type aggregates of the chromophores. In fact, their energies match those of the shoulders in the corresponding UV/Vis spectrum (***Figure 4.57***, **bottom**). Due to the positive sign of the CD-signals a right-handed helical arrangement of the

quaterthiophenes can be assessed. Temperature-dependent CD experiments carried out on the THF/water (1:9) solution showed only a slight decrease of intensity of both maximum and minimum going from 30 °C to 70 °C (***Figure 4.59***); this indicates that the species formed in the THF/water (1:9) solution are thermodynamically stable.

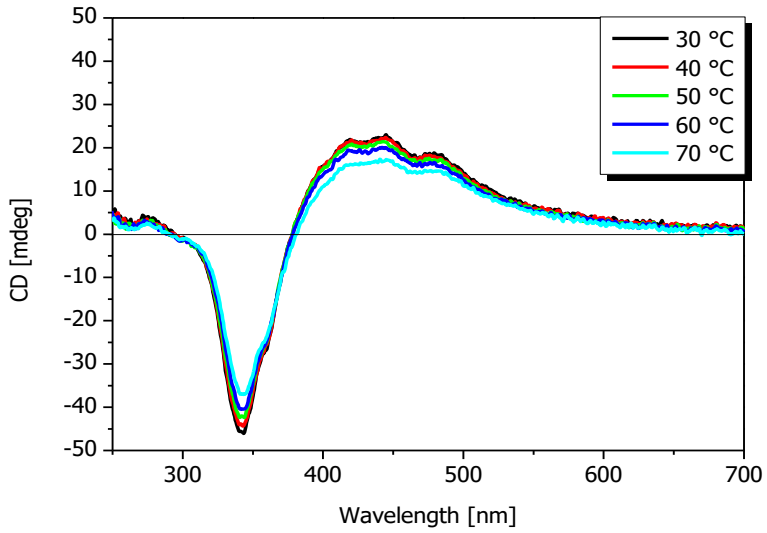

Figure 4.59. *Temperature-dependent CD-spectra of hybrid* ***3.7*** *in the THF/water (1:9) solution, [c] = 10^{-5} M. Black curve: CD-spectrum at 30 °C; red curve: CD-spectrum at 40 °C; green curve: CD-spectrum at 50 °C; blue curve: CD-spectrum at 60 °C; cyan curve: CD-spectrum at 70 °C.*

At room temperature DLS measurements showed the presence of aggregates with the averaged hydrodynamic diameter of ~300 nm (***Figure 4.60***) and, in particular, most of them have a narrow hydrodynamic diameter distribution.

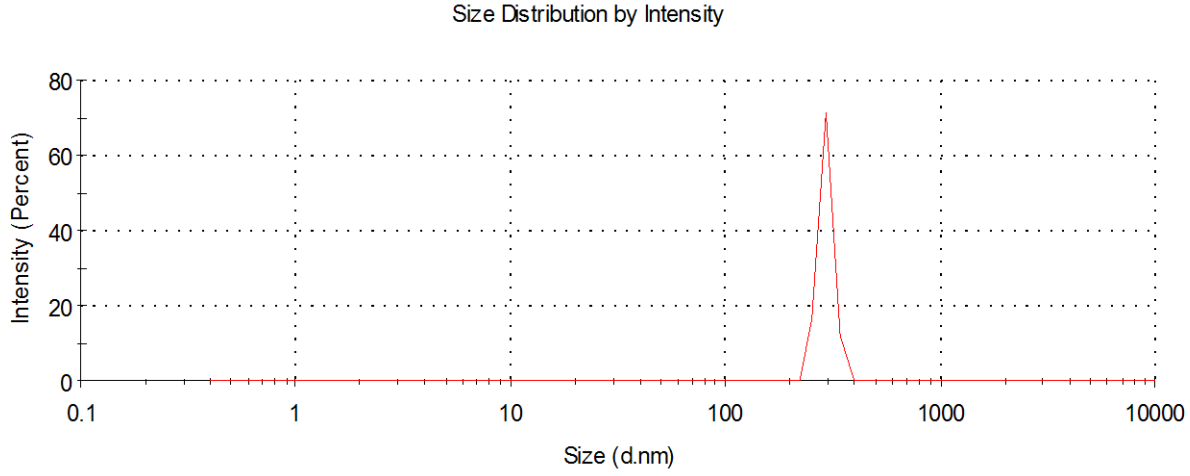

Figure 4.60. *DLS measurement of the aggregate size of hybrid* ***3.7*** *formed in the THF/water (1:9) solution, [c] = 10^{-5} M.*

4.3.2.7 UV/Vis-, Fluorescence-, CD-Spectroscopy, and DLS Measurements of DCV-Quaterthiophene-Proline **3.9**

The self-assembly behavior of hybrid **3.9** (***Chart 4.10***) was also investigated.

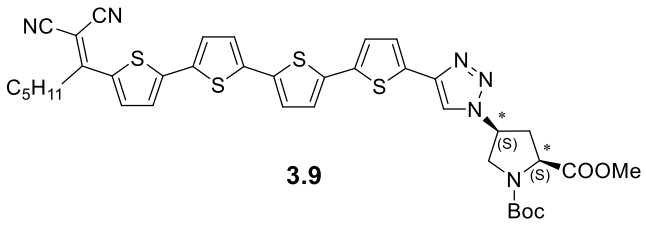

Chart 4.10. *Molecular structure of DCV-quaterthiophene-methyl ester proline hybrid* ***3.9****.*

Self-aggregation of the system was induced by titration of the pure THF solution with water. As observed in ***Figure 4.61***, a slight quenching of the ICT curve accompanied by a blue shift of the absorption maximum and the appearance of a shoulder in the low energy region was detected upon increasing the amount of water.

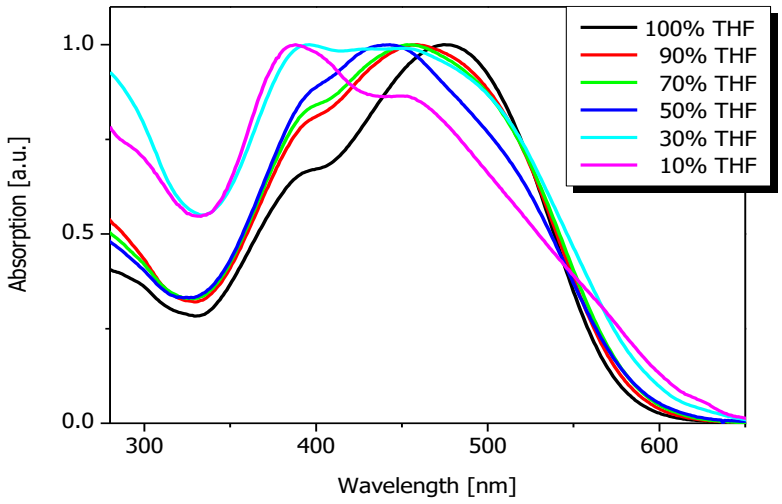

Figure 4.61. *Normalized absorption spectra of hybrid* ***3.9*** *upon titration of the THF solution with water, [c] = 5 x* 10^{-5} *M. Black curve: absorption spectrum of the 100% THF solution; red curve: absorption spectrum of the THF/water (9:1) solution; green curve: absorption spectrum of the THF/water (7:3) solution; blue curve: absorption spectrum of the THF/water (1:1) solution; cyan curve: absorption spectrum of the THF/water (3:7) solution; magenta curve: absorption spectrum of the THF/water (1:9) solution.*

Many studies have examined the effect of the solvent polarity on the energy of ICT absorption in donor-acceptor-substituted systems.[13-15] In general, when the excited state is more polar than the ground state, the ICT absorption band red-shifts to higher wavelength as the solvent polarity increases due to the stabilization of the Franck-Condon excited state compared to the ground state by polar solvents. However, this situation is most often observed for donor-acceptor-substituted molecules which have comparatively non-polar ground states. On the contrary, the situation is more complicated for aromatic DCV compounds, because in these systems the ground state is polar. The situation is further complicated by the fact that the polarity of the ground state increases as the solvent polarity increases. These factors may account for the relatively small change observed in the ICT absorption band of **3.9**. If μ_g increases with solvent polarity, then the difference in dipole moment between the ground and excited states ($\Delta\mu$) will decrease as the solvent polarity increases. The decrease of $\Delta\mu$ with increased solvent polarity will tend to mitigate the effect of solvent polarity on the energy of the ICT transition meaning that the solvent polarity influences the energy of the ground state and the ICT in a parallel manner. [13-15] Concomitantly, blue-shift of the maximum relative to the π-π^* transition band of the quaterthiophene moiety along the long axis of the molecule was observed suggesting that the molecules still prefer to organize in *H*-like aggregates (***Figure 4.61***).

The stability of the species in the THF/water (1:9) solution was investigated by temperature-dependent UV/Vis measurements (***Figure 4.62***). Upon increasing the temperature the absorption band whose maximum is located at 389 nm was not particularly affected, whereas the change relative to the ICT band is more prominent. In fact, the transition regains the intensity showed in pure THF. These results indicate that the aggregates formed in aqueous environment are not stable.

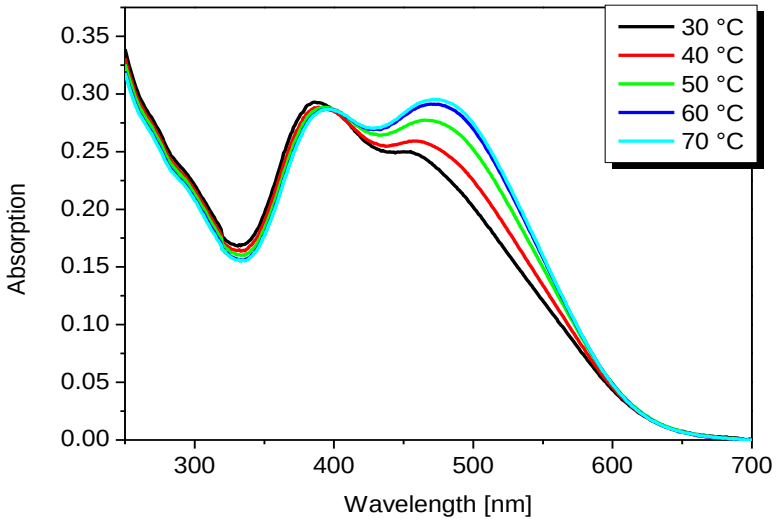

Figure 4.62. *Temperature-dependent absorption spectra of DCV-quaterthiophene-proline hybrid* ***3.9*** *in the THF/water (1:9) solution, [c] = 10^{-5} M. Black curve: absorption spectrum at 30 °C; red curve: absorption spectrum at 40 °C; green curve: absorption spectrum at 50 °C; blue curve: absorption spectrum at 60 °C; cyan curve: absorption spectrum at 70 °C.*

The self-assembling process was further studied by emission spectroscopy. In the THF/water (1:9) solution the emission intensity decreased to 95% of its previous emission intensity in pure THF and the emission maximum was bathochromically shifted ($\Delta\lambda$ = 36 nm) (***Figure 4.63***). This confirms the formation of aggregates in the aqueous environment.

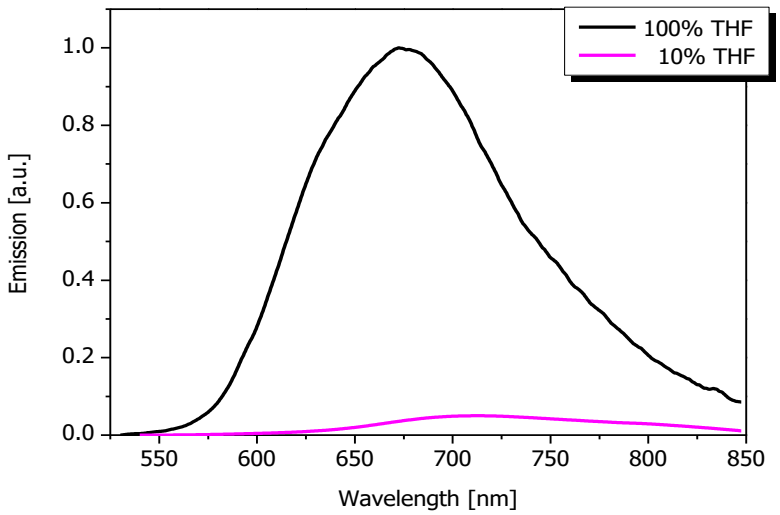

Figure 4.63. *Comparison of the normalized emission spectrum of* ***3.9****, [c] = 10^{-7} M in THF (black curve) and the quenched emission spectrum in THF/water (1:9) solution (magenta curve).*

Additional investigations on the aggregates formed in aqueous solutions were accomplished by CD spectroscopy. As shown in ***Figure 4.64***, the formation of chiral supramolecular structures started in the THF/water (3:7) solution, reaching its highest intensity in the THF/water (1:9) mixture. A negative Cotton-effect with the minimum situated at 475 nm and a positive CD-signal (λ_{max} = 361 nm) were observed. The correlation between the zero-crossing of the bisignate Cotton-effect and the maximum of the absorption band relative to the π-π^* transition of the quaterthiophene moiety along the long axis of the molecule (λ = 390 nm) evidences the exciton-coupled character of the transition. Additionally, it can be assessed that the chomophores are arranged in the suprastructures in a left-handed helical way.

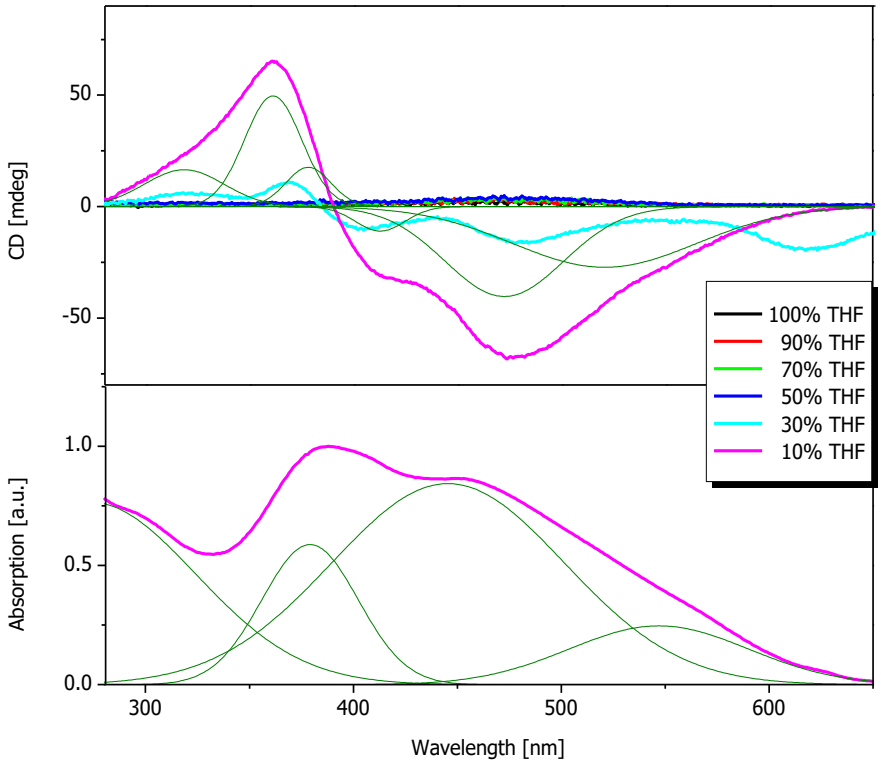

Figure 4.64. *CD-spectra of hybrid* ***3.9*** *upon titration of the THF solution with water (top), [c] = 5 x 10^{-5} M. Black curve: CD-spectrum of the 100% THF solution; red curve: CD-spectrum of the THF/water (9:1) solution; green curve: CD-spectrum of the THF/water (7:3) solution; blue curve: CD-spectrum of the THF/water (1:1) solution; cyan curve: CD-spectrum of the THF/water (3:7) solution; magenta curve: CD- (top) and absorption (bottom) spectra of the THF/water (1:9) solution; olive curves: deconvoluted CD- and absorption spectra.*

As already observed in the temperature-dependent UV/Vis measurements, the instability of the aggregates present in solution was also proven by CD-spectroscopy

(***Figure 4.65***). In fact, a loss of intensity of the maximum and minimum of the CD-signals could be detected indicating disassembly of the aggregates.

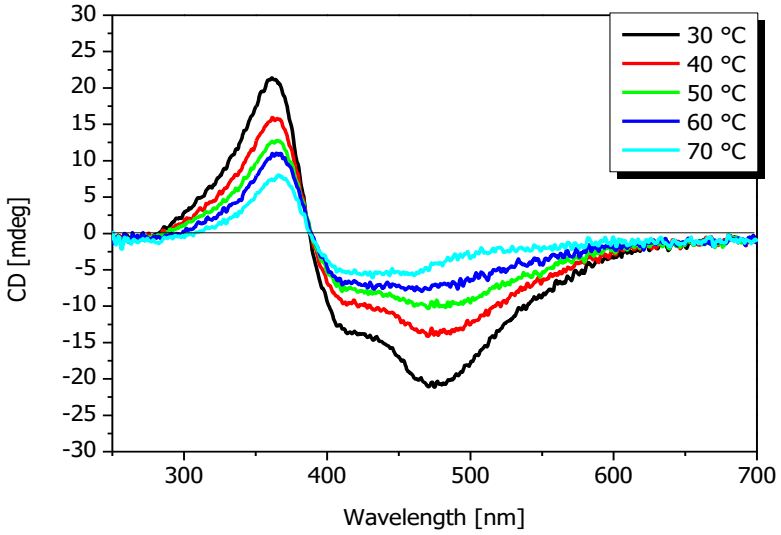

Figure 4.65. *Temperature-dependent CD-spectra of hybrid* ***3.9*** *in the THF/water (1:9) solution, [c] = 5 x 10^{-5} M. Black curve: CD-spectrum at 30 °C; red curve: CD-spectrum at 40 °C; green curve: CD-spectrum at 50 °C; blue curve: CD-spectrum at 60 °C; cyan curve: CD-spectrum at 70 °C.*

In particular, the quenching in percent of the positive and negative Cotton-effect in correspondence to their maximum (361 nm) and minimum (475 nm), respectively, was plotted against the temperature (***Figure 4.66***).

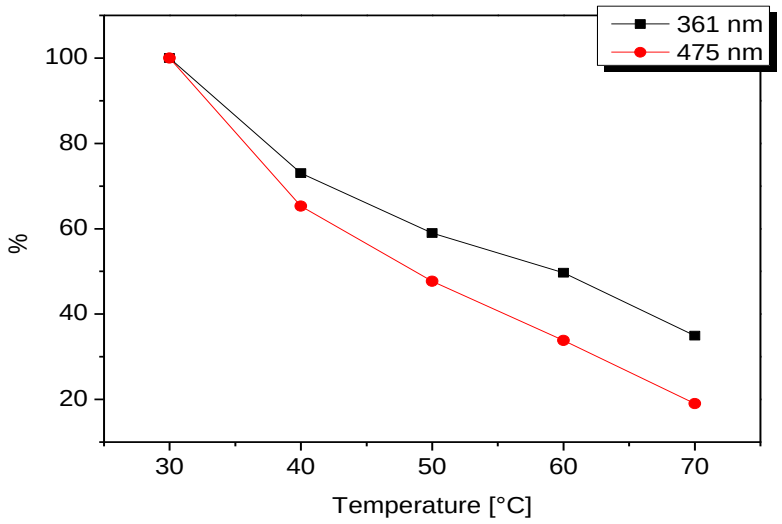

Figure 4.66. *Intensity quenching in percent of the Cotton-effects at 361 nm (black curve) and 475 nm (red curve) against the temperature.*

It was observed that both CD-signals were quenched with similar velocity upon increasing the temperature.

At room temperature, presence of particles with a averaged hydrodynamic diameter of ~145 nm were detected via DLS experiments (***Figure 4.67***).

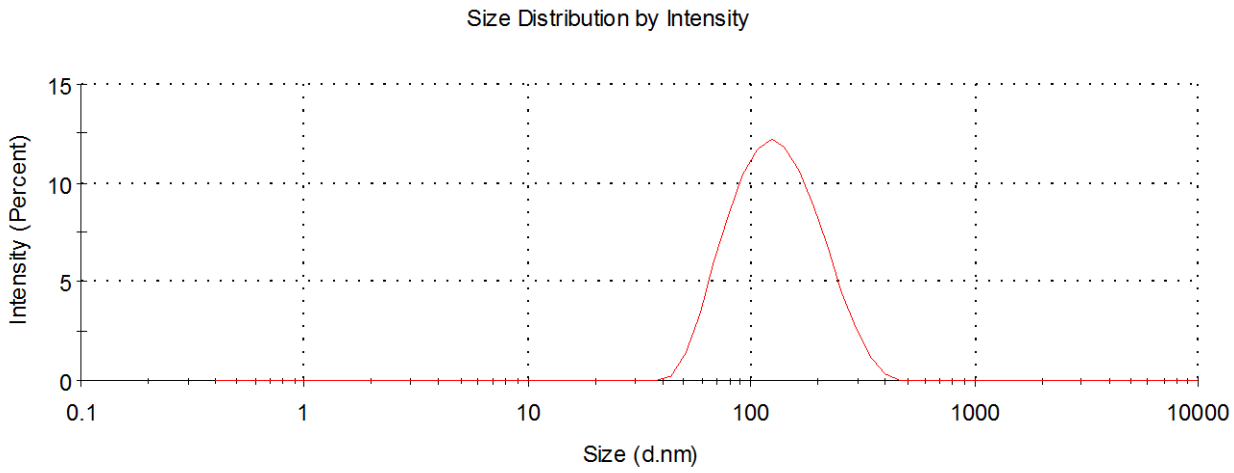

Figure 4.67. *DLS measurement of the aggregate size of hybrid* ***3.9*** *in THF/water (1:9) solution at room temperature, [c] = 5 x 10 -5 M.*

*4.2.3 Summary of the Self-Assembling Behaviour of Quaterthiophene-Proline Hybrids **3.2**, **3.3**, **3.4**, **3.5**, **3.7**, and **3.9***

In the second part of ***Chapter 4***, the study of the self-assembly revealed the importance of the forces involved during this process. In general, in carboxylic acid-substituted systems such as **3.2**, **3.3**, **3.4**, and **3.5**, the interactions responsible for the suprastructures formation are both hydrophobic (π-π stacking and van der Waals interactions) and hydrophilic (*H*-bonding interactions between the hydrogen bonding donor carboxylic acid and the hydrogen bond acceptors such as carbonyl group or triazole unit). When the molecules are surrounded by an aqueous environment, the forces behave orthogonal: the hydrophobic interactions bring the π-systems in proximity in order to minimize their contact with the water molecules, and at the same time, the water molecules stabilize the aggregates by forming *H*-bonds with the *H*-bond acceptor sites of the hybrid (nitrogen atoms of the triazole unit and oxygen atoms of the Boc-protecting group and of the carbonyl group of the carboxylic acid) (***Figure 4.68***).

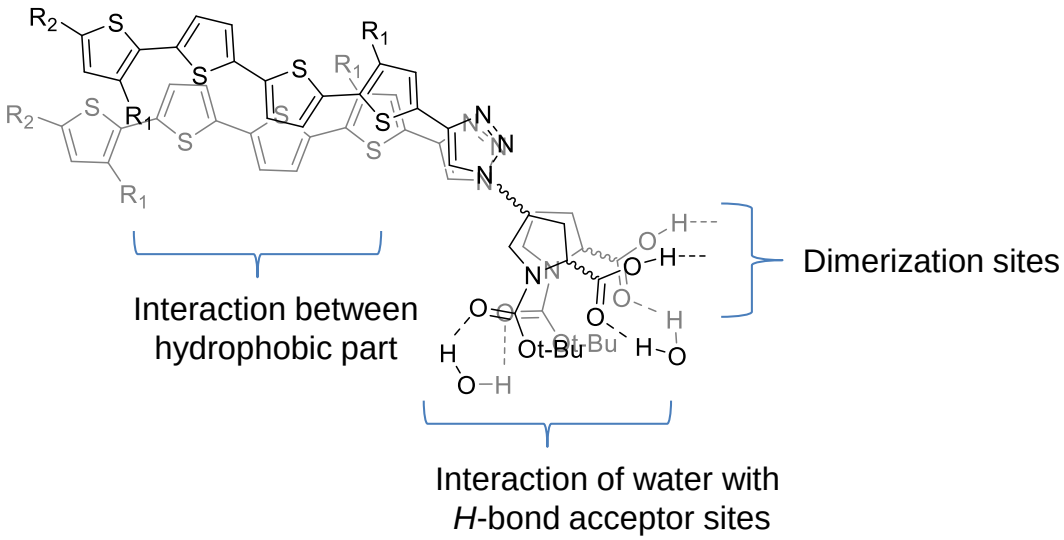

Figure 4.68. *Model of interactions between two molecules.*

In this model, the interactions between two molecules are represented. From the information obtained from the UV/Vis spectra of the hybrids in the aqueous solutions, it is hypothesized that the systems have the transition dipole relative to the π-π* transition of the oligothiophenes backbone, parallelly aligned (*H*-like aggregate). Furthermore, it is suggested that the systems further interact with each other in order to form dimers, having the transition dipoles antiparallel aligned (absorption at higher wavelength). This could occur through the formation of *H*-bonding interactions between the carboxylic acid groups of the molecules.

Furthermore, the CD-spectra of the carboxylic acid-substituted biohybrids indicated that the chirality is transferred from the proline to the π-conjugated backbones. As the hybrids have shown to be very stable, it is hypothesized that interactions of water molecules with the H-bond acceptor sites of the molecule are also involved in stabilizing the suprastructures. In particular, by comparing quaterthiophene-proline hybrids **3.2** and **3.5** (***Chart 4.11***) it was observed that the position of the substitution on the quaterthienylic core influenced the self-assembling behaviour of the hybrids.

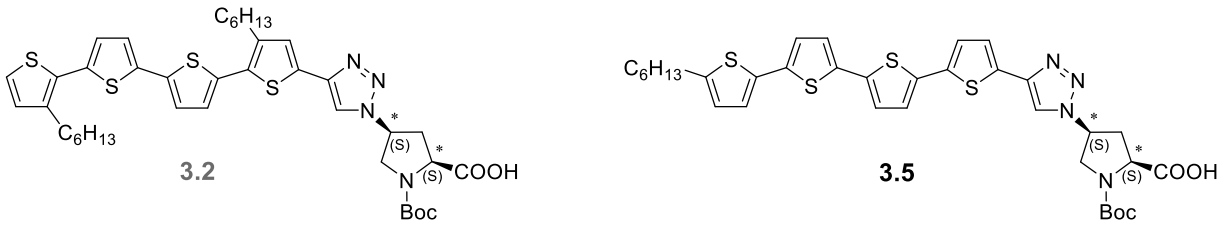

Chart 4.11. *Molecular structures of quaterthiophene-proline hybrids* ***3.2*** *and* ***3.5****.*

Looking at the absorption spectra measured in THF/water (1:9) solution (***Figure 4.69***, ***bottom***), the absorption band of β-substituted hybrid **3.2** is broader than the one displayed by α-substituted 4T **3.5**. This indicates that the supramolecular structures of **3.2** have less defined structure than the aggregates formed by α-substituted **3.5**. This statement is in agreement with the CD-measurements showed in **Figure 4.69** (**top**). In fact, for both hybrids the formation of chiral left-handed helical suprastructures was detected, but the intensity of the bisignate Cotton-effect was definitely lower for hybrid **3.2** than for **3.5**. This might be due to the presence of the β-hexyl substituents on the quaterthiophene **3.2** which hinder the π-π stacking of the chromophores. Additionally, it can be assessed that oligothiophenes **3.2** and **3.5** self-organize in diverse type of supramolecular structures.

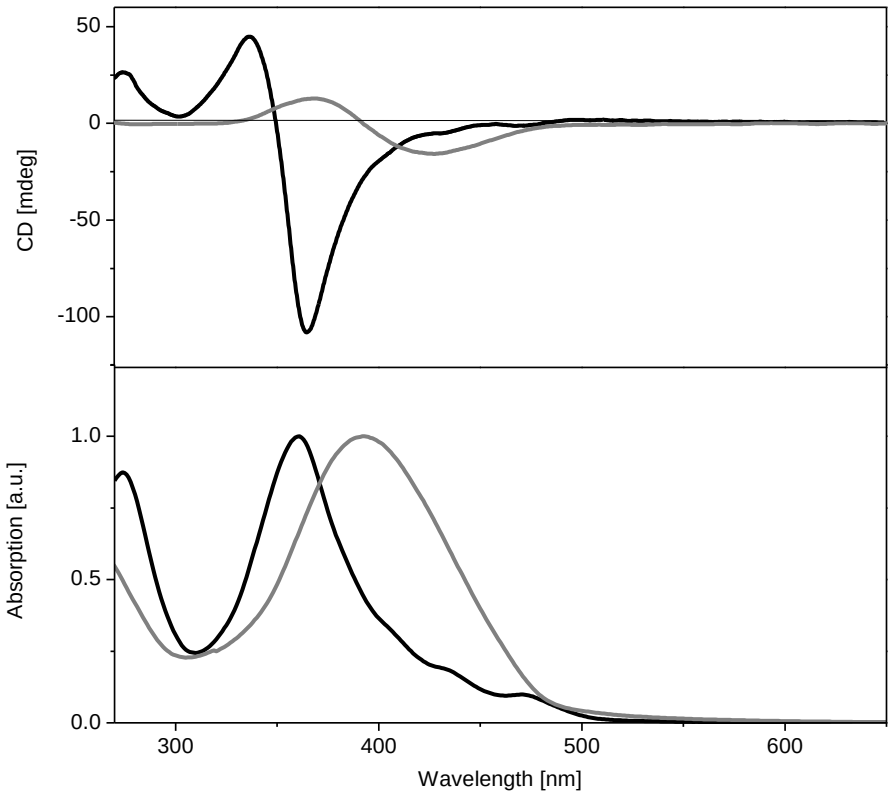

Figure 4.69. *Comparison of CD- (top) and UV/Vis absorption (bottom) spectra of **3.2** (grey curve) and **3.5** (black curve) in THF/water (1:9) solution, [c] = 5 x 10^{-5} M.*

The influence of the diverse α-substitutions of the quaterthiophene on the self-organisation process of the biohybrids was analysed by comparing the self-assembling properties of hybrids **3.3**, **3.4**, and **3.5** (***Chart 4.12***) in the THF/water (1:9) solution.

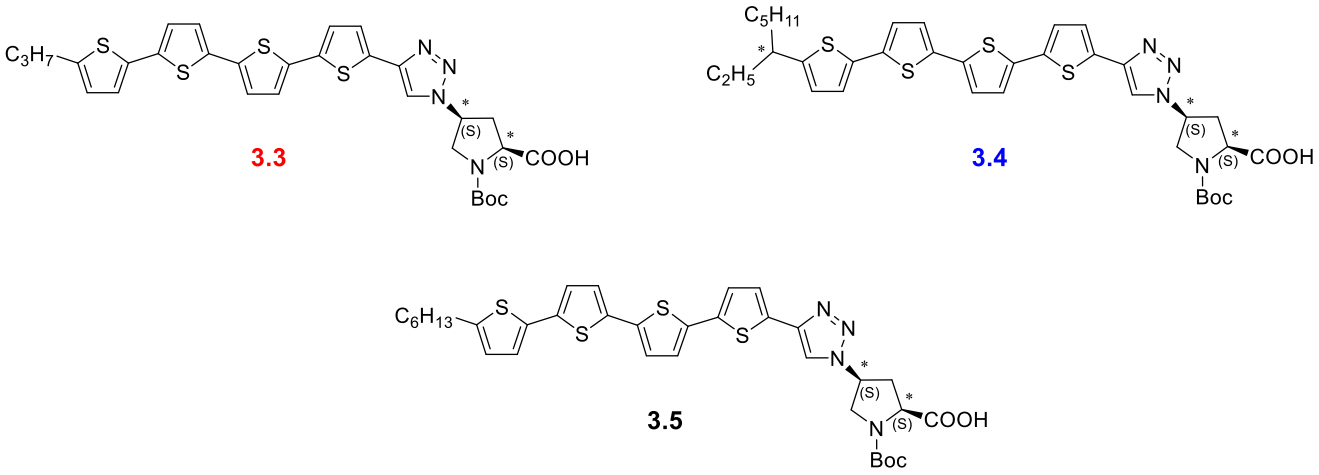

Chart 4.12. *Molecular structures of quaterthiophene-proline hybrids* ***3.3****,* ***3.4*** *and* ***3.5****.*

In ***Figure 4.70*** (**bottom**) it could be observed that the absorption maximum of α-propyl **3.3** was located at lower wavelength than the λ_{max} of α-ethylhexyl **3.4** and α-hexyl **3.5** quaterthiophenes, whereas hybrid **3.4** displayed a broader absorption band in comparison the other two biosystems. In general, it can be assessed that all three hybrids self-assembled in *H*-like aggregates. The CD-spectra of both quaterthiophenes **3.3** and **3.5** (***Figure 4.70***, ***black and red curves***) displayed a negative Cotton-effect at 363 nm and a positive Cotton-effect at 337 nm. Additionally, the $\lambda_{zero\text{-}crossing}$ of both bisignated CD-signals are also similar. This may indicate that in the THF/water (1:9) solution hybrids **3.3** and **3.5** self-organize building same chiral suprastructures in which the chromophores are arranged in a left-handed helical fashion. The CD-spectrum of hybrid **3.4** displayed also the negative Cotton-effect at 363 nm but additional positive Cotton-effect at higher wavelengths and a positive CD-signal whose maximum was located at 393 nm were observed. This indicates that the α-branched alkyl chain influences in a different way the self-assembly of the quaterthiophene and a different type of chiral aggregates is formed. Furthermore, two additional CD-bands at 444 nm and 477 nm could be also detected and are caused by *J*-type aggregates of the chromophores. In fact, their energies match those of the shoulders in the corresponding UV/Vis spectrum (***Figure 4.69***, **blue curve**). Due to the negative sign of the Cotton bands a left-handed helical arrangement of the quaterthiophenes in the *J*-type supramolecular packing of hybrid **3.4** can be assessed.

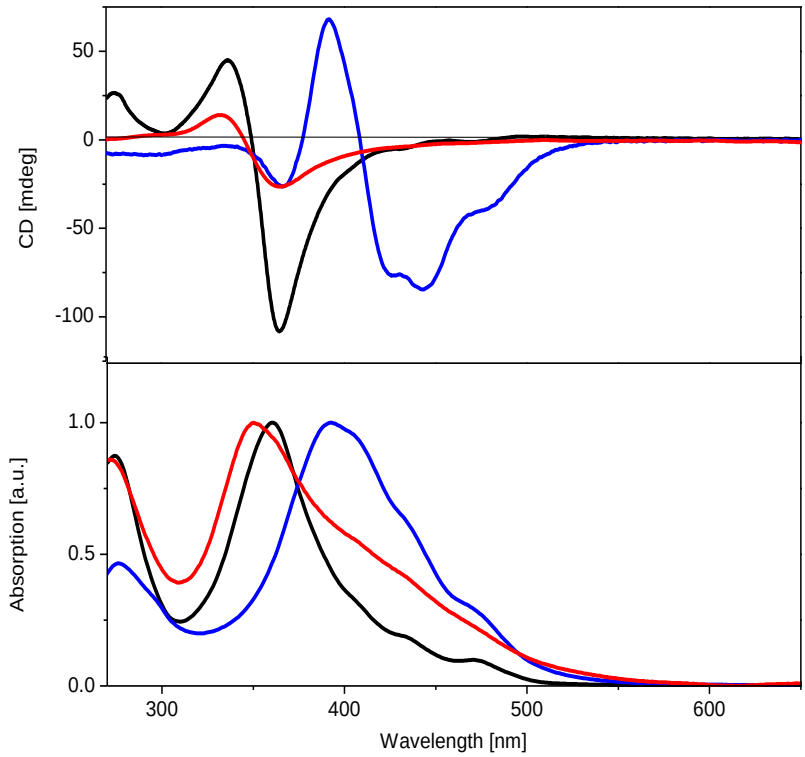

Figure 4.70. *Comparison of CD- (top) and UV/Vis (bottom) spectra of* ***3.3*** *(red curve),* ***3.4*** *(blue curve) and* ***3.5*** *(black curve) in THF/water (1:9) solution, [c] = 5 x 10^{-5} M.*

Additional experiments in the apolar mixture chloroform/*n*-hexane were carried out for hybrid **3.5**. It was observed that the biosystem showed different optical and chiroptical behaviour than in the polar mixture, above all the loss of the thermodynamic stability, which was so extraordinary high in the aqueous solutions and less order in the self-organization (***Figure 4.51***). These findings lead to hypothesize that different interactions are involved in the assembling process. In fact, because of the apolar environment, it is suggested that the hydrophobic forces are not anymore predominant, but the *H*-bonding interactions are just responsible for the ordering of the systems (***Figure 4.71***).

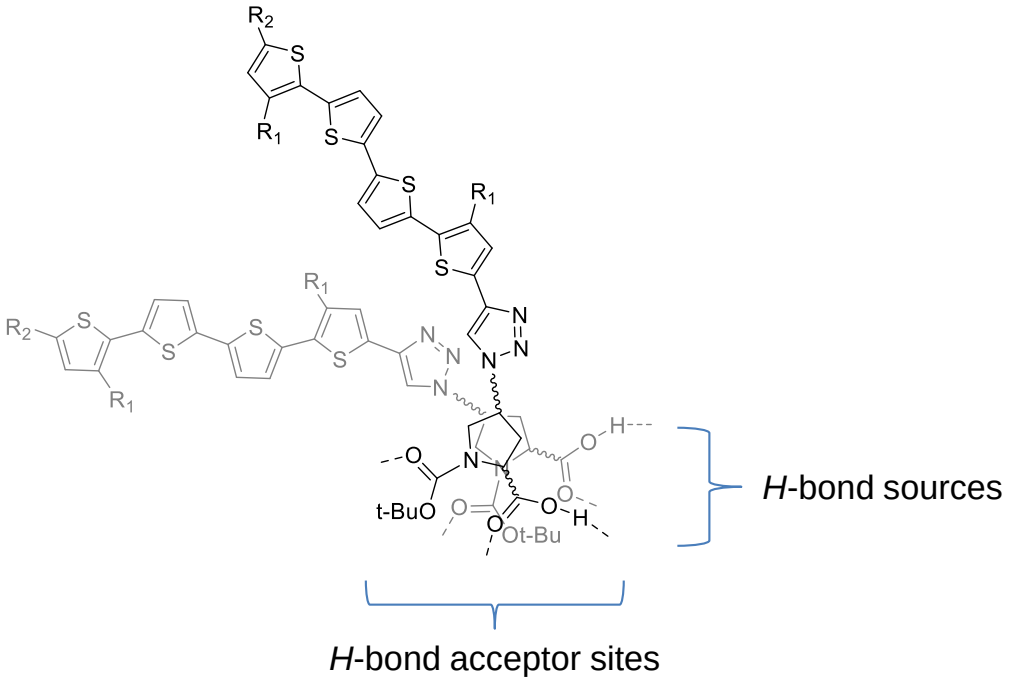

Figure 4.71. *Model of interactions between two molecules.*

This assumption could be corroborated by carrying out the same experiments on methyl ester-substituted hybrid **3.7**, in which the possibility to have *H*-bonding interactions is suppressed. It was observed that under apolar conditions no CD-signals could be detected meaning that formation of chiral ordered suprastructures does not occur (***Figure 4.72***).

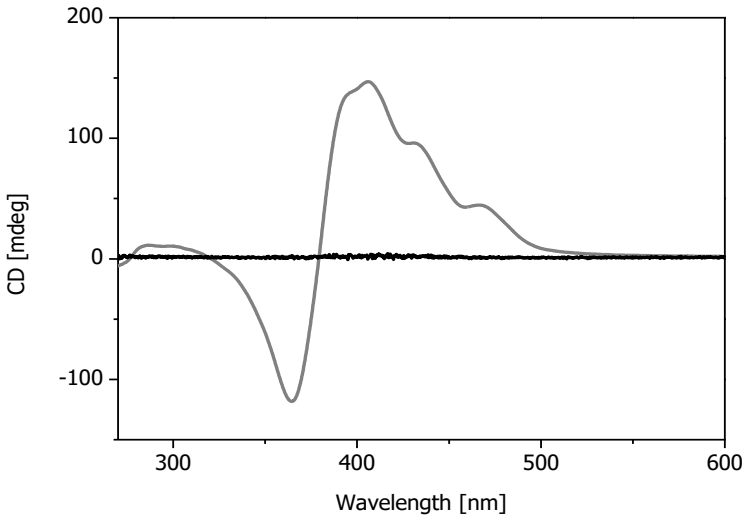

Figure 4.72. *Comparison of CD-spectra of* ***3.5*** *(grey curve) and* ***3.7*** *(black curve) in chloroform/n-hexane (3:7) solution.*

A comparison between quaterthiophenes **3.5** and **3.7** shows the consequence of the suppression of the *H*-bonding interactions in the self-assembly process.

In ***Chart 4.13*** the structures of the two α-hexyl substituted quaterthiophenes are once more reported.

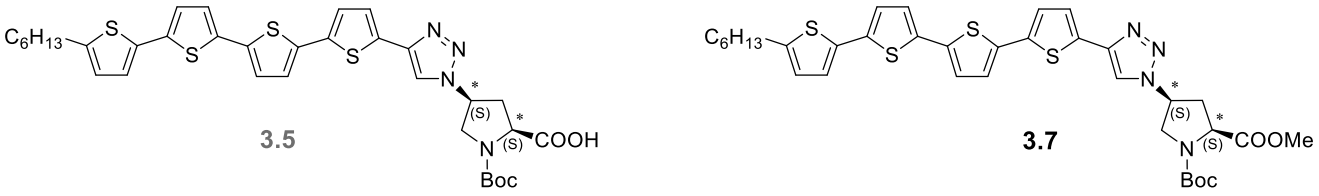

Chart 4.13. *Molecular structures of quaterthiophene-proline hybrids **3.5** and **3.7**.*

The structural change is responsible for the different optical and chiroptical behaviours of the two biosystems in aqueous environment (***Figure 4.73***).

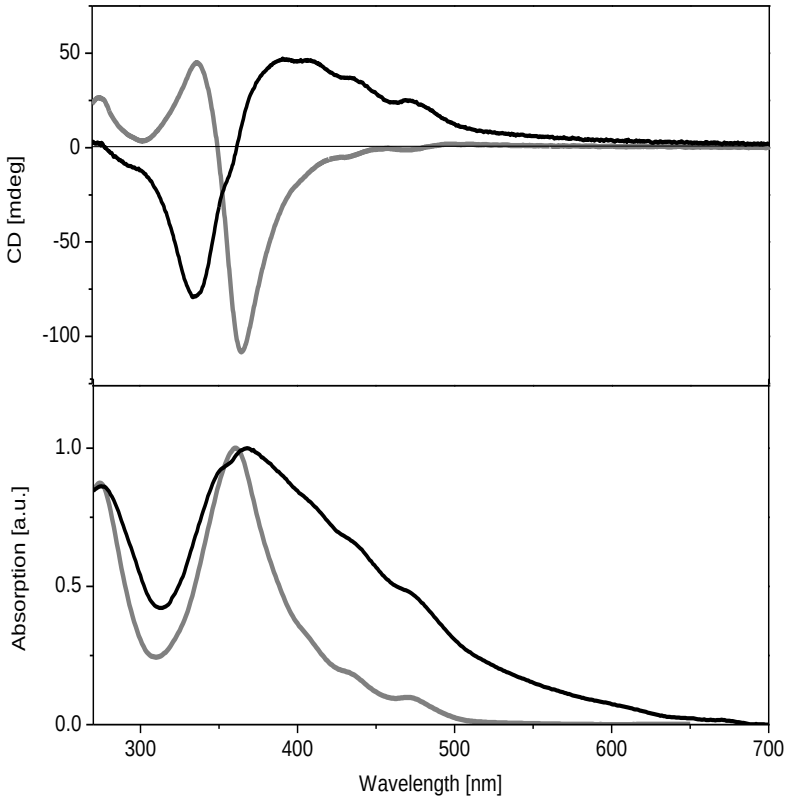

Figure 4.73. *Comparison of CD- (top) and UV/Vis absorption (bottom) spectra of **3.5** (grey curve) and **3.7** (black curve) in THF/water (1:9) solution, [c] = 5 x 10^{-5} M.*

In fact, thanks to the orthogonality of the forces involved in the self-organization process of **3.5**, an almost pure bisignate CD signal and absorption band could be de-

tected, hint of a high order of the molecules in the left-handed suprastructures. On the contrary, the suppression of the *H*-bond interactions in the self-assembly of **3.7** causes right-handed assembles of molecules with less defined structure, which is suggested by the broadening of the absorption spectrum and the presence of different signals at higher wavelength in the CD-spectrum. All in all, it can be assessed that the involvement of both hydrophobic and hydrophilic interactions is fundamental to obtain well-ordered and stable supramolecular structures.

Furthermore, it was observed that the introduction of an acceptor function, as the DCV group, in the molecular structure caused completely different optical and chiroptical behaviours.

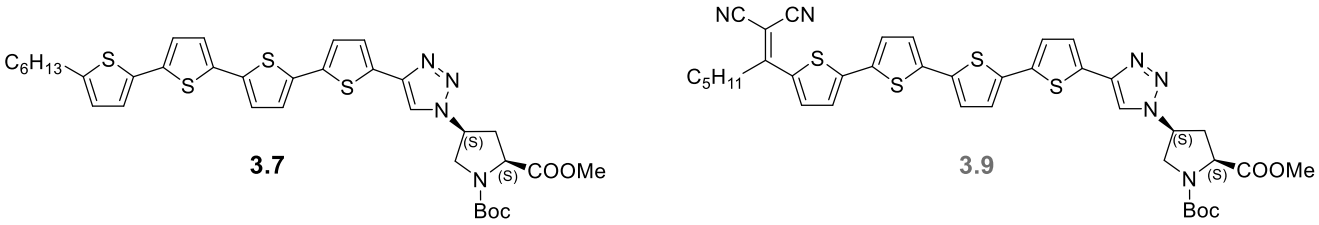

Chart 4.14. *Molecular structures of quaterthiophene-proline hybrids **3.7** and **3.9**.*

Comparing biosystems **3.7** and **3.9** (***Chart 4.14***) in their aggregation states, it can be observed that they have diverse optically and chiroptically properties (***Figure 4.74***). The introduction of the DCV acceptor group in the quaterthiophene hybrid affects the dipole moment of the quaterthiophene-proline which decreases from μ = 7.65 D in case of **3.7** to μ = 4.45 D for **3.9**. This change may have strong influence on the dipole-dipole interactions between the chromophores leading to the formation of completely diverse type of aggregates. In particular, looking at the CD spectra in ***Figure 4.74*** a turn-over of the handedness of the aggregates was observed. In fact, differently from quaterthiophene **3.7**, DCV-quaterthiophene-proline hybrid **3.9** self-assembles in Suprastructures, in which the chromophores are arranged in a left-handed helical fashion.

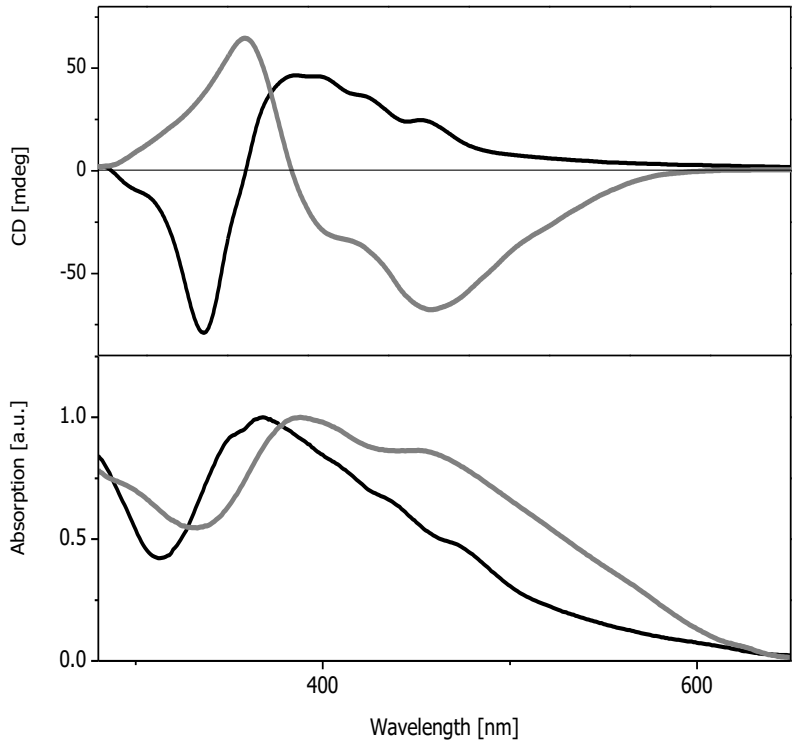

Figure 4.74. *Comparison of CD- (top) and UV/Vis absorption (bottom) spectra of* ***3.7*** *(black curve) and* ***3.9*** *(grey curve) in THF/water (1:9) solution, [c] = 5 x* 10^{-5} *M.*

References

[1] L. W. Hartzel, F. R. Benson, *J. Am. Chem. Soc.* **1954**, *76*, 667–670.

[2] E.-K. Schillinger, *PhD Thesis*, University of Ulm, **2010**.

[3] T. Johansson, W. Mammo, M. Svensson, M. R. Anderson, O. Inganäs, *J. Mater. Chem.* **2003**, *13*, 1316–1323.

[4] Z. Wu, C. Li, Z. Wei, P. Ying, Q. Xin, *J. Phys. Chem. B* **2002**, 106, 979–987.

[5] J. S. Kwiatkowskia, J. Leszczyński, I. Teca, *J. Mol. Struct.* **1997**, *436-437*, 451–480.

[6] D. A. Lightner, J. E. Gurst in *Organic Conformational Analysis and Stereochemistry from Circular Dichroism Spectroscopy*, Wiley-VCH: New York, **2000**, 423.

[7] E. E. Jelley, *Nature* **1936**, *138*, 1009–1010.

[8] K. Kieser, *Angew. Chem.* **1936**, *49*, 562–564.

[9] G. Scheibe, *Angew. Chem.* **1937**, *50*, 212–219.

[10] N. Berova, L. D. Bari, G. Pescitelli, *Chem. Soc. Rev.* **2007**, *36*, 914–931.

[11] R. Winter, F. Noll, *Methoden der Biophysikalischen Chemie*, B. G. Teubner: Stuttgart, **1998**.

[12] N. Harada, K. Nakanishi, *Circular Dichroic Spectroscopy- Exciton Coupling in Organic Stereochemistry*; Oxford University Press: Oxford. **1983**.

[13] P. Suppan, *J. Photochem. Photobiol., A: Chem.* **1990**, *50*, 293.

[14] C. Reichardt, *Solvents and Solvent Effects in Organic Chemistry*; VCH Pubishers: Weinheim, **1988**.

[15] R. Katritzky, D.-W. Zhu, K. S. Schanze, *J. Phys. Chem.* **1991**, *95*, 5737–5742.

Chapter 5

Own Work: Supramolecular Self-Organization in the Solid State

5.1 Introduction

In ***Chapter 4*** the ability of the biohybrids to self-organize in solution in ordered chiral suprastructures was proven. In this part, the study of the self-assembling behaviour of the quaterthiophenes will be extended to the solid state. First of all, it has to be taken into account that the molecules synthesized so far are amphiphiles; this means that the molecules are characterized by a hydrophilic and a hydrophobic part. The major forces that govern the self-assembly of amphiphiles in well-defined structures such as micelles or bilayers, derive from the hydrophobic attraction at the hydrophobic part-water interface, which induces the molecules to associate, and the hydrophilic or steric repulsion of the headgroups, which imposes the opposite requirement: the contact with water. These two interactions compete as two opposing forces and they act mainly in the interfacial region: the one tending to decrease and the other to increase the interfacial area per molecule exposed to the aqueous phase.

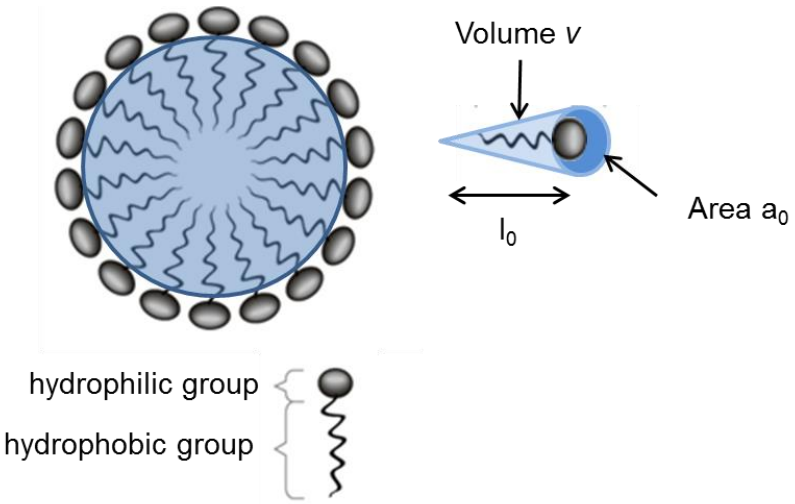

Figure 5.1. *Representation of a micelle where the hydrophilic part point out and the hydrophobic part inside the structure. v = hydrophobic volume, l_0 = hydrophobic length, a_0 = headgroup area.*

Once it is established which interactions between amphiphilic molecules within an aggregate are involved, the most favoured structures have to be determined. These depend on the optimal area a_0 of the headgroup, the maximum effective length of the hydrophobic part and its volume v, which will be assumed to be fluid and incompressible. The maximum effective length sets a limit on how far the hydrophobic part can extend: smaller extensions are allowed but further extensions are not. Once the optimal surface area a_0, and the volume v and the length l_0 of the hydrophobic part are

specified for a specific molecule, it may be possible to determine which structure the molecules can pack into, by calculating the *packing parameter* (***Equation 5.1***, ***Table 5.1***).[1]

$$P = \frac{v}{a_0 l_0} \quad (5.1)$$

Table 5.1 *Relation between packing parameter and structure formed.*

$P = \frac{v}{a_0 l_0}$	Structure formed
0-1/3	Spherical micelles
1/3-1/2	Cylindrical micelles
1/2-1	Vesicles or bilayer
>1	Inverted micelles

In order to predict the supramolecular structure of the quaterthiophenes, the values a_0 of the proline, v and l_0 of the hydrophobic part were calculated by Dr. Elena Mena-Osteritz, and the *packing parameter* estimated (***Table 5.2***).

The a_0 value is for all molecules equivalent and corresponds to 164 Å^2. For hybrids **3.4**, **3.5**, **3.7** and **3.9** the same v and l_0 values (390.71 Å^3 and 27 Å) are obtained because of the high structural similarity of the quaterthiophene skeletons, whereas higher hydrophobic values and shorter hydrophobic length for **3.2** (485.50 Å^3 and 19 Å) and lower hydrophobic values and longer hydrophobic length in case of **3.3** 344.49 Å^3 and 22 Å) were calculated.

Table 5.2 *Values of v, l_0, and packing parameter and structure formed by hybrids **3.2**-**3.5**, **3.7** and **3.9**.*

Hybrid	V [Å^3]	l_0[Å]	$P = \frac{v}{a_0 l_0}$	Structure formed
3.2	**485.50**	**19**	**0.15**	Spherical micelles
3.3	**344.49**	**22**	**0.095**	Spherical micelles
3.4, 3.5, 3.7, 3.8	**390.71**	**27**	**0.088**	Spherical micelles

As one can see from the values reported in ***Table 5.2***, in theory all hybrids should form spherical micellar suprastructures.[1]

5.1.1 Instrumental Analytical Methods

In order to analyse the self-assembled structures of the quaterthiophene-proline hybrids, atomic force microscopy (AFM) and transmission electron microscopy (TEM) were implemented. In fact, by using scanning probe techniques assemble features can be visualized and the morphologies characterized, in case the aggregates survive the transfer to the substrate and the loss of the stabilizing solvent. In particular, AFM has a good lateral resolution (10-20 nm) and a high vertical resolution (1-2 Å) to the height variations of the sample surface. In the intermittent contact mode the cantilever is oscillating with a larger amplitude which allows the transient contact of the tip with the sample at the bottom of the swing.[2] The tapping-mode is a compromise between contact and non-contact mode and is frequently applied for biomolecules and supramolecular morphologies.[3-6] Due to the contact of the tip with the sample the resolution is almost as good as in the contact mode but no shear forces influence the sample surface. Therefore, this almost non-invasive method was applied to visualize the self-assembled features of my biosystems. Highly Oriented Pyrolytic Graphite (HOPG) was employed as an inert, hydrophobic substrate for AFM measurements. It is indeed well known that such surface is widely used for the formation of oligothiophenes assemblies together with the silicon wafer.[7] Moreover, the experimental protocol followed for the sample deposition on the surface is of extreme importance, since deposition techniques, drying process, temperature, or concentration of the measured solution strongly influence the self-assembly properties. While spin-coating leads to a fast and uniform evaporation of the solvent, drop-casting is a much slower process and allows the growth of larger aggregates onto the surface. For this reason, the drop-casting was preferred as deposition method also because strong shear forces influence the aggregates during the spin-coating deposition technique. The same method was also utilized in TEM measurements. In this case, the sample was deposited on a carbon substrate, which covers a support copper grid. Here, in order to withstand the instrument vacuum and facilitate the handling, the sample is fixated using a negative staining material such as uranyl acetate. In general, in the transmission electron microscopy a beam of electrons is transmitted through an ultra-thin specimen and the image contrast is given by the absorption of electrons in the material and depends on the thickness and composition of this, in the atomic force microscopy a cantilever with a sharp tip at its end is used to scan the specimen surface.

In this case, a laser light from a solid-state diode is reflected off the back of the cantilever and collected by a position-sensitive detector (PSD) consisting of two closely spaced photodiodes whose output signal is collected by a differential amplifier, which translate such signals in images.

In order to gain more informations about the supramolecular organization in the solid state, dedicated morphological characterization tools are the Grazing incidence X-ray Diffraction (GIXD), which includes Grazing-incidence small-angle scattering (GISAXS) and Grazing-incidence wide-angle scattering (GIWAXS). In particular, the GIWAXS technique has emerged in the last two decades as a powerful tool that allows the investigation of the crystallinity of surfaces and thin films. The advantages of such technique are that it is non-destructive, it yields statistical information averaged on a large number of nano-objects, it allows probing both the surface or deep below it, by changing the incident angle of the X-ray beam; it can be used in very different sample environments, in particular *in situ* in the course of a given process such as growth, annealing, gas exposure.[8,9]

Below, a schematic representation of the GIWAX geometry is shown.

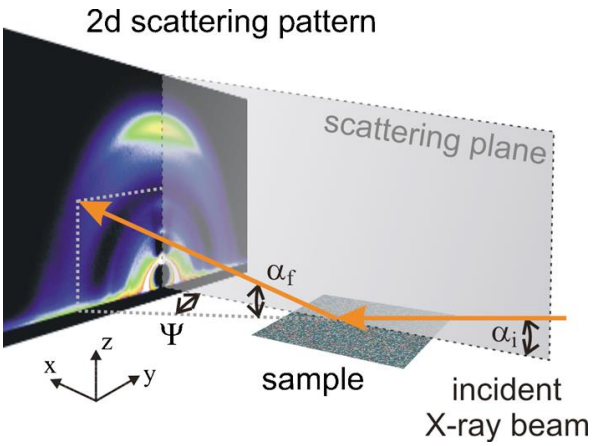

Figure 5.2. *Schematic representation of the GIWAX geometry.*[8] Reprinted with permission from *Rev. Sci. Instrum.* **2010**, *81*, 105105. Copyright 2010 AIP Publishing LLC.

The sample surface is placed horizontally, the X-ray beam with wavelength λ impinges on the sample surface with a fixed angle of incidence α_i. The scattered beam is described by the exit angle α_f and the horizontal scattering angle ψ. The area detector resembles the q_y dependence along the horizontal axis and the q_z dependence along the vertical axis, neglecting the small q_x dependence. The detected two-dimensional scattering pattern shows the wide angle scattering originating from

the sample. The primary beam and the intensity from the small angle scattering (GISAXS) are shielded with a rod-like beam stop.[9]

Here, GIWAX together with powder X-ray diffraction technique were applied to gain deeper insights into the supramolecular organization of the proline-quaterthiophene conjugate **3.5**, which has revealed so far to be the most interesting hybrid, due to its self-assembly properties in solution.

5.2 AFM and TEM Investigations of Quaterthiophene-Proline Hybrids 3.2 and 3.5

AFM and TEM investigations on quaterthiophenes **3.2** and **3.5** (***Chart 5.1***) will be reported in the next subchapters. Because of the similar *packing parameter* values of the α-substituted quaterthiophene-proline hybrids, just the self-assembly behaviour of **3.5** will be shown. On the other hand, quaterthiophene **3.2** was chosen as the only derivative bearing β-substitutions on the conjugated backbone.

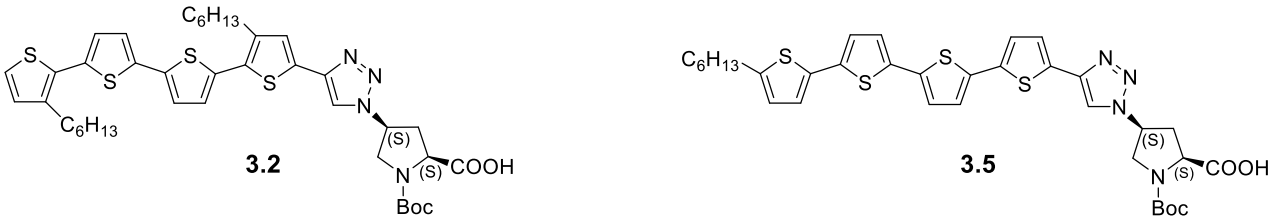

Chart 5.1. *Molecular structures of quaterthiophene-proline hybrids **3.2** and **3.5.***

*5.2.1 β-Hexyl-Substituted Quaterthiophene-Proline **3.2** from THF/Water (1:9) Solution*

A THF/water (1:9) solution ([c] = 5 x 10^{-5} M) of **3.2** was drop-casted on freshly cleaved HOPG. The sample was measured 24 hours after the deposition, in order to let the solvent evaporate.

Figure 5.3 depicts AFM micrographs of the prepared samples. In both topography (***a***) and phase (***c***) images the presence of widespread and flat granular particles can be detected. They are characterized by a height between 2 and 5 nm and have a diameter between 40 and 70 nm, as shown in the profile diagram (***Figure 5.3***, ***b***). A

change in phase of ca. 4 degree (***Figure 5.3***, ***c***) indicates that the structures covering the substrate are all of the same kind.

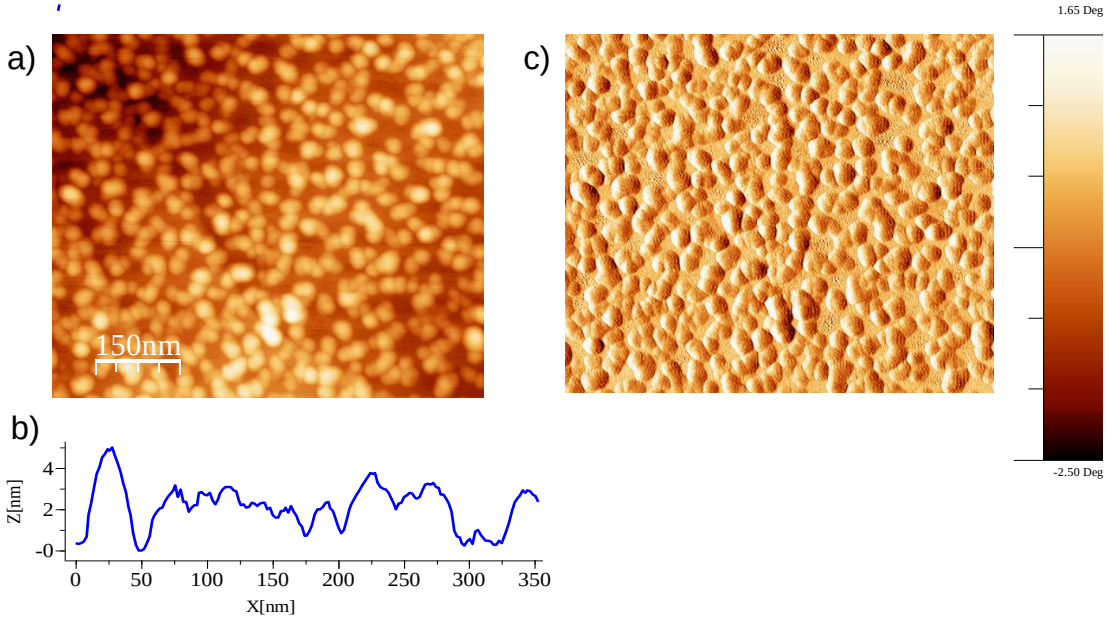

Figure 5.3. *AFM micrograph (740 x 630 nm^2) of* ***3.2****/HOPG drop-casted from the THF/water (1:9) solution a) topography ΔZ = 8 nm; b) height profile; c) phase image $\Delta\Phi$ = 4 °.*

By zooming in the topography micrograph, the analysis of a single aggregate is possible (***Figure 5.4***): the structure is characterized by height of 3 nm and a diameter of 40 nm.

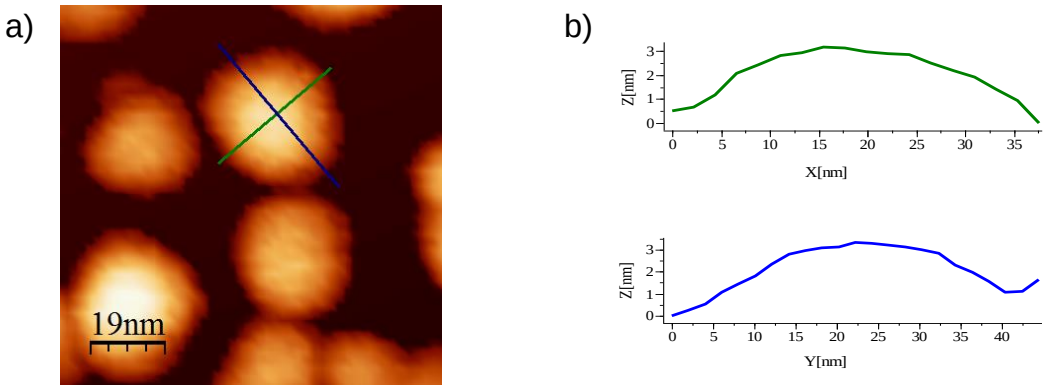

Figure 5.4. *Close up of* ***3.2****/HOPG. a) Topography micrograph, 100 x 100 nm^2 ΔZ = 4 nm; b) height profile in the two labelled directions.*

In general, these findings indicate that quaterthiophene **3.2** aggregates in the solid state by forming "*pancake-like*" suprastructures, which becomes more evident by looking at the 3D image (***Figure 5.5***).

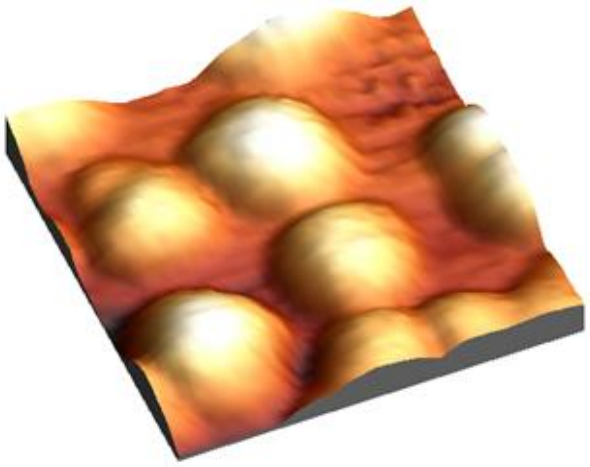

Figure 5.5. 3.2*/HOPG. 3D Representation of the topography micrograph, 100 x 100 nm^2 ΔZ = 4 nm.*

This kind of shape is often observed for micelles and small unilamellar vesicles, when deposited on a substrate, as it will be explained in ***Paragraph 5.3***.[10]

*5.2.2 β-Hexyl-Substituted Quaterthiophene-Proline **3.2** from 100% THF Solution*

A solution of hybrid **3.2** in pure THF ([c] = 5 x 10^{-5} M) was drop-casted on freshly cleaved HOPG; the sample was measured after 24 hours.

In ***Figure 5.6***, the substrate structure, which is characterized by the presence of terraces and steps, is still recognisable. While in the topography image it is not clear, whether the substrate is covered by material, the phase micrograph, due to a small variation in $\Delta\Phi$, shows that HOPG is covered by a close layer of substance (***Figure 5.6***). As expected, it can be assessed that no aggregates are present, when **3.2** is deposited from the pure THF solution.

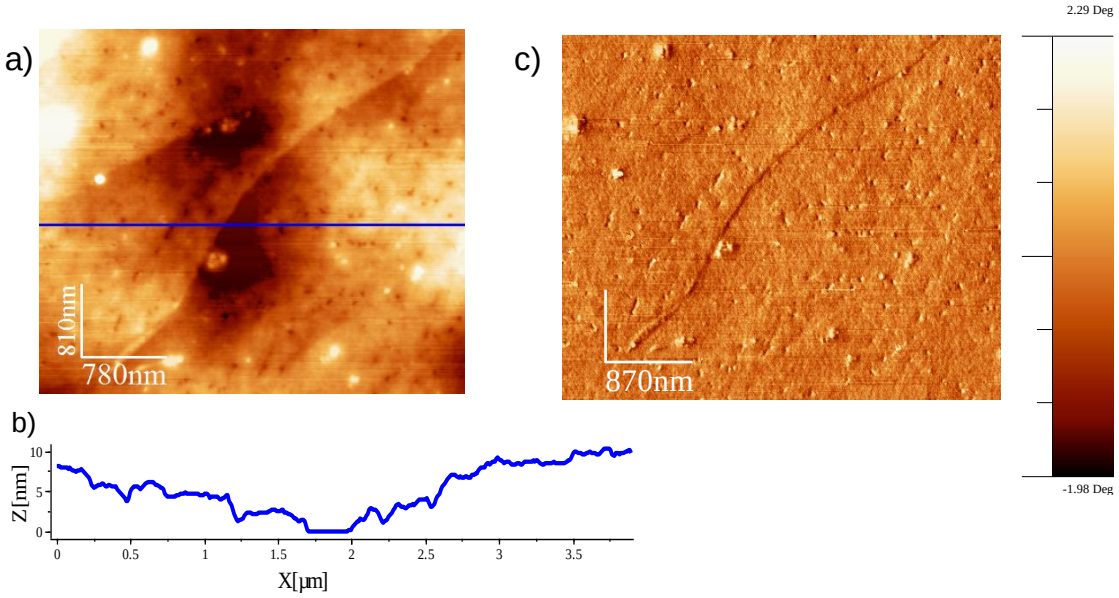

Figure 5.6. *AFM micrograph (4.4 x 4.4 µm^2) of* ***3.2****/HOPG drop-casted from the THF a) topography ΔZ = 14 nm; b) height profile; c) phase image ΔΦ = ~4 °.*

5.2.3 α-Hexyl Substituted Quaterthiophene-Proline ***3.5*** from THF/Water (1:9) Solution

A THF/water (1:9) solution ([c] = 10^{-4} M) of quaterthiophene **3.5** was drop-casted on freshly cleaved HOPG.

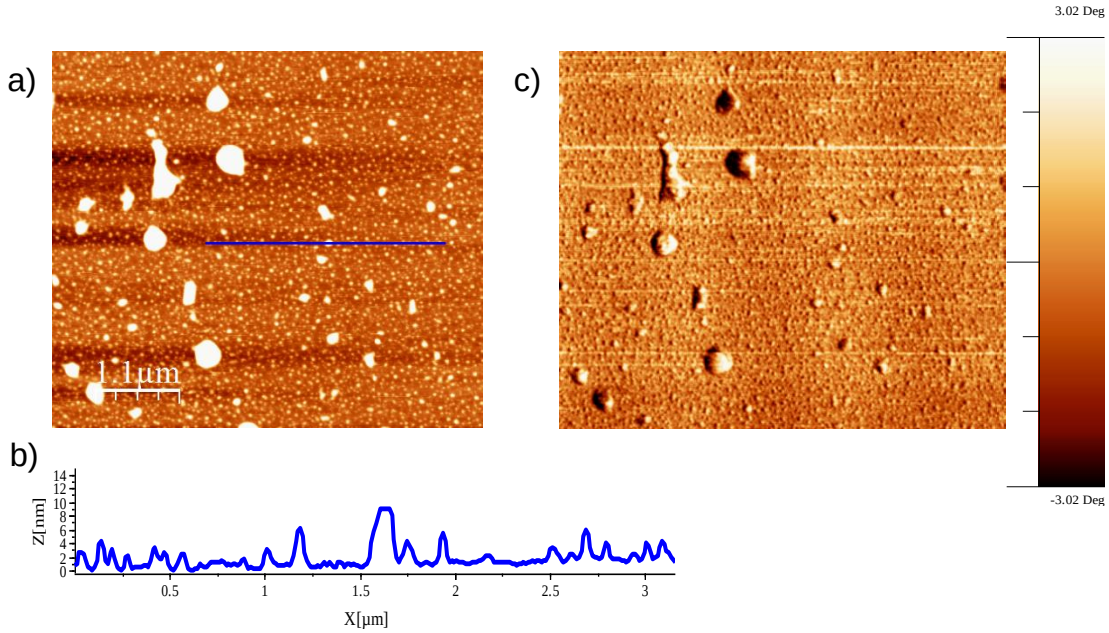

Figure 5.7. *AFM micrograph (5.2 x 5.7 µm^2) of* ***3.5****/HOPG drop-casted from the THF/water (1:9) solution: a) topography ΔZ = 12nm; b) height profile in the labelled direction; c) phase image, ΔΦ = ~ 6 °.*

Also in this case, the sample was measured 24 hours after deposition. ***Figure 5.7*** shows two types of structures: few bigger aggregates, ca. 500 nm broad and 12 nm high, and smaller ones, 80 to 100 nm broad and 2 to 4 nm high. Additionally, it is possible to discern into two kinds of material: sporadic clusters, which are represented by the colour green (***Figure 5.8***, ***a***), and small aggregates, which cover most of the surface and have a yellow/brown contrast. Because of the high distribution of the small round-shaped particles on the surface (***Figure 5.8***, ***b***), it might be hypothesized that these correspond to the suprastructures which were originally detected by UV/Vis and CD-spectroscopy in the THF/water (1:9) solution of hybrid **3.5**.

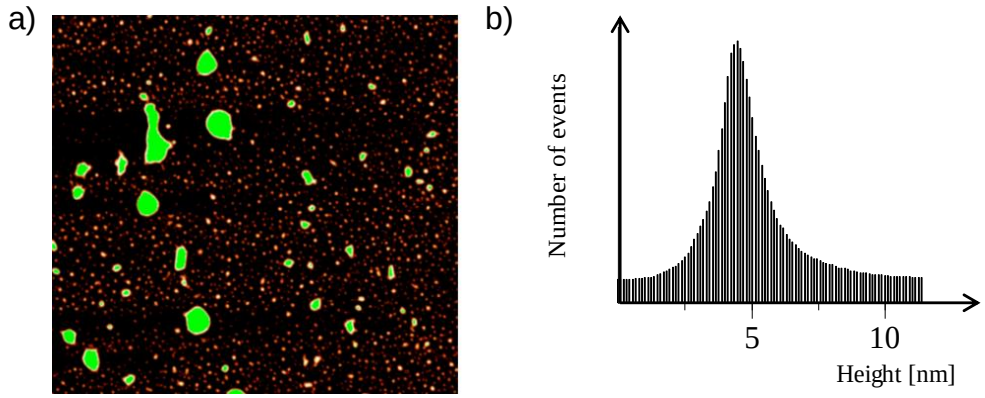

Figure 5.8. 3.5*/HOPG drop-casted from the THF/water (1:9) solution, 5.2 x 5.7 µm*^{2}*. a) Flooding topography, b) height histogram.*

By zooming into the topography and in particular on a single structure a better analysis of this is possible. The aggregate is characterized by 3 nm height and 85/100 nm broadness (***Figure 5.9***).

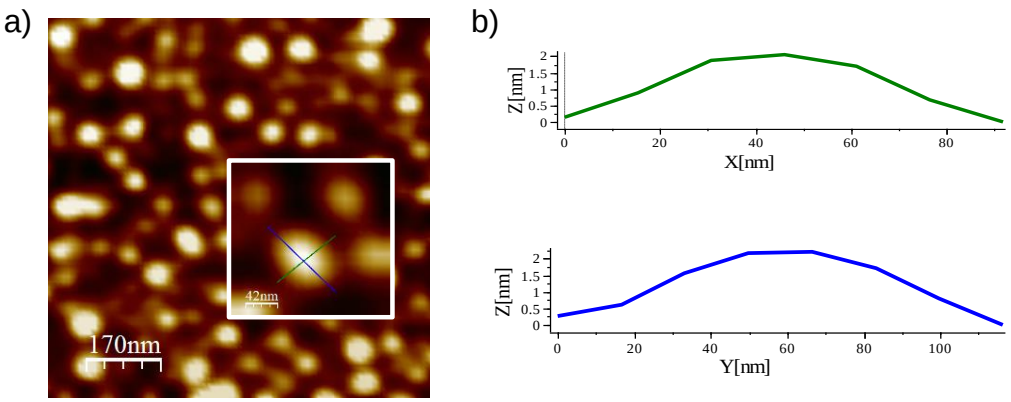

Figure 5.9. *Close up of* ***3.5****/HOPG. a) Topography micrograph, 850 x 850 nm*^{2} *ΔZ = 3 nm, and 210 x 210; b) height profile in the two labelled directions.*

Additionally, the histogram of the statistical distribution of the area of the aggregates detected in the close up topography image is reported (***Figure 5.10***). This kind of analysis shows the number of structures which display the same dimension of the aggregate described above.

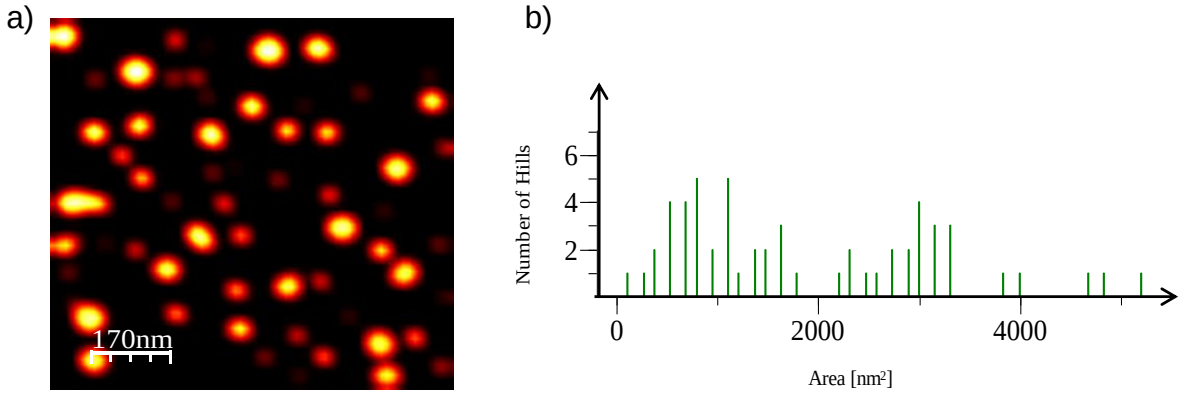

Figure 5.10. 3.5*/HOPG drop-casted from the THF/water (1:9) solution, 850 x 850 nm^2. Flooding topography (left) and area distribution histogram (right).*

As already observed for hybrid **3.2**, the structures show "*pancake-like*" shape, which can be again better seen in the 3D representation (***Figure 5.11***).

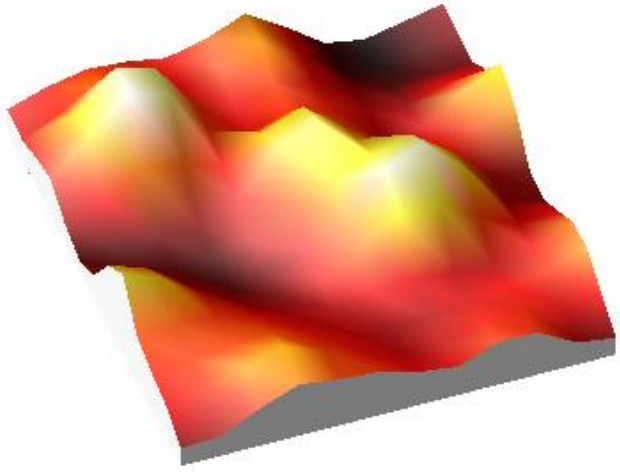

Figure 5.11. 3.5*/HOPG. 3D representation of the topography micrograph, 210 x 210 nm^2 ΔZ = 3 nm.*

The dimensions of the aggregates in the AFM images correlate with those obtained on the TEM experiment. Here, the sample was drop-casted from THF/water (1:9) so-

lution ([c] = 10^{-4} M) on a copper grid and uranyl acetate was added as staining agent (***Figure 5.12***).

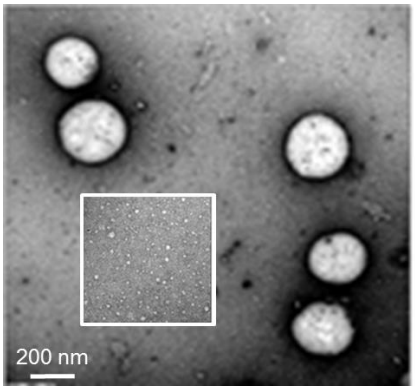

Figure 5.12. *TEM micrographs 9 x9 mm^2 and 2 x 2 µm^2 obtained from drop-casting of a THF/water (1:9) solution of hybrid* ***3.5****.*

Two borderline dimensions have been analysed: the large aggregates evidence a well-defined perimeter with a reflecting halo and strong contrast inside, which is indicative of a vesicular structure (***Figure 5.12***). The size of the big vesicles ranges from 0.5 to 1.7 µm diameter. The small structures (diameters between 25 and 75 nm) were randomly distributed in the micrographs and showed as well a brighter contrast inside. No evidence of intermediate aggregates was found.

The self-assembly behaviour of hybrid **3.5** on silicon wafer was also investigated in order see whereas the nature of the aggregates is influenced by the surface chosen for the measurements.

The THF/water (1:9) solution ([c] = 10^{-4} M) of **3.5** was drop-casted on silicon wafer. The sample was left to ripen on the surface for 24 hours.

The presence of big round-shaped aggregates embedded in an unstructured layer of material was detected. Looking at the phase micrograph (***Figure 5.13***, ***b***), it was observed that the structures cover the entire surface; in fact a very small contrast was registered. Furthermore, the height profile shows that the assemblies are comprised between 1.5 nm and 4 nm in height.

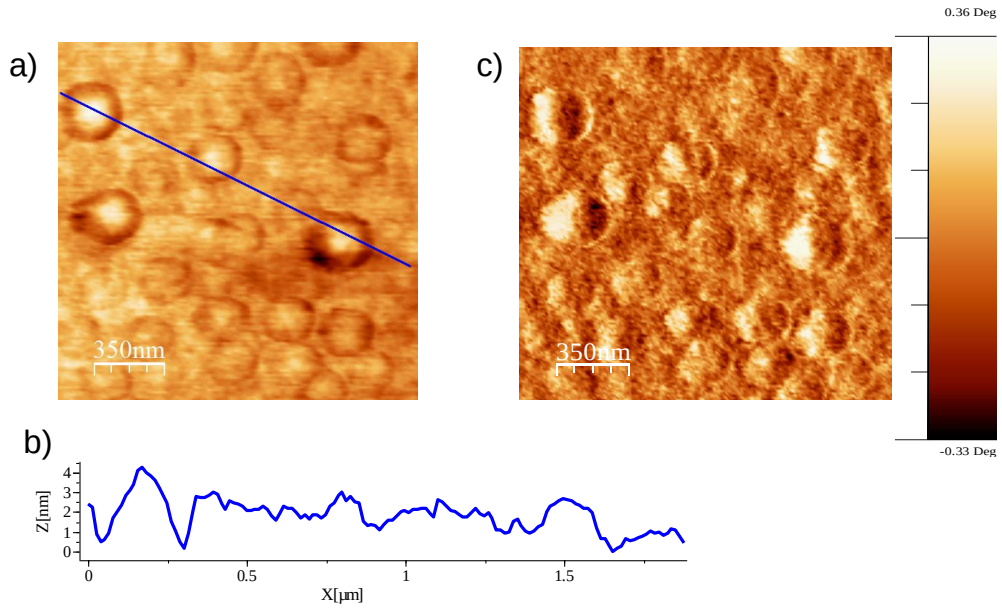

Figure 5.13. *AFM micrograph (1.7 x 1.7 nm^2) of* ***3.5****/silicon wafer drop-casted from the THF/water (1:9) solution a) topography ΔZ = 6 nm; b) height profile in the labelled direction; c) phase image $\Delta\Phi$ = ~ 0.6 °.*

These findings suggest that the nature of the surface does not influence the shape of the aggregates, but just their dimensions: on silicon wafer the structures are indeed two times bigger than the ones measured on HOPG.

*5.2.4 α-Hexyl Substituted Quaterthiophene-Proline **3.5** from THF solution*

A solution of hybrid **3.5** in pure THF was drop-casted on freshly cleaved HOPG. The sample was measured after 24 hours. Interestingly, ***Figure 5.14*** shows the presence of agglomerates in the micrometer range, which reach a maximum of 70 nm in height. Besides these structures, smaller aggregates are recognizable.

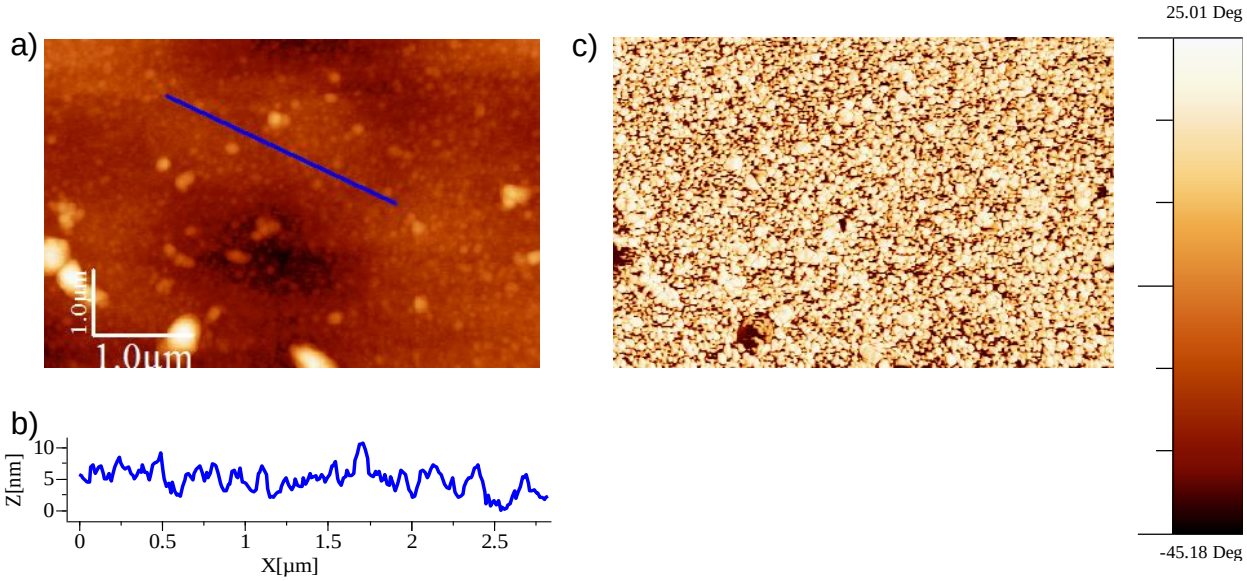

Figure 5.14. *AFM micrograph (5 x 3 µm^2) of* ***3.5****/HOPG drop-casted from THF solution a) topography ΔZ = 12 nm; b) height profile; c) phase image ΔΦ = ~ 70 °.*

In order to have a better overview on the smaller aggregates, a close up in the area under investigation is necessary. Now, two kinds of aggregates can be detected: crystalline structures and grains (***Figure 5.15***).

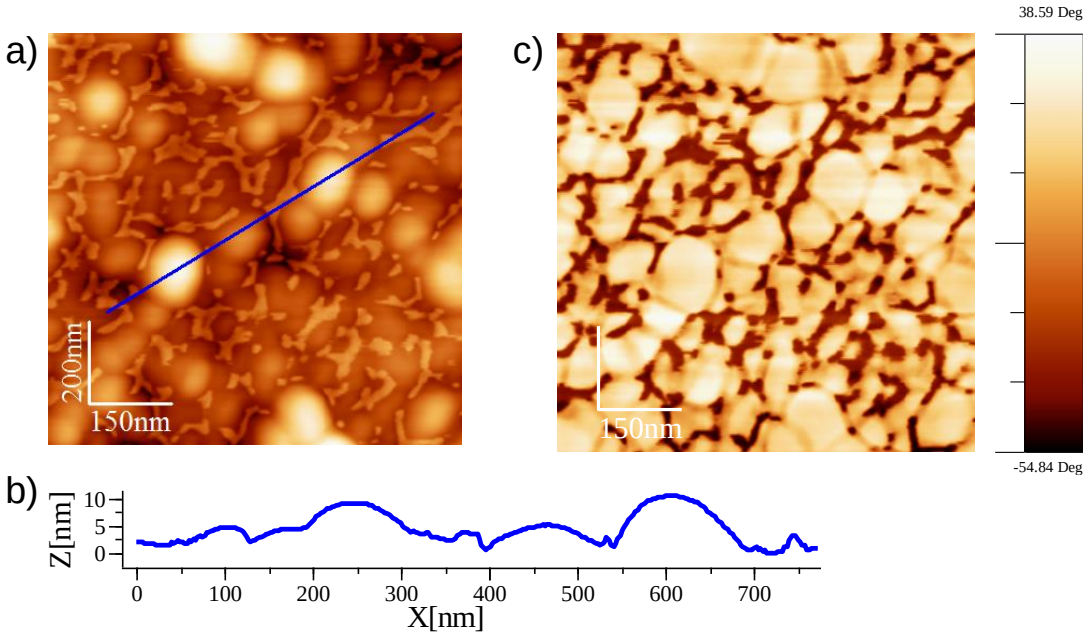

Figure 5.15. *Close up of* ***3.5****/HOPG. a) Topography micrograph, 1 x 0.75 µm^2, ΔZ = 12 nm; b) height profile in the labelled direction; c) phase image, ΔΦ = ~ 96 °.*

The crystalline structures are characterized by a height between 3 and 4 nm. These structures can be formed by more crystalline aggregates versus the rest high phase structures. The granular aggregates are more defined; they reach a maximum height of 10 nm and diameter between 100 and 150 nm.

Unlike hybrid **3.2**, quaterthiophene **3.5** shows still self-assembling ability, when deposited on a substrate from a neat THF solution. The aggregates detected under such conditions are different with respect to those observed when the sample was deposited from the water/THF (1:9) solution.

5.3 Proposed Model

As discussed in the ***Introduction***, and because of the *packing parameter* values, it was suggested that the quaterthiophene hybrids self-assemble in micelles. This hypothesis was further corroborated by the AFM and TEM findings.

Since the measurements carried out in the solid state were performed depositing a solution of the hybrids in THF/water, a model is proposed: the molecules aggregate in the mixture solution leaving the hydrophilic proline part facing towards the aqueous environment and the hydrophobic part pointing inside the supramolecular structures, without THF in the center, as depicted in ***Figure 5.16***. Here, quaterthiophene **3.5** was chosen as representative for all biosystems.

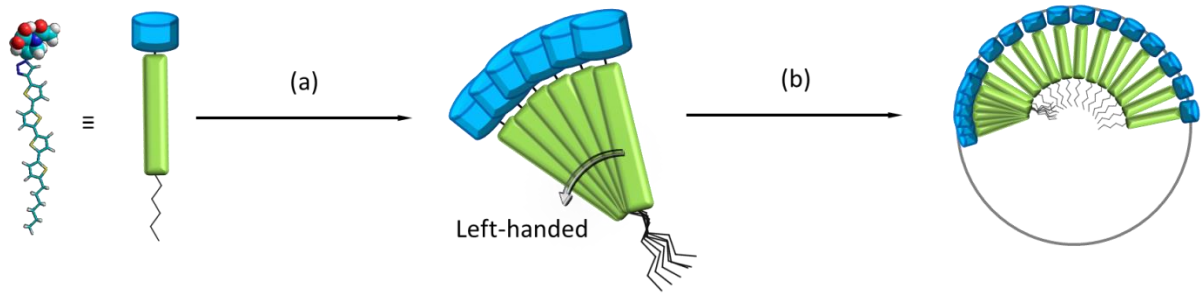

Figure 5.16. *Proposed model for the aggregates of* ***3.5****, (a) π-π interacting ensemble formation, (b) micelle formation.*

Once the supramolecular structures are investigated on a substrate, new parameters start to play a role in the aggregates' behaviour, such as the surface tension and the radius of the suprastructures. In fact, it is known that for a given surface tension, the pressure in a vessel is inversely proportional to the radius, meaning that a smaller radius results in a higher pressure difference. Practically, this means that the radial

force toward the centre of the structure is much higher than the surface forces, causing a partial disaggregation of the micelle or of the vesicle when they are in contact with the surface.[8] This could be indeed the reason why the aggregates detected in the AFM and TEM images have a "*pancake-like"* shape.

When a polar surface, as silicon wafer is utilized for the investigations, it can be suggested that the structures, which are characterized by an all hydrophilic surface, will get directly in contact with the substrate, and, afterwards, they will assume the already described "*pancake-like"* shape (***Figure 5.17***).

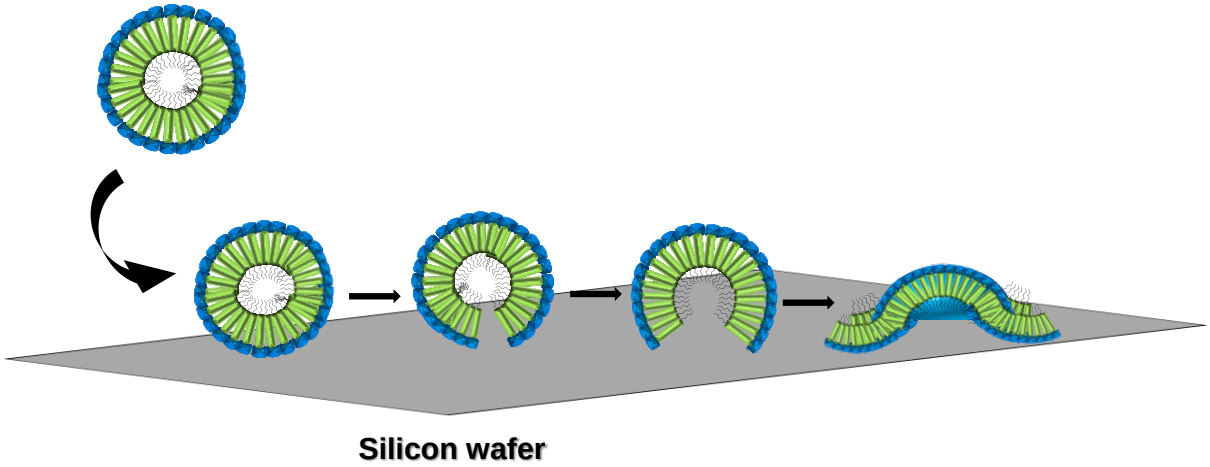

Figure 5.17. *Proposed model of the behaviour of aggregates of* ***3.5*** *on silicon wafer substrate.*

When HOPG is employed, it is hypothesized that the molecules passivate the substrate by forming a laye(***Figure 5.18***).

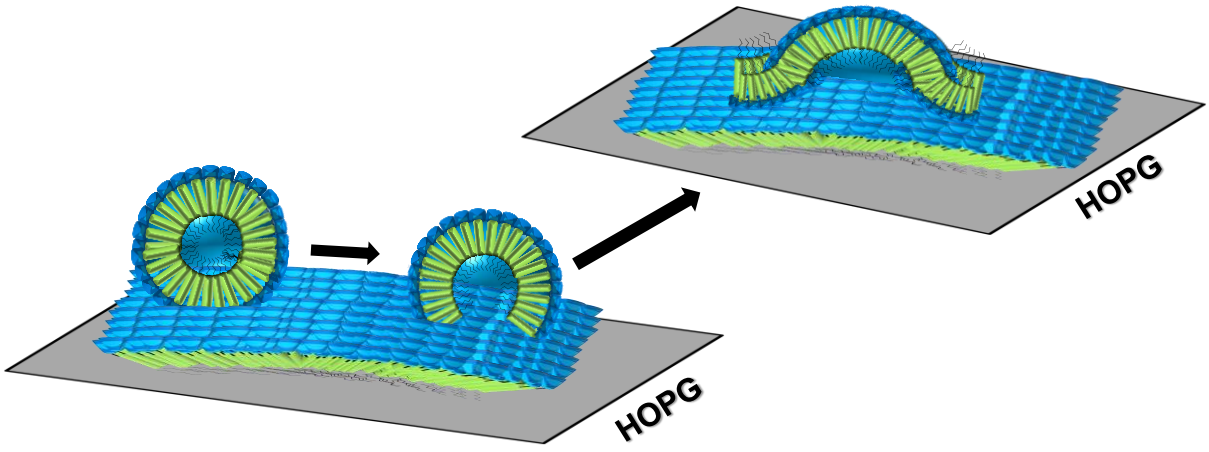

Figure 5.18. *Proposed model for the behaviour of aggregates of* ***3.5*** *on HOPG substrate.*

Now, a polar surface is formed and the micelles can interact with it. In this case, it is suggested that the hydrophilic interactions between the spherical suprastructures and the polar passivating layer are the one responsible of bringing the molecule to assume the characteristic flat shape (***Figure 5.18***).

Because on silicon wafer the circularly-shaped aggregates showed bigger dimensions than those detected on HOPG, it is hypothesized that the structures do not just interact with the surface but also with each other (coalescence), forming bigger assemblies (***Figure 5.19***).

Figure 5.19. *Coalescence on silicon wafer substrate.*

5.4 GIWAX and XRD Investigations of Quaterthiophene-Proline Hybrid 3.5

The experiments were carried out in the Müllen group by Dr. Wojciech Zajaczkowski at the Max Planck Institute for Polymer Research in Mainz. The sample was prepared by drop-casting the THF/water (1:9) solution of hybrid **3.5** ([c] = 10^{-4} M) on SiO_2 previously washed with acetone and isopropanol, afterwards the sample was left to incubate for seven days. The GIWAXS patterns of the biosystem are indicative of supramolecular order. The data revealed wide-angle equatorial scattering corresponding to d-spacing of 0.37 nm; such value is assigned to the π-stacking distance, while the reflection on d-spacing of 0.56 nm is assigned to width of the molucule. The reflections at 0.43 nm could be attributed to the typical alkyl-packing distance. Reflections on meridional plane in the small angle range correspond to a d-spacing of 2.72 nm, which is assigned to the interlayer distance (100 according Miller index). Furthermore, visible higher orders reflections (1.35 nm) suggest well-ordered lamella structure. Meridional positions of reflections assigned to interlayer distance suggest edge-on organization with long molecular axis perpendicular to the surface. It is extraordinary to see the perfect correlation between the reflections detected in the GIWAX and in the XRD experiments (***Figure 5.20***).

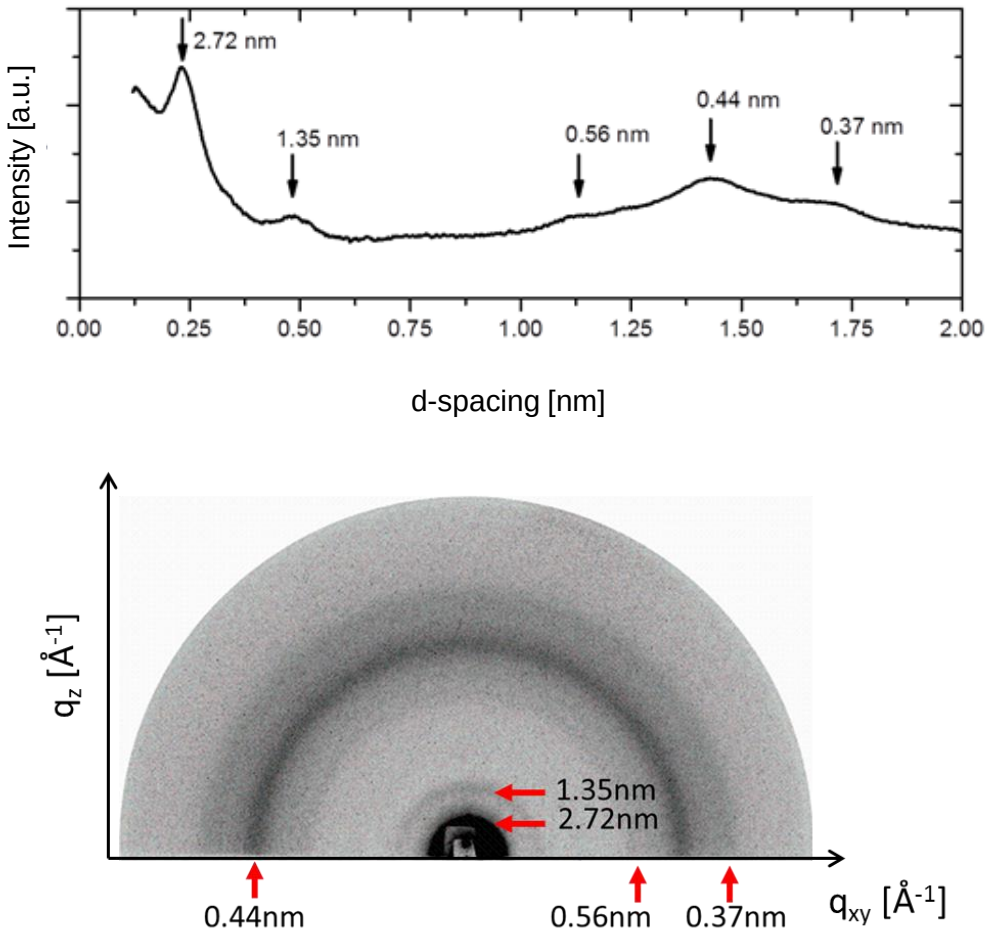

Figure 5.20. *XRD (top) and GIWAXS (bottom) of* ***3.5*** *after deposition from THF/water (1:9) solution and seven days of incubation.*

In order to visualize the just described outcomes, a semi-empirical model of hybrid **3.5** was calculated (***Figure 5.21***) and a model of the supramolecular organization is proposed (***Figure 5.22***).

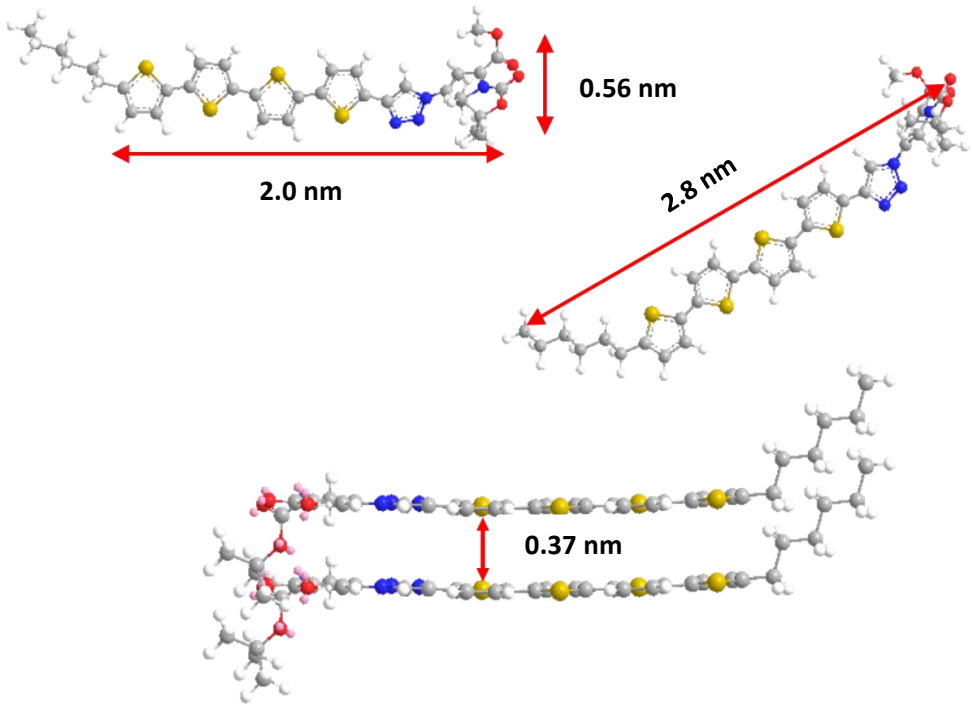

Figure 5.21. *Semi-empirical model of* ***3.5****, grey: carbon, blue: nitrogen, red: oxygen, yellow: sulfur and white: hydrogen with length of 2.8 nm and height of 0.66 nm. π-π stacking distance = 37 nm.*

Since SiO_2 is a polar substrate, one could hypothesize that the molecules organize with the polar proline directed to the surface and the hydrophobic part far away from it (***Figure 5.22***). In the model the individual oligomers are arranged in a lamella-type orientation and are separated by about 3.7 nm from the adjacent ones.

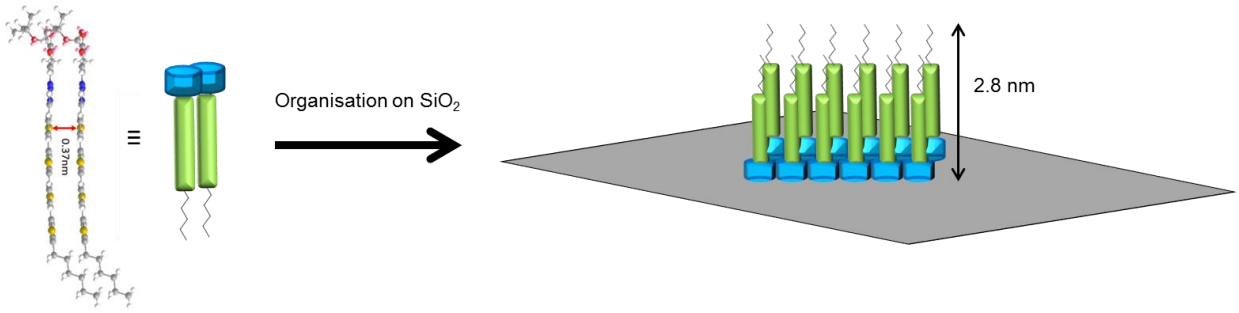

Figure 5.22. *Model of the molecular organization of* ***3.5*** *on SiO_2. Blue: proline, green: triazolylquater-thiophene, and black: alkyl chain.*

References

[1] J. N. Israelachvilli, *Intermolecular and Surface forces*, Academic Press: Boston, **1992**.

[2] C. Bustamante, D. Keller, *Phys. Today* **1995**, *48*, 32–38.

[3] S. N. Magonov, M.-H. Whangbo, *Surface Analysis with STM and AFM;* VCH Verlagsgesellschaft mbH: Weinheim, **1996**.

[4] M. Surin, R. Lazzaroni, W. J. Feast, A. Schenning, E. W. Meijer, P. Leclére, *Synth. Met.* **2004**, *147*, 67–72.

[5] F. Brustolin, M. Surin, V. Lamaur, G. Romanazzi, Q. Sun, J. Cornil, R. Lazzaroni, N. A. J. M. Sommerdijk, P. Leclére, E. W. Meijer, *Bull. Chem. Soc. Jpn.* **2007**, *80*, 1703–1715.

[6] P. Jonkheijm, F. Hoeben, R. Kleppinger, J. van Herrikhuyzen, A. Schenning, E. W. Meijer, *J. Am. Chem. Soc.* **2003**, *125*, 15941–15949.

[7] P. Jonkheijm, P. van der Schoot, A. Schenning, E. W. Meijer, *Science* **2006**, *313*, 80–83.

[8] I. F. Perepichka, D. F. Perepichka, *Handbook of Thiophene-Based Materials*; John Wiley & Sons Ltd, **2009**.

[9] J. Perlich, J. Rubeck, S. Botta, R. Gehrke, S. V. Roth, M. A. Ruderer, S. M. Prams, M. Rawolle, Q. Zhong, V. Körstgens, P. Müller-Buschbaum, *Rev. Sci. Instrum.* **2010**, *81*, 105105.

[10] G. Renaud, R. Lazzari, F. Leroy, *Surface Science Report* **2009**, *64*, 255–280.

[11] A. I. Mechler, *Nanobiotechnology of Biomimetic Membranes*; D. Martin, Spring Science + Buisness Media, LLC, **2007**, 104.

Chapter 6

Own Work: Solution-Processed Organic Solar Cells

6.1 Introduction

Recently, the demand for the development of new materials for applications in organic bulk-heterojunction solar cells (BHJSCs) has been growing.[1-3] In response, the field has been expanding rapidly with the number of new molecules being synthesized at an increasingly faster rate,[3-5] and very recently, a record efficiency of 10.1% for single-junction small molecule-organic photovoltaics (SM-OPVs) was achieved.[6] In particular, it has been observed that the organization of the active layer plays a critical role in the device performance. As it was already discussed in ***Chapter 2*** (***State of the Art***), one way to achieve this morphology is to use supramolecular materials capable of self-assembling in defined nanostructures.[7-17]

For this reason, and because the hybrids studied so far have shown a very good ability to self-organize in stable supramolecular structures, they were employed as donor materials in solution-process solar cells. In particular, 5'''-hexyl-2,2';5',2'';5'',2'''-quaterthiophene-proline hybrid **3.5** and DCV-functionalised quaterthiophene-proline hybrid **3.9** were considered the most suitable one with respect to their solubility, their optoelectronic properties, and their self-assembling ability (***Chart 6.1***).

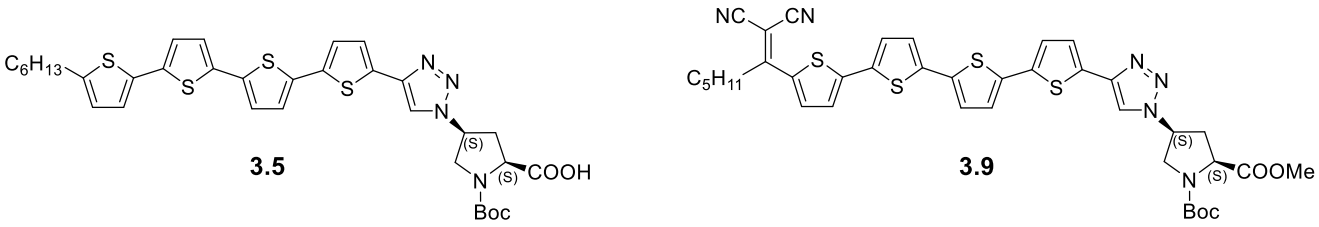

Chart 6.1. *Molecular structures of quaterthiophene-proline hybrids **3.5** and **3.9** employed as donor material in solution-processed bulk-heterojunction solar cells.*

It is already known that oligothiophenes end-capped with electron-withdrawing dicyanovinylen groups have excellent performance in BHJSCs.[5,6,18,19] Oligothiophenes of various lengths (from 3 to 7 thiophene units), which contain various alkyl side chains (methyl to octyl) with different substitution patterns, have been incorporated in photoactive layers of BHJSCs. When vacuum deposition is used, the highest efficiency for single-junction solar cells to date, with regard to DCV-end-capped oligothiophenes, has been reported to be 8.3% for dicyanovinyl quinquethiophene with methyl substituents on the central thiophene unit **DCV5T-Me (3,3)** blended with C_{60} in a ratio of 2:1.[18] In the case of solution-processed BHJSCs, a quinquethiophene derivative in-

corporating regioregular octyl chains, capped with 2-(1,1-dicyanomethylene)rhodanine groups **DRCN5T**, and blended with [6,6]-phenyl-C_{71}-butyric acid methyl ester ($PC_{71}BM$), displayed a *PCE* of 10.1% when spin-coated from a chloroform solution (***Chart 6.2***).[6]

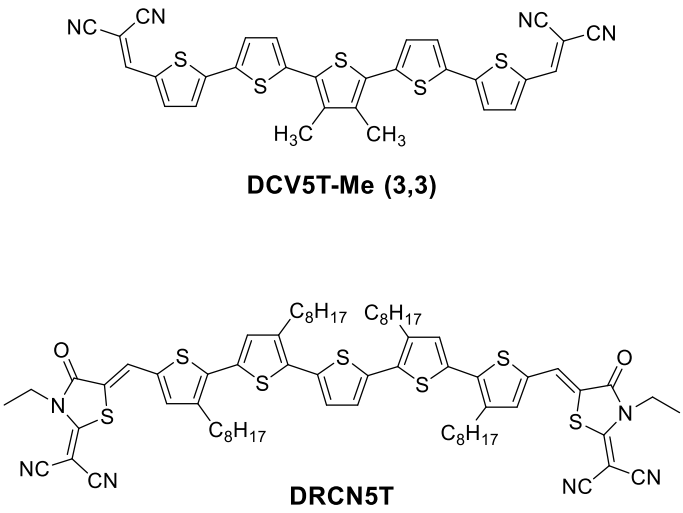

Chart 6.2. *Quinquethiophene* ***DCV5T-Me (3,3)*** *and quinquethiophene* ***DRCN5T*** *employed as donor material in vacuum-processed BHJSCs and solution-processed BHJSCs, respectively.*

6.2 Photovoltaic Properties of Oligomers 3.5 and 3.9

Hybrids **3.5** and **3.9** were implemented as donor component in solution-processed bulk heterojunction solar cells and the bulk layers were fabricated by spin-coating donor:acceptor blends from solution. Blend-layer thickness was varied using different spin-coating speeds. Due to the deep HOMO energy levels, V_{OC} values of 1.17 V for **3.5** and 1.05 V for **3.9** were calculated using empirical ***Equation 6.1***.[20]

$$V_{OC} \approx \frac{1}{e} \left| E_{HomO}\,(donor) - E_{LUMO}(acceptor) \right| - 0.3\ \text{V} \qquad (6.1)$$

Commonly used acceptors are fullerenes and the most popular soluble derivative is $PC_{61}BM$ with a LUMO level of -4.0 eV.[21] A difference of 0.3-0.4 eV[20] between the LUMO of the donor and the LUMO of the acceptor was found to be favourable for a good charge separation in organic photovoltaic.

The HOMO energy levels of quaterthiophene-proline hybrids **3.5** and **3.9** and the LUMO energy level of **3.9** were calculated from the onset values of the first oxidation and reduction waves using the standard approximation that the Fc/Fc^+ HOMO energy level is -5.1 eV versus vacuum.[22] The LUMO energy level of hybrid **3.5** was calculated from the HOMO and optical gap (***Equation 6.2***).

$$|E_{LUMO}| = |E_{HOMO}| - E_{g,optical} \quad (6.2)$$

The HOMO energy levels of hybrids **3.5** and **3.9** are similar, -5.47 eV and -5.35 eV respectively, whereas the LUMO energy level of hybrid **3.5** is clearly higher in comparison to the LUMO energy level of **3.9** resulting in a higher E_g value. These results are graphically shown in **Figure 6.1** and compared to the HOMO energies of PEDOT:PSS and $PC_{61}BM$ and the LUMO energies of $PC_{61}BM$ and aluminium.

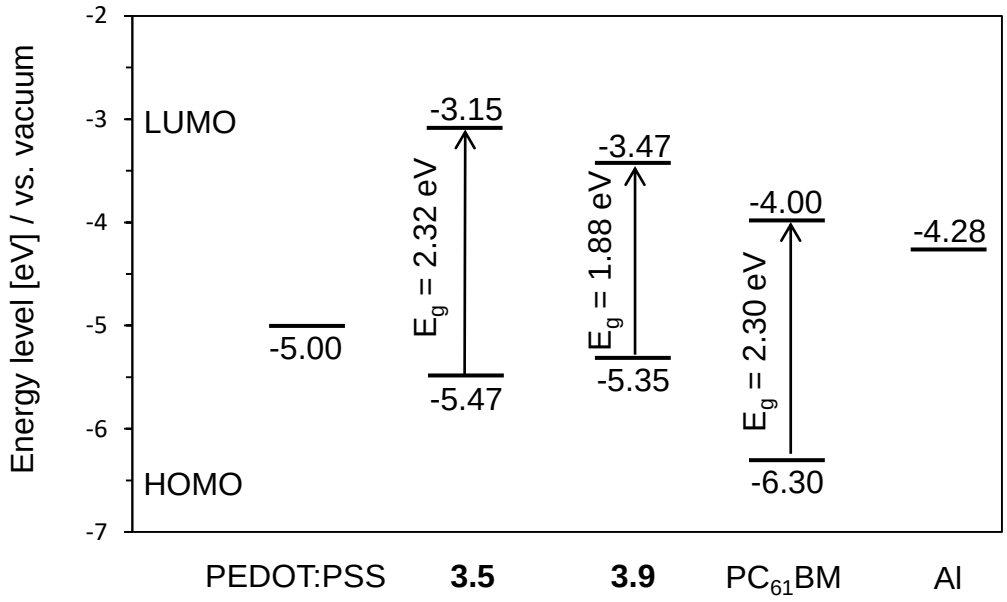

Figure 6.1. *Representation of the HOMO and LUMO energies of hybrids **3.5** and **3.9** compared to PEDOT:PSS and $PC_{61}BM$.*

6.2.1 Solar Cell Results of Quaterthiophene-Proline Hybrid ***3.5***

Devices were prepared with THF as solvent and were fabricated by spin-coating the **3.5**:$PC_{61}BM$ blend from hot solution (60 °C) on heated indium tin oxide | hole transporting layer (ITO | HTL)-coated glass substrates (60 °C). Subsequently, 0.7 nm lithium fluoride (LiF) was deposited, followed by 100 nm aluminium (Al) via thermal

evaporation. Poly(3,4-ethylenedioxythiophene) poly(styrenesulfonate) (PEDOT:PSS) was used as hole transporting material. General device structure with layer sequences of ITO/PEDOT:PSS/**3.5**:$PC_{61}BM$ /LiF/Al was investigated and is schematically shown in ***Figure 6.2***.

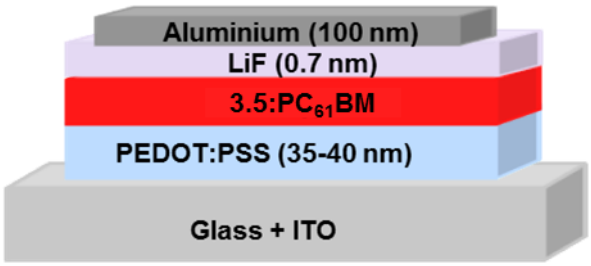

Figure 6.2. *Device architecture of investigated solution processed bulk heterojunction solar cells for hybrid **3.5**.*

The resulting solar cells did not show good results: all donor:acceptor ratios showed *PCE*s of 0% (***Table 6.1***). The main problems were the very low current of ≤ 32 µA cm^{-2} and *FF*s between 11% and 33%. The low *fill factor* is a hint for a limited charge transport in the active layer, and since the difference between the LUMO of the donor and the LUMO of the acceptor is higher than 0.4 eV, a good charge separation was also not to be expected.

Table 6.1. *Photovoltaic parameters of BHJ solar cells of quaterthiophene-proline **3.5**.*

Solvent[a]	D:A	T [°C]	Acceptor	Speed [rpm]	J_{SC} [µA/cm^2]	V_{OC} [V]	*FF* [%]	*PCE* [%]
THF	1:3	60 °C	$PC_{61}BM$	4000	15	0.03	33	0.00
THF	1:3	60 °C	$PC_{61}BM$	6000	27	0.16	25	0.00
THF	1:3	60 °C	$PC_{61}BM$	6000	23	0.69	12	0.00
THF	1:2	60 °C	$PC_{61}BM$	6000	53	0.32	19	0.00
THF	1:2	60 °C	$PC_{61}BM$	6000	33	0.79	10	0.00
THF	1:2	60 °C	$PC_{61}BM$	6000	28	0.85	12	0.00
THF	1:1	60 °C	$PC_{61}BM$	6000	32	0.78	9	0.00
THF	1:1	60 °C	$PC_{61}BM$	6000	17	0.72	17	0.00
THF	1:1	60 °C	$PC_{61}BM$	6000	11	0.44	16	0.00

[a] Films prepared from solution with a total concentration of 12 mg mL^{-1}; temperature of solution/substrate: 60 °C/60 °C.

Additionally, oligomer **3.5** showed a very low solubility. Despite the fact that the solution was filtered before spin-coating in order to remove materials which was still not dissolved, the films appeared not amorphous, and scattered light and also particles were visible resulting in bad BHJSCs.

6.2.2 Solar Cell Results of Quaterthiophene-Proline Hybrid ***3.9***

Devices were prepared with $CHCl_3$ as solvent and were fabricated by spin coating the **3.9**:$PC_{61}BM$ blend from hot solution (60 °C) on heated indium tin oxide. As for quaterthiophene **3.5**, the general device structure investigated was ITO/PEDOT:PSS/**3.9**:$PC_{61}BM$/LiF/Al and is schematically shown in ***Figure 6.3***.

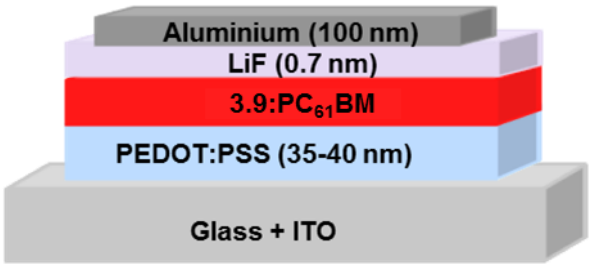

Figure 6.3. *Device architecture of investigated solution processed bulk heterojunction solar cells for hybrid **3.9**.*

Improved results were obtained utilizing hybrid **3.9** as donor material. In fact, the J_{SC}, *FF* and *PCE* values are higher than those obtained using **3.5** as electron donor (***Table 6.2***).This could be attributed to a better morphology of the film with respect to hybrid **3.5.** This could be due to the higher solubility of **3.9**. Additionally, the higher HOMO energy level of the DCV-functionalized donor should favour a better charge separation. Still, a low current density was recorded: after spin-coating it was evident by eye that particles were present in the film resulting in leakage currents in the *J-V* curve.

Table 6.2. *Photovoltaic parameters of bulk heterojunction solar cells of quaterthiophene-proline **3.9**.*

Solvent[a]	**D:A**	**T [°C]**	**Acceptor**	**Speed [rpm]**	**J_{SC} [mA/cm^2]**	**V_{OC} [V]**	***FF*** **[%]**	***PCE*** **[%]**
$CHCl_3$	1:3	60 °C	$PC_{61}BM$	2000	0.50	0.56	36	0.10
$CHCl_3$	1:3	60 °C	$PC_{61}BM$	4000	0.80	0.53	38	0.19

$CHCl_3$	1:3	60 °C	$PC_{61}BM$	6000	0.80	0.58	37	0.20
$CHCl_3$	1:2	60 °C	$PC_{61}BM$	2000	0.48	0.59	30	0.12
$CHCl_3$	1:2	60 °C	$PC_{61}BM$	4000	0.45	0.55	3	0.11
$CHCl_3$	1:2	60 °C	$PC_{61}BM$	6000	0.57	0.62	30	0.10
$CHCl_3$	1:1	60 °C	$PC_{61}BM$	2000	0.03	0.60	16	0.00
$CHCl_3$	1:1	60 °C	$PC_{61}BM$	4000	0.004	0.38	17	0.00
$CHCl_3$	1:1	60 °C	$PC_{61}BM$	6000	0.002	0.45	2	0.01

[a] Films prepared from solution with a total concentration of 15 mg mL^{-1}; temperature of solution/substrate: 60 °C/60 °C.

Furthermore, from previous experiences in our group it was observed that the replacement of the vinylic proton of the DCV acceptor via alkyl side chain, in this specific case hexyl chain, resulted in weaker intramolecular interactions and a decrease of the acceptor strength. This could partially explain the low efficiency of the solar cells.[23]

However, it is evident that by increasing the acceptor content in the active layer slightly higher *PCE*s values could be achieved.

Anyway, the device fabricated utilizing oligomer **3.9** as donor component is comparable to those shown by A. B. Holmes and colleagues in 2011.[24] They synthesized an asymmetric sexithiophene functionalized via Click chemistry with a single amino acid, L-lysine **6.1**, and **6.2**, and they employed these hybrids as donor in BHJSCs (***Chart 6.3***).

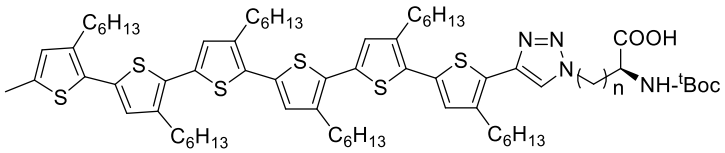

6.1 (n = 7)

6.2 (n = 11)

Chart 6.3. *L-lysine-sexithiophene hybrids **6.1** and **6.2** synthesized in Holmes´s group.*[24]

The architecture of their devices was glass/ITO/PEDOT:PSS/**6.1**:$PC_{61}BM$/Ca/Al and glass/ITO/PEDOT:PSS/**6.2**:$PC_{61}BM$/Ca/Al. They implemented calcium as electron transporting layer instead of lithium fluoride and they deposited the active layer by spin coating the film from chlorobenzene instead of chloroform.

Table 6.3. *Comparison of photovoltaic parameters of bulk heterojunction solar cells of* ***6.1****,* ***6.2****, and* ***3.9****.*

Hybrid	Solvent	D:A	T [°C]	Acceptor	Speed [rpm]	J_{SC} [mA/cm^2]	V_{OC} [V]	*FF* [%]	*PCE* [%]
6.1	**CB**	1:2	RT	$PC_{61}BM$	3000	0.76	0.59	26.3	0.12
6.2	**CB**	1:2	RT	$PC_{61}BM$	3000	1.30	0.61	27.7	0.22
3.9	**$CHCl_3$**	1:3	60 °C	$PC_{61}BM$	6000	0.80	0.58	37	0.20

By comparing the J_{SC}, V_{OC}, *FF*, and *PCE* values, it is evident that the two BHJ solar cells have really similar outcomes, and in particular the device fabricated using **3.9** has a *PCE* value comparable to **6.2**.

6.3 Conclusion

Hybrids **3.5** and **3.9** were implemented in solution-processed BHJSC with $BC_{61}BM$ as acceptor. DCV-functionalized hybrid **3.9** showed higher efficiency than quater-thiophene **3.5**, and comparable outcomes with the literature known sexithiophenes **6.1** and **6.2**. The main problem of the fabricated solar cells were the dramatic low current density, which could be attributed to the suboptimal morphology of the film, together with the λ_{max} values in absorption of both quaterthiophenes (417 nm for **3.5** and 475 nm for **3.9**). Room of improvement is still possible, though; for example, an alternative could be the employment of hybrid **3.9** in tandem solar cells.[25,26] In fact, the combination of the biohybrid with a complementary absorbing semiconducting material, which can allow for a larger coverage of the solar spectrum, would probably lead to more promising results.

References

[1] H. Spanggaard, F. C. Krebs, *Sol. Energy Mater. Sol. Cells* **2004**, *83*, 125–146.

[2] S. Günes, H. Neugebauer, N. S. Sariciftci, *Chem. Rev*. **2007**, *107*, 1324–1338.

[3] P.-L. Boudreault, A. Najari, M. Leclerc, *Chem. Mater.* **2011**, *23*, 456–469.

[4] B. Walker, C. Kim, T.-Q. Nguyen, *Chem. Mater.* **2010**, *23*, 470–482.

[5] A. Mishra, P. Bäuerle, *Angew. Chem.* **2012**, *124*, 2060; *Angew. Chem., Int. Ed.* **2012**, *51*, 2020–2067.

[6] B. Kan, M. Li, Q. Zhang, F. Liu, X. Wan, Y. Wang, W. Ni, G. Long, X. Yang, H. Feng, Y. Zuo, M. Zhang, F. Huang, Y. Cao, T. P. Russell, Y. Chen, *J. Am. Chem. Soc.* **2015,** *137*, 3886–3893.

[7] Y. Yamamoto, *Sci. Technol. Adv. Mater.* **2012**, *13*, 33001.

[8] D. Gonzàlez-Rodrìguez, A. P. H. J. Schenning, *Chem. Mater.* **2011**, *23*, 310–325.

[9] G. Bottari, O. Trukhina, M. Ince, T. Torres, *Coord. Chem. Rev.* **2012**, *256*, 2453–2477.

[10] M. Wang, F. Wudl, *J. Mater. Chem.* **2012**, *22*, 24297–24314.

[11] F. Würthner, Z. Chen, F. J. M. Hoeben, P. Osswald, C. C. You, P. Jonkheijm, J. V. Herrikhuyzen, A. P. H. J. Schenning, P. P. A. van der Schoot, E. W. Meijer, E. H. A. Beckers, S. C. J. Meskers, R. A. J. Janssen, *J. Am. Chem. Soc.* **2004**, *126*, 10611–10618.

[12] T. Hasobe, S. Fukuzumi, P. V. Kamat, *Angew. Chem., Int. Ed.* **2006**, *45*, 755–759.

[13] K. Sugiyasu, S. I. Kawano, N. Fujita, S. Shinkai, *Chem. Mater.* **2008**, *20*, 2863–2865.

[14] A. A. Gorodetsky, C. Y. Chiu, T. Schiros, M. Palma, M. Cox, Z. Jia, W. Sattler, I. Kymissis, M. Steigerwald, C. Nuckolls, *Angew. Chem*. **2012**, *124*, 1–5; *Angew. Chem., Int. Ed.* **2010**, *49*, 7909–7912.

[15] a) Y. Hizume, K. Tashiro, R. Charvet, Y. Yamamoto, A. Saeki, S. Seki, T. Aida, *J. Am. Chem. Soc.* **2010**, *132*, 6628–6629; b) W. Zhang, W. Jin, T. Fukushima, A. Saeki, S. Seki, T. Aida,*Science* **2011**, *334*, 340–343.

[16] a) N. Sakai, R. Bhosale, D. Emery, J. Mareda, S. Matile, *J. Am. Chem. Soc.* **2010**, *132*, 6923–6925; b) R. Bhosale, A. Perez-Velasco, V. Ravikumar, R. S. K. Kishore, O. Kel, A. Gomez-Casado, P. Jonkheijm, J. Huskens, P. Maroni, M. Borkovec, T. Sawada, E. Vauthey, N. Sakai, S. Matile, *Angew. Chem*. **2009**, *121*, 6583–6586; *Angew. Chem., Int. Ed.* **2009**, *48*, 6461–6464; c) R. Bhosale, J. Míšek, N. Sakai, S. Matile, *Chem. Soc. Rev.* **2010**, *39*, 138–149.

[17] W. W. H. Wong, T. B. Singh, D. Vak, W. Pisula, C. Yan, X. Feng, E. L. Williams, K. L. Chan, Q. Mao, D. J. Jones, C.-Q. Ma, K. Müllen, P. Bäuerle, A. B. Holmes, *Adv. Funct. Mater.* **2010**, *20*, 927–938.

[18] K. Meerheim, C. Korner, K. Leo, *Appl. Phys. Lett.* **2014**, *105*, 063306-1–63306-4.

[19] G. L. Schulz, M. Urdanpilleta, R. Fitzner, E. Brier, E. Mena-Osteritz, E. Reinold, P. Bäuerle, *Beilstein J. Nanotechnol.* **2013**, *4*, 680–689.

[20] M. C. Scharber, D. Mühlbacher, M. Koppe, P. Denk, C. Waldauf, H. J. Heeger, C. J. Brabec, *Adv. Mater.* **2006**, *18*, 789–794.

[21] C. J. Brabec, C. Winder, N. S. Sariciftci, C. J. Hummelen, A. Dhanabalan, P. A. van Hal, R. A. J. Janssen, *Adv. Funct. Mater.* **2002**, *12,* 709–712.

[22] T. Johansson, W. Mammo, M. Svensson, M. R. Andersson, O. Inganäs, *J. Mater. Chem.* **2003**, *13*, 1316-1323.

[23] M. Loebert *Ph.D. Thesis,* University of Ulm, **2013.**

[24] R. J. Kumar, J. M. McDonald, T. B. Singh, L. J. Waddington, A. B. Holmes, *J. Am. Chem. Soc.* **2011**, *133*, 8564–8573.

[25] T. Ameri, G. Dennler, C. Lungenschmied, C. J. Brabec, *Energy Environ. Sci.* **2009**, *2*, 347–363.

[26] A. De Vos, *J. Phys. D: Appl. Phys.***1980**, *13*, 839–846.

Chapter 7

Experimental Section

Methods:

NMR spectra were recorded on a Bruker AMX 400 spectrometer at 25 °C (^{1}H NMR: 400 MHz, 500 MHz, ^{13}C NMR: 100 MHz). Chemical shifts values (δ) are expressed in parts per million [ppm] using the internal standard tetramethylsilane (^{1}H NMR, δ_H = 0.00) or the solvent as reference (^{1}H, NMR δ_H = 7.26 for $CDCl_3$; ^{1}H NMR δ_H = 3.58, δ_H = 1.72 for THF-d_8, ^{13}C NMR, δ_C = 67.21 for $CDCl_3$, δ_C = 25.31 for THF-d_8). The following abbreviations reflect the multiplicity of the signals obtained: *s* = singlet, *d* = doublet, *t* = triplet, *m* = multiplet, combination of *dd* = doublet of doublets. Infrared (FT-IR) spectra were recorded on a Perkin-Elmer FTIR Spectrum 2000. Matrix-assisted laser desorption ionisation time-of-flight mass spectrometry (MALDI-TOF MS) measurements were carried out on a Bruker Daltonik Reflex III mass spectrometer using trans-2-[3-(4-tert-butylphenyl)-2-methyl-2-propenylidene]malononitrile (DCTB) as matrix. Chemical ionization (CI) and electron ionization (EI) mass spectrometry was performed on a Finnigan MAT SSQ-7000. High resolution mass spectra were carried out on a Bruker solariX. High performance liquid chromatography (HPLC) was performed on a Hitachi instrument equipped with a UV/Vis detector L-7420, column (Nucleosil 100-5 NO_2 with a pore size of 100 Å) from Macherey-Nagel. Dynamic light scattering (DLS) was performed on a Malvern Zetasizer Nano ZS (angle: 173°, λ: 633 nm) at 20 °C. Absorption spectra were recorded on a Perkin Elmer Lambda 19 spectrometer and fluorescence emission spectra on a Perkin Elmer LS 55 spectrometer in 1 cm cuvettes. Electrochemistry was performed using a Metrohm Autolab PGSTAT 10 Potentiostat in a three-electrode single-compartment cell with a platinum working electrode, a platinum wire counter electrode, and an Ag/AgCl reference electrode. In CV-measurements, all potentials were internally referenced to the ferrocene/ ferrocenium couple (Fc/Fc^+). Melting points were determined using Büchi B-545 apparatus. CD spectra were recorded on a JASCO J 600 spectropolarimeter. The transmission electron microscopy (TEM) images were carried out with a Jeol 1400 Transmissions-Elektronenmikroskop. The atomic force microscopy (AFM) was performed with a Nanoscope IIIa (Veeco Instruments Inc.) using standard silicon-cantilevers (spring constant: 50 N/m, frequency: 300 kHz) in tapping mode. Height, phase, and amplitude images were recorded simultaneously. The samples were drop-casted on freshly cleaved highly pyrolytic graphite (HOPG) substrates.

Chemicals:

N-Bromosuccinimide, magnesium turnings, mercury acetate, sodium azide, sodium bicarbonate, sodium hydride (60% suspension in paraffin oil), potassium carbonate, potassium fluoride, tetrabutylammonium fluoride, trimethylsilylacetylene, copper powder, bromine, iodine, phosphorylchloride, malonodinitrile, ammonium acetate, glacial acetic acid, ethylene diamine tetraacetic acid, triethylamine, diisopropylamine, diethyl ether, tetrahydrofuran, N,N-dimethylformamide, 1,2-dichloroethane, dichloromethane, and methanol were purchased from Merck. Trimethyltin chloride, 1-bromohexane, 1-bromo-2-ethylhexane, titanium isopropoxide, dimethyl(2-oxopropyl)-phosphonate, dichloro(1,3-bis(diphenylphosphino)propane)nickel, tetrakis (acetonitrile)-copper(I) hexafluorophosphate, and *N*-Boc–cis-4-azido-L-proline (dicyclohexylammonium) salt were purchased from Sigma Aldrich. *n*-Butyl lithium (1.6 M in *n*-hexane) was purchased from Acros Organics. Toluene and mesyl chloride were purchased from VWR. *N,O*-Dimethylhydroxylamide hydrochloride was purchased from Alfa Aesar. All reactions were performed using dried glassware under argon and were followed by thin layer chromatography (TLC) using aluminium plates, pre-coated with silica gel 60 F_{254} (Merck). Preparative flash column chromatography was performed using glass columns packed with silica gel 60 (particle size 0.040-0.063 mm Merck). All solvents were distilled prior to use.

3,3'''-Dihexyl-2,2';5',2'';5'',2'''-quaterthiophene-5-carbaldehyde 3.17[1,2]

Phosphorylchloride (0.460 g, 3 mmol) was added dropwise to a solution of 0.230 mL of dry DMF (3 mmol) in 3.3 mL of dry DCE. The resulting mixture was stirred at room temperature for 2 h. Afterwards, the Vilsmeier reagent was added dropwise to a refluxing solution of 0.900 g of quaterthiophene **3.16** (1.80 mmol) in 7 mL of dry DCE. After stirring for 2.5 h, the dark red solution was quenched with 25 mL of a saturated $NaHCO_{3(aq)}$ solution. The organic layer was separated and the aqueous layer extracted with DCM four times. The combined organic layers were dried over Na_2SO_4, filtered and the solvent removed under vacuum. The crude product was purified by column chromatography (silica, eluent: DCM) to give quaterthiophene **3.17** as bright orange solid in 55% yield (0.522 g, 1 mmol).

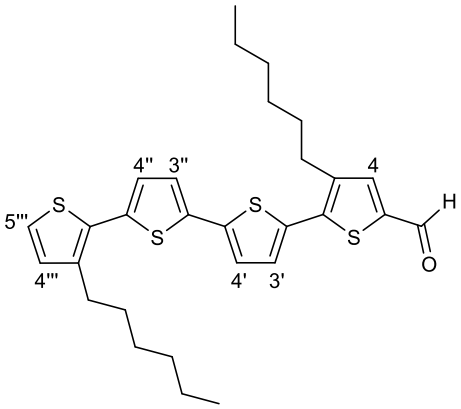

M. p. 53-55 °C (52-54 °C[1]);

^{1}H NMR (400 MHz, $CDCl_3$): δ 9.83 (s, 1H, *H*-aldehyde); 7.69 (s, 1H, *H*-4); 7.26-7.16 (m, 4H, *H*-4', *H*-3'', *H*-4''', *H*-5'''); 7.04 (d, *J* = 3.7 Hz, 1H, *H*-3'); 6.95 (d, *J* = 5.1 Hz, 1H, *H*-4''); 2.85-2.76 (m, 4H, Ar-CH_2); 1.70-1.63 (m, 4H, Ar-CH_2-CH_2); 1.40-1.31 (m, 12H, ArCH_2CH_2-CH_2-CH_2-CH_2); 0.90-0.89 (m, 6H, -CH_3) ppm;

MALDI-TOF MS (DCTB): *m/z* $[M+H]^+$ = 526.2.

3,3'''-Dihexyl-5-ethynyl-2,2';5',2'';5'',2'''-quaterthiophene 3.22[1,2]

Dimethyl(2-oxopropyl)phosphonate **3.21** (0.573 ml, 4.15 mmol) was added dropwise to a suspension of 0.275 g of sodium hydride (11.4 mmol) in 45 mL of dry THF at 0 °C. The resulting mixture was stirred at 0 °C for 1 h. Afterwards, 0.850 g of tosylazide (4.31 mmol) were added and the mixture was stirred for additional 10 min at 0 °C. The reaction mixture was quickly filtered through a short filtration column (silica, eluent: ethyl acetate) and the solvent was removed under reduced pressure. The resulting colourless oil was dissolved in 21 mL of dry THF and added to a suspension of 1.070 g of K_2CO_3 (7.7 mmol) and 0.225 g of the aldehyde **3.17** (0.43 mmol) in 24 mL of dry MeOH. The resulting yellow-orange mixture was stirred at room temperature for 24 h. After removal of the solvent, the residue was redissolved in DCM and washed with a saturated $NH_4Cl_{(aq)}$ solution. The organic layer was separated and the aqueous layer was repeatedly extracted with DCM. The combined organic layers were dried over Na_2SO_4 and the solvent removed under reduced pressure. The crude product was purified by column chromatography (silica, eluent: *n*-hexane) to give quaterthiophene **3.22** as brown oil in 92% yield (0.207 g, 0.4 mmol).

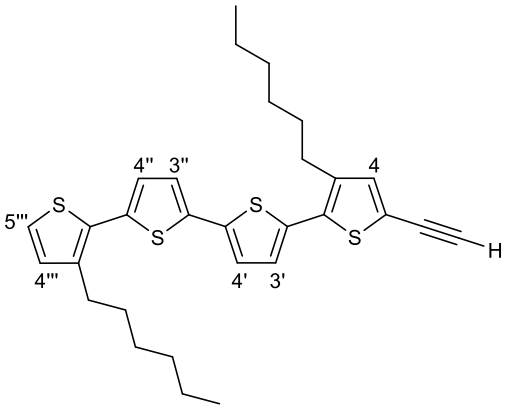

^{1}H NMR (400 MHz, $CDCl_3$): δ 7.18 (d, *J* = 5.2 Hz, 1H, *H*-4); 7.15-7.10 (m, 3H, *H*-4''', *H*-4', *H*-3'); 7.04 (d, *J* = 3.6 Hz, 1H, *H*-5'''); 7.03 (dd, *J* = 5.5, 3.8 Hz, 1H, *H*-3''); 6.94 (d, *J* = 5.2 Hz, 1H, *H*-4''); 3.38 (s, 1H, *H*-alkyne); 2.82-2.70 (m, 4H, *H*-8); 1.70-1.63 (m, 4H, *H*-9); 1.42-1.28 (m, 12H, *H*-10, *H*-11, *H*-12); 0.89 (m, 6H, *H*-13) ppm;

MALDI-TOF MS (DCTB): *m/z* $[M+H]^+$ = 522.3.

(4*S*)-1-*Tert*-butoxycarbonyl-[(3,3'''-dihexyl-2,2';5',2'';5'',2'''-quaterthien-5-yl)-1*H*-1,2,3-triazol-1yl]-L-proline 3.2

N-Boc–cis-4-azido-L-proline dicyclohexylammonium salt (0.117 g, 0.27 mmol), 0.002 g of copper powder (0.026 mmol) and 0.060 g of tetrakis(acetonitrile) copper(I) hexafluorophosphate (0.16 mmol) were added under argon to a solution of 0.070 g (0.13 mmol) of 3,3'''-dihexyl-5-ethynyl-2,2';5',2'';5'',2'''-quaterthiophene **3.22** in 2 mL of DCM. The reaction was stirred at room temperature for 16 h. The reaction mixture was washed several times with a saturated $EDTA_{(aq)}$ solution. The aqueous layers were repeatedly extracted with DCM. The organic layers were combined and the solvent was removed. The crude product was suspended in dry *n*-hexane and filtered off to give quaterthiophene-proline hybrid **3.2** as brown solid in 95% yield (0.103 g, 0.13 mmol).

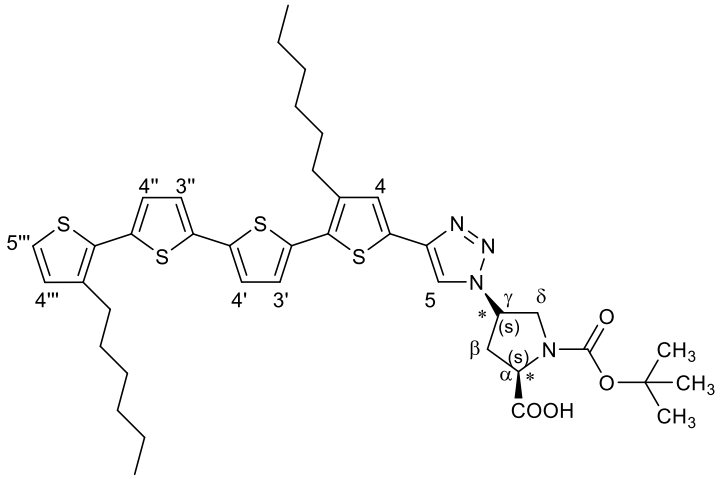

M. p. 158-226 °C (decomposition);

^{1}H-NMR (500 MHz, $CDCl_3$): δ 7.99 (s, 1H, *H*-5 triazole); 7.75-7.71 (d, J = 3.6 Hz, 1H, *H*-4); 7.23 (d, J = 3.6 Hz, 1H, *H*-4); 7.18-7.10 (m, 4H, *H*-4', *H*-3', *H*-4''', *H*-5'''); 7.01 (d, J = 3.6 Hz, 1H, *H*-3''); 6.72 (d, J = 3.6 Hz, 1H, *H*-4''); 5.12 (bs, 1H, *H*-γ); 4.34 (bs, 1H, *H*-δ); 4.19 (bs, 1H, *H*-δ); 3.79 (bs, 1H, *H*-β); 3.51 (bs, 1H, *H*-β); 3.29-3.15 (bs, 1H, *H*-carboxylic acid); 3.01 (m, 2H, Ar-CH_2); 2.93 (bs, 1H, *H*-α); 2.70 (d, *J* = 6.7 Hz, 2H, $ArCH_2$-CH_2); 2.58 (bs, 1H, *H*-α); 2.12 (m, 3H, Boc-CH_3), 1.98 (m, 3H, Boc-CH_3), 1.80 (m, 3H, Boc-CH_3); 1.60 (m, 4H, $ArCH_2$-CH_2); 1.35-1.21 (m, 12H, $ArCH_2CH_2$-CH_2-CH_2-CH_2); 0.89 (m, 6H, -CH_3) ppm;

^{13}C-NMR (126 MHz, $CDCl_3$): δ 140.4, 139.9, 137.0, 136.6, 135.5, 134.7, 130.2, 130.1, 129.5, 129.4, 127.5, 126.6, 126.5, 123.9, 123.9, 123.9, 53.8, 49.3, 49.2, 49.0, 31.6, 30.9, 30.8, 30.6, 30.4, 29.4, 29.3, 29.2, 29.1, 28.2, 28.1, 24.8, 24.5, 22.6 ppm;

HRMS (MALDI, (DCTB)): *m/z* $[M+H]^+$ calc. for $C_{40}H_{50}N_4O_4S_4$: 778.2715; found : 778.2703; δm/m = 1.5 ppm.

5'-Propyl-2,2'-bithiophene 3.27

A mixture of 2.750 g of (5-propylthien-2-yl)trimethyl stannane **3.25** (9.5 mmol), 2,000 g of 2-iodothiophene **3.26** (7.9 mmol) and 0.045 g of tetrakis(triphenylphosphine) palladium (0.04 mmol) in 50 mL dry DMF was heated up to 100 °C. The reaction mixture was stirred for one hour under argon. After cooling down the mixture to room temperature, the solvent was removed under reduced pressure. Subsequently, the crude residue was redissolved in DCM, and the organic phase was washed with water. The phases were separated, and the aqueous layer was further extracted with DCM (2 x 10 mL). The organic layers were combined and washed with 2% sodium hydroxide aqueous solution, brine, and water, and dried over $MgSO_4$. After removal of solvent, the crude product was purified by HPLC (eluent: *n*-hexane) to give 5'-propyl-2,2'-bithiophene **3.27** as colorless liquid in 86% yield (0.763 g, 2.05 mmol).

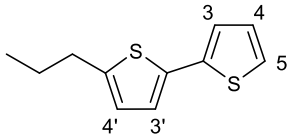

^{1}H NMR (400 MHz, $CDCl_3$) δ 7.45-7.41 (m, 2H, *H*-5, *H*-3); 7.39 (d, *J* = 2.4 Hz, 1H, *H*-4); 7.28 (d, *J* = 3.4 Hz, 1H, *H*-3'); 6.97 (d, *J* = 3.3 Hz, 1H, *H*-4'); 3.06 (t, *J* = 7.4 Hz, 2H, Ar-CH_2); 2.07-1.94 (m, 2H, $ArCH_2$-CH_2); 1.29 (t, *J* = 7.3 Hz, 3H, CH_3) ppm;

MS (EI): *m/z* = 208 $[M]^+$, 194 $[M\text{-}CH_2]^+$, 148 $[M\text{-}S(CH_2)_2]^+$.

[5'-Propyl(2,2'-bithien)-5-yl]trimethyl-stannane 3.28

A solution of *n*-butyl lithium in *n*-hexane 1.6 M (4.3 mL, 6.9 mmol) was added drop-wise to a solution of 1.300 g of 5'-propyl-2,2'-bithiophene **3.27** (6.3 mmol) in 20 mL of dry THF at -78 °C, under argon. The reaction was stirred for 1 h at -78 °C; therefore, 1.500 g of Me_3SnCl (7.5 mmol) were added and the reaction was stirred at room temperature overnight. After the removal of solvent, the residue was redissolved in DCM and washed with water several times. The organic layer was separated and dried over Na_2SO_4, and the solvent removed under reduced pressure to give without further purification [5'-propyl(2,2'-bithien)-5-yl]trimethyl-stannane **3.28** as yellow oil in 91% yield (1.760 g, 4.7 mmol).

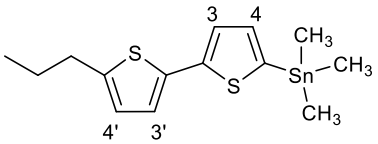

^{1}H NMR (400 MHz, $CDCl_3$): δ 7.23 (d, *J* = 3.3, Hz, 1H, *H*-4); 7.09 (d, *J* = 3.3, Hz, 1H, *H*-3); 6.99 (d, *J* = 3.6 Hz, 1H, *H*-3'); 6.69 (d, *J* = 3.6 Hz, 1H, *H*-4'); 2.78 (t, *J* = 7.4 Hz, 2H, Ar-CH_2); 1.78-1.68 (m, 2H, $ArCH_2$-CH_2); 1.01 (t, *J* = 7.3 Hz, 3H, -CH_3); 0.47-0.32 (m, 9H, Sn-CH_3) ppm;

MS (EI): *m/z* = 372 $[M]^+$, 372 $[M-(CH_3)_3]^+$, 224 $[M-Sn(CH_3)_2]^+$, 195 $[M-Sn(CH_3)_3CH_2]^+$, 162 $[M-Sn(CH_3)_3CH_2SH]^+$.

5'''-Propyl-2,2';5',2'';5'',2'''-quaterthiophene 3.30

A mixture of 0.912 g of [5'-propyl(2,2'-bithien)-5-yl]trimethyl-stannane **3.28** (2.5 mmol), 0.482 g of 5-bromo-2,2'-bithiophene **3.29** (1.97 mmol), and 0.012 g of tetrakis(triphenylphosphine) palladium (0.010 mmol) in 20 mL dry DMF was de-gassed for 20 min and heated up to 100 °C. The reaction mixture was stirred for one hour under argon. After cooling down the mixture to room temperature, the solvent was removed under reduced pressure. Subsequently, the crude residue was redis-solved in DCM and the organic phase was washed with water. The phases were separated and the aqueous layer was further extracted with DCM (4 x 10 mL). The

organic layers were combined and washed with 2% $NaOH_{(aq)}$ solution, brine, and water, and dried over $MgSO_4$. After removal of solvent, the crude product was purified by column chromatography (silica, eluent: DCM/*n*-hexane, 1:1) to give quaterthiophene **3.30** as golden solid in 83% yield (0.763 g, 2.05 mmol).

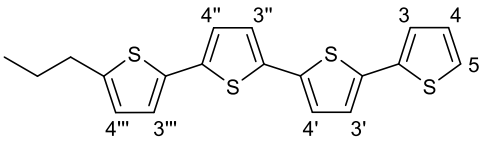

M. p. 158.4-161.9 °C;

^{1}H NMR (400 MHz, $CDCl_3$): δ 7.22 (dd, J = 5.1, 1.1 Hz, 1H, *H*-5); 7.17 (dd, J = 3.6, 1.1 Hz, 1H, *H*-3); 7.08 (d, *J* = 3.8 Hz, 1H, *H*-3'); 7.05 (dd, J = 3.8, 1.0 Hz, 2H, *H*-4'', *H*-3''); 7.03 (dd, J = 5.1, 3.6 Hz, 1H, *H*-4); 6.99 (m, 2H, *H*-4', *H*-3'''); 6.69 (dd, J = 3.5, 0.8 Hz, 1H, *H*-4'''); 2.78 (t, J = 7.5 Hz, 2H, Ar-CH_2), 1.77-1.66 (m, 2H, $ArCH_2$-CH_2); 0.99 (td, J = 7.3, 2.7 Hz, 3H, -CH_3) ppm;

^{13}C NMR (101 MHz, $CDCl_3$): δ 145.4, 137.1, 136.9, 136.1, 136.1, 135.1, 134.4, 127.9, 125.0, 124.5, 124.3, 124.2, 124.0, 123.7, 123.6, 123.5, 32.2, 30.9, 24.8 ppm;

HRMS (MALDI, (DCTB)): *m/z* $[M+H]^+$ calc. for $C_{19}H_{16}S_4$: 372.0135; found : 372.0132; δ m/m = 0.8 ppm.

5'''-Propyl-2,2';5',2'';5'',2'''-quaterthiophene-5-carbaldehyde 3.31

20 Equivalents of phosphorylchloride (3.280 g, 21.39 mmol) was added dropwise to a solution of 1.66 mL of dry DMF (21.47 mmol) in 12 mL of dry DCE. The resulting mixture was stirred at room temperature for 2 h. Afterwards, the Vilsmeier reagent was added dropwise to a solution of 0.400 g of 5'''-propyl-2,2';5',2'';5'',2'''-quaterthiophene **3.30** (1.07 mmol) in 30 mL of dry DCE. The reaction mixture was stirred for 3 h under reflux before being quenched with 100 mL of a saturated $NaHCO_{3(aq)}$ solution. The mixture was stirred for additional two days at room temperature. The organic layer was separated and the aqueous layer extracted three times with DCM. The combined organic layers were dried over Na_2SO_4. After removal of solvent, the crude

product was purified by column chromatography (silica, eluent: DCM/*n*-hexane, 1:1) to give 5'''-propyl-2,2';5',2'';5'',2'''-quaterthiophene-5-carbaldehyde **3.31** as orange solid in 90% yield (0.390 g, 0.97 mmol).

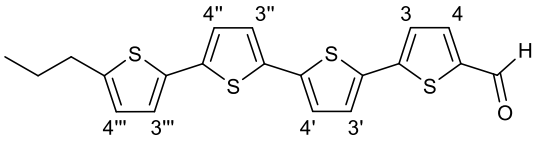

M. p. 206-209 °C;

^{1}H NMR (500 MHz, THF-d_8): δ 9.85 (s, 1H, *H*-aldehyde); 7.67 (d, *J* = 4.0 Hz, 1H, *H*-4); 7.27 (d, *J* = 3.9 Hz, 1H, *H*-3'); 7.23 (d, *J* = 4.0 Hz, 1H, *H*-3); 7.11 (dd, *J* = 3.8, 2.7 Hz, 2H, *H*-4', *H*-3''); 7.01 (t, *J* = 3.8 Hz, 2H, *H*-4'', *H*-3'''); 6.70 (d, *J* = 3.6 Hz, 1H, *H*-4'''); 2.78 (t, J = 7.3 Hz, 2H, Ar-CH_2), 1.77-1.66 (m, 2H, ArCH$_2$-CH_2); 1.00 (t, J = 7.3 Hz, 3H, -CH_3) ppm;

^{13}C NMR (126 MHz, THF-d_8): δ 182.6, 146.6, 143.6, 139.7, 139.0, 137.9, 135.7, 135.6, 135.3, 128.0, 126.2, 125.6, 125.3, 124.8, 124.8, 68.1, 33.0, 30.5, 25.9 ppm;

HRMS (MALDI, (DCTB)): *m/z* $[M+H]^+$ calc. for $C_{20}H_{16}OS_4$: 400.0084; found : 400.0079; δm/m = 1.2 ppm.

5-Ethynyl-5'''-propyl-2,2';5',2'';5'',2'''-quaterthiophene 3.32

Dimethyl(2-oxopropyl)phosphonate **3.21** (1 mL, 7.19 mmol) was added dropwise to a suspension of 0.196 g of sodium hydride (8.16 mmol) in 45 mL of dry THF at 0 °C. The resulting mixture was stirred at 0 °C for 1 h. Afterwards, 1.418 g tosylazide (7.19 mmol) were added and the mixture was stirred for additional 40 min at 5 °C. The reaction mixture was quickly filtered through a short filtration column (silica, eluent: ethyl acetate) and the solvent was removed under reduced pressure. The resulting colourless oil was dissolved in 45 mL of dry THF and added to a suspension of 2.920 g of K_2CO_3 (21.12 mmol) and 0.288 g of the aldehyde **3.31** (0.72 mmol) in 24 mL of dry MeOH. The resulting mixture was stirred at room temperature for four days. After

the removal of solvent under vacuum, the residue was redissolved in DCM and washed three times with a saturated $NH_4Cl_{(aq)}$ solution. The organic layer was separated and the aqueous layer was repeatedly extracted with DCM. The combined organic layers were dried over Na_2SO_4 and the solvent removed under reduced pressure. The crude product was purified by column chromatography (silica, eluent: DCM/*n*-hexane, 1:1) to give 5-ethynyl-5'''-propyl-2,2';5',2'';5'',2'''-quaterthiophene **3.32** as brown solid in 74% yield (0.210 g, 0.53 mmol).

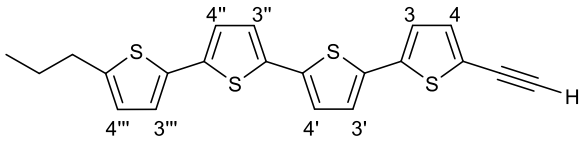

M. p. 190-194 °C;

^{1}H NMR (500 MHz, $CDCl_3$): δ 7.18 (d, *J* = 3.6 Hz, 1H, *H*-4); 7.09 (d, *J* = 3.6 Hz, 1H, *H*-3); 7.06 (d, *J* = 3.9 Hz, 2H, *H*-3', *H*-4'); 7.01 (d, *J* = 4.0 Hz, 2H, *H*-3'', *H*-4''); 6.99 (d, *J* = 3.5 Hz, 1H, *H*-3'''); 6.69 (d, *J* = 3.3 Hz, 1H, *H*-4'''); 5.4 (s, 1H, *H*-alkyne); 2.78 (t, J = 7.5 Hz, 2H, Ar-CH_2), 1.71-1.63 (m, 2H, ArCH_2-CH_2); 1.00 (t, J = 7.3 Hz, 3H, -CH_3) ppm;

^{13}C NMR (126 MHz, THF-d_8): δ 146.4, 139.5, 138.4, 138.0, 135.9, 135.8, 135.4, 134.9, 126.3, 126.2, 125.7, 125.3, 124.7, 124.6, 124.4, 122.2, 84.6, 77.2, 33.0, 30.4, 28.2 ppm;

HRMS (MALDI, (DCTB)): *m/z* $[M+H]^+$ calc. for $C_{21}H_{16}S_4$: 396.0135; found : 396.0130; δm/m = 1.2 ppm.

(4*S*)-1-*Tert*-butoxycarbonyl-[(5'''-propyl-2,2';5',2'';5'',2'''-quaterthien-5-yl)-1*H*-1,2,3-triazol-1yl]-L-proline 3.3

N-Boc–cis-4-azido-L-proline dicyclohexylammonium salt (0.175 g, 0.40 mmol), 0.001 g of copper powder (0.020 mmol) and 0.044 g of tetrakis(acetonitrile) copper(I) hexafluorophosphate (0.12 mmol) were added under argon to a solution of 0.040 g (0.10 mmol) of 5-ethynyl-5'''-propyl-2,2';5',2'';5'',2'''-quaterthiophene **3.32** in a mixture of 2

mL of DCM and 2 mL of THF. The reaction was stirred at room temperature for 16 h. The reaction mixture was washed several times with a saturated $EDTA_{(aq)}$ solution. The aqueous layers were repeatedly extracted with DCM. The organic layers were combined and the solvent was removed. The crude product was suspended in dry *n*-hexane and filtered off to give quaterthiophene-proline hybrid **3.3** as a brown solid in 95% yield (0.103 g, 0.13 mmol).

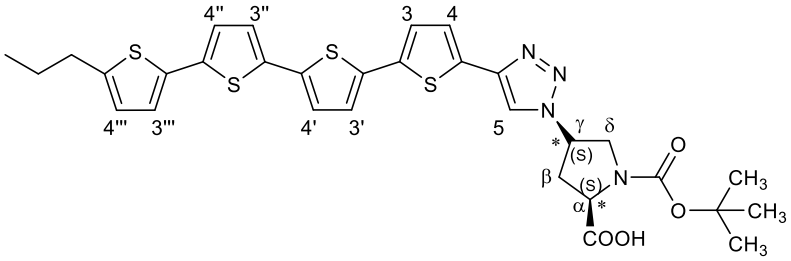

M. p. 301 °C (decomposition);

Recording ^{1}H NMR, ^{13}C NMR was not possible due to low solubility;

HRMS (MALDI, (DCTB)): *m/z* $[M+H]^+$ calc. for $C_{40}H_{50}N_4O_4S_4$: 652.1306; found : 652.1296; Δ m/m = 1.5 ppm.

(5-Ethylhexylthien-2-yl)trimethyl stannane 3.35

A solution of *n*-butyl lithium in *n*-hexane 2.5 M (6.7 mL, 16.8 mmol) was added drop-wise to a solution of 3.000 g of 2-(2-ethylhexyl)-thiophene (15.3 mmol) in 50 mL of THF at -78 °C, under argon. The reaction was stirred for 10 min at -78 °C and for 1 h at 0 °C. After cooling down the reaction to -78 °C, 3.400 g of Me_3SnCl (16.8 mmol) were added. The reaction was stirred for 1 h at -78 °C and for 20 h at room temperature. Subsequently, the reaction was quenched and the solvent evaporated. The residue was dissolved in chloroform and washed with water. The organic phase was dried over $MgSO_4$ and the solvent removed under reduced pressure to give (5-ethylhexylthien-2-yl)trimethyl stannane **3.35** without further purification as light yellow liquid in 90% yield (4.900 g, 13.7 mmol).

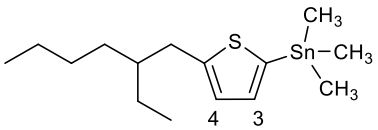

^{1}H NMR (400 MHz, $CDCl_3$): δ 7.08 (d, *J* = 3.2 Hz, 1H, *H*-4), 6.96 (d, *J* = 3.2 Hz, 1H, *H*-3), 2.73 (d, *J* = 6.8 Hz, 2H, $ArCH_2CHCH_2$-C*H*$_2$), 1.37–1.28 (m, 9H, $ArCH_2$-C*H*-C*H*$_2$-C*H*$_2$-C*H*$_2$, $ArCH_2CH$-(C*H*$_2$)), 0.90 (d, *J* = 14.8 Hz, 6H, ArC_5H_9-C*H*$_3$, $ArCH_2CH(CH_2$-C*H*$_3$)) ppm;

MS (EI): *m/z* = 359 $[M]^+$, 344 $[M-(CH_3)]^+$, 314 $[M-(CH_3)_3]^+$, 181 $[M-Sn(CH_3)_3]^+$.

5’’-(2-Ethylhexyl)-2,2';5',2''-terthiophene 3.39[3]

A mixture of 0.242 g of 5-iodo-2,2´-bithiophene **3.37** (0.83 mmol), 0.357 g of (5-ethylhexylthien-2-yl)trimethyl stannane **3.35** (0.99 mmol), and 0.004 g of tetrakis(triphenylphosphine) palladium (4 µmol) in 10 mL dry DMF was heated up to 100 °C and was stirred for 24 hours under argon. After cooling down the mixture to room temperature, the solvent was removed in vacuum. Subsequently, the crude residue was directly purified by column chromatography (silica, eluent: petrol ether) to give 5’’-(2-Ethylhexyl)-2,2';5',2''-terthiophene **3.39** as yellowish solid in 49% yield (0.146 g, 0.40 mmol).

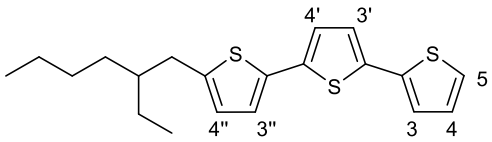

^{1}H NMR (400 MHz, $CDCl_3$): δ 7.21 (dd, *J* = 5.1 Hz, 1H, *H*-4), 7.16 (dd, *J* = 3.6 Hz, 1H, *H*-3’) 7.06 (d, *J* = 3.7 Hz, 1H, *H*-4’), 7.03-6.98 (m, 3H, *H*-5, *H*-3, *H*-3’’), 6.67 (d, *J* = 3.5 Hz, 1H, *H*-4’’), 2.73 (d, *J* = 6.8 Hz, 2H, $ArCH_2CHCH_2$-C*H*$_2$), 1.40-1.28 (m, 9H, $ArCH_2$-C*H*-C*H*$_2$-CH_2-C*H*$_2$, $ArCH_2CH$-(C*H*$_2$)), 0.91 (d, *J* = 7.4 Hz, 6H, ArC_5H_9-C*H*$_3$, $ArCH_2CH(CH_2$-C*H*$_3$)) ppm.

5-Bromo-5''-(2-ethylhexyl)-2,2';5',2''-terthiophene 3.40

A solution of 0.123 g of NBS (0.69 mmol) in 8 mL DMF was added dropwise to a solution of 0.250 g of terthiophene **3.39** (0.69 mmol) in 6 mL dry DMF at 0 °C under argon. The mixture was stirred at room temperature for 24 h. After the removal of solvent, the residue was redissolved in DCM, and washed with a saturated solution of sodium bisulfite, and several times with water. The organic layer was separated and dried over Na_2SO_4, and the solvent removed under reduced pressure. The crude residue was purified by column chromatography (silica, eluent: petrol ether) and the solvent was evaporated under vacuum to give 5-bromo-5''-(2-ethylhexyl)-2,2';5',2''-terthiophene **3.40** as yellow solid in 85% yield (0.258 g, 0.59 mmol).

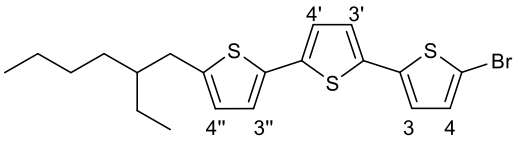

M. p. 84-85.9 °C

^{1}H NMR (400 MHz, $CDCl_3$): δ 6.97 (m, 4H, *H*-3, *H*-4', *H*-3, *H*-3'), 6.89 (d, *J* = 3.8 Hz, 1H, *H*-3''), 6.66 (d, *J* = 3.6 Hz, 1H, *H*-4''), 2.73 (d, *J* = 6.8 Hz, 2H, $ArCH_2CHCH_2$-CH_2), 1.37-1.28 (m, 9H, $ArCH_2$-C*H*-CH_2-CH_2-CH_2, $ArCH_2CH$-(CH_2)), 0.90 (d, *J* = 14.8 Hz, 6H, ArC_5H_9-CH_3, $ArCH_2CH(CH_2$-CH_3) ppm;

^{13}C NMR (101 MHz, $CDCl_3$): δ 144.3, 138.6, 137.2, 134.2, 134.1, 130.4, 125.8, 124.3, 123.3, 123.3, 123.3, 110.6, 41.2, 34.0, 32.2, 30.7, 28.7, 25.3, 22.8, 10.6 ppm;

MS (CI) *m/z* = 440 $[M]^+$, 359 $[M\text{-}Br]^+$, 344 $[M\text{-}BrCH_3]^+$, 216 $[M\text{-}SBrC_8H_{17}]^+$.

5'''-(2-Ethylhexyl)-2,2';5',2'';5'',2'''-quaterthiophene 3.42

A mixture of 0.570 g of 5-bromo-5''-(2-ethylhexyl)-2,2';5',2''-terthiophene **3.40** (1.1 mmol), 0.191 g of trimethylstannylthiophene **3.41** (0.91 mmol), and 0.004 g of tetrakis(triphenylphosphine) palladium (4 µmol) in 15 mL dry DMF was degassed for 20 min and heated up to 100 °C. The reaction mixture was stirred for 24 hours under

argon. After cooling down the reaction mixture to room temperature, the solvent was removed under reduced pressure. Subsequently, the crude residue was directly purified by column chromatography (silica, eluent: *n*-hexane) to give 5'''-(2-ethylhexyl)-2,2';5',2'';5'',2'''-quaterthiophene **3.42** as yellowish solid in 71% yield (0.343 g, 0.77 mmol).

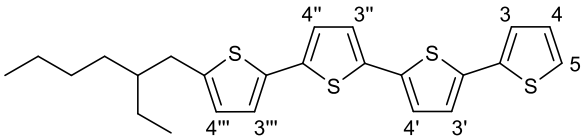

M. p. 128.3-130.1 °C;

^{1}H NMR (400 MHz, $CDCl_3$): δ 7.23 (dd, *J* = 5.1, 1.1 Hz, 1H, *H*-5), 7.18 (dd, *J* = 3.6, 1.1 Hz, 1H, *H*-3), 7.09 (d, *J* = 3.8 Hz, 1H, *H*-3'), 7.06 (d, *J* = 4.7 Hz, 2H, *H*-3'', *H*-4'), 7.03 (dd, *J* = 5.1, 3.6 Hz, 1H, *H*-4), 7.00 (dd, *J* = 5.3, 3.7 Hz, 2H, *H*-4'', *H*-3'''), 6.68 (d, *J* = 3.6 Hz, 1H, *H*-4'''), 2.74 (d, *J* = 6.7 Hz, 2H, $ArCH_2CHCH_2$-CH_2), 1.41-1.27 (m, 9H, $ArCH_2$-C*H*-CH_2-CH_2-CH_2, $ArCH_2CH$-(CH_2)), 0.91 (t, *J* = 7.4 Hz, 6H, ArC_5H_9-CH_3, $ArCH_2CH(CH_2$-CH_3)) ppm;

^{13}C NMR (101 MHz, $CDCl_3$): δ 144.3, 137.1, 137.0, 136.1, 135.1, 134.6, 127.9, 125.9, 124.5, 124.4, 124.2, 124.0, 123.7, 123.5, 123.4, 76.7, 41.4, 34.1, 32.3, 30.9, 28.8, 25.5, 23.0, 10.8. ppm;

HRMS (MALDI, (DCTB)): *m/z* $[M+H]^+$ calc. for $C_{24}H_{26}S_4$: 442.0917; found : 442.0913; δm/m = 0.9 ppm.

5-Bromo-5'''-(2-ethylhexyl)-2,2';5',2'';5'',2'''-quaterthiophene 3.43

A solution of 0.138 g of NBS (0.77 mmol) in 5 mL DMF was added dropwise to a solution of 0.343 g of 5'''-(2-ethylhexyl)-2,2';5',2'';5'',2'''-quaterthiophene **3.42** (0.77 mmol) in 15 mL dry chloroform at 0 °C, under argon. The mixture was stirred at rt for 24 h. After removing the solvent, the residue was redissolved in DCM and washed with a saturated solution of sodium bisulfite and several times with water.

The organic layer was separated and dried over Na_2SO_4 and the solvent removed under reduced pressure. The crude residue was purified by column chromatography (silica, eluent: *n*-hexane) to give 5-bromo-5'''-(2-ethylhexyl)-2,2';5',2'';5'',2'''-quaterthiophene **3.43** as yellow solid in 92% yield (0.371 g, 0.71 mmol).

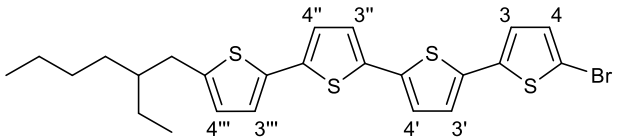

M. p. 169.8-175.2 °C;

^{1}H NMR (400 MHz, THF-d_8): δ 7.16-7.12 (m, 3H, *H*-4, *H*-3, *H*-3'), 7.08-7.06 (m, 2H, *H*-4', *H*-3''), 7.04 (t, *J* = 3.7 Hz, 2H, *H*-4'', *H*-3'''), 6.72 (d, *J* = 3.6 Hz, 1H, *H*-4'''), 2.77 (d, *J* = 6.8 Hz, 2H, $ArCH_2CHCH_2$-CH_2), 1.34 (m, 9H, $ArCH_2$-C*H*-CH_2-CH_2-CH_2, $ArCH_2CH$-(CH_2)), 0.91 (m, 6H, ArC_5H_9-CH_3, $ArCH_2CH(CH_2$-CH_3)) ppm;

^{13}C NMR (101 MHz, $CDCl_3$): δ 144.4, 138.6, 137.2, 136.6, 134.8, 134.2, 130.7, 126.0, 124.6, 124.4, 124.0, 123.7, 123.5, 123.4, 110.8, 76.7, 41.4, 34.1, 32.3, 30.9, 28.8, 25.5, 23.0, 10.8 ppm;

HRMS (MALDI, (DCTB)): *m/z* $[M+H]^+$ calc. for $C_{24}H_{25}BrS_4$: 520.0022; found : 520.0016; δ m/m = 1.2 ppm.

5-([Trimethylsilyl]ethynyl)-5'''-(2-ethylhexyl)-2,2';5',2'';5'',2'''-quaterthiophene 3.45

Trimethylsilylacetylene **3.44** (0.48 mL, 3.35 mmol) was dropped into a solution of 0.351 g of 5-bromo-5'''-(2-ethylhexyl)-2,2';5',2'';5'',2'''-quaterthiophene **3.43** (0.67 mmol), 0.011 g of bis(triphenylphosphine)palladium(II) dichloride (0.016 mmol) and 6 mg of CuI (0.034 mmol) in a mixture of 10 mL dry THF and 5 mL triethylamine. The reaction mixture was stirred for 48 hours at 60 °C under argon. After cooling down the reaction to room temperature, the solvent was removed under reduced pressure. The crude residue was directly purified by column chromatography (silica,

eluent: *n*-hexane) to give 5-([trimethylsilyl]ethynyl)-5'''-(2-ethylhexyl)-2,2';5',2'';5'',2'''-quaterthiophene **3.45** as brownish solid in 75% yield (0.270 g, 0.50 mmol).

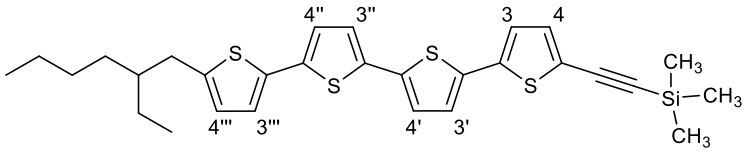

M. p. 136-139.4 °C;

^{1}H NMR (400 MHz, THF-d_8) δ 7.19 (d, J = 3.8 Hz, 1H, *H*-4), 7.16 (t, J = 3.7 Hz, 3H, *H*-3, *H*-3', H-4'), 7.12 (d, J = 3.8 Hz, 1H, *H*-3''), 7.07 (d, J = 3.8 Hz, 1H, *H*-4''), 7.05 (d, J = 3.6 Hz, 1H, *H*-3'''), 6.72 (d, J = 3.6 Hz, 1H, *H*-4'''), 2.77 (d, J = 6.8 Hz, 2H, $ArCH_2CHCH_2$-CH_2), 1.43-1.27 (m, 9H, $ArCH_2$-C*H*-CH_2-CH_2-CH_2, $ArCH_2CH$-(CH_2)), 0.91 (td, J = 7.3, 3.9 Hz, 6H, ArC_5H_9-CH_3, $ArCH_2CH(CH_2$-CH_3)), 0.25-0.22 (m, 9H, Si-CH_3) ppm;

^{13}C NMR (126 MHz, THF-d_8): δ 155.2, 145.0, 137.2, 136.6, 133.7, 126.1, 125.1, 124.6, 124.2, 123.5, 123.4, 123.3, 121.7, 98.4, 53.8, 41.4, 38.4, 33.7, 32.2, 29.4, 28.7, 25.4, 23.0, 13.3, 10.2, 1.2 ppm;

HRMS (MALDI, (DCTB)): *m/z* $[M+H]^+$ calc. for $C_{29}H_{34}S_4Si$: 538.1313; found : 538.1306; δ m/m = 1.3 ppm.

(4*S*)-1-*Tert*-butoxycarbonyl-{[5'''-(2-ethylhexyl)-2,2';5',2'';5'',2'''-quaterthien-5-yl]-1*H*-1,2,3-triazol-1-yl}-L-proline 3.4

Potassium fluoride (0.002 g , 0.040 mmol) was added to a solution of 0.020 g (0.037 mmol) of 5-([trimethylsilyl]ethynyl)-5'''-(2-ethylhexyl)-2,2';5',2'';5'',2'''-quaterthiophene **3.45**, 0.016 g of N-Boc–cis-4-azido-L-proline dicyclohexyl-ammonium salt (0.037 mmol), 0.001 g of copper powder (0.007 mmol) and 0.016 g of tetrakis(acetonitrile) copper(I) hexafluorophosphate (0.044 mmol) in 2 mL of DCM. The reaction was stirred at room temperature for four days. The reaction mixture was washed several times with a saturated $EDTA_{(aq)}$ solution. The organic layers were combined and dried over Na_2SO_4, and the solvent was removed under reduced pressure. The crude

product was suspended in dry methanol and filtered off to give quaterthiophene-proline hybrid **3.4** as a brown solid in 90% yield (0.024 g, 0.033 mmol).

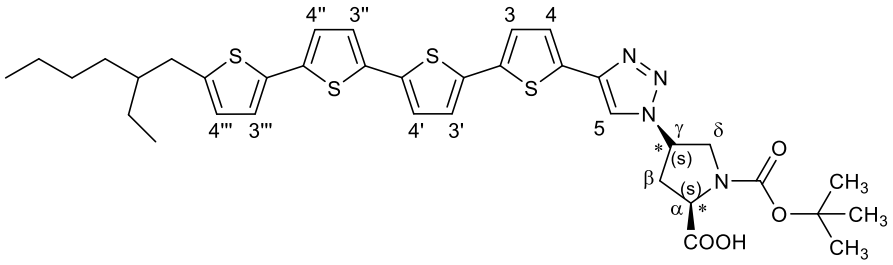

M. p. 180 °C (decomposition);

^{1}H NMR (400 MHz, THF-d_8): δ 8.29 (s, 1H, *H*-5 triazole), 7.29 (d, *J* = 3.7 Hz, 1H, *H*-4), 7.19 (dd, *J* = 3.7, 2.5 Hz, 2H, *H*-3, *H*-3'), 7.17-7.12 (m, 2H, *H*-4', *H*-3''), 7.07 (d, *J* = 3.8 Hz, 1H, *H*-4''), 7.05 (d, *J* = 3.5 Hz, 1H, *H*-3'''), 6.72 (d, *J* = 3.6 Hz, 1H, *H*-4'''), 5.22 (bs, 1H, *H*-γ), 4.36 (bs, 1H, *H*-δ), 4.15 (bs, 1H, *H*-δ), 3.82 (bs, 1H, *H*-β), 2.95 (bs, 1H, *H*-β), 2.77 (d, J = 6.8 Hz, 2H, $ArCH_2CHCH_2$-C*H*$_2$), 2.65 (bs, 1H, *H*-α) 1.49-1.40 (m, 9H, $ArCH_2$-C*H*-C*H*$_2$-CH_2-C*H*$_2$, $ArCH_2CH$-(C*H*$_2$)), 1.33-1.21 (m, 9H, Boc-C*H*$_3$), 0.91 (td, *J* = 7.4, 4.0 Hz, 6H, ArC_5H_9-C*H*$_3$, $ArCH_2CH(CH_2$-C*H*$_3$)) ppm;

^{13}C NMR (126 MHz, THF-d_8) δ 203.4, 185.1, 137.2, 136.7, 133.6, 126.1, 125.1, 124.6, 124.2, 123.5, 123.4, 123.3, 121.7, 53.8, 41.5, 33.8, 32.3, 29.3, 28.8, 25.4, 24.8, 24.0, 22.8, 13.4, 10.1, 6.0 ppm;

HRMS (MALDI, (DCTB)): *m/z* $[M+H]^+$ calc. for $C_{36}H_{42}N_4O_4S_4$: 722.2086; found : 722.2073; δ m/m = 1.8 ppm.

5'''-Hexyl-2,2';5',2'';5'',2'''-quaterthiophene 3.48[4,6]

A mixture of 0.335 g of 5-(trimethylstannyl)-5'-hexyl-2,2'-bithiophene **3.47** (0.8 mmol), 0.160 g of 5-bromo-2,2'-bithiophene **3.29** (0.65 mmol), and 0.004 g of tetrakis(triphenylphosphine) palladium (0.003 mmol) in 10 mL dry DMF was de-gassed for 30 min and heated up to 80 °C. The reaction mixture was stirred for 1 h under argon. After cooling down the mixture to room temperature, the solvent was

removed under reduced pressure. Subsequently, the crude residue was redissolved in DCM and the organic phase was washed with water. The phases were separated, and the aqueous layer was extracted with DCM (2 x 20 mL). The organic layers were combined and washed with 2% $NaOH_{(aq)}$ solution, brine, and water and dried over $MgSO_4$. After removal of solvent, the crude product was purified by column chromatography (silica, eluent: *n*-hexane) to give 5'''-hexyl-2,2';5',2'';5'',2'''-quaterthiophene **3.48** as yellow solid in 86% yield (0.232 g, 0.56 mmol).

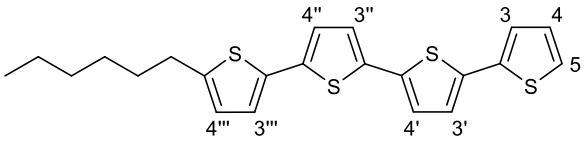

M. p. 182-185 °C (194 °C[4]);

^{1}H NMR (400 MHz, $CDCl_3$) δ 7.22 (dd, *J* = 5.1, 1.1 Hz, 1H, *H*-5); 7.17 (dd, *J* = 3.6, 1.1 Hz, 1H, *H*-3); 7.07 (d, *J* = 3.8 Hz, 1H, *H*-3'); 7.05 (d, *J* = 4.7 Hz, 1H, *H*-4''); 7.02 (dd, *J* = 5.1, 3.6 Hz, 2H, *H*-4, *H*-3'''); 6.99 (dd, *J* = 5.8, 3.8 Hz, 2H, *H*-3'', *H*-4'); 6.68 (d, *J* =3.6 Hz, 1H, *H*-4'''); 2.79 (t, *J* = 7.6 Hz, 2H, Ar-CH_2); 1.68 (m, 2H, $ArCH_2$-CH_2); 1.32 (m, 6H, $ArCH_2CH_2$-*C*H_2-*C*H_2-CH_2); 0.89 (t, *J* = 6.8 Hz, 3H, -CH_3) ppm;

MS (CI): *m/z* = 415 $[M]^+$, 344 $[M\text{-}C_5H_{11}]^+$, 222 $[M\text{-}SC_{12}H_{17}]^+$.

5'''-Hexyl-2,2';5',2'';5'',2'''-quaterthiophene-5-carbaldehyde 3.49[5,6]

For the generation of the Vilsmeier reagent, 0.86 mL dry DMF (11.2 mmol) were dissolved in 6 mL of dry DCE and 1.1 mL of phosphoryl chloride (11.7 mmol) were added dropwise. The resulting mixture was stirred for 2 h at room temperature. In a two-neck flask equipped with a reflux condenser 0.232 g of 5-hexyl-2,2':5',2'':5'',2'''-quaterthiophene **3.48** (0.56 mmol) were dissolved in 15 mL of dry DCE. The solution was warmed up to reflux and the Vilsmeier reagent was added dropwise. After refluxing for three hours, the mixture was allowed to cool down to room temperature before being quenched with 25 mL of saturated $NaHCO_{3(aq)}$ solution and stirred overnight. The layers were separated and the aqueous layer was extracted three times with DCM. The combined organic layers were washed with water and dried over $MgSO_4$.

The solvent was removed under reduced pressure. The crude product was purified by column chromatography (silica, eluent: DCM/*n*-hexane 1:1) to give 5'''-hexyl-2,2';5',2'';5'',2'''-quaterthiophene-5-carbaldehyde **3.49** as orange solid in 70% yield (0.170 mg, 0.38 mmol).

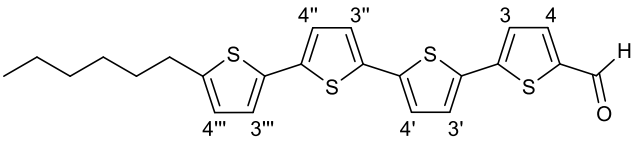

M. p. 169-170 °C (174 °C[5]);

^{1}H-NMR (400 MHz, $CDCl_3$): δ 9.86 (s, 1H, *H*-aldehyde); 7.67 (d, *J* = 4.0 Hz, 1H, *H*-4); 7.27 (d, *J* = 3.9 Hz, 1H, *H*-3); 7.23 (d, *J* = 4.0 Hz, 1H, *H*-3'); 7.07 (dd, *J* = 3.8, 2.7 Hz, 2H, *H*-4', *H*-3''); 7.01 (dd, *J* = 5.2, 3.8 Hz, 2H, *H*-4'', *H*-3'''); 6.70 (d, *J* = 3.8 Hz, 1H, *H*-4'''); 2.79 (t, *J* = 7.5 Hz, 2H, Ar-CH_2); 1.68 (m, 2H, $ArCH_2$-CH_2); 1.32 (m, 6H, $ArCH_2CH_2$-*C*H_2-*C*H_2-CH_2); 0.89 (t, *J* = 6.9 Hz, 3H, -CH_3) ppm;

MS (CI): *m/z* = 442 $[M]^+$, 113 $[M\text{-}S_2OC_{11}H_{17}]^+$.

5-Ethynyl-5'''-hexyl-2,2';5',2'';5'',2'''-quaterthiophene 3.50

A suspension of 0.060 g of NaH (2.5 mmol) in 15 mL of dry THF was cooled to 0 °C. Dimethyl(2-oxopropyl) phosphonate (2.5 mmol, 0.345 mL) was added dropwise to the solution. The resulting mixture was stirred at 0 °C for 1 h. Then, 0.493 g of tosyl-azide (2.5 mmol) were added and the mixture was stirred for another 10 min at 0 °C. The reaction mixture was quickly passed through a short filtration column (silica, eluent: ethyl acetate) and the solvent was removed under reduced pressure. The resulting colourless oil was dissolved in 16 mL of dry THF and was added to a previously prepared suspension of 0.585 g of K_2CO_3 (4.2 mmol) and 0.104 g 5'''-hexyl-2,2';5',2'';5'',2'''-quaterthiophene-5-carbaldehyde **3.49** (0.24 mmol) in 4 mL of dry MeOH. The resulting intensely yellow-orange mixture was allowed to stir at room temperature for 16 h under argon. The solvent was removed and the residue was re-dissolved in DCM. After washing the organic phase with a saturated solution of $NH_4Cl_{(aq)}$, the layers were separated and the aqueous phase was repeatedly extract-

ed with DCM. The combined organic layers were dried over Na_2SO_4 and the solvent was removed under reduced pressure at room temperature, due to the high sensitivity of the compound against oxygen. The crude product was purified by column chromatography (silica, eluent: *n*-hexane) to give 5-ethynyl-5'''-hexyl-2,2';5',2'';5'',2'''-quaterthiophene **3.50** as brown solid in 70% yield (0.072 g, 0.16 mmol).

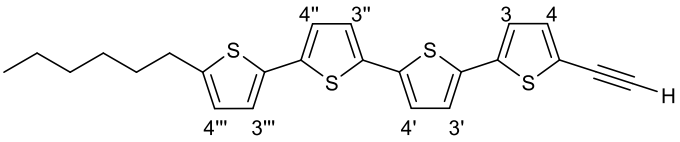

M. p. 165 °C (decomposition);

^{1}H-NMR (400 MHz, THF-d_8): δ 7.19 (d, *J* = 1.7 Hz, 1H, *H*-4); 7.18 (d, *J* = 1.7 Hz, 1H, *H*-3); 7.15 (d, *J* = 2.0 Hz, 1H, *H*-3'); 7.14 (d, *J* = 2.8 Hz, 1H, *H*-4'); 7.11 (d, *J* = 3.8 Hz, 1H, *H*-3''); 7.06 (d, *J* = 3.8 Hz, 1H, *H*-4''); 7.03 (d, *J* = 3.6 Hz, 1H, *H*-3'''); 6.71 (d, *J* = 3.6 Hz, 1H, *H*-4'''); 4.00 (s, 1H, *H*-alkyne); 2.79 (t, *J* = 7.5 Hz, 2H, Ar-CH_2); 1.67 (m, 2H, ArCH$_2$-CH_2); 1.34 (m, 6H, ArCH$_2$CH$_2$-*CH$_2$*-*CH$_2$*-CH_2); 0.89 (m, 3H, -CH_3) ppm;

^{13}C-NMR (101 MHz, THF-d_8): δ 146.3, 139.1, 137.9, 137.5, 135.6, 135.4, 135.0, 134.6, 125.0, 125.8, 125.4, 125.0, 124.3, 124.2, 124.0, 121.8, 84.3, 77.0, 32.4, 30.5, 30.4, 29.4, 23.3, 14.2 ppm;

MS (CI): *m/z* = 438 $[M]^+$, 369 $[M\text{-}C_5H_{11}]^+$.

(4S)-1-*Tert*-butoxycarbonyl-[(5'''-hexyl-2,2';5',2'';5'',2'''-quaterthien-5-yl)-1*H*-1,2,3-triazol-1yl]-L-proline 3.5

To a solution of 0.050 g (0.11 mmol) of 5-ethynyl-5'''-hexyl-2,2';5',2'';5'',2'''-quaterthiophene **3.50** in a mixture of 2 mL THF and 2 mL of DCM 0.060 g of the *N*-Boc–cis-4-azido-L-proline dicyclohexylammonium salt **3.23** (0.13 mmol), 0.002 g of copper powder (0.023 mmol) and 0.051 g of tetrakis(acetonitrile) copper(I) hexafluorophosphate (0.13 mmol) were added under argon. The reaction was stirred at room temperature for 16 h. The reaction mixture was washed several times with a saturat-

ed $EDTA_{(aq)}$ solution. The aqueous layers were repeatedly extracted with DCM. The organic layers were combined and the solvent was removed. The crude product was suspended in dry *n*-hexane and filtered off to give quaterthiophene-proline hybrid **3.5** as dark brown solid in 89% yield (0.071 mg, 0.1 mmol).

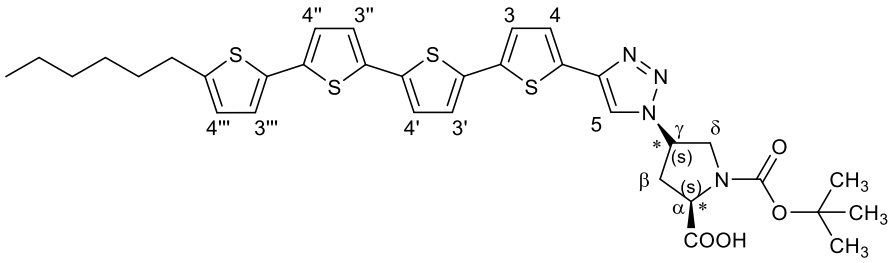

M. p. 282 °C (decomposition);

^{1}H-NMR (400 MHz, THF-d_8): δ 8.31 (s, 1H, *H*-5 triazole); 7.28 (d, *J* = 3.6 Hz, 1H, *H*-4); 7.18 (dd, *J* = 3.6, 2.4 Hz, 2H, *H*-3, *H*-3'); 7.14 (m, 2H, *H*-4', *H*-3''); 7.05 (d, *J* = 3.8 Hz, 1H, *H*-4''); 7.03 (d, *J* = 3.6 Hz, 1H, *H*-3'''); 6.72 (d, *J* = 3.6 Hz, 1H, *H*-4'''); 5.22 (bs, 1H, *H*-γ); 4.32 (bs, 1H, *H*-δ); 4.12 (bs, 1H, *H*-δ); 3.80 (bs, 1H, *H*-β); 3.51 (bs, 1H, *H*-α); 2.93 (bs, 1H, *H*-β); 2.80 (t, *J* = 7.5 Hz, 2H, Ar-CH_2); 2.52 (bs, 1H, *H*-carboxylic acid); 1.67 (m, 2H, $ArCH_2$-CH_2); 1.34 (m, 15H, $ArCH_2CH_2$-CH_2-CH_2-CH_2, Boc-CH_3); 0.89 (m, 3H, -CH_3) ppm;

HRMS (MALDI, (DCTB)): *m/z* $[M+H]^+$ calc. for $C_{34}H_{38}N_4O_4S_4$: 694.1776; found : 694.1762; δm/m = 2 ppm.

(4*R*)-1-*Tert*-butoxycarbonyl-[(5'''-hexyl-2,2';5',2'';5'',2'''-quaterthien-5-yl)-1*H*-1,2,3-triazol-1yl]-D-proline 3.6

To a solution of 0.050 g (0.11 mmol) of 5-ethynyl-5'''-hexyl-2,2';5',2'';5'',2'''-quaterthiophene **3.50** in a mixture of 2 mL THF and 2 mL of DCM 0.035 g of **3.51** (0.13 mmol), 0.002 g of copper powder (0.023 mmol) and 0.051 g of tetrakis(acetonitrile) copper(I) hexafluorophosphate (0.13 mmol) were added under argon. The reaction was stirred at room temperature for 16 h. The reaction mixture was washed several times with a saturated $EDTA_{(aq)}$ solution. The aqueous layers were repeatedly extracted with DCM. The organic layers were combined and the sol-

vent was removed. The crude product was suspended in dry *n*-hexane and filtered off to give quaterthiophene-proline hybrid **3.6** as brown solid in 90% yield (0.072 mg, 0.1 mmol).

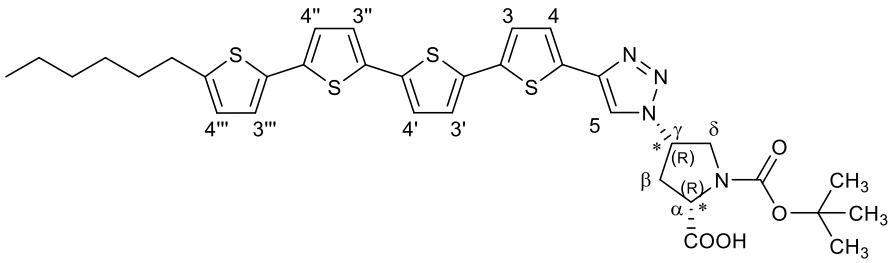

M. p. 295 °C (decomposition);

^{1}H-NMR (400 MHz, THF-d_8): δ 8.28 (s, 1H, *H*-5 triazole); 7.28 (d, *J* = 3.6 Hz, 1H, *H*-4); 7.18 (dd, *J* = 3.6, 2.7 Hz, 2H, *H*-3, *H*-3'); 7.14 (t, *J* = 4.0 Hz, 2H, *H*-4', *H*-3''); 7.05 (d, *J* = 3.7 Hz, 1H, *H*-4''); 7.03 (d, *J* = 3.5 Hz, 1H, *H*-3'''); 6.72 (d, *J* = 3.5 Hz, 1H, *H*-4'''); 5.22 (bs, 1H, *H*-γ); 4.37 (bs, 1H, *H*-δ); 4.13 (bs, 1H, *H*-δ); 3.81 (bs, 1H, *H*-β); 2.96 (bs, 1H, *H*-β); 2.80 (t, *J* = 7.5 Hz, 2H, Ar-CH_2); 2.63 (bs, 1H, *H*-α); 2.50 (bs, 1H, *H*-carboxylic acid); 1.68 (m, 2H, ArCH$_2$-CH_2); 1.37 (m, 15H, ArCH$_2$CH$_2$-*CH*$_2$-*CH*$_2$-CH_2, Boc-CH_3); 0.89 (m, 3H, -CH_3) ppm;

MS (MALDI-TOF, DCTB): *m/z* $[M+H]^+$ = 694.5 (calc. for $C_{34}H_{38}N_4O_4S_4$: 694.95).

(4*S*)-1-*Tert*-butoxycarbonyl-[(5'''-hexyl-2,2';5',2'';5'',2'''-quaterthien-5-yl)-1*H*-1,2,3-triazol-1yl]-L-proline methyl ester 3.7

To a solution of 0.045 g (0.10 mmol) of 5-ethynyl-5'''-hexyl-2,2';5',2'';5'',2'''-quaterthiophene **3.50** in a mixture of 2 mL THF and 2 mL of DCM, 0.035 g of **3.54** (0.12 mmol), 0.001 g of copper powder (0.02 mmol) and 0.044 g of tetrakis(acetonitrile) copper(I) hexafluorophosphate (0.12 mmol) were added under argon. The reaction was stirred at room temperature for 16 h. The reaction mixture was washed several times with a saturated $EDTA_{(aq)}$ solution. The organic layers were combined and the solvent was removed. The crude product was at first suspended in dry methanol and then in *n*-hexane and filtered off to give quaterthiophene-proline hybrid **3.7** as brown solid in 90% yield (0.064 mg, 0.09 mmol).

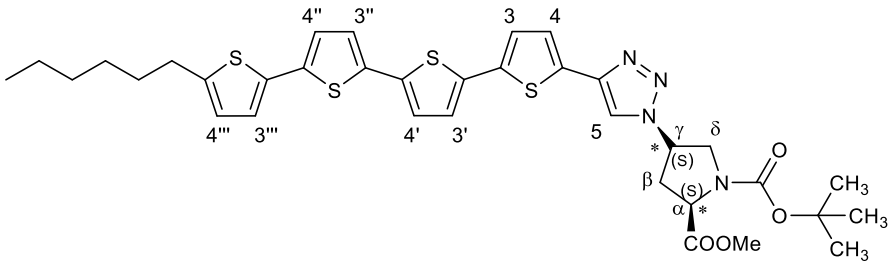

M. p. 200-201 °C;

^{1}H NMR (500 MHz, THF-d_8): δ 8.08 (s, *H*-5, triazole), 7.28 (d, *J* = 3.7 Hz, 1H, *H*-4), 7.15 (dd, *J* = 6.4, 3.7 Hz, 2H, *H*-3, *H*-3'), 7.13-7.10 (m, 2H, *H*-4', *H*-3''), 7.02 (dd, *J* = 11.6, 3.6 Hz, 2H, *H*-4'', *H*-3'''), 6.70 (d, *J* = 3.5 Hz, 1H, *H*-4'''), 5.31-5.23 (bs, 1H, *H*-γ), 4.59-4.53 (bs, 1H, *H*-δ), 4.02 (bs, 1H, *H*-δ), 3.90-3.83 (bs, 1H, *H*-β), 2.97-2.87 (bs, 1H, *H*-β), 2.81 (t, *J* = 7.5 Hz, 2H, Ar-CH_2), 2.61-2.52 (bs, 1H, *H*-α), 1.70-1.65 (m, 2H, ArCH$_2$-CH_2), 1.36 (m, 18H, ArCH$_2$CH$_2$-*CH*$_2$-*CH*$_2$-CH_2, Boc-CH_3, methyl ester-CH_3), 0.90 (t, *J* = 7.1 Hz, 3H, -CH_3) ppm;

^{13}C NMR (126 MHz, THF-d_8): δ 146.5, 143.1, 138.1, 138.0, 137.1, 137.0, 136.1, 135.3, 125.8, 125.7, 125.2, 125.2, 125.2, 125.1, 124.9, 124.5, 124.4, 119.3, 80.6, 52.6, 52.0, 32.5, 30.8, 29.6, 28.5, 23.3, 14.2 ppm;

HRMS (MALDI, (DCTB)): *m/z* $[M+H]^+$ calc. for $C_{35}H_{40}N_4O_4S_4$: 708.1932; found : 708.1925; δ m/m = 1 ppm.

(4*R*)-1-*Tert*-butoxycarbonyl-[(5'''-hexyl-2,2';5',2'';5'',2'''-quaterthien-5-yl)-1*H*-1,2,3-triazol-1yl]-L-proline methyl ester 3.8

To a solution of 0.060 g (0.14 mmol) of 5-ethynyl-5'''-hexyl-2,2';5',2'';5'',2'''-quaterthiophene **3.50** in a mixture of 2 mL THF and 2 mL of DCM 0.072 g of the *N*-Boc–trans-4-azido-L-proline **3.55** (0.17 mmol), 0.002 g of copper powder (0.028 mmol) and 0.042 g of tetrakis(acetonitrile) copper(I) hexafluorophosphate (0.13 mmol) were added, under argon. The reaction was stirred at room temperature for 16 h. The reaction mixture was washed several times with a saturated $EDTA_{(aq)}$ solution. The aqueous layers were repeatedly extracted with DCM. The organic layers were

combined and the solvent was removed. The crude product was suspended in dry *n*-hexane and filtered off to give hybrid **3.8** as dark brown solid in 94% yield (0.093 mg, 0.13 mmol).

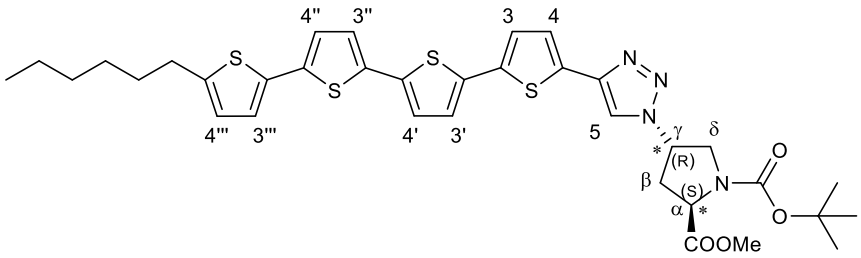

M. p. 194-195 °C;

^{1}H NMR (500 MHz, THF-d_8): δ 8.08 (s, *H*-5 triazole), 7.28 (d, *J* = 3.7 Hz, 1H, *H*-4), 7.15 (dd, *J* = 6.4, 3.7 Hz, 2H, *H*-3, *H*-3'), 7.13-7.10 (m, 2H, *H*-4', *H*-3''), 7.02 (dd, *J* = 11.6, 3.6 Hz, 2H, *H*-4'', *H*-3'''), 6.70 (d, *J* = 3.5 Hz, 1H, *H*-4'''), 5.31-5.23 (bs, 1H, *H*-γ), 4.59-4.53 (bs, 1H, *H*-δ), 4.02 (bs, 1H, *H*-δ), 3.90-3.83 (bs,1H, *H*-β), 2.97-2.87 (bs, 1H, *H*-β), 2.81 (t, *J* = 7.5 Hz, 2H, Ar-CH_2), 2.61-2.52 (bs, 1H, *H*-α), 1.70-1.65 (m, 2H, ArCH$_2$-CH_2), 1.36 (m, 18H, ArCH$_2$CH$_2$-*CH*$_2$-*CH*$_2$-CH_2, Boc-CH_3, methyl ester-CH_3), 0.90 (t, *J* = 7.1 Hz, 3H, -CH_3) ppm;

^{13}C NMR (126 MHz, THF-d_8): δ 146.5, 143.1, 138.1, 138.0, 137.1, 137.0, 136.1, 135.3, 125.8, 125.7, 125.2, 125.2, 125.2, 125.1, 124.9, 124.5, 124.4, 119.4, 80.6, 52.6, 52.0, 32.5, 30.8, 29.6, 28.5, 23.3, 14.2 ppm;

HRMS (MALDI, (DCTB)): *m/z* $[M+H]^+$ calc. for $C_{35}H_{40}N_4O_4S_4$: 708.1932; found : 708.1925; δ m/m = 1 ppm.

(5'-Bromo-[2,2'-bithien)]-5-yl)-1-hexanone 3.60

A solution of 1.350 g of NBS (7.58 mmol) in 10 mL DMF was added dropwise to a solution of 2.000 g of [2,2'-bithien]-5-yl-1-hexanone **3.59** (7.58 mmol) in 28 mL dry DMF at 0 °C under argon. The mixture was stirred at room temperature for 16 h. After removing the solvent, the residue was redissolved in DCM and washed with a

saturated solution of sodium bisulfite and several times with water. The organic layer was separated and dried over Na_2SO_4 and the solvent removed under reduced pressure. The residue was purified by column chromatography (silica, eluent: petroleum ether/DCM 2:8) to give (5'-bromo-[2,2'-bithien)]-5-yl)-1-hexanone **3.60** as yellow solid in 98% yield (2.560 g, 0.78 mmol).

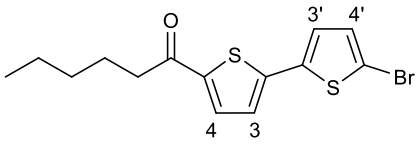

M. p. 79.2-81.5 °C;

^{1}H NMR (400 MHz, $CDCl_3$): δ 7.57 (d, *J* = 4.0 Hz, 1H, *H*-4), 7.09 (d, *J* = 3.9 Hz, 1H, *H*-3), 7.05 (d, *J* = 3.9 Hz, 1H, *H*-3'), 7.01 (d, *J* = 3.9 Hz, 1H, *H*-4'), 2.89-2.81 (m, 2H, Ar(C=O)-CH_2), 1.79-1.70 (m, 2H, Ar(C=O)CH_2-CH_2), 1.36 (dq, *J* = 7.2, 3.6 Hz, 4H, Ar(C=O)CH_2CH_2-CH_2-CH_2), 0.95-0.87 (m, 3H, CH_3) ppm;

^{13}C NMR (101 MHz, $CDCl_3$): δ 193.0, 143.8, 142.6, 137.6, 132.2, 130.8, 125.3, 124.0, 113.1, 38.8, 31.3, 24.3, 22.3, 13.7 ppm;

MS (CI): *m/z* = 344 $[M]^+$, 286 $[M\text{-}C_3H_6O]^+$, 264 $[M\text{-}Br]^+$.

1-(2,2';5',2'';5'',2'''-Quaterthien-5-yl)-1-hexanone 3.68

A mixture of 1.200 g of [2,2'-bithien]-5-yl-(trimethyl)stannane **3.67** (3.6 mmol), 1.000 g of (5'-bromo-[2,2'-bithien)]-5-yl)-1-hexanone **3.60** (2.9 mmol), and 0.017 g of tetrakis(triphenylphosphine) palladium (0.015 mmol) in 30 mL dry DMF was degassed for 25 min and heated up to 80 °C for 30 min. The reaction mixture was directly filtered off. In order to remove all the impurity, the crude product was washed with petroleum ether to give 1-(2,2';5',2'';5'',2'''-quaterthien-5-yl)-1-hexanone **3.68** as dark yellow solid in 83% yield (1.000 g, 2.4 mmol).

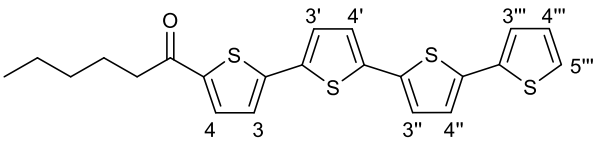

M. p. 209-210 °C;

^{1}H NMR (500 MHz, $C_2D_2Cl_4$_100 °C): δ 7.57 (d, *J* = 4.0 Hz, 1H, *H*-4), 7.23 (d, *J* = 5.2 Hz, 1H, *H*-3'''), 7.21 (d, *J* = 3.9 Hz, 1H, *H*-3), 7.18 (d, *J* = 3.5 Hz, 1H, *H*-5'''), 7.15 (d, *J* = 3.9 Hz, 1H, *H*-3'), 7.12-7.07 (m, 3H, *H*-4'', *H*-3'', *H*-4'), 7.02 (dd, *J* = 5.1, 3.6 Hz, 1H, *H*-4'''), 2.82 (t, *J* = 7.4 Hz, 2H, Ar(C=O)-CH_2), 1.78-1.71 (m, 2H, Ar(C=O)CH_2-CH_2), 1.40-1.34 (m, 4H, Ar(C=O)CH_2CH_2-CH_2-CH_2), 0.92 (t, *J* = 7.1 Hz, 3H, CH_3) ppm;

^{13}C NMR (126 MHz, $C_2D_2Cl_4$_100 °C): δ 193.0, 144.7, 143.0, 138.4, 137.6, 137.1, 135.7, 135.6, 132.5, 128.2, 126.5, 125.3, 125.2, 124.9, 124.8, 124.4, 120.7, 39.5, 31.8, 24.8, 22.5, 14.0 ppm;

HRMS (MALDI, (DCTB)): *m/z* $[M+H]^+$ calc. for $C_{22}H_{20}OS_4$: 428.0397; found : 428.0393; δ m/m = 0.9 ppm.

1-(5'''-Bromo-[2,2';5',2'';5'',2'''-quaterthien]-5-yl)-1-hexanone 3.69

A solution of 0.214 g of NBS (1.2 mmol) in 15 mL DMF was added dropwise to a solution of 0.515 g of 1-(2,2';5',2'';5'',2'''-quaterthien-5-yl)-1-hexanone **3.68** (1.2 mmol) in 15 mL dry chloroform at 0 °C under argon. The mixture was stirred at room temperature for 16 h. In order to remove all the impurities, the crude product was directly filtered off and washed with *n*-hexane to give 1-(5'''-bromo-[2,2';5',2'';5'',2'''-quaterthien]-5-yl)-1-hexanone **3.69** as a red solid in 82% yield (0.500 g, 0.99 mmol).

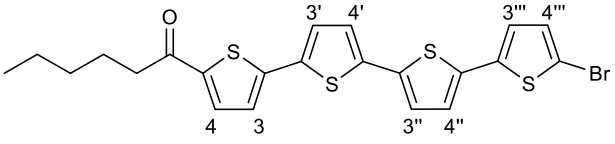

M. p. 203- 205 °C;

^{1}H NMR (500 MHz, $C_2D_2Cl_4$_100 °C): δ 7.57 (d, *J* = 4.0 Hz, 1H, *H*-4), 7.20 (d, *J* = 3.8 Hz, 1H, *H*-4'''), 7.15 (d, *J* = 4.0 Hz, 1H, *H*-3), 7.11-7.08 (m, 2H, *H*-4', *H*-3''), 7.02 (d, *J* = 3.8 Hz, 1H, *H*-3'), 6.98 (d, *J* = 3.9 Hz, 1H, *H*-4''), 6.92 (d, *J* = 3.8 Hz, 1H, *H*-3'''), 2.82 (t, *J* = 7.4 Hz, 2H, Ar(C=O)-CH_2), 1.78-1.71 (m, 2H, Ar(C=O)CH_2-CH_2), 1.38 (dd, *J* = 9.0, 5.8 Hz, 4H, Ar(C=O)CH_2CH_2-CH_2-CH_2), 0.92 (t, *J* = 7.1 Hz, 3H, -CH_3) ppm;

^{13}C NMR (126 MHz, $C_2D_2Cl_4$_100 °C): δ 193.1, 144.7, 143.5, 138.7, 138.0, 136.3, 135.8, 132.5, 131.1, 126.5, 125.3, 125.2, 125.1, 124.5, 124.4, 120.6, 39.5, 31.8, 29.9, 24.8, 22.5, 14.0 ppm;

HRMS (MALDI, (DCTB)): *m/z* $[M+H]^+$ calc. for $C_{22}H_{19}BrOS_4$: 505.9502; found : 505.9504; δ m/m = 0.4 ppm.

1-(5'''-[(Trimethylsilyl)ethynyl]-[2,2';5',2'';5'',2'''-quaterthien]-5-yl)-1-hexanone 3.70

Trimethylsilylacetylene **3.44** (0.4 mL, 2.8 mmol) was dropped into a solution of 0.288 g of 1-(5'''-bromo-[2,2';5',2'';5'',2'''-quaterthien]-5-yl)-1-hexanone **3.69** (0.56 mmol), 0.012 g of bis(triphenylphosphine)palladium(II) dichloride (0.016 mmol) and 0.006 g of CuI (0.033 mmol) in a mixture of 30 mL dry THF and 15 mL triethylamine. The reaction was stirred for four days at 60 °C under argon. After cooling down the reaction to room temperature, the mixture was washed several times with water. The organic layer was separated and dried over Na_2SO_4 and the solvent removed under reduced pressure. The residue was purified by column chromatography (silica, eluent: *n*-hexane/chloroform 1:1) to give 1-(5'''-[(trimethylsilyl)ethynyl]-[2,2';5',2'';5'',2'''-quaterthien]-5-yl)-1-hexanone **3.70** as golden solid in 72% yield (0.215 g, 0.41 mmol).

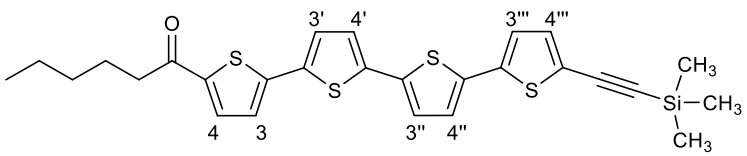

M. p. 200-203 °C;

^{1}H NMR (500 MHz, $C_2D_2Cl_4$_100 °C): δ 7.57 (d, *J* = 4.0 Hz, 1H, *H*-4), 7.21 (d, *J* = 3.8 Hz, 1H, *H*-4'''), 7.15 (d, *J* = 3.9 Hz, 1H, *H*-3), 7.09 (m, 2H, *H*-4', *H*-3''), 7.01 (dd, *J* = 7.8, 3.8 Hz, 1H, *H*-3'), 6.98 (d, *J* = 3.9 Hz, 1H, *H*-4''), 6.92 (d, *J* = 3.8 Hz, 1H, *H*-3'''), 2.82 (t, *J* = 7.4 Hz, 2H, Ar(C=O)-CH_2), 1.74 (dd, *J* = 14.5, 7.3 Hz, 2H, Ar(C=O)CH_2-CH_2), 1.41-1.35 (m, 4H, Ar(C=O)CH_2CH_2-CH_2-CH_2), 0.92 (t, *J* = 7.1 Hz, 3H, -CH_3), 0.26 (s, 9H, Si-CH_3) ppm;

Recording ^{13}C NMR was not possible due to low solubility;

HRMS (MALDI, (DCTB)): *m/z* $[M+H]^+$ calc. for $C_{27}H_{28}OS_4Si$: 524.0792; found : 524.0785; δm/m = 1.3 ppm.

2-[1-(5'-Bromo[2, 2'-bithien]-5-yl)hexylidene]-propanedinitrile 3.62

(5'-Bromo-[2,2'-bithien)]-5-yl)-1-hexanone **3.59** (2.000 g, 5.83 mmol), 7.690 g of malononitrile (58.30 mmol) and 44.700 g of ammonium acetate (583 mmol) were dissolved in 20 mL of 1,2-dichloroethane. The reaction mixture was stirred for five days at 100 °C under argon. After cooling down to room temperature, the reaction mixture was washed several times with water. The organic layer was separated and dried over Na_2SO_4 and the solvent removed under reduced pressure. The crude oily residue was purified by column chromatography (silica, eluent: *n*-hexane/DCM 1:1) to give 2-[1-(5'-bromo[2,2'-bithien]-5-yl)hexylidene]-propanedinitrile **3.62** as orange solid in 87% yield (1.950 g, 5.04 mmol).

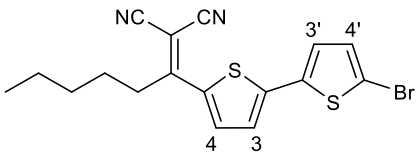

M. p. 106-108.5 °C;

^{1}H NMR (400 MHz, $CDCl_3$): δ 7.93 (d, *J* = 4.2 Hz, 1H, *H*-4); 7.20 (d, *J* = 4.1 Hz, 1H, *H*-3); 7.12 (d, *J* = 3.9 Hz, 1H, *H*-3'); 7.05 (d, *J* = 3.8 Hz, 1H, *H*-4'); 2.95-2.88 (m, 2H, Ar(C=O)-CH_2), 1.75-1.64 (m, 2H, Ar(C=O)CH_2-CH_2), 1.49-1.31 (m, 4H, Ar(C=O)CH_2CH_2-CH_2-CH_2), 0.92 (t, *J* = 7.1 Hz, 3H, -CH_3) ppm;

^{13}C NMR (101 MHz, $CDCl_3$): δ 193.5, 144.2, 143.0, 138.1, 132.6, 131.3, 130.0, 125.8, 124.5, 113.5, 39.3, 31.7, 24.8, 22.7, 14.2 ppm;

MS (CI): *m/z* $(M)^+$ = 391 $[M]^+$, 313 $[M\text{-}Br]^+$.

{5'-([Trimethylsilyl]ethynyl)[2,2'-bithien]-5-yl}trimethyl-stannane 3.64

Lithium diisopropylamide (0.6 mL, 4.2 mmol) was added dropwise to a solution of 1.000 g of 5´-trimethylsilyl-2,2´-bithiophene **3.63** (3.8 mmol) in 35 mL of THF at -78 °C under argon. The reaction was stirred for 1 h at -78 °C. Trimethyltin chloride (0.834 g, 4.2 mmol) was added. The reaction was stirred for 1 h at -78 °C and for 16 h at room temperature. Subsequently, the reaction was quenched and the solvent evaporated. The residue was dissolved in DCM and washed with water. The organic phase was dried over $MgSO_4$ and the solvent removed under reduced pressure to give {5'-([trimethylsilyl]ethynyl)[2,2'-bithien]-5-yl}trimethyl-stannane **3.64** without further purification.

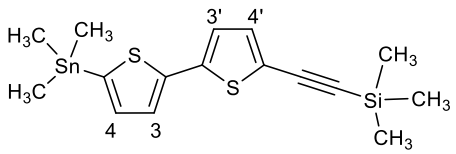

^{1}H NMR (400 MHz, $CDCl_3$) δ 7.28 (dd, *J* = 5.3, 3.4 Hz, 1H, *H*-4'), 7.22 (dd, *J* = 5.4, 3.5 Hz, 1H, *H*-4'), 7.17 (d, *J* = 3.8 Hz, 1H, *H*-4), 7.14-7.11 (m, 2H, *H*-4, *H*-3), 7.10-7.07 (m, 1H, *H*-3), 7.04 – 6.98 (m, 2H, *H*-3', *H*-3'), 3.39 (s, 1H, *H*-acetylene), 0.41-0.22 (m, 27H, Sn-CH_3, Si-CH_3) ppm;

MS (CI): *m/z* = 355 $[M]^+$, 252 $[M\text{-}(SiCH_3)_6]^+$.

2-{1-(5'''-Ethynyl-[2,2';5',2'';5'',2'''-quaterthien]-5-yl)-hexylidene}-propane-dinitrile 3.71

1-(5'''-[(Trimethylsilyl)ethynyl]-[2,2';5',2'';5'',2'''-quaterthien]-5-yl)-1-hexanone **3.70** (0.200 g, 0.38 mmol), 0.251 g of malononitrile (3.8 mmol), 0.162 g of titanium iso-

propoxide (0.57 mmol) were dissolved in a mixture of 10 mL of 1,2-dichloroethane and 10 mL of 2-propanol. The reaction mixture was stirred at 70 °C overnight and quenched with a 1 N HCl solution. The organic layer was washed several times with water and dried over Na_2SO_4. The solvent was removed under reduced pressure and the crude product was purified by column chromatography (silica, eluent: petrol ether/DCM 1:2) to give 2-{1-(5'''-ethynyl-[2,2';5',2'';5'',2'''-quaterthien]-5-yl)-hexylidene}-propanedinitrile **3.71** as a red solid in 75% yield (0.142 g, 0.28 mmol).

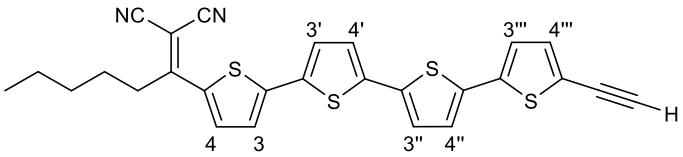

M. p. 140 °C (decomposition);

^{1}H NMR (400 MHz, $CDCl_3$): δ 7.96 (d, *J* = 4.2 Hz, *H*-4), 7.29 (d, *J* = 3.9 Hz, *H*-4'''); 7.25 (d, *J* = 4.1Hz, *H*-3) 7.19 (d, *J* = 3.8 Hz, *H*-3'''); 7.15 – 7.10 (m, 3H, *H*-3'', *H*-4', *H*-3') 7.04 (d, *J* = 3.8 Hz, *H*-4''); 3.44 (s, *H*-alkyne) 1.75-1.67 (m, 2H, Ar(C=O)-CH_2), 1.43-1.33 (m, 2H, Ar(C=O)CH_2-CH_2), 1.29-1.23 (m, 4H, Ar(C=O)CH_2CH_2-CH_2-CH_2), 0.93 (t, *J* = 7.1 Hz, 3H, -CH_3) ppm;

Recording ^{13}C NMR was not possible due to decomposition;

HRMS (MALDI, (DCTB)): *m/z* $[M+H]^+$ calc. for $C_{27}H_{20}N_2S_4$: 500.0509; found : 500.0500; δ m/m = 1.7 ppm.

(4*S*)-1-*Tert*-butoxycarbonyl-{2-[(1-[2,2';5',2'';5'',2'''-quaterthien]-5-yl)-hexylidene]-propanedinitrile}-1*H*-1,2,3-triazol-1yl}-L-proline methyl ester 3.9

To a solution of 0.055 g (0.11 mmol) of 2-{1-(5'''-ethynyl-[2,2';5',2'';5'',2'''-quaterthien]-5-yl)-hexylidene}-propanedinitrile **3.71** in 4 mL of DCM, 0.040 g of the *N*-Boc–trans-4-azido-L-proline **3.54** (0.13 mmol), 0.001 g of copper powder (0.02 mmol) and 0.042 g of tetrakis(acetonitrile) copper(I) hexafluorophosphate (0.13 mmol) were added under argon. The reaction was stirred at room temperature for 16 h. The reaction mixture was washed two times with a saturated $EDTA_{(aq)}$ solution.

The aqueous layers were repeatedly extracted with DCM. The organic layers were combined and the solvent was removed. The crude product was suspended in dry methanol and petrol ether, and filtered off to give quaterthiophene-proline hybrid **3.9** as purple solid in 60% yield (0.050 g, 0.06 mmol).

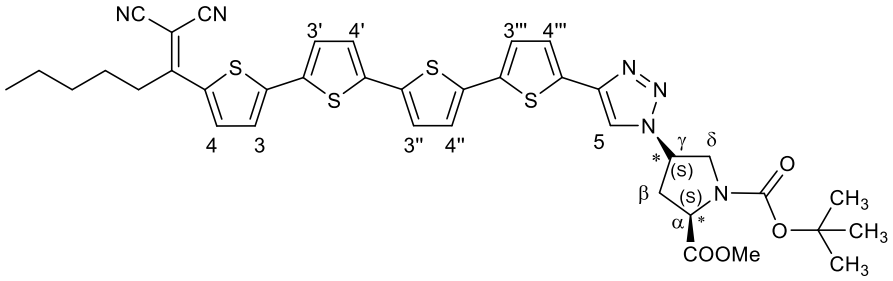

M. p. 180 °C (decomposition);

Recording ^{1}H NMR and ^{13}C NMR were not possible due to strong aggregation;

HRMS (MALDI, (DCTB)): *m/z* $[M+H]^+$ calc. for $C_{38}H_{38}N_6O_4S_4$: 770.1837; found : 770.1831; δm/m = 0.7 ppm.

References

[1] A. Jatsch, *PhD Thesis*, University of Ulm, **2010**.

[2] E.-K. Schillinger, *PhD Thesis*, University of Ulm, **2010**.

[3] E. A. Kleymyuk, P. A. Troshin, E. A. Khakina,Y. N. Luponosov, Y. L. Moskvin, S. M. Peregudova, S. D. Babenko, T. Meyer-Friedrichsen, S. A. Ponomarenko, *Energy Environ. Sci.* **2010**, *3*, 1941–1948.

[4] R. Hajlaoui, D. Fichou, G. Horowitz, B Nessakh, M. Constant, F. Garnier, *Adv. Mater.* **1997**, *9*, 557-561.

[5] M. Melucci, G. Barbarella, M. Zambianchi, M. Benzi, F. Biscarini, M. Cavallini, A. Bongini, S. Fabbroni, M. Mazzeo, M. Anni, G. Gigli, *Macromolecules* **2004**, *37*, 5692–5702.

[6] A. Digennaro, H. Wennemers, G. Joshi, S. Schmid, E. Mena-Osteritz, P. Bäuerle, *Chem. Commun.* **2013**, *49*, 10929–10931.

Summary

The aim of my thesis was to synthesize new asymmetric A-B systems, which are able to self-assemble in chiral suprastructures due to the presence of a single amino acid and to investigate them with respect to their self-assembling behaviour in solution and in the solid state. Firstly, a synthetic protocol was developed to efficiently link the biomotive to the π-conjugated scaffold (***Chapter 3***). This was accomplished by applying a Cu(I)-catalyzed 1,3-dipolar cycloaddition of azides and terminal alkynes, better known as click-reaction. In fact, this kind of reaction allows the exclusive formation of the desired products in very good yields. Therefore, a series of *N*-Boc-proline-quaterthiophene hybrids was synthesized and characterized (***Chart 1***).

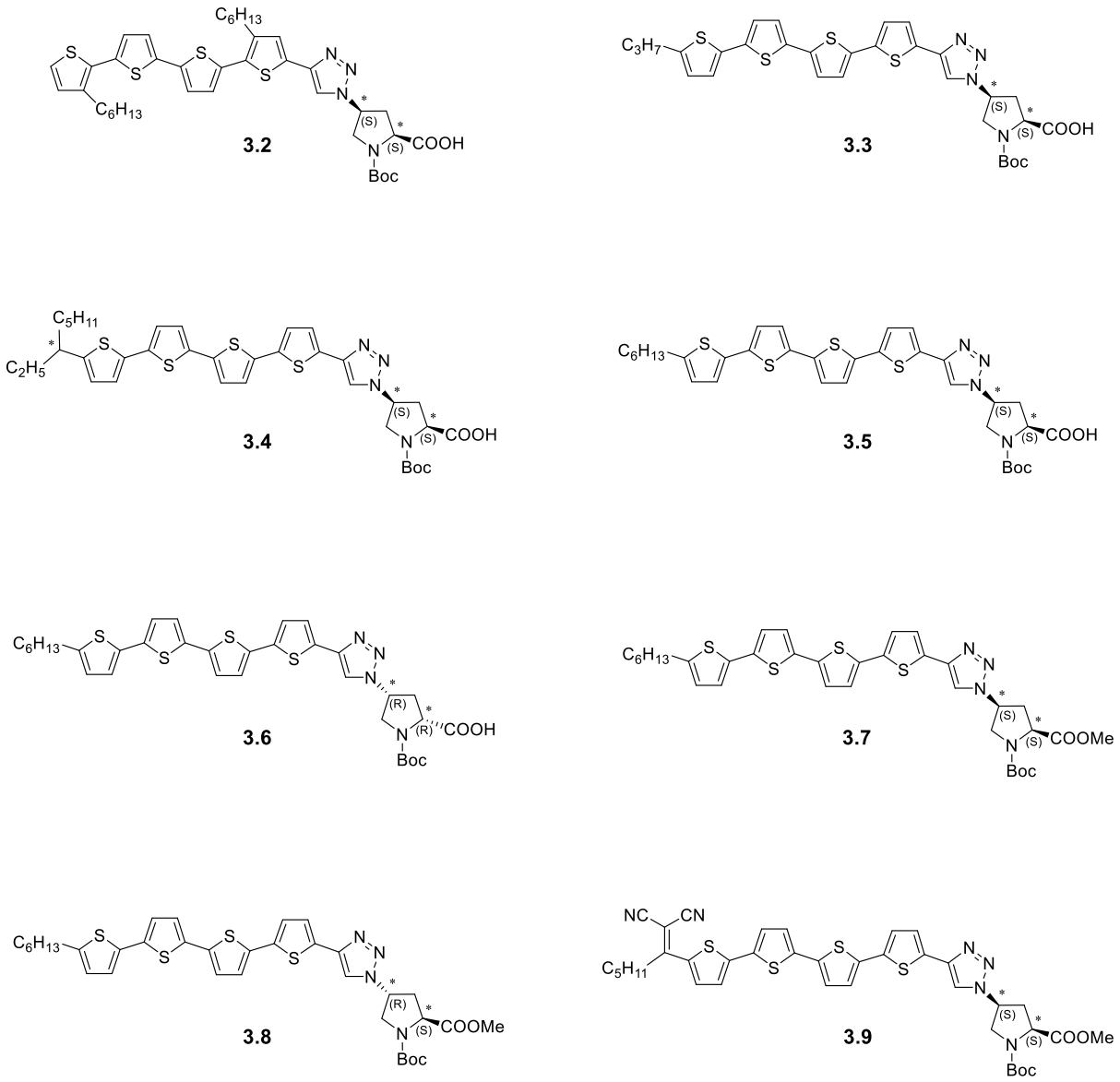

Chart 1*. Molecular structures of the synthesized proline-quaterthiophene hybrids* ***3.2****-****3.9****.*

In order to avoid the often used synthesis and isolation of larger peptides, a single proline was instead utilized. In fact, this simple biomoiety, characterized by two stereo-centres, is enough to influence the self-assembling behaviour of the oligothiophenes in solution and in the solid state. The choice of proline as amino acid derived from its ability, in both oligomeric and polymeric forms, to exist in two solvent-dependent well-defined helical conformations: PPI and PPII. These differ in handedness, residues per helical turn, and helical pitch length. The combination of such scaffold with π-conjugated oligomers results in new hybrids, which promise interesting results with respect to their self-organizing behaviours.

Firstly, the self-assembly process of the synthesized oligothiophenes was investigated in solution by UV/Vis, fluorescence, and CD-spectroscopy (***Chapter 4***). The optical and chiroptical properties pointed out to the formation of aggregates in which the π-conjugated systems interact with each other confirming the influence of the proline scaffold.

In aqueous environment, for carboxylic acid-substituted systems **3.2**, **3.3**, **3.4**, and **3.5** the interactions responsible for the superstructure formation were both hydrophobic (π-π stacking and van der Waals interactions) and hydrophilic (*H*-bonding interactions) (***Figure 1***).

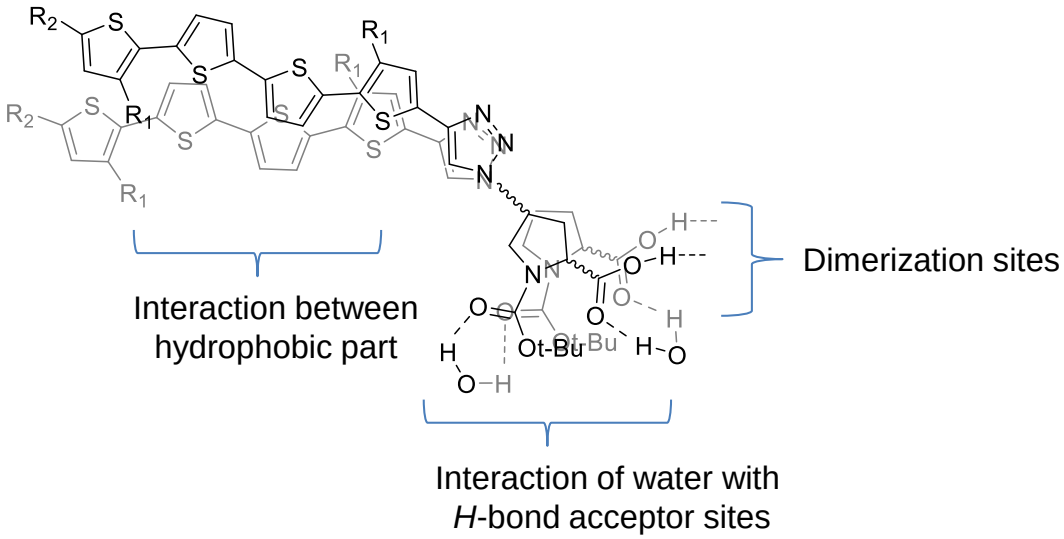

Figure 1. *Model of interactions between two hybrids in polar environment.*

In apolar solutions hybrid **3.5** showed different optical and chiroptical behaviour than in the polar mixture: above all the loss of the thermodynamic stability of the formed

chiral aggregates, which was so extraordinary high in the aqueous solutions. This finding suggested that diverse interactions are involved in the assembling process: the hydrophobic forces are not anymore predominant, but the *H*-bonding interactions are just responsible for the formation of the aggregates (***Figure 2***).

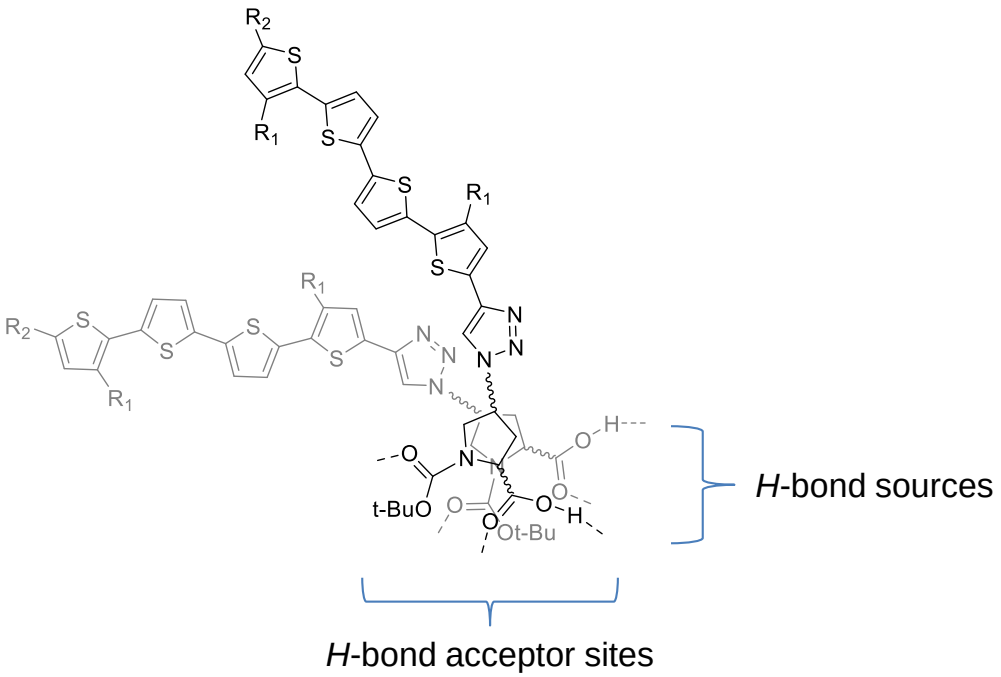

Figure 2. *Model of interactions between two hybrids in apolar environment.*

It was indeed assessed that the involvement of both hydrophobic and hydrophilic interactions is fundamental to obtain well-ordered and very stable supramolecular structures. Furthermore, the introduction of the DCV group into the molecular structure affected the self-assembling behaviour of the quaterthiophene-proline. This structural change had strong influence on the dipole-dipole interactions between the chromophores leading to the formation of aggregates in which the π-systems are differently organized.

Additionally, investigation of the self-assembly properties of hybrids **3.2** and **3.5** in the solid state was performed by AFM and TEM. For both quaterthiophenes, the formation of micelles was observed, according to the calculated *packing parameter* values (***Figure 3***).

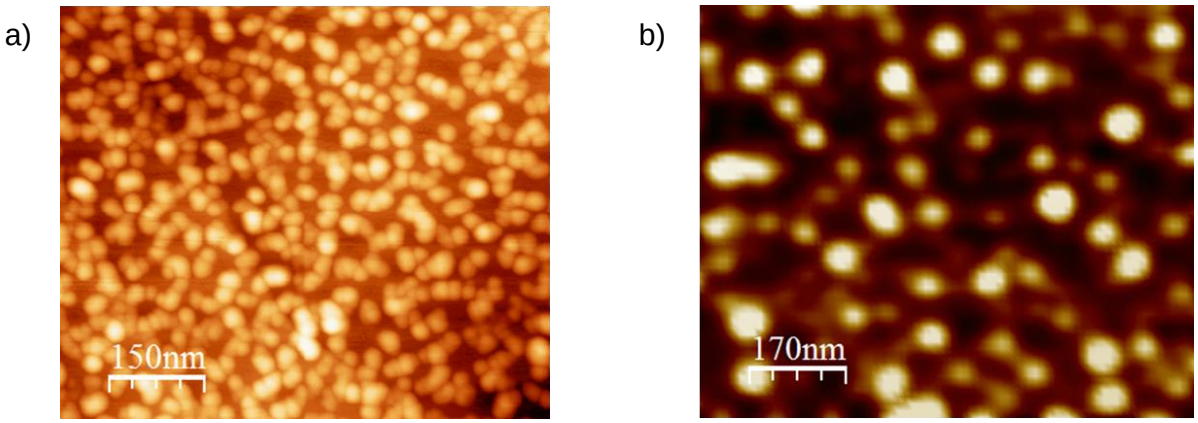

***Figure 3**. a) **3.2**/HOPG drop-casted from the THF/water (1:9) solution, topography micrograph, 740 x 630 nm^2, ΔZ = 8 nm; b) **3.5**/HOPG drop-casted from the THF/water (1:9) solution, topography micrograph, 210 x 175 nm^2, ΔZ = 8 nm.*

Furthermore, a model was proposed, in which the molecules aggregate by leaving the hydrophilic proline part facing towards the aqueous environment, and the hydrophobic part pointing inside the supramolecular structure, as depicted in ***Figure 4***.

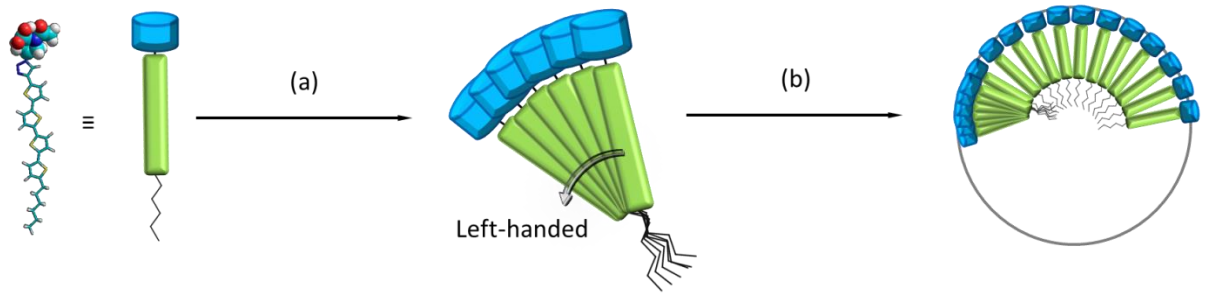

***Figure 4.** Proposed model for the aggregates of **3.5**, (a) π-π interacting ensemble formation, (b) micelle formation.*

Finally, first tests on hybrids **3.5** and **3.9** in solution-processed BHJSC, with $BC_{61}BM$ as acceptor, were also carried out. It was observed that DCV-functionalized hybrid **3.9** showed higher efficiency than quaterthiophene **3.5**, and comparable outcomes with literature known sexithiophene hybrids (Ref. 24, ***Chapter 6***).

"CV was removed for data privacy protection reasons."

"CV was removed for data privacy protection reasons."

CONFERENCE CONTRIBUTIONS

Lectures

Tagung über Konjugierte Polymere und Quaterthiophene Oligomere (Würzburg, September 2013)	'Chiral Asymmetric Proline-Hybrids'.
International Winterschool of Bioelectronics Proline (Kirchberg in Tirol, February 2014)	'Chiral Asymmetric Oligothiophene-Hybrids'.

Poster

11th International Symposium on „Functional π-Electron System" (Arcachon, France, July 2013) : A. Digennaro, H. Wennemers, G. Joshi, S. Schmid, E. Mena-Osteritz, P. Bäuerle, `*Self-Organizing Proline-Fuctionalized Oligothiophene´*.